Numerical (FEA) Evaluation of Crane End Buffer Impact Forces

by

Trevor Neville Haas

Dissertation presented for the degree of

Doctor of Philosophy in Engineering

at the University of Stellenbosch

Department of Civil Engineering
University of Stellenbosch
Private Bag X1, 7602, Matieland, South Africa

Promoters:
Dr. P. Maincon
Prof. P. E. Dunaiski

December 2007

Declaration

I, the undersigned, hereby declare that the work contained in this dissertation is my own original work and that I have not previously in its entirety or in part submitted it at any university for a degree.

Signature: ……..

T. N. Haas

Date: ……..

SYSNOPSIS

Numerical (FEA) Evaluation of Crane End Buffer Impact Forces

T.N. Haas

Department of Civil Engineering
University of Stellenbosch
Private Bag X1, 7602, Matieland, South Africa

Dissertation: PhD (Engineering)

December 2007

The current codes of practice for the design of structures which were studied during this investigation do not explicitly account for the flexibilities and interactions of the Electric Overhead Travelling Crane (EOHTC) and the crane support structure. This leads to analysing the EOHTC and the gantry structure as a decoupled system for ease of computation. Thus, the interaction of the various components of the EOHTC and gantry structure is ignored, which may result in an incorrect assessment of the forces computed in the gantry structure's members.

This led to a study to determine the effects of a EOHTC on the gantry structure. The research was conducted through a series of limited experimental tests and extensive advanced Finite Element Analysis (FEA) simulations.

This resulted in developing a computationally efficient FEA model of the full scale experimental EOHTC testing facility in the structural engineering laboratory at Stellenbosch University. The FEA model was developed to conduct simulations for the various load models, namely, vertical wheel load, horizontal longitudinal load and the horizontal lateral load models, as prescribed by the various codes. The research was then focussed at determining the maximum end buffer impact force responses when the crane runs into the end stops. The other load models were investigated by another researcher using the same FEA model.

The results from the experimental tests were used to calibrate the FEA simulations. This proved exceptionally challenging due to the various structural response phenomena which occur during the impact of the crane against the end stops. A good correlation between the experimental values and the values predicted by the FEA simulations was achieved for the first impact.

Modal analysis and modal superposition methods of analysis were used to determine the effect of the modes of vibration on the structural response to the end buffer impact.

A FEA sensitivity analysis was conducted on a set of identified parameters which have a significant effect on the structural response to the end buffer impact.

The maximum end buffer impact force was determined for a chosen level of reliability based on the responses from the sensitivity analysis using the Lagrange Multiplier method.

These maximum end buffer impact forces are then compared with the forces prescribed by the codes. SABS 0160 slightly underestimates, while SANS 10160 severely overestimates the end buffer impact force obtained from the constraint optimization technique for a target level of reliability of $\beta = 3$.

SAMEVATTING

Numerical (FEA) Evaluation of Crane End Buffer Impact Forces

T.N. Haas

Departement Siviele Ingenieurwese
Universiteit van Stellenbosch
PrivaatSak X1, 7602, Matieland, Suid-Afrika

Proefskrif: PhD (Ingenieurwese)

Desember 2007

Die huidige praktyk kodes vir die ontwerp van strukture wat in hierdie ondersoek bestudeer is, maak nie eksplisiet voorsiening vir die buigbaarheid van die Oorhoofse Elektriese Kraan (OEK) en die interaksie van die OEK met die ondersteunings struktuur nie. Dit lei tot die analise van die OEK en die ondersteunings struktuur as ′n ontkoppelde stelsel vir die gemak van berekeninge. Dus word die interaksie tussen die verskillende komponente van die OEK en die ondersteunings struktuur geignoreer, wat dan ′n foutiewe skatting van die kragte in die struktuur komponente veroorsaak.

Hierdie tekortkomings het gelei tot die studie om die effekte van ′n OEK op die struktuur te bepaal. Die navorsing behels ′n stel beperkte eksperimentele toetse en uitgebreide gevorderde Eindige Element Analiese (EEA) simulasies.

Hierdie ondersoek het tot die ontwikkeling van ′n doeltreffende EEA model van die volskaalse eksperimentele OEK toetsfasiliteit in die struktuurlaboratorium van die Universiteit van Stellenbosch gelei. Die EEA model is ontwikkel om simulasies van die verskillende lasmodelle te ondersoek, naamlik die vertikale wielkrag, die horisontale longitudinale krag en horisontale laterale krag modelle soos voorskryf deur die verskillende kodes. Hierdie navorsing is dan verder gefokus om die maksimum entbuffer kragte te bepaal wanneer die OEK teen die

entbuffers bots. Die ander lasmodelle is deur ′n mede-navorser met behulp van dieselfde EEA model ondersoek.

Die resultate van die eksperimentele ondersoek is gebruik om die EEA simulasies te kalibreer. Hierdie kalibrasie proses is aansienlik bemoeilik deur die verskillende strukturele gedrags verskynsels wat tydens die impak van die kraan teen die entbuffers ontstaan. ′n Goeie korrelasie tussen die eksperimenteel bepaalde waardes en die waardes soos bepaal met behulp van die EEA simulasies is vir die eerste impak verkry.

′n Modale analise en modale superposisie metodes is gebruik om te bepaal of enige van die modes van vibrasie ′n effek op die strukturele gedrag van die entbuffer kragte het.

′n EEA sensitiwiteitsanalise is op ′n stel van ge-indentifiseerde parameters, wat ′n betekenisvolle effek op die strukturele gedrag as gevolg van die impak op die entbuffers het, uitgevoer.

Die maksimum entbuffer krag is bepaal vir ′n bepaalde vlak van betroubaarheid gebaseer op die resultate van die sensitiwiteitsanalise deur van die Lagrange vermenigvuldiger metode gebruik te maak.

Hierdie maksimum entbuffer kragte is met die voorskrifte van die praktyk kodes vergelyk. SABS 0160 onderskat die entbuffer impakkragte, terwyl SANS 1060 die entbuffer impakkragte oorskat soos bereken deur van die Lagrange vermenigvuldiger metode gebruik te maak vir ′n bepaalde vlak van betroubaarheid van $\beta = 3$.

ACKNOWLEDGEMENTS

I take this opportunity to express my heartfelt gratitude to all and especially those mentioned below during the course of my study at Stellenbosch University. Without you, my studies would not have been a success. Once again, Thank You.

- To Walter Sisulu University of Science and Technology (former Eastern Cape Technikon) for leave to pursue my studies.

- My promoters, Dr. P. Maincon and Prof. P. Dunaiski, for their constant support and academic guidance during my academic study.

- Helmut Bowles from FEAS (ABAQUS) for always being available to answer all my ABAQUS questions with enthusiasm.

- To all staff and students in the structural engineering division for their encouragement and support.

- My families for their encouragement and all the countless wonderful times spent together while in Cape Town.

- My parents, for providing the educational foundation which allowed me to attain this pinnacle. Thank you for your unending support, encouragement, love and prayers during my entire academic career and life. Baie dankie.

- My wife and children, Michelle, Cheyenne, Chaska and Chayton for enduring all the sacrifices to allow me to pursue my goal. Thank you Cheyenne, Chaska and Chayton for cheering me up when I was down. Only you Michelle knew the extent of the difficulties which I experienced. Michelle, thank you for also being by my side and always believing in me when at times I did not believe in myself. No amount of words can express my appreciation for the support and understanding I received from all of you, THANK YOU.

- To my LORD and GOD for always being by my side to guide, protect and help me thus far.

Table of Contents

LIST OF FIGURES

CHAPTER 5

LIST OF TABLES

CHAPTER 1: INTRODUCTION

1.1 General Discussion of Electric Overhead Travelling Cranes and the Crane Supporting Structure

Electric Overhead Travelling Cranes (EOHTC) are predominantly used in industrial buildings to move heavy and / or cumbersome equipment or material from one position to another. EOHTC are used to increase the mobility of the operational process within a building, thereby improving production and ultimately reducing the production costs of the manufactured item. Without EOHTC, many industries would be immobilised due to the lack of efficiency which the EOHTC provides. The hoist loads range from insignificant to several hundred tons, sometimes under very demanding conditions, such as in steel manufacturing environments. The crane supporting structure forms an integral part of the EOHTC system. For the EOHTC to transverse smoothly, the crane supporting structure must be adequately designed. The members of the crane and the crane supporting structure must be designed to have sufficient strength and stiffness to prevent failure at the Ultimate Limit State and excessive deflection and vibrations under the Serviceability Limit State.

The type of EOHTC which the designer chooses depends on a unique set of criteria to which it will be exposed during its lifetime. The factors which influence the choice of the EOHTC and the crane support structure include, but are not limited to; the maximum hoist load, the horizontal lateral span of the crane, the type of lifting attachment, the vertical height restriction, the speed of the crane and crab, the location of the crane, the environmental conditions, the use of standalone crane columns, etc. Figure 1.1 shows a picture of the EOHTC and of the crane support structure, used for the experimental tests in the Structural Engineering Laboratory of the Civil Engineering Department at the University of Stellenbosch. This study is limited to overhead travelling cranes of which both rails are at the same level on top of the crane girder. Portal cranes and semi-portal cranes, as well as under-slung cranes are excluded from this study. The in-depth study of the various types of cranes is outside the scope of this investigation. The reader is referred to Roswell [1.1] for more information on the subject.

Figure 1.1 Picture of the experimental configuration of the EOHTC and the crane support structure with all the members

1.2 Definition of the Problem

The South African Bureau of Standards, SABS 0160-1989 code of practice as amended in 1990 is simplistic in its approach of prescribing the forces to be applied to the crane supporting structure. The code does not explicitly account for the flexibility and interaction of the crane and crane support structure. The code assumes that the crane is rigid while only the crane supporting structure is allowed to deform. This is a simplification to allow for easier analysis and design methods.

A proposal to adopt the Eurocode EN 1991:3 (Actions Induced by Cranes and Machinery) is currently being discussed and will most likely be implemented with some changes in the new SANS 10160 loading code. The Eurocode EN 1991:3 addresses the load models with a more scientific approach based on the mechanics of the crane and its movement. A substantial

reduction in certain forces, notably the vertical wheel forces, is obtained when using the EN 1991:3 code as opposed to the SABS 0160-1989 code. There is apparently very little scientific basis or literature to support the multiplication factors to account for the dynamic effects as specified in SABS 0160. The result of the vertical wheel forces as prescribed by EN 1991:3 is based on the vertical hoisting speed, resulting in more realistic forces applied to the crane girder.

Both codes ignore the flexibilities of the crane and the crane support structure when specifying the loads which the crane exerts on the crane support structure. Thus, the interaction of the various components of the crane and the crane support structure is ignored, which results in an incorrect assessment of the forces computed in the crane support structure's members. This leads to greater forces in the crane support structure's members and ultimately in bigger steel sections which increases the costs of the overall structure. To obtain accurate member forces in the crane support structure's members under the various loading conditions, it is imperative to study the crane with the crane support structure as a coupled system.

1.3 History of the Crane Project

This investigation forms part of a comprehensive study of the EOHTC Project at the Institute of Structural Steel's Centre for Development of Steel Structures. The overall goal of the EOHTC project is to provide guidelines for the design of the crane supporting structure. Various investigations have been conducted by former and current students.

Barnard [1.2] was responsible for the design and construction of the full scale 5-ton EOHTC testing facility in the Structural Engineering laboratory. The experimental EOHTC facility was constructed with the option of adjusting various parameters during the experimental tests.

Viljoen [1.3], studied the local behaviour of a simply supported crane girder when subjected to vertical and horizontal lateral loading by experimental and Finite Element Analysis (FEA) simulations.

Perez-Winkler [1.4], studied the interaction between the crane wheel, rail and girder using experimental and FEA simulations.

Dymond [1.5], conducted a reliability calibration of the proposed crane load models.

De Lange [1.6], performed the experimental tests on the 5-ton EOHTC in the Structural Engineering laboratory at Stellenbosch University.

Kohlhaas [1.7], conducted experimental investigations into the end buffer impact force when the crane collides into the end stops. The investigation is explored in detail in chapter 2.3.

McKenzie [1.8], conducted FEA simulations on the horizontal lateral forces and the vertical wheel loads which are imposed by the crane on the crane supporting structure.

The overall objective of the project is to develop a proper understanding of EOHTC behaviour and to eventually produce guidelines for the design of the crane supporting structures.

1.4 Objectives of the Dissertation

The first objective of this research is to develop a FEA model which will capture the global interactions of all the components of the EOHTC and of the crane support structure, while being computationally efficient, by using various modelling techniques suitable for practical applications. The FEA model will be used in this research and future work to assess the maximum forces for the various load models (cases), i.e., vertical wheel load, horizontal longitudinal load and the horizontal lateral load.

The FEA simulations on the vertical wheel load and horizontal lateral load models were investigated by McKenzie [1.8], using the same FEA model developed by the author.

The second objective is to determine the maximum end buffer impact force when the crane collides with the end stops. The FEA model will be calibrated against the results of the experimental investigations, where after the FEA model will be used to perform more advanced simulations to assess the maximum end buffer impact force. A set of parameters were identified which could have a substantial effect on the impact response. These parameters were used to perform a sensitivity analysis using the FEA model. The FEA results of the various parameters, which substantially influence the impact forces, will be compared to the SABS 0160-1989 and the proposed SANS 10160 (based on EN 1991:3) codes. In addition, the key parameters which substantially influence the end buffer impact force response will also be documented.

1.5 Overview of the Dissertation Chapters

A brief review is provided of the subsequent chapters;

Chapter 2, “Literature Review and Problem Definition”, summarizes the latest information with regard to determining the end buffer impact forces as specified by the various codes of practice. The end buffer impact forces are determined for each of the codes reviewed. The end buffer impact forces as obtained from the various codes were compared.

The problem definition is examined in detail with the aims of the research project clearly identified. A research methodology is presented describing how the study will be performed.

Chapter 3, “Finite Element Analysis Modelling”, describes the modelling techniques used to create a computationally efficient model of the experimental 5-ton EOHTC in the Structural Engineering laboratory. Emphasis is also placed on the implications and limitations of the element choices made for the crane and the crane supporting structure’s members.

Chapter 4, “FEA Model Calibration”, describes how the FEA model was calibrated to the experimental test responses. The FEA model was calibrated to the experimental test results when the payload was hoisted to 0.15m above ground level. The cable lengths were adjusted in the FEA model and the responses compared to the experimental results when the payload was hoisted to 2.20m above ground level. The chapter also explains the differences in responses specifically when the payload is hoisted to 2.20m above ground level.

Chapter 5, “Modal Analysis and Modal Superposition”, explains the necessity to perform the modal analysis and modal superposition on the crane with the payload. The chapter presents the modal analysis data obtained from a FEA modal analysis for the crane with payload, excluding the crane supporting structure. An introduction to the modal analysis theory is also presented.
Two methods for obtaining the modal superposition response are presented. These responses are compared and the differences discussed. Recommendations are made on the correct choice of method to use for low and high frequencies.

Chapter 6, “Sensitivity Study”, explores the various parameters which have a significant effect on the end buffer impact response. A sensitivity analysis was performed on each parameter and its responses obtained from the FEA simulations. The maximum impact force of each parameter was compared to obtain the maximum end buffer impact force.

Chapter 7, “Comparison between the FEA and Codified Results” compares the FEA impact force responses of each parameter with the current SABS 0160 and the proposed SANS 10160 codes of practice. The FEA impact force responses were obtained by adjusting a single parameter at a time.

The maximum impact force was obtained from a constraint optimisation procedure using the Lagrange multiplier method by considering all the parameters. The maximum impact force was compared to the current SABS 0160 and the proposed SANS 10160 codes of practice to assess the codes adequacy in estimating the maximum end buffer impact force.

Chapter 8, “Summary, Conclusions and Recommendations”, presents the summary of the various chapters, the conclusions of the research project together with the recommendations.

CHAPTER 2: LITERATURE REVIEW AND PROBLEM DEFINITION

2.1 Introduction

After an extensive literature search, no peer reviewed journal publications were found relating to crane end buffer (end stop) impact forces. Other sources of information which exist are; experimental investigations, the crane manufacturer's guidelines for the selection of crane buffers, the various codes of practice for structural design and the guidelines presented by various professional associations. A limited number of journal publications exist on the estimation of forces imposed by the crane on the crane supporting structure, other than the crane end buffer impact forces.

A brief overview of the chapter 2 is presented below.

Chapter 2.2 reviews research conducted to determine the end buffer impact force using the FEA method.

The only experimental crane impact test studies found during this study are those conducted by Kohlhaas [1.7], at the University of Stellenbosch. This could be due to the significant cost of establishing a full scale testing facility to perform the tests. Kohlhaas' [1.7], experimental crane impact test report will be studied in detail in chapter 2.3.

The crane manufacturer, DEMAG, provides guidelines for determining the impact force, which are used to select the appropriate buffer type for specific conditions. The manufacturer's guidelines will be examined in detail in chapter 2.4.

In chapter 2.5, the different design philosophies used by the various codes to determine the impact forces are examined, calculated and compared.

Chapter 2.6 provides a summary of the criteria used to determine the estimated end buffer impact response when the crane collides into the end stops as proposed by the various codes of practice for structural design and professional associations.

Other literature not specifically related to end buffer impact forces, but relating to the estimation of forces imposed by the crane on the crane support structure is briefly reviewed in chapter 2.7.

Chapter 2.8, presents a review of the current practice, the objectives of the research project and a methodology to achieve the objectives of the research project.

2.2 Finite Element Analysis of the End Buffer Impact Forces

This study found no report of finite element analysis, previously conducted to obtain the end buffer impact response when the crane including payload, the crane supporting structure and end buffers are analyzed as a coupled system when the crane collides into the end stops.

2.3 Experimental End Buffer Impact Tests Performed by Kohlhaas

Kohlhaas[1.7], conducted experimental investigations into the end buffer impact response when the crane including payload, the crane supporting structure and end buffers are considered as a coupled system when the crane collides with the end stops. The experimental investigations were conducted on the 5-ton EOHTC at the Department of Civil Engineering at Stellenbosch University. The investigation provided valuable information and insight into the behaviour of the crane and the crane supporting structure during impact, especially with the payload attached.

2.3.1 End Buffer Characteristics

Kohlhaas [1.7], measured the deformation of the end buffers, the force in the end buffers and the speed of the crane as a function of time during the collision. From this information, the 1st cycle of the hysteresis of a set of experimental, force vs. displacement graphs of the end buffer's response during impact for a varying strain rates is presented in Figure 2.3.1.1. Figure 2.3.1.1 shows the variance in the response between the crane's LHS and RHS end buffers during a series of experimental tests. The LHS buffer is positioned on the LHS of the crane when the crane moves towards the end stops. The variance can be attributed to the slightly different properties of the end buffers and the slight unsymmetrical experimental configuration.

Figure 2.3.1.2 compares the representative experimental LHS and RHS end buffers responses to the manufacturer's stiffness curves at various speeds. The manufacturer's stiffness curve for an impact speed of 0.55m/s approximates the loading cycle of the experimental stiffness of the buffers. The experimental stiffness responses were obtained under a varying strain rate, i.e. starting at an initial velocity of 0.55m/s and reducing to 0m/s when the buffer is maximally compressed. It can be

assumed that the manufacturer's stiffness curves are also for a varying strain rate as it approximates the experimental stiffness response closely.

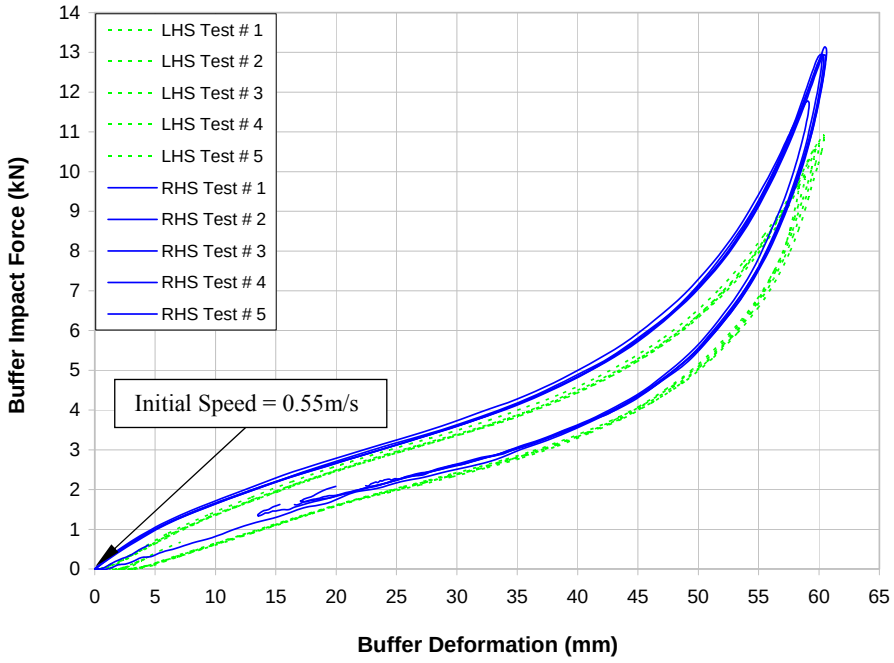

Figure 2.3.1.1 Comparison of the elastic characteristics of the 1st cycle of the LHS and RHS buffer's response for a varying strain rate. (Initial impact speed = 0.55m/s)

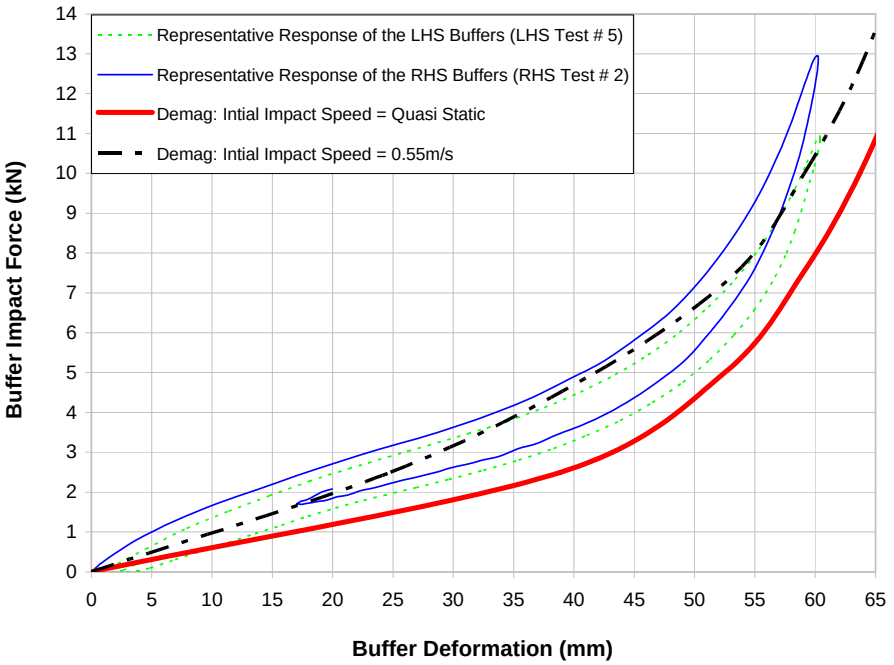

Figure 2.3.1.2 Comparison of the experimental and manufacturer's stiffness responses

2.3.2 Payloads

The first payload comprised of 4 concrete blocks connected to each other using a steel spreader frame as shown in Figure 2.3.2.1. The bulky nature of the payload resulted in a limited hoisting height which restricted Kohlhaas [1.7], from performing impact tests with the payload hoisted close to the crane bridge. The experimental tests were performed when the payload was hoisted to 0.15m and 0.8m above ground level. It was also difficult to account for energy losses between the concrete blocks due to their relative movement during impact. This spurred the design and construction of a compact payload which could be raised just below the crane bridge as shown in Figure 2.3.2.2. Kohlhaas only performed the impact tests with the original payload configuration.

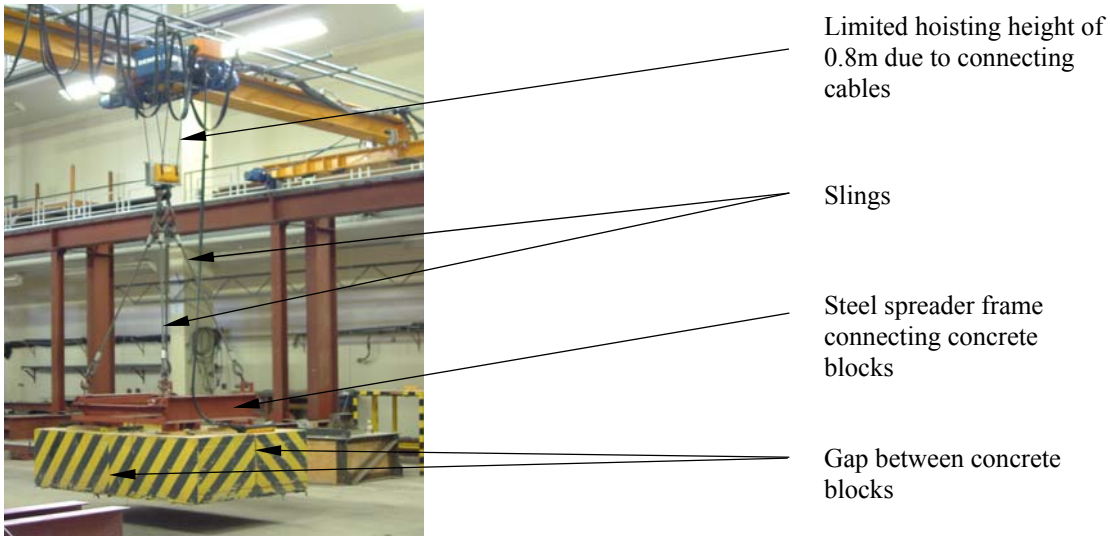

Figure 2.3.2.1 Original payload configuration with limited vertical travel distance

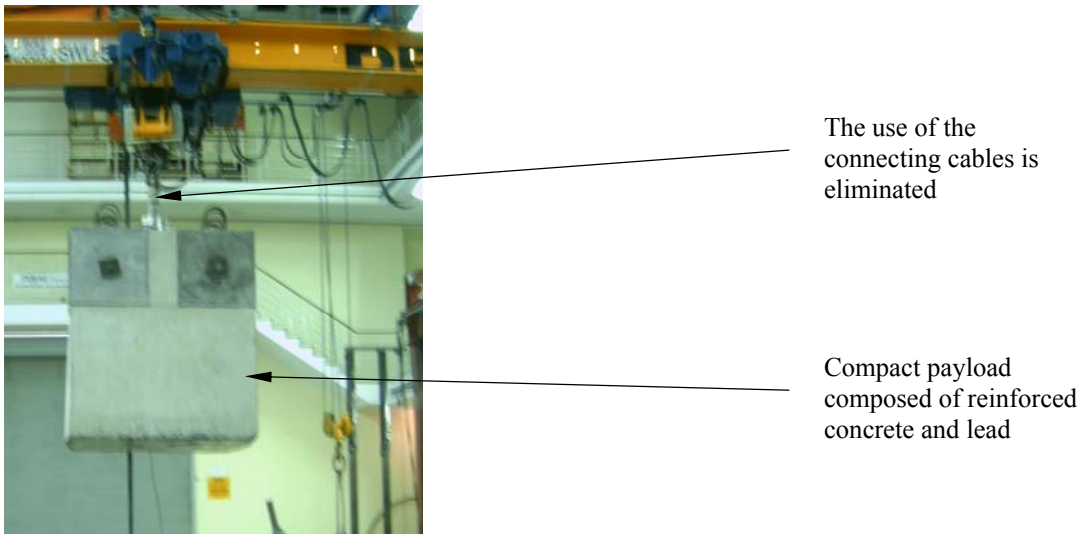

Figure 2.3.2.2 Compact (new) payload hoisted below crane bridge

2.3.3 Codified End Buffer Impact Forces

Kohlhaas [1.7], calculated the end buffer impact forces using the various codes of practice for an impact speed of 0.55m/s as presented in Table 2.3.3.1. It is evident that there is a large discrepancy between the end buffer impact forces as determined by the different codes of practice due to the different analysis philosophies used. Kohlhaas [1.7], shows that the European code, EN 1991-3: 2003 predicts much larger impact forces than the other codes of practice.

Table 2.3.3.1 End buffer impact forces obtained for the various codes for an impact speed of 0.55m/s

Code of Practice	**Velocity (m/s)**	**Estimated Impact Force (kN)**
South African Bureau of Standard *SABS 0160 – 1989* Method (a) Method (b) **Use lesser of the two**	 Not applicable 0.55	 21.9 12.0 Therefore **F = 12.0**
European Code *EN 1991-3: 2003* *(Proposed SANS 10160)*	0.7 x 0.55 = 0.42	**F = 22.7**
Australian Code of Practice *AS 1418.18 – 2001*	0.55	**F = 7.5**
Australian Code of Practice *AS 1418.1 – 1994*	0.55	**F = 7.4**

2.3.4 Scrutiny of the Experimental End Buffer Impact Test Responses

Kohlhaas [1.7], conducted a series of 5 different impact test experiments by including the payload and by varying the position of the payload during the collision. These tests were repeated by horizontally longitudinally misaligning the LHS buffer by 20mm. The results obtained revealed some interesting phenomena. Figure 2.3.4.1 shows the end buffer impact force vs. time response when the crane collides into the end stops without the payload attached. Interestingly, the 1st peak is followed by 2 consecutive peaks which occur approximately 1.0s and 1.8s after the 1st peak. The additional peaks are due to the step down torque in the drive motors for the longitudinal motion of

the crane after the operator releases the acceleration button. The torque present in the drive motors for the longitudinal motion of the cranes after the 1st impact is sufficient to drive the crane back into the end stops for a second and even a third time. The crane manufacturer did not provide information on the magnitude of the residual torque in the drive motors for the longitudinal motion of the crane.

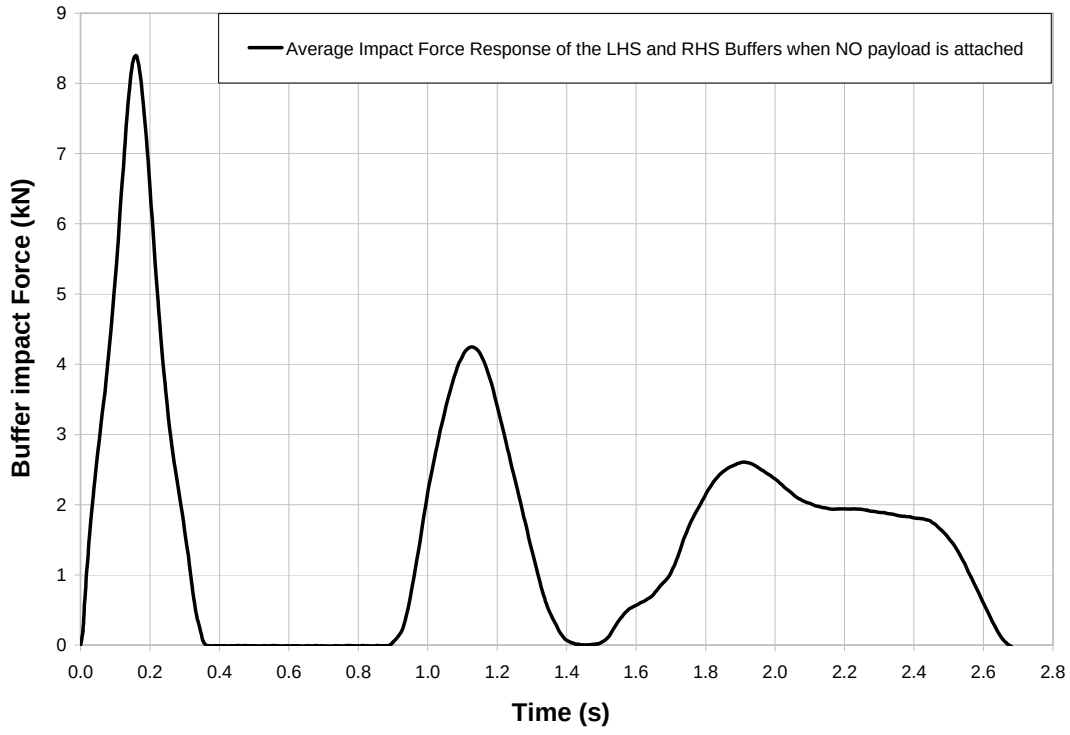

Figure 2.3.4.1 Shows the average end buffer impact force vs. time response when the crane collides into the end stops without the payload attached

On average, the end buffer impact force increases by 34%, from 8.41kN to 11.26kN for the crane without payload compared to the crane with payload. When the load is eccentric and one end stop is misaligned by 20mm, the impact force increases by 94%, from 8.41kN to 16.31kN.

Kohlhaas' [1.7], investigation highlighted that the payload, position of the payload, offset of the end stops and the step down torque on the drive motors for the longitudinal motion of the crane has a significant effect on the end buffer impact response when the crane collides into the end stops.

2.4 DEMAG, The Manufacturer's Assessment of the Buffer Impact Forces

The estimation of the end buffer impact force as determined by the manufacturer, DEMAG [2.1], is based upon the German code of practice, DIN 15018. The code specifies that only rigidly connected masses should be considered when determining the end buffer impact force. Thus, the mass of the payload should be ignored when determining the estimated end buffer impact force on the end stops if the mass is not rigidly connected to the crane bridge. The manufacturer assumes that the crane supporting structure is sufficiently braced to prevent any significant horizontal longitudinal deflections of the crane supporting structure during the collision between the crane and the end stops. Thus only the end buffers, which can deform significantly during impact, are considered to be flexible.

The manufacturer uses the end buffer's resilience, the mass of the rigid elements of the crane, the impact velocity and the relevant Energy vs. Deformation and Deformation vs. Impact Force graphs to determine the estimated buffer forces. The absorbed energy at the moment of impact is determined using the manufacturer's revised kinetic energy formula,

$$E_{PU} = \frac{m_{PU} \times v^2}{9965} \tag{2.4.1}$$

where,

E_{PU} = Absorbed energy at the moment of impact in Nm

m_{PU} = Mass of the rigid elements of the crane in kg

v = Impact velocity in metres per minute at the moment of impact

9965 = Constant

When converting metres per minute to metres per second in equation 2.4.1, the value of the denominator should be 7200.

The method proposed by the manufacturer comprises of determining the absorbed energy (E_{PU}) as specified by equation 2.4.1. The end buffer's deformation can then be read from Figure 2.4.1, "Energy (E_{PU}) vs. Flexibility Ranges" using the absorbed energy and the relevant impact speed of the crane. Finally, the estimated impact force can be read from Figure 2.4.1, "Flexibility Ranges vs. Buffer Final Forces (F_{PU})" using the deformation of the end buffer and the relevant impact speed of the crane.

Table 2.4.1 presents the estimated maximum end buffer impact forces for the crane with the relevant criteria used in the experimental tests, for varying impact speeds according the DEMAG's

assessment.

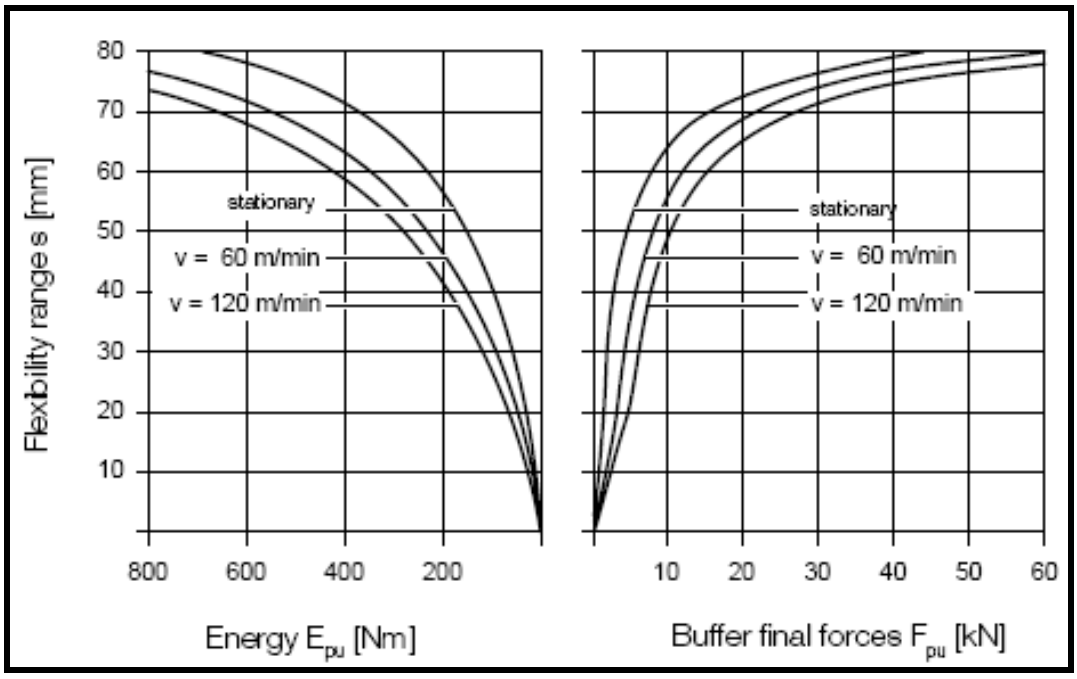

Figure 2.4.1 "Energy vs. Flexibility Ranges" and "Flexibility Ranges vs. Buffer Final Force" graphs of the DPZ 100 buffer

Table 2.4.1 Maximum end buffer impact forces for various impacts speeds according to DEMAG's assessment using a DPZ 100 cellular plastic buffer

Longitudinal crane velocity **[v]** (m/sec)	Mass of the crane excluding payload **[m_{PU}]** (kg)	Absorbed energy **[E_{PU}]** (Nm)	Flexibility range {Buffer deformation} **[δ]** (mm)	Estimated buffer impact force per manufacturer's assessment **[F_{PU}]** (kN)
0.30	2233	73	31.4	2.4
0.50	2233	202	51.1	6.1
0.55	2233	244	56.3	8.1
0.60	2233	290	58.3	9.4
0.70	2233	395	65.5	15.0
0.80	2233	516	70.2	23.3
0.90	2233	653	73.3	27.6

Based upon the manufacturer's assessment of the buffer impact force, the DPZ 100 buffer will not be able to sustain impact speeds greater than 0.9 m/s, since the calculated absorbed energy exceeds the Energy vs. Flexibility graph of figure 2.4.1.

The manufacturer's assessment of the impact forces does not explicitly account for the contributions of the following factors at the moment of impact:

(i) Mass of the payload
(ii) Vertical position of the payload below the crane bridge
(iii) Horizontal longitudinal position of the hoist load relative to the crane bridge
(iv) Damping characteristics of the end buffers
(v) Resilience of the crane supporting structure
(vi) Dynamic effects
(vii) Longitudinal misalignment of the end stops or crane at the moment of impact
(viii) "Power-off" / "Power-on" (Torque present from the moment of impact)

2.5 Codified Estimations of the End Buffer Impact Forces

The impact forces need to be assessed for the design of the end stops on the gantry structure and the longitudinal bracing system on the crane supporting structure. The estimation of the end buffer impact forces as specified by the various codes of practice will be examined in detail in this section.

2.5.1 Estimation of the End Buffer Impact Forces According to:

SABS 0160-1989 (As Amended 1989), "South African Standard: *Code of Practice For: The General Procedure And Loadings To Be Applied In The Design Of Buildings*"

Clause 5.7.6 of SABS 0160: 1989, [2.2], provides two methods with different approaches to estimate the maximum end buffer impact force (horizontal longitudinal force) when the crane collides with the end stops. These two methods are presented and investigated in detail.

To obtain the estimated maximum end buffer impact forces clause 5.7.6 of SABS 0160-1989, states;

"Take the horizontal force imposed on each end stop by a crane in the direction of travel to be the ***lesser*** *of the following:*

(a) A force equal to the combined weight of the crane bridge (crane) and the crab;

(b) A force calculated on the assumption that the crane strikes the end stop while travelling at its full rated speed, taking into account the resilience of the end stops and crane buffers.

Note: In (a) and (b), the weight of the load carried by the crane may be ignored unless it is restrained in a horizontal direction as in a mast or claw crane"

To obtain the most severe buffer impact forces clause 5.7.7 states SABS 0160-1989;
"In determining the crane loads set out in clause 5.7.6, assume the magnitude of the load lifted by the crane (up to its rated capacity), the position of the crab on the crane bridge, and the position of the crane on the crane supporting structure, to be such as will produce the most adverse effect upon the building or part of the building being designed"

In method (a), the estimated end buffer impact force is determined by taking the product of the mass of the crane with the crab and gravity, i.e. estimated end buffer impact force = (mass of crane with crab) × 9.81m/s^2. Method (a) yields a constant impact force of 21.9kN for a crane mass of 2233kg. Method (a) of clause 5.7.6 of SABS 0160-1989, does not explicitly account for the contributions of the following factors at the moment of impact:

(i) The impact speed of the crane
(ii) Mass of the payload
(iii) Vertical position of the payload below the crane bridge
(iv) Horizontal longitudinal position of the hoist load with respect to the crane bridge
(v) Elastic characteristics of the crane buffers
(vi) Damping characteristics of the crane buffers
(vii) Resilience of the crane supporting structure
(viii) Dynamic effects
(ix) Longitudinal misalignment of the end stops or crane at the moment of impact
(x) "Power-off" / "Power-on" (Torque present from the moment of impact)

In method (b), the impact force is a function of the weight of the crane with the crab, the maximum impact speed, the resilience of the end stops and the resilience of the crane buffers. Since the crane supporting structure and the end stops are not expected to significantly displace longitudinally during impact, its resilience is assumed to be zero. Thus, it is assumed that only the crane's buffers is flexible and can deform significantly during impact.

The method proposed in method (b) of SABS 0160-1989 is the same as that specified for DEMAG's approach, except for the way the energy is determined. The absorbed energy is

determined using the conventional kinetic energy approach, where,

$$E_K = E_{PU} = \frac{m_{PU} \times v^2}{2}; \quad (2.5.1.1)$$

where,

E_K = Absorbed energy at the moment of impact in Nm

m_{PU} = Mass of the rigid elements of the crane in kg

v = Impact velocity in metres per second (m/s) at the moment of impact

If the impact velocity in equation 2.5.1.1 is converted to metres per minute, then equation 2.5.1.1 changes to;

$$E_K = E_{PU} = \frac{m_{PU} \times v^2}{7200}; \quad (2.5.1.2)$$

Equations 2.4.1 and 2.5.1.2 are identical; except that equation 2.4.1 uses a magnitude of 9965 as the denominator. The greater the denominator the smaller the absorbed energy, which results in a reduced end buffer impact force. Thus DEMAG's approach is un-conservative.

Table 2.5.1.1 presents the end buffer impact forces for the crane with the relevant criteria used in the experimental tests, for various impact speeds according to clause 5.7.6 (b) of SABS 0160-1989.

Table 2.5.1.1 Maximum end buffer impact forces for various impacts speeds based on clause 5.7.6, method (b) of SABS 0160-1989 using a DPZ 100 cellular plastic buffer

Longitudinal crane velocity **[v]** (m/sec)	Mass of the crane excluding payload **[m_{PU}]** (kg)	Absorbed energy **[E_{PU}]** (Nm)	Flexibility range {End buffer deformation} **[δ]** (mm)	Manufacturer's assessment of end buffer forces **[F_{PU}]** (kN)
0.30	2233	100	37.4	3.3
0.50	2233	279	59.4	9.1
0.55	2233	338	63.5	11.9
0.60	2233	402	66.6	15.0
0.70	2233	547	71.7	21.9
0.80	2233	715	76.6	37.3

Based upon SABS 0160-1989, method (b)'s assessment of the end buffer impact force, the DPZ 100 buffer will not be able to sustain impact speeds greater than 0.8m/s, since the calculated absorbed energy exceeds the Energy vs. Flexibility graph of figure 2.4.1.

Although the end buffer impact force varies as a function of the impact velocity, it does not explicitly account for the contributions of the following factors at the moment of impact:

(i) Vertical position of the payload below the crane bridge
(ii) Horizontal longitudinal position of the hoist load with respect to the crane bridge
(iii) Damping characteristics of the crane buffers
(iv) Dynamic effects
(xi) Longitudinal misalignment of the end stops or crane at the moment of impact
(xii) "Power-off" / "Power-on" (Torque present from the moment of impact)

Clause 5.7.6 of SABS 0160-1989 specifies that the impact force is the lesser of the values determined from methods (a) and (b). Thus the estimated maximum impact forces based on SABS 0160-1989, clause 5.7.6 is presented in Table 2.5.1.2,

Table 2.5.1.2 Estimated maximum end buffer impact forces at various velocities based on clause 5.7.6 of SABS 0160-1989 using a DPZ 100 cellular plastic buffer

Longitudinal crane velocity **[v]** (m/sec)	Mass of the crane excluding payload **[m_{PU}]** (kg)	Impact force as per SABS 0160-1989, clause 5.7.6, **Method (a)** **[F_{PU}]** (kN)	Impact force as per SABS 0160-1989, clause 5.7.6, **Method (b)** **[F_{PU}]** (kN)	Estimated maximum impact force as per SABS 0160-1989, clause 5.7.6, **[F_{PU}]** (kN)
0.30	2233	21.9	3.3	3.3
0.50	2233	21.9	9.1	9.1
0.55	2233	21.9	11.9	11.9
0.60	2233	21.9	15.0	15.0
0.70	2233	21.9	21.9	21.9
0.80	2233	21.9	37.3	21.9

Clause 5.7.6, method (a) of SABS 1060-1989 provides conservative results for low impact speeds. Clause 5.7.6, method (b) of SABS 1060-1989 provides reasonable estimates of the maximum impact forces at various speeds.

2.5.2 Estimation of the End Buffer Impact Forces According to the Proposed SANS 10160, Working document on SANS 10160, "South African National Standards 10160: *Basis Of Structural Design And Actions For Buildings And Industrial Structures, Section 10: Action Induced By Cranes and Machinery*"

The proposed SANS 10160, [2.3], section 10, clause 10.2.12.1 to determine the estimated end buffer impact force is adopted verbatim from the European code EN 1991-3:2003 [2.4]. Thus the force obtained from EN 1991-3:2003 applies for the proposed SANS 10160: Section 10, clause 10.2.12.1 as well.

2.5.3 Estimation of the End Buffer Impact Forces According to: EN 1991-3:2003, European Standard 1991-3: EUROCODE 1 – "*Actions On Structures, Part 3: Actions Induced By Cranes and Machinery*"

To obtain the estimated maximum end buffer impact force clause 2.11.1 of EN 1993-3:2003, states;

"(1) Where buffers are used, the forces on the crane supporting structure arising from collision with the buffers shall be calculated from the kinetic energy of all relevant parts of the crane moving at 0.7 to 1.0 times the nominal speed.

(2) The buffer forces multiplied by φ_7 according Table 2.10 of EN 1991-3:2003 to make allowance for the dynamic effects may be calculated taking into account the distribution of relevant masses and the buffer characteristics;

$$H_{B,1} = \varphi_7 \times v_1 \times \sqrt{m_c \times S_B},$$

where;

$H_{B,1}$ = *Horizontal Longitudinal Force due to Impact*

φ_7 = *Dynamic Factor obtained from Table 2.10 of EN 1991-3:2003*

v_1 = *is 70% of the Maximum Longitudinal Velocity (m/s)*

m_c = *is the mass of the crane and the hoist load (kg)*

S_B = *is the spring constant of the buffer (N/m)"*

Table 2.5.3.1 Dynamic factor φ_7

Table 2.10 of EN 1991-3: 2003	
$\varphi_7 = 1.25$	If $0.0 \leq \xi_b \leq 0.5$
$\varphi_7 = 1.25 + 0.7*(\xi_b - 0.5)$	If $0.5 \leq \xi_b \leq 1.0$

For the method presented by EN1991-3:2003, the impact force is a function of the weight of the crane including the crab and the payload, the maximum impact speed, the resilience of the end stops and the resilience of the crane buffers and a dynamic factor. As is the case with method (b) in 2.5.1, the gantries and the end stops are not expected to significantly displace longitudinally during impact, thus its resilience can be assumed to be zero. Thus, it is assumed that only the cranes' buffers are flexible and can deform significantly during impact.

The codes specify that where automatic speed retarding mechanisms are provided the impact speed can be reduced to 70% of the maximum longitudinal crane speed. At the moment of impact the maximum kinetic energy is determined by;

$$E_K = 0.5 \times m_C \times (0.7 \times v_1)^2 \qquad (2.5.3.1)$$

where,

m_C = Mass of the crane, crab and payload in kg

v_1 = Crane impact velocity in metres per second at the moment of impact

The mass of the crane, crab and payload, (m_C), and the maximum longitudinal velocity, (v_1), of the crane are known. The only unknown parameters are the end buffers' spring stiffness, S_B, and the dynamic factor, φ_7. The buffer's spring stiffness, S_B, is determined by dividing the estimated end buffer impact force f_{PU} with the buffer deformation using the appropriate graphs as supplied by the manufacturer. The method of determining the end buffer displacements and end buffer forces is the same as described in section 2.4. The dynamic factor φ_7 is obtained from Table 2.5.3.1 to account for the end buffer type which is presented in Table 2.5.3.2 for the various end buffer types.

Table 2.5.3.2 Dynamic factor φ7 based upon the buffer type

Buffer type	**Buffer Characteristic factor, ξ_b**	**Dynamic factor φ_7**
Hydraulic	1.00	1.60
Elastic spring	0.50	1.25
Cellular elastic	0.25	1.25

The estimated maximum end buffer impact forces based on clause 2.11 of EN 1991-3: 2003, are presented in Table 2.5.3.3.

Table 2.5.3.3 Estimated maximum end buffer impact forces at various velocities based on clause 2.11 of EN 1991-3: 2003 using a DPZ 100 cellular plastic buffer

Longitu-dinal crane velocity **[v]** (m/sec)	Mass of the crane including payload **[m_{PU}]** (kg)	Absor-bed energy **[E_{PU}]** (Nm)	Flexibility range {End buffer defor-mation} **[δ]** (mm)	Estimated end buffer impact force **[F_{PU}]** (kN)	Buffer spring constant **[S_B]** (kN/m)	Dyna-mic factor **[φ_7]**	Estimated final maximum end buffer impact force as per EN 1991-3: 2003, **[F_{PU}]** (kN)
0.30	7361	162	49.0	4.9	100	1.25	7.1
0.50	7361	451	71.2	19.5	274	1.25	19.6
0.55	7361	546	73.3	24.7	337	1.25	23.9
0.60	7361	649	76.5	34.1	446	1.25	30.1

Based on clause 2.11 of EN 1991-3: 2003's assessment of the end buffer impact force, the DPZ 100 buffer will not be able to sustain impact speeds greater than 0.6m/s, since the calculated absorbed energy exceeds the Energy vs. Flexibility graph of figure 2.4.1.

The impact forces obtained from EN 1991-3: 2003 are conservative relative to other codes. The reason for the extremely conservative impact forces is due to the use of the total mass of the crane

with payload which is used to calculate the impact energy and leads to greater end buffer displacements and end buffer impact forces.

Although the impact force varies as a function of the impact velocity, it does not explicitly account for the contributions of the following factors at the moment of impact:

(i) Vertical position of the payload below the crane bridge

(ii) Horizontal longitudinal position of the hoist load with respect to the crane bridge

(iii) Damping characteristics of the crane buffers

(xiii) Longitudinal misalignment of the end stops or crane at the moment of impact

(iv) "Power-off" / "Power-on" (Torque present from the moment of impact)

2.5.4 Estimation of the End Buffer Impact Forces According to: AS 1418.18:2001, Australian Standard, "*Cranes (Including Hoists and Winches), Part 18: Crane Runways and Monorails*", Appendix B

To obtain the estimated maximum end buffer impact force Appendix D of AS 1418.18: 2001 [2.5], states;

"Forces on end buffer stops shall be determined as specified in AS 1418.1. In the absence of the vendor's information on buffer characteristics, the buffer force shall be determined from;
$P_b = C_b \times$ *(sum of all wheel reactions for a crane without lifted load) where the coefficient* C_b *is given in Table B4 of AS 1418.18.*

The stopping distance depends on the buffer type. It shall not be less than 50mm and not more than 300mm. The buffer force so determined shall be used for the design of each buffer and the supporting structure.

Table 2.5.4.1 Coefficient C_b used to determine the buffer force

Table B4 of AS 1418.18: Coefficient C_b used to determine the buffer force			
Longitudinal travel velocity (m/s)	*Stopping Distance (m)*		
	≤ 0.10	*0.20*	*≥ 0.30*
0.50	*0.26*	*0.13*	*0.08*
1.00	*1.02*	*0.51*	*0.34*
1.50	*2.29*	*1.15*	*0.74*

The buffer impact force presented by Appendix B of 1418.14, is a function of the vertical wheel loads excluding the hoistload, the longitudinal crane speed and the stopping distance of the crane during impact. This method is used when the buffer characteristics are unknown and should be used to assess the initial buffer forces in the preliminary design. The buffer impact force is obtained from the product of the vertical wheel loads, excluding the hoistload and the coefficient C_b; i.e. $P_b = C_b \times$ vertical wheel loads. The impact force varies due to the coefficient C_b, which is a function of the travel speed and the stopping distance.

The maximum end impact forces based on Appendix B of AS 1418.14, are presented in Table 2.5.4.2. The magnitudes of the Coefficient, C_b, used in Table 2.5.4.2 were interpolated from Table 2.5.4.1 using a stopping distance of less than 100mm with the various longitudinal crane velocities.

Table 2.5.4.2 Estimated maximum end buffer impact forces at various speeds based on Appendix B of AS 1418.14

Longitudinal crane velocity (m/s)	Stopping distance (m)	Σ of Vertical wheels loads (Excluding hoistload) (kN)	Coefficient C_b	Estimated end buffer impact forces based on Appendix B of AS 1418.18, (kN)
0.50	≤ 0.10	21.97	0.26	5.7
0.55	≤ 0.10	21.97	0.31	6.8
0.60	≤ 0.10	21.97	0.37	8.1
0.70	≤ 0.10	21.97	0.50	10.9
0.80	≤ 0.10	21.97	0.65	14.3
0.90	≤ 0.10	21.97	0.83	18.2
1.00	≤ 0.10	21.97	1.02	22.4
1.50	≤ 0.10	21.97	2.29	50.3

The crude method yields plausible results even though it does not explicitly account for the contributions of the following factors at the moment of impact:

(i) Mass of the payload

(ii) Vertical position of the payload below the crane bridge

(iii) Horizontal longitudinal position of the hoist load with respect to the crane bridge

(iv) Dynamic effects

(v) Longitudinal misalignment of the end stops or crane at the moment of impact

(vi) "Power-off" / "Power-on" (Torque present from the moment of impact)

2.5.5 Estimation of the End Buffer Impact Forces According to: AS 1418.1: 1994, "Standards Australia AS 1418.1 -1994: *Cranes (Including Hoists and Winches), Part 1: General Requirements*"

Extracts from clause 4.7.5 of AS 1418.1: 1994, [2.6], pertaining to the estimation of the maximum end buffer impact force for a single running crane state,

"It is assumed that in normal operation, cranes or crabs only rarely collide with each other or with buffer stops. The impact force (P_B), due to cranes or crabs running against stops or against each other shall be absorbed by buffers or similar energy-absorbing means.

The total buffer capacities required and the maximum buffer force (P_B) shall be determined for the longitudinal travel at 85% of full travel velocity and for transverse at 100%. Where automatic retarding means are provided, the maximum buffer force (P_B) shall be determined for cranes and crabs at not less than 70% of full travel velocity.

The total energy (E) is to be absorbed by all buffers engaged in the collision, with each taking its share in proportion to its rigidity.

Where a crane of mass m and having a velocity V collides with an end stop, the kinetic energy released on collision shall be calculated by the following equation;

$$E = 0.5 \times m \times V^2$$

Loads suspended from hoisting equipment and freely swinging loads need not be taken into account.

The resulting forces as well as the horizontal inertia forces in balance with the buffer forces shall be multiplied by a factor (ϕ_6) to account for elastic effects which cannot be evaluated using a rigid body analysis. Factor ϕ_6 shall be taken as 1.25 in the case of buffers with linear characteristics (e.g. springs) and 1.60 in the case of buffers with rectangular characteristics (e.g. hydraulic constant force buffers). For buffers with other characteristics, other values justified by calculation or test shall be used as detailed below;

$\phi_6 = 1.25$ *for* $0.0 \leq \xi \leq 0.5$

$\phi_6 = 1.25 + 0.7\ x\ (\xi - 0.5)$ *for* $0.5 \leq \xi \leq 1.0$

where;

ξ *is defined in the same manner as per EN 1991:3-2003, Table 2.5.3.2.*

The method presented by clause 4.7.5 of AS 1418.1, is the same as for method (b) in SABS 0160-1989, clause 5.7.6, except for the reduction in the maximum impact velocity. Assuming that the supporting structure has automatic retarding devices and cellular plastic buffers are used, the estimated maximum end buffer impact forces are presented in Table 2.5.5.1.

Table 2.5.5.1 Estimated maximum end buffer impact forces at various speeds based on clause 4.7.5 of AS 1418.1 using a DPZ 100 cellular plastic buffer

Longitudinal crane velocity **[v]** (m/sec)	Mass of the crane excluding payload **[m]** (kg)	Absorbed energy **[E]** (Nm)	Flexibility range {End buffer deformation} **[δ]** (mm)	Dynamic factor **[ϕ_6]**	Estimated maximum end buffer impact force as per AS 1418.1, clause 4.7.5 **[F_{PU}]** (kN)
0.3	2233	49	26.8	1.25	3.5
0.50	2233	137	42.3	1.25	5.1
0.55	2233	165	45.9	1.25	6.1
0.60	2233	197	48.5	1.25	7.6
0.70	2233	268	57.2	1.25	11.7
0.80	2233	350	61.4	1.25	13.9
0.90	2233	443	67.1	1.25	20.3
1.00	2233	547	70.7	1.25	27.8

Based on clause 4.7.5 of AS 1418.1's assessment of the end buffer impact force, the DPZ 100 buffer is capable of withstanding an initial impact speed of just above 1.0m/s

Although the impact force varies as a function of the impact velocity, it does not explicitly account for the contributions of the following factors at the moment of impact:

(i) Mass of the payload

(ii) Vertical position of the payload below the crane bridge

(iii) Horizontal longitudinal position of the hoist load with respect to the crane bridge

(iv) Damping characteristics of the crane buffers

(v) Dynamic effects

(vii) Longitudinal misalignment of the end stops or crane at the moment of impact

(vi) "Power-off" / "Power-on" (Torque present from the moment of impact)

2.5.6 Estimation of the End Buffer Impact Forces According to: AISE Technical Report 6, October 2000, "*Specification for Electric Overhead Travelling Cranes for Steel Mill Service*"

To obtain the estimated maximum end buffer impact force clause 3.8 of AISE Technical Report No. 6 of 2000, [2.7], states;

"Provision in the design of the runway and the design of the runway stops shall consider the energy absorbing or storage device used in the crane bumper. The device may be nonlinear (e.g. hydraulic bumpers) or a linear device such as a coil spring.

The maximum deceleration rate for both bridge and trolley shall not exceed 16 fps^2 at 50% of the full load rated speed (full load rated speed shall be used unless adequate information is supplied by owner to determine the actual maximum attainable speed). Additionally, bumpers shall be capable of absorbing the total energy at 100% full load rated speed. See the sample problem calculations for hydraulic and spring bumpers.

Between cranes or trolleys (if two trolleys are located on one bridge) bumpers shall be capable of absorbing the energy from 70% of full rated speed of both cranes or trolleys traveling in opposite directions, or the energy from 100% of full load rated speed of either crane or trolley, whichever is the greatest.

The design of all bumpers shall include safety cables to prevent parts from dropping to the floor.

The height of bumpers above the top of the rail shall be as specified on the OIS or as determined by the crane builder.

For computing bridge bumper energy, the trolley shall be placed in the end approach which will produce the maximum end reaction from both the bridge and trolley. This end reaction shall be

used as the maximum weight portion of the crane that can act on each bridge bumper. The energy absorbing capacity of the bumper shall be based on power-off and shall not include the lifted load if free to swing. Bridge bumpers shall have a contact surface of not less than 5inches in diameter, be located on the rail centerline and mounted to provide proper clearance when bumpers of two cranes come together and both are fully compressed. Where practical, they shall be mounted to provide for easy removal of bridge track wheels.
Note: The building and end stops shall be designed to withstand those forces of the fully load crane at 100% rated speed (power off). The recommended increase in allowable stresses for this case is 50%. Please refer to AISE technical Report No. 13.

It should be noted that these forces may be reduced by increasing bumper stroke. In the example, increasing the bumper stroke(s) from 4.19 inches to 10 inches reduces end forces (F_A) from 69 kips to 28.5 kips".

For the method presented by AISE Technical report No. 13, the impact force is a function of the weight of the crane and the position and weight of the crab, the full rated impact speed of the crane, the specified maximum allowable deceleration of the crane at 0.5g = 4.905m/s^2, the efficiency of the end buffers and the buffer deformation during impact.

Table 2.5.6.1 presents the estimated maximum impact forces for the crane with the relevant criteria used in the experimental tests, for various impact speeds. The end buffer impact forces were determined using the commentary clause 7.6.3.

Table 2.5.6.1 Estimated maximum end buffer impact forces at various speeds based on AISE, Technical Report No.13 using a DPZ 100 cellular plastic buffer

Longi-tudinal crane velocity **[v]** (m/sec)	Weight of the crane and crab transferred to one end stop **[W_E]** (kN)	Kinetic energy at 100% of full load rated speed **[K_E]** (Nm)	Kinetic energy at 50% of full load rated speed **[K_H]** (Nm)	Maximum allowable end buffer force to decelerate crane at 0.5g **[F_A]** (kN)	End buffer defor-mation using 0.5g **[S]** (mm)	Effi-ciency of the end buffer **η**	Revised maximum allowable end buffer force when limiting **S** to 0.07m **[$F_{A\ Revised}$]** (kN)
0.30	10.9	0.49	0.12	5.5	34.6	0.65	2.8
0.50	10.9	1.30	0.34	5.5	96.2	0.65	7.5
0.55	10.9	1.66	0.41	5.5	116.3	0.65	9.1
0.60	10.9	1.97	0.49	5.5	138.5	0.65	10.8
0.70	10.9	2.68	0.67	5.5	188.5	0.65	14.8
0.80	10.9	3.56	0.88	5.5	246.2	0.65	19.3
0.90	10.9	4.44	1.11	5.5	311.5	0.65	24.4
1.00	10.9	5.48	1.37	5.5	380.5	0.65	30.1

The method proposed by AISE Technical Report No. 13, June 1997, does not explicitly account for the contributions of the following factors at the moment of impact:

(i) Vertical position of the payload below the crane bridge

(ii) Horizontal longitudinal position of the hoist load with respect to the crane bridge

(iii) Damping characteristics of the crane buffers

(iv) Dynamic effects

(v) Longitudinal misalignment of the end stops or crane at the moment of impact

(vi) “Power-off” / “Power-on” (Torque present from the moment of impact)

2.6. Summary of the Estimated End Buffer Impact Forces and the Criteria Used to Determine the End Buffer Impact Forces

The summary of the criteria used by the various codes and guidelines is presented in Table 2.6.1 for comparison.

Table 2.6.1 Summary of the criteria used to determine the end buffer impact forces specified by the various codes and guidelines

Code / Guideline	Impact speed	Impact speed reduction factor	Crane and crab mass	Payload mass	Dynamic factor to account for dynamic effects	Vertical position of the payload during impact	Horizontal position of the payload during impact	Damping characteristics (Energy absorption of end buffers)	Longitudinal misalignment of the end stops	Power off (Minimum load during impact)	Power on (Maximum load during impact)
SABS 0160- 1989 Method (a) & Method (b)	× √	× ×	√ √	× ×	× ×	× ×	× ×	× √	× ×	√ √	× ×
DEMAG	√	×	√	×	×	×	×	√	×	√	×
EN 1991:3 & SANS 10160	√	√	√	√	√	×	×	√	×	√	×
AS 1418.18 : 2001	√	×	√	×	×	×	×	√	×	√	×
AS 1418.1 : 1994	√	√	√	×	×	×	×	√	×	√	×
AISE No. 13: 1997	√	×	√	×	×	×	×	√	×	√	×

A summary of the estimated end buffer impact forces as obtained from the various codes and guidelines is presented in Table 2.6.2. All the calculations were performed based on the experimental 5-ton EOHTC in the Department of Civil Engineering at Stellenbosch University.

Table 2.6.2 Summary of the end buffer impact forces obtained at various speeds based upon the various codes and guidelines using a DPZ 100 cellular plastic buffer

Code / Guideline	**Estimated end buffer impact forces as a function of impact speed**							
	Impact Speed (m/s)							
	0.3	0.5	0.55	0.6	0.7	0.8	0.9	1.0
DEMAG	2.4	6.1	8.1	9.4	15.0	23.3	27.6	-
SABS 0160- 1989								
Method (a) &	21.0	21.9	21.9	21.9	21.9	21.9	21.9	21.9
Method (b)	3.3	9.1	11.9	15.0	21.9	37.3	-	-
Lesser of (a) & (b)	3.3	9.1	11.9	15.0	21.9	21.9	21.9	21.9
EN 1991:3 & SANS 10160	7.1	19.6	23.9	30.1	-	-	-	-
AS 1418.18 : 2001	5.7	6.8	8.1	10.9	14.3	18.2	22.4	50.3
AS 1418.1 : 1994	3.5	5.1	6.1	7.6	11.7	13.9	20.3	27.8
AISE No. 13: 1997	2.8	7.5	9.1	10.8	14.8	19.3	24.4	30.1

Figure 2.6.1 shows the graphical summary of the end buffer impact forces obtained at various speeds based upon the various codes and guidelines.

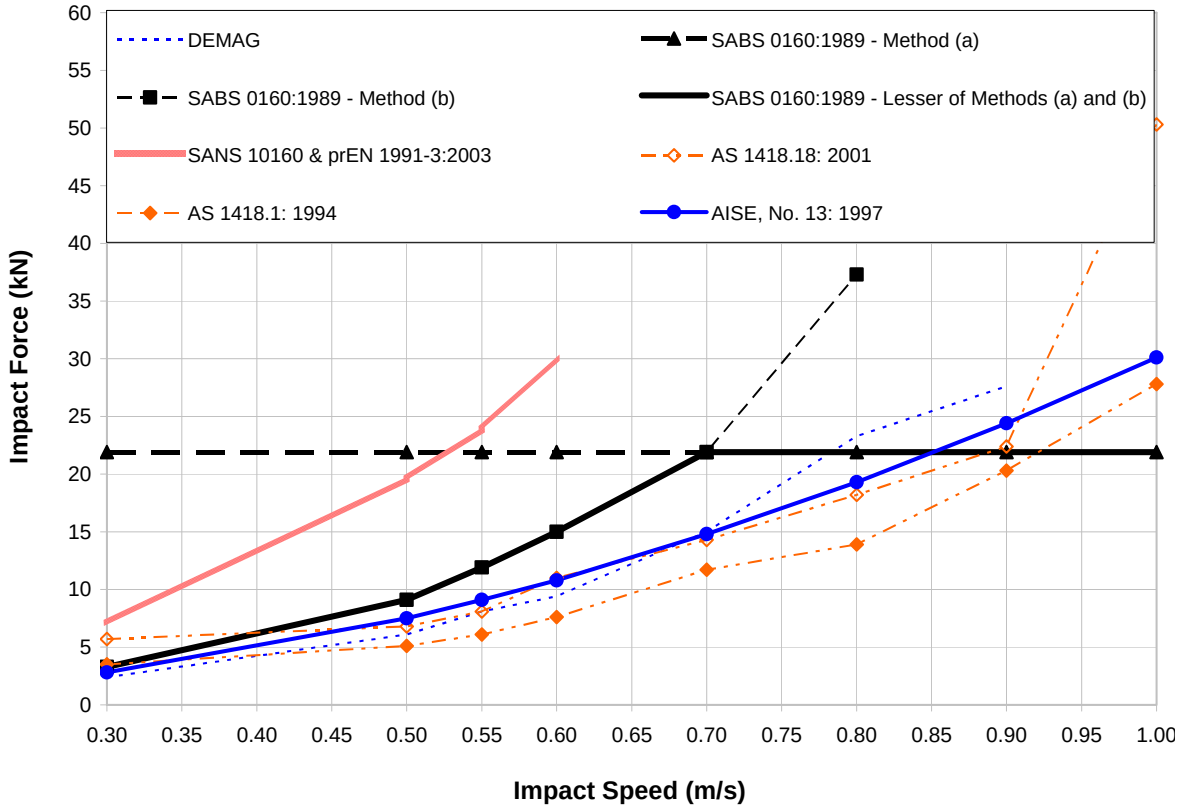

Figure 2.6.1 Graphical representation of the end buffer impact forces as a function of the impact velocity based upon the various codes and guidelines using a DPZ 100 cellular plastic buffer

2.7 Other Related Crane Studies

Various authors have investigated actions induced by cranes onto the supporting structure mainly through theoretical work.

Lobov [2.8 to 2.12], published several refereed journal articles on the actions induced by cranes on the crane supporting structures, based on analytical methodologies. A selection of his published work is reviewed below.

Lobov [2.8] analytically investigated the dynamic effects of an electric overhead traveling crane during its movement. The author proposes formulae to determine the horizontal lateral dynamic load when the crab transverses on the crane bridge.

Lobov [2.9] analytically investigated the additional loads applied to the crane rails as a result of the transverse and rotatory motion of the crane bridge and end carriages. The author proposes formulae for the calculation of the above loads.

Lobov [2.10] analytically investigated how skewing of the crane occurs and the resulting horizontal lateral forces imposed by the wheels onto the crane rails. The author proposes formulae for determining the horizontal lateral wheel forces under various conditions.

Lobov [2.11] analytically investigated whether a crane can travel in a straight line with a constant skew angle of the crane. The author proposes formulae for determining the horizontal lateral wheel forces under various conditions.

Karmakar [2.12] et al, investigated the dynamics of electric overhead travelling cranes using the bond method to simulate the hoisting of the load, braking of the crane as the load is lowered and crane motion of three different type of rail joints. The authors conclude that the bond graph method is suitable for simulating crane dynamics due to its efficiency, ease of modifications during the design phase and can include effects such as the motor hoisting the payload.

Grigor'ev [2.13] et al, investigated the effect which tapered wheels have on the rotational stability of overhead travelling cranes. The authors show that driven tapered wheels assists in the self alignment of the crane when skewing occurs.

2.8 Problem Definition

2.8.1 Review of Current Practice

The various codes provide a guideline to estimate the maximum end buffer impact force when the crane collides with the end stops. Figure 2.6.1 graphically shows the disparity between the various codes of practice estimations of the end buffer impact forces. This leads to the conclusion that the codified estimations of the end buffer impact force is not properly understood.

Also, the literature review has revealed that the estimation of the end buffer impact forces is not entirely based on scientific justification. This is due to the assumptions made by the code specifications and guidelines which subjectively prescribe load multipliers and omit certain critical

criteria which have a substantial influence on the end buffer impact forces. During this investigation no scientific justification was found for the load multipliers used in the code specifications and guidelines which creates uncertainty for the designer. The codes also implicitly assume that the crane and the crane supporting structure act as a decoupled system. Thus, the combination of the load multipliers and the omission of the critical parameters could lead to severe underestimation of the real (actual) end buffer impact forces, when considering the system as decoupled. The critical parameters which are omitted from virtually all code specifications and guidelines are:

(i) The mass of the payload and its vertical and horizontal positions at the moment of impact
(ii) The dynamic effects of the end buffers
(iii) The longitudinal misalignment of one of the end stops
(iv) The effect of the "power-on" condition during impact

2.8.2 Aims of the Research Project

As described in Chapter 1, this investigation forms part of a comprehensive study of the EOHTC Project at the Institute of Structural Steel's Centre for Development of Steel Structures. The overall goal of the EOHTC project is to provide guidelines for the design of crane support structures. Several research projects have already been investigated by various students to gain a better understanding into the behaviour of the EOHTC.

This research project will contribute to the understanding of how forces are imposed by the crane on the crane supporting structure, complementing the goals of the overall project. The aims of the research project are;

(i) Identify the physical parameters which have an effect on the impact force response.
(ii) Develop a set of criteria which the designer should include in the FEA model to accurately simulate the end buffer response when the crane collides into the end stops.
(iii) Develop a computationally efficient FEA model of the experimental 5-ton electric overhead travelling crane including the crane supporting structure, which will be used to investigate various load models.
(iv) Using the FEA model, conduct simulations on the various parameters to determine the maximum end buffer impact force when the crane collides with the end stops. This will be performed by analyzing one parameter at a time, where after the maximum impact

force will be obtained from a constraint optimisation using the Lagrange multiplier method.

Hence, the research work will provide the background for future code specifications.

2.8.3 Methodology of the Research Project

The research will be conducted through a series of experimental tests, finite element analysis simulations and analytical computations to estimate the end buffer impact forces.

A series of experimental tests under set conditions were performed by De Lange [1.6], to determine the impact response of the end buffers during the collision between the crane and the end stops. The critical information which was extracted from these experimental tests are; the force vs. time and the deformation vs. time responses of the end buffers and the velocity vs. time responses of the crane. The experimental tests were performed on a full scale testing facility in the Structural Engineering Laboratory of the Civil Engineering Department at the University of Stellenbosch.

A finite element analysis model of the full scale testing facility was modelled to simulate the experimental tests under the set conditions. The various modelling techniques used to create a computationally efficient model are described in detail in chapter 3. The FEA model was calibrated to the basic experimental tests performed under set conditions. Upon calibration of the FEA model, more extensive FEA simulations were performed by adjusting the parameters in a sensitivity study. The parameters which should be investigated to provide realistic end buffer impact forces are;

(i) The impact speed of the crane at the moment of impact
(ii) The vertical position of the payload at the moment of impact
(iii) The horizontal position of the payload at the moment of impact
(iv) The type of end buffers used and their elastic and damping characteristics
(v) The longitudinal misalignment of one of the end buffers
(vi) The effect of the “power-on” condition during impact

These parameters can be easily adjusted in the FEA model which is difficult to replicate in the experimental configuration.

From the advanced FEA model simulations, a set of criteria will be developed which need to be accurately modelled and included in a FEA simulation to accurately predict realistic end buffer impact force responses under various conditions.

CHAPTER 3: FINITE ELEMENT ANALYSIS MODELLING

3.1 General Discussion

A finite element analysis (FEA) model of the experimental 5-ton electric overhead traveling crane (EOHTC) and of the crane supporting structure was created to determine its global response when subjected to various loading conditions. The purpose of the FEA model is to accurately predict the global behaviour of the 5-ton EOHTC and the crane supporting structure. Due to the complexity of the 5-ton EOHTC, the crane supporting structure and numerous members used in the experimental model shown in Figure 3.1, many simplifications were required to obtain a FEA model which is computationally efficient.

Figure 3.1 A view of the experimental model of the 5-ton electric overhead travelling crane and the crane supporting structure with its numerous components

This section explains the assumptions and simplifications introduced in the FEA model, and the implications thereof. The finite element analysis model was created in ABAQUS [3.1], a commercially available general-purpose FEA software.

3.2 Overview of the Crane and Crane Supporting Structure

An EOHTC is generally composed of the crane and the crane supporting structure as shown in Figures 3.2.1 and 3.2.2. The purpose of the crane is to hoist and move loads from one position to another in a factory environment. The purpose of the crane supporting structure is to allow the crane to transverse smoothly along the crane rails by providing a suitable supporting structure.

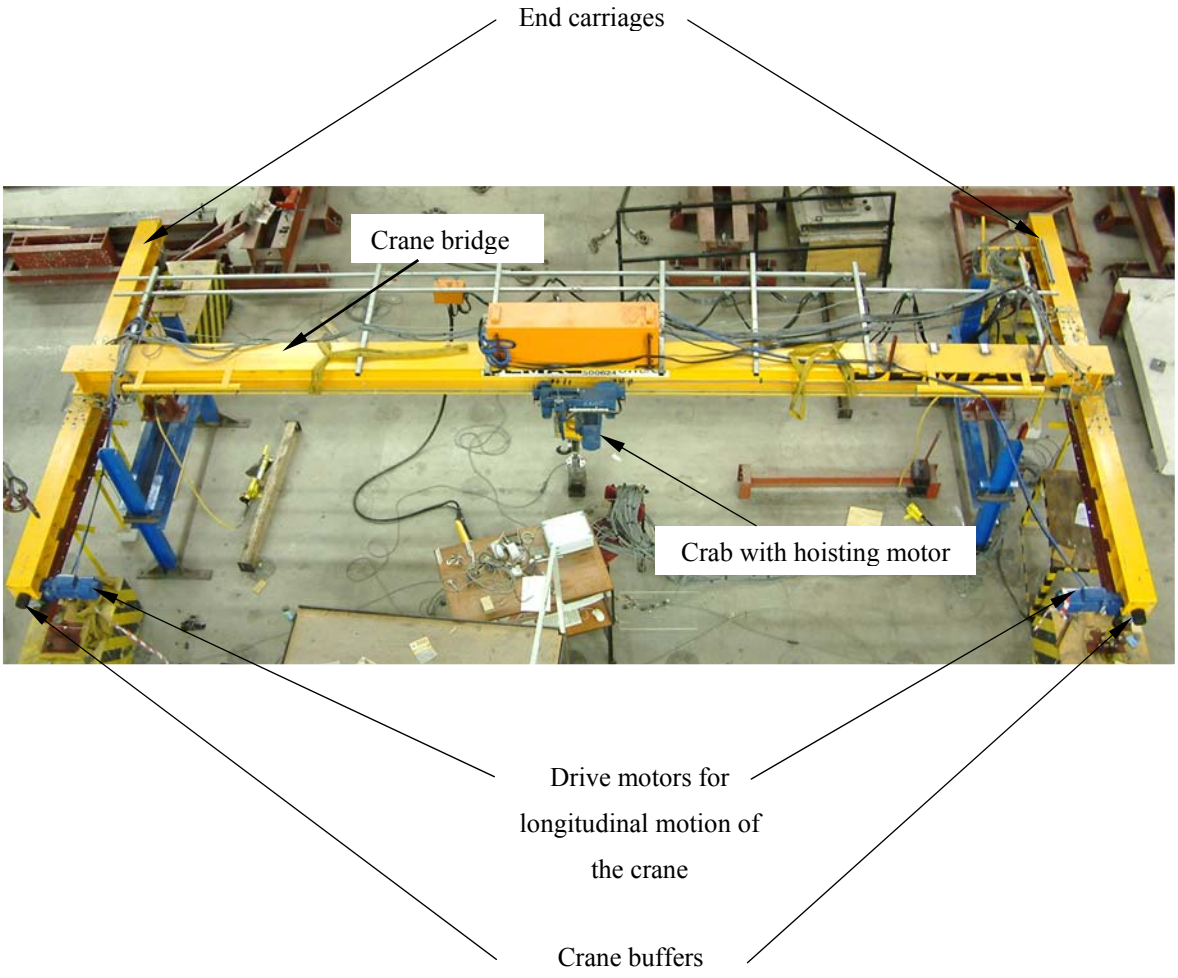

Figure 3.2.1 Picture of the crane identifying all the crane members

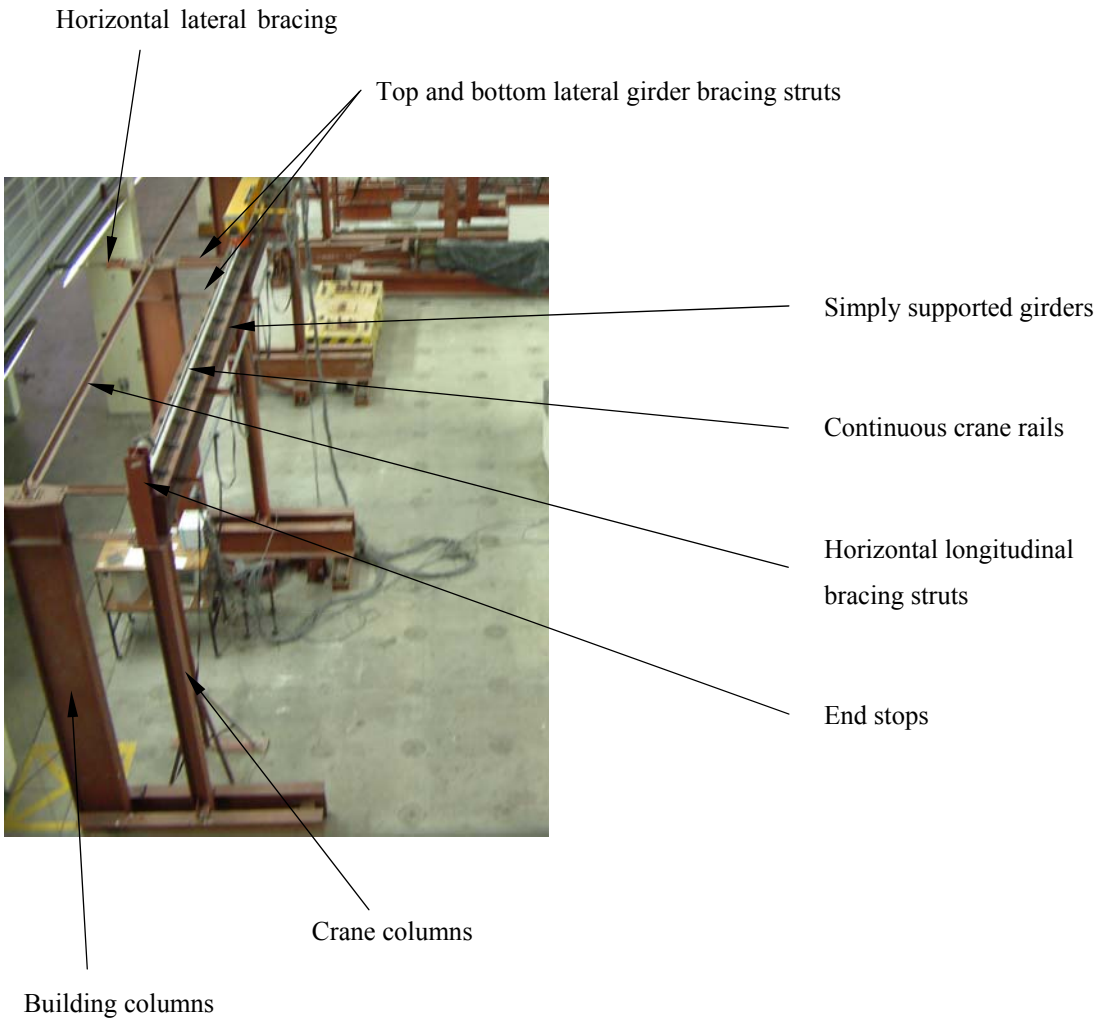

Figure 3.2.2 Picture of the crane supporting structure identifying all the members

3.2.1 Composition of the Crane

The crane usually consists of the following members as shown in Figure 3.2.1:

- Crane bridge
- End carriages
- Wheel blocks with wheels
- Drive motors for the longitudinal motion of the crane
- Crab with hoisting motor
- Crane buffers

Each of the crane members are described in detail in the later part of this chapter. Where the span between the crane supporting structure's supports is large or when the payload which must be hoisted is substantial the crane usually has a double crane bridge as shown in Figure 3.2.1.1. The crab with the hoisting motor is positioned between the crane bridges, which allows the crab to move transversely.

Figure 3.2.1.1 Crane with a double box girder crane bridge

3.2.2 Composition of the Crane Supporting Structure

The crane supporting structure usually consists of the following members as shown in Figure 3.2.2.1:

- Simply supported girders
- Continuous elastomeric pads between the crane rail and the top flange of the girder
- Continuous crane rails
- Crane columns, back columns and roof structure
- Horizontal lateral bracing system
- Horizontal longitudinal bracing system
- Top and bottom lateral girder bracing struts
- Horizontal longitudinal bracing struts
- End stops

Each of the crane supporting structure's members are described in detail in the later part of this chapter.

3.2.3 Purpose of Modelling the Crane Supporting Structure

The FEA end buffer impact simulations could have been conducted without modelling the crane supporting structure. The modelling of the crane supporting structure was included to determine the response of the crane and crane supporting structure as a coupled system. The crane and crane support structure was modelled as a entity to be able to investigate all relevant load models.

In future additional research work will be conducted when the crane supporting structure will be converted into a portal frame structure as shown in Figure 3.2.3.1.

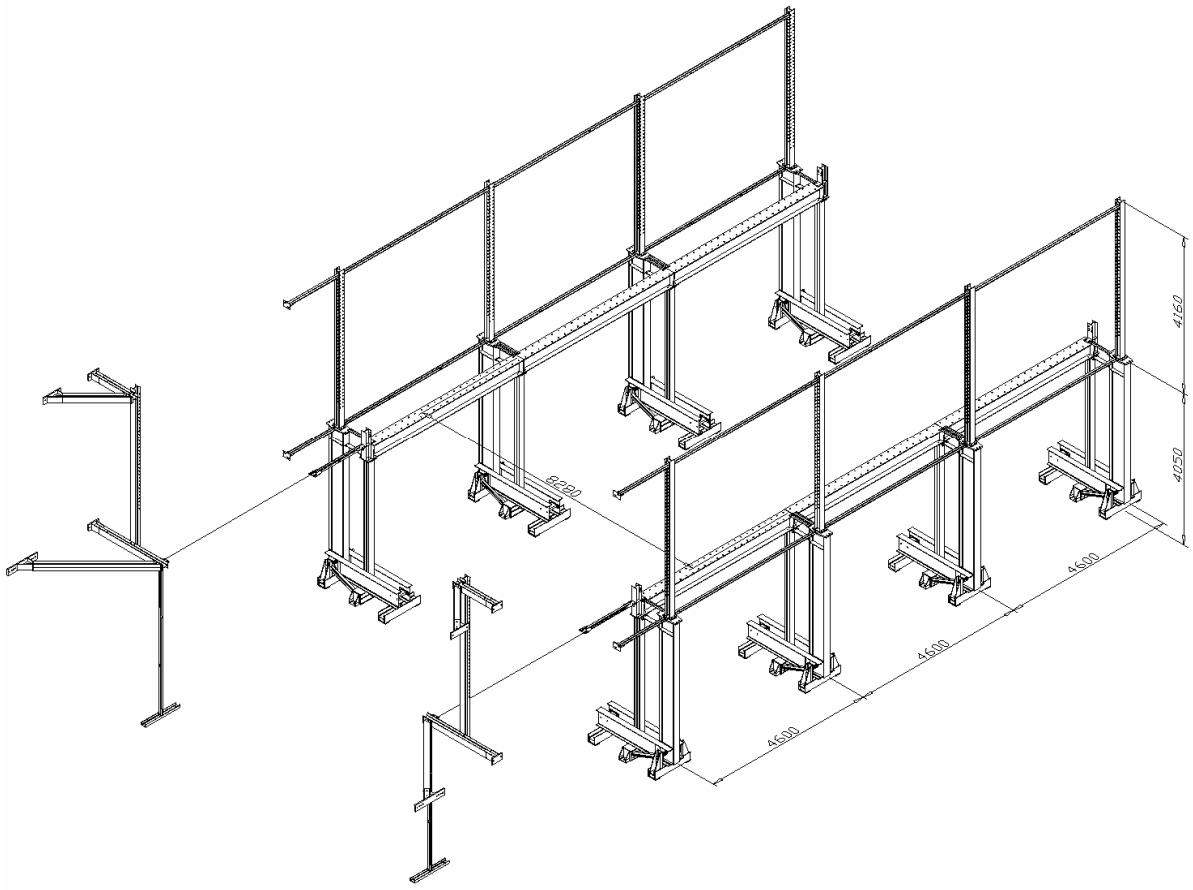

Figure 3.2.3.1 The crane supporting structure for future research work (Drawn by H. Barnard [1.2])

3.3 Crane Bridge

The crane bridge is composed of an $305 \times 305 \times 118$ H section, which is 8.485m long and oriented with its strong axis in the vertical direction as shown in Figure 3.3.1. The purpose of the crane bridge is to transfer the loads arising from the hoisted payload to the end carriages.

The purpose of the FEA model of the crane bridge is to accurately compute the global transverse displacements along the length of the beam. The crane bridge was modelled using beam elements. Brick (solid) or shells elements would yield a computationally inefficient model due to the large number of degrees of freedom (DOF).

The vertical and lateral displacements due to shear along the length of the beam could be significant depending on the slenderness ratio. It is imperative that the transverse displacement due to shear be accounted for to accurately compute the transverse displacement along the length of the crane bridge. This is achieved using three node shear flexible (Timoshenko) beam elements instead of the usual Euler-Bernoulli beam elements. Although the shear flexible (Timoshenko) beam elements are computationally slightly more expensive than the Euler-Bernoulli beam elements, the shear flexible elements provide results which are more accurate and thus the additional computational time of this choice can be accepted.

The vertical displacement for a beam with both ends fixed and a point load at midspan taking account of the shear displacement is given in equation 3.3.1;

$$\delta = \frac{PL^3}{192EI} + \frac{PL}{2GA} \tag{3.3.1}$$

where,

δ = Transverse vertical displacement of the member
P = Applied load on the member
L = Length of the member
E = Young's Modulus of the material of the member
I = Moment of Inertia of the member about the strong axis
G = Shear Modulus
A = Effective Shear Area about the strong axis

The first part of equation 3.3.1 is due to bending, which is the manner in which Euler-Bernoulli computes the transverse displacement for the above conditions. The only difference between Euler-Bernoulli and Timoshenko is the later part of equation 3.3.1, which allows for the transverse displacement due to shear.

The crane bridge was meshed into 40 beam elements to accurately compute the transverse displacements compared with the experimental results, thereby limiting the number of DOF to 486, i.e. 6 DOF per node for 81 nodes of the crane bridge. A supporting reason for meshing the beam into 40 elements was the placement of the crab at various positions along the crane bridge if required.

Thus, the crane bridge was modelled using 40 three dimensional three node shear flexible (Timoshenko) quadratic beam elements (B32) as shown in Figure 3.3.2. Only the centre line is displayed for the representation of all beam elements, as shown in Figure 3.3.2.

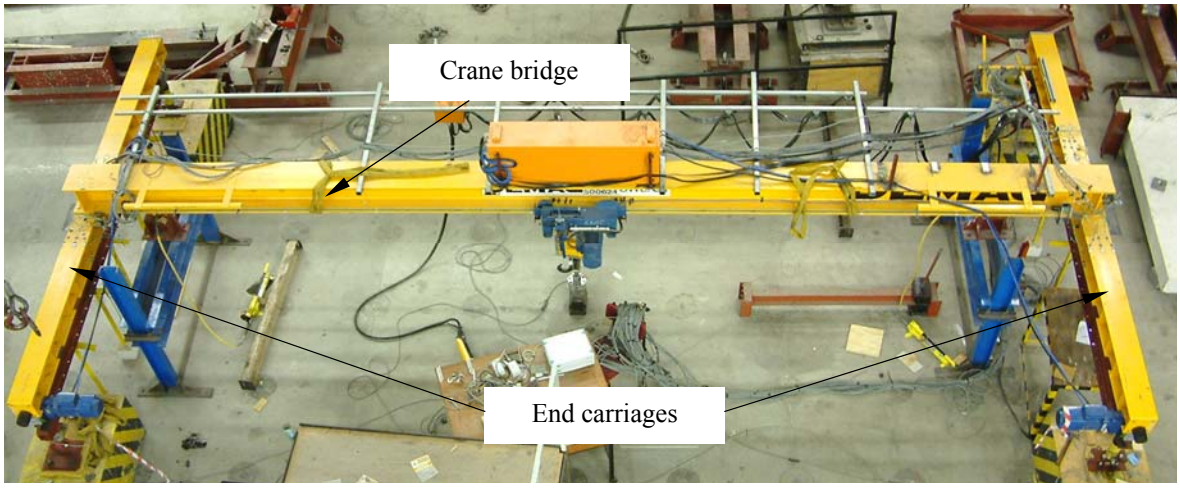

Figure 3.3.1 Experimental model of the crane consisting of crane bridge, end carriages, crab and wheels

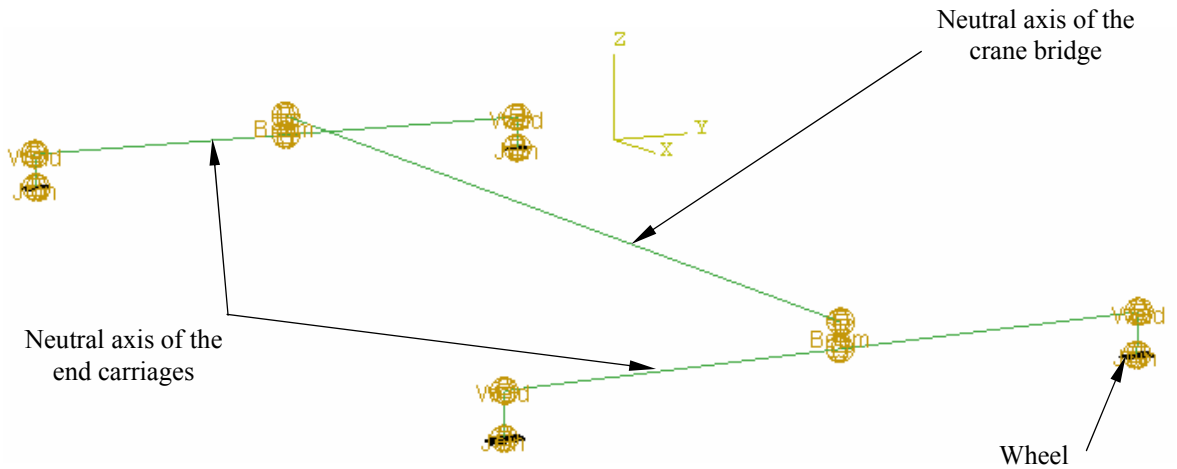

Figure 3.3.2 FEA representation of the neutral axis of the crane bridge and end carriages with the wheels, showing the various types of connectors

3.4 End Carriages

The end carriages are composed of $203 \times 203 \times 60$ H sections, which are 4.260m long and oriented with the web in the vertical direction as shown in Figure 3.3.1. The purpose of the end carriages is to transfer the loads from the crane bridge to the crane wheels as the payload is hoisted.

The end carriages behave in a similar manner to the crane bridge and can thus be modelled using the same techniques used for the crane bridge.

The end carriages are meshed into 20 beam elements each, to accurately compute the transverse displacements for comparison with the experimental results, thereby limiting the number of DOF to 246, i.e. 6 DOF per node for 41 nodes for each of the end carriages. The total number of nodes and the number of DOF for both end carriages are 82 and 492, respectively.

Thus, the end carriages are modelled using 20 three dimensional three node shear flexible (Timoshenko) quadratic beam elements (B32) as shown in Figure 3.3.2.

3.5 Connection between the Crane Bridge and the End Carriages

The ends of the crane bridge are rigidly connected to the middle of the end carriages as shown in Figure 3.5.1, using bolts. The rigid connections are thus able to transfer moments from the crane bridge to the end carriages.

This connection must be accurately modelled to allow the end carriages to deform in translation and rotation along the length of the beam, as the crane bridge deflects under the induced load caused by the hoisting of the payload. As the payload is hoisted, the crane bridge deflects vertically in the Z-direction (see Figure 3.3.2 for axis direction), while the end carriages deflect vertically but also rotates about their axis in the Y direction. The rotations are prominent at the connection between the crane bridge and the end carriages. “Beam connectors” were used in the FEA model to obtain the correct rotation and transverse displacements of the beam as shown in Figure 3.5.2. The Beam connectors constrain the translational and rotational DOF of the respective nodes so that they behave concordantly creating a rigid link between the two elements.

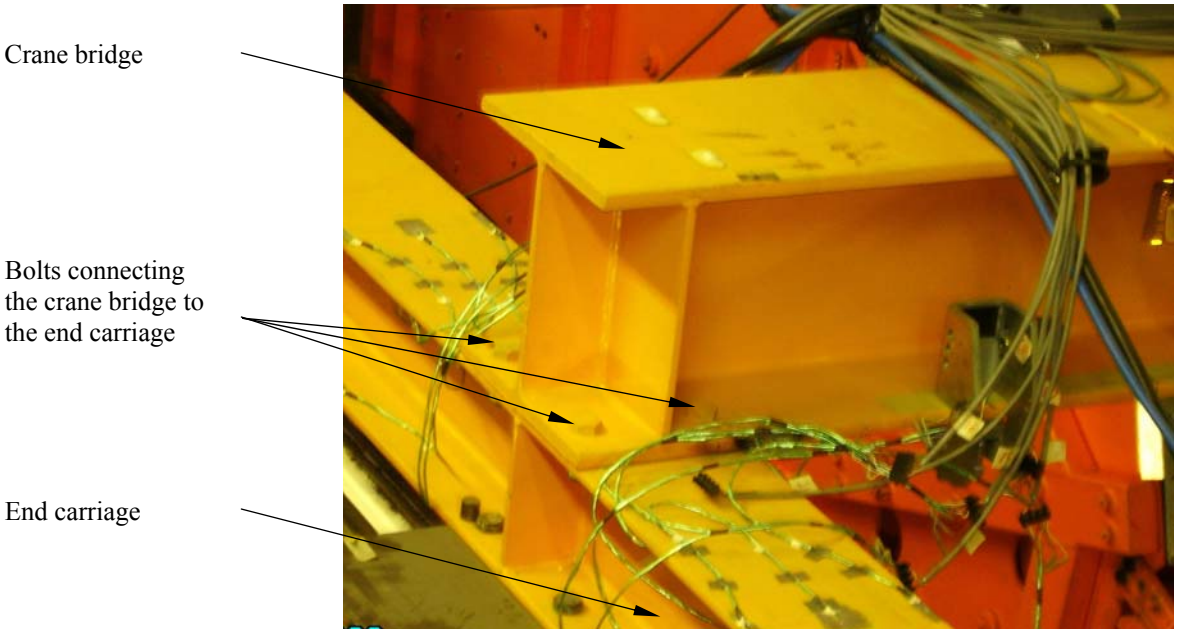

Figure 3.5.1 Detailed view of the actual connection between the crane bridge and end carriage

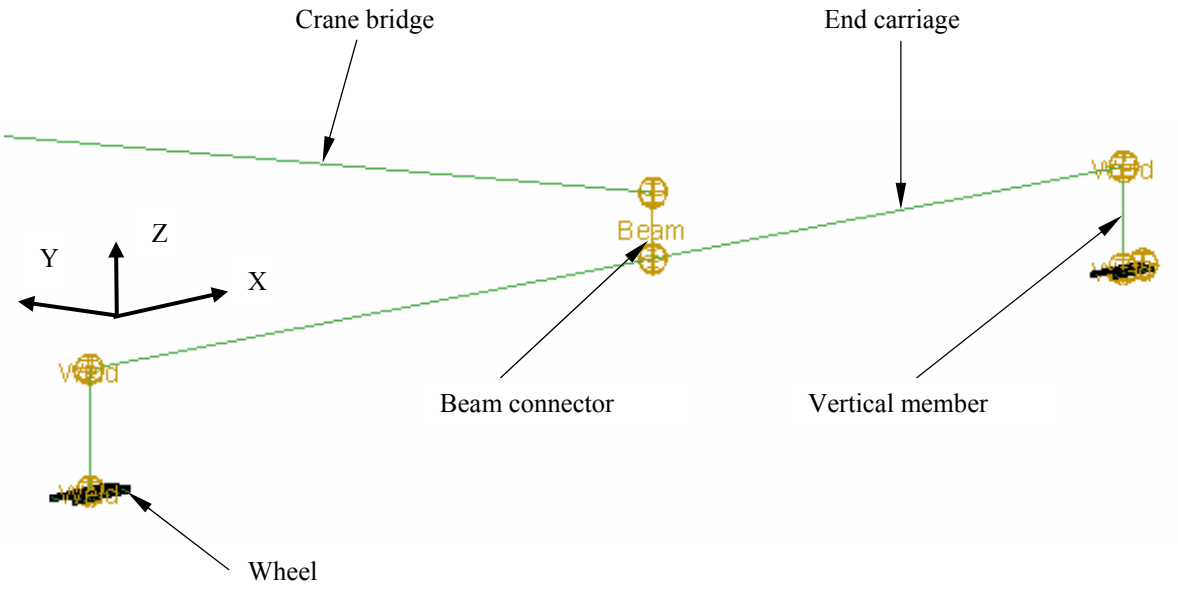

Figure 3.5.2 FEA representation of the beam connector between the crane bridge and the end carriage

3.6 Vertical Members

The experimental model does not have physical vertical members. These members are only encountered in the FEA model due to the offset arising from the distance from the centre line of the crane bridge to the bottom surface of the wheel as shown in Figure 3.6.1. The distance between the centre line of the crane bridge to the bottom surface of the wheel is 0.265m. These vertical members are used to join the ends of the end carriages to the crane wheels.

The purpose of the vertical members in the FEA model is to transfer the forces from the end carriages to the crane wheels. Beam elements instead of rigid links were used to model the vertical members to allow the bending moment of inertia's to be adjusted. The bending stiffness of the vertical beam members between the wheels and the end carriages need to be much greater than the torsional stiffness of the end carriages in order to correctly simulate the wheel block – end carriage connection.

The vertical members are modelled using 1 three dimensional two node (Euler-Bernoulli) linear beam element (B31) shown in Figure 3.6.1.

The connection between the ends of the end carriages and the vertical members are rigid.

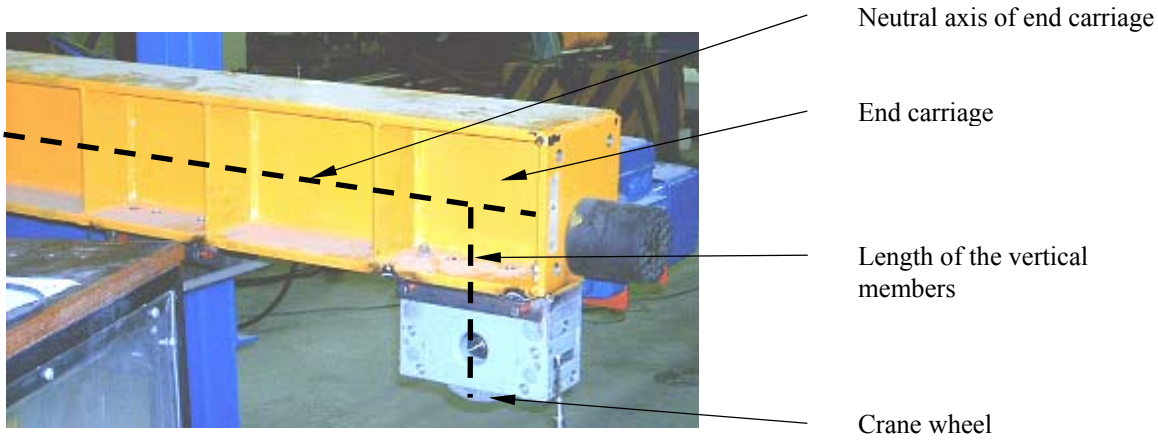

Figure 3.6.1 View of the experimental configuration of the end carriage, wheel block and wheel

3.7 Crane Wheels

3.7.1 Conventional Crane Wheels

The experimental crane wheels are 0.125m in diameter with a cylindrical surface width of 0.062m and a flange width of 0.013m. The purposes of the crane wheels are to transfer the forces from the end carriages to the crane rails and also to ensure smooth translations of the crane along the crane rails.

The purpose of the crane wheels in the FEA model are to efficiently transfer the forces to the crane rails and also to ensure smooth longitudinal and lateral translations of the crane. Initially, the solid rotating wheels were modelled as conventional wheels in the FEA simulations. The crane bounced vertically during its longitudinal travel when large crane rail elements with a length of 500mm were used. To eliminate the bouncing effect of the crane during its longitudinal travel the crane rail element length were reduced to 25mm. This resulted in a FEA model which was computationally inefficient and extremely time consuming.

The vertical bouncing of the crane can be eliminated with the remodelling of the conventional crane wheels and adjusting the interaction properties between the crane wheels and crane rails. The interaction properties between the skis (crane wheels) and the crane rails comprise of friction and a contact pressure relationship.

The contact pressure relationship needs to be accurately simulated to ensure the smooth travel of the crane wheels on the crane rails. A contact pressure relationship which is too "severe" will exacerbate the bouncing effect. Thus a gradual increase in the contact pressure vs. the contact clearance was incorporated to prevent the vertical bouncing of the crane on the crane rails.

Since the detailed modelling of the crane wheels proved computationally expensive, a computationally efficient alternative needed to be employed.

3.7.2 Ski's: An Alternative Approach to the Conventional Crane Wheels

Ski's are introduced as a computationally efficient and cost effective alternative to the conventional crane wheels. The ski's are modelled using an inverted channel section as shown in figure 3.7.2.1. The dimensions of the cylindrical horizontal surface of the channel section are 200mm x 62mm, while the flanges are 200mm x 13mm. The inside dimensions between the flanges and the height of the flanges are obtained from the conventional wheels. The channel-shaped "wheels" (skis) are modelled with 8 node shell elements, which are meshed into 70 elements to allow for even distribution of the forces to the crane rails.

The channel shaped skis will not be adequate to study the skewing effect between the wheels and the crane rail head. To achieve this, the dimensions of the skis must be adjusted to match the experimental configuration dimensions.

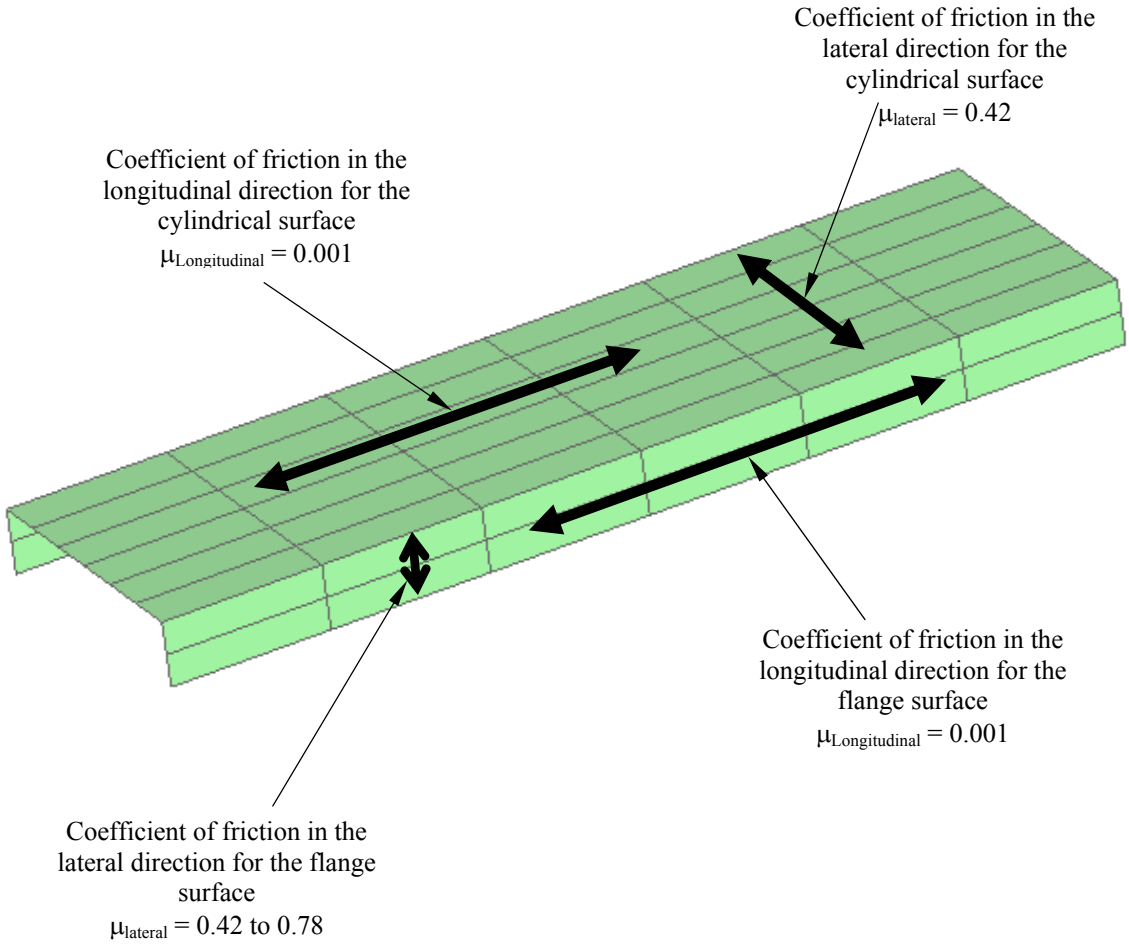

Figure 3.7.2.1 FEA representation of the inverted channel shaped meshed ski wheel

3.7.3 Friction Coefficient Between the Ski Surfaces and the Crane Railhead

The friction behaviour is comprised of the longitudinal and lateral slip between the crane wheels and the crane rails. The various coefficients of friction for different materials were obtained from Royal Institute of Mechanical Engineering's website [3.2].

The coefficient of friction when the cylindrical surface of the crane wheels roll in a longitudinal direction on the crane rails is approximately equal to 0.000 5 ($\mu_{longitudinal} \approx 0.000\ 5$). The energy losses due the various components in the motors cannot be neglected and must be accounted for as this increases the coefficient of friction in the longitudinal direction. Thus, the total coefficient of friction in the longitudinal direction can be estimated as $\mu_{longitudinal} \approx 0.001$.

The coefficient of friction in the lateral direction cannot be ignored as no rolling action occurs, but rather a sliding action as the crane wheels translates laterally. The static friction must be overcome before the crane wheels can translate laterally across the crane rails. The coefficient of friction for steel against steel ranges from 0.42 to 0.78 depending on the abrasiveness between the surfaces. Thus, the longitudinal friction coefficient, $\mu_{longitudinal} = 0.001$, while the lateral friction coefficient, $\mu_{lateral} = 0.42$, will be used in the FEA model to simulate the friction between the cylindrical surfaces of the crane wheels and crane rails.

Since different friction coefficients can be specified in two directions this leads to anisotropic friction behaviour model which can be implemented in the FEA model. The anisotropic friction behaviour obviates the need to model the conventional rolling wheels which is computational expensive as contact surface element lengths on the crane rails need to be exceptionally small. A flat surface which acts as skis will be used to model the cylindrical surface of the solid rotating wheels. The same techniques can be employed for the flanges. The conventional wheels are now replaced with an channel shaped section (skis) with the relevant anisotropic friction and contact behaviour for the cylindrical and flange surfaces. The channel shaped section with the relevant friction parameters are shown in Figure 3.7.2.1.

A limiting factor to using the ski model is that it will not be able to adequately capture the physics of the conventional wheel "mounting" the head of the crane rail.

3.8 Compound Beams (Girders, Elastomeric Pad and Crane Rail)

The experimental configuration of the compound beam consists of 3 abutted simply supported mono-symmetric girders, a continuous crane rail and a continuous elastomeric pad sandwiched between the crane rail and the top flange of the crane girder as shown in Figure 3.8.1. The mono-symmetric girders, which are supported on the crane columns, are 4 596mm long, thus resulting in an overall length of the crane supporting structure of 13 788mm. The mono-symmetric crane girder is a plate girder with a top flange $(300 \times 16\text{mm})$, a bottom flange $(250 \times 10\text{mm})$ and a web $(350 \times 20\text{mm})$. The crane rail consists of a 30 kg/m railway rail section and is continuous over 13 788mm in length. The purpose of the compound beams is to transfer the forces arising from the crane wheels to the crane columns. A close-up view of the girder, elastomeric pad, crane rail and gantrex clips are shown in Figure 3.8.2.

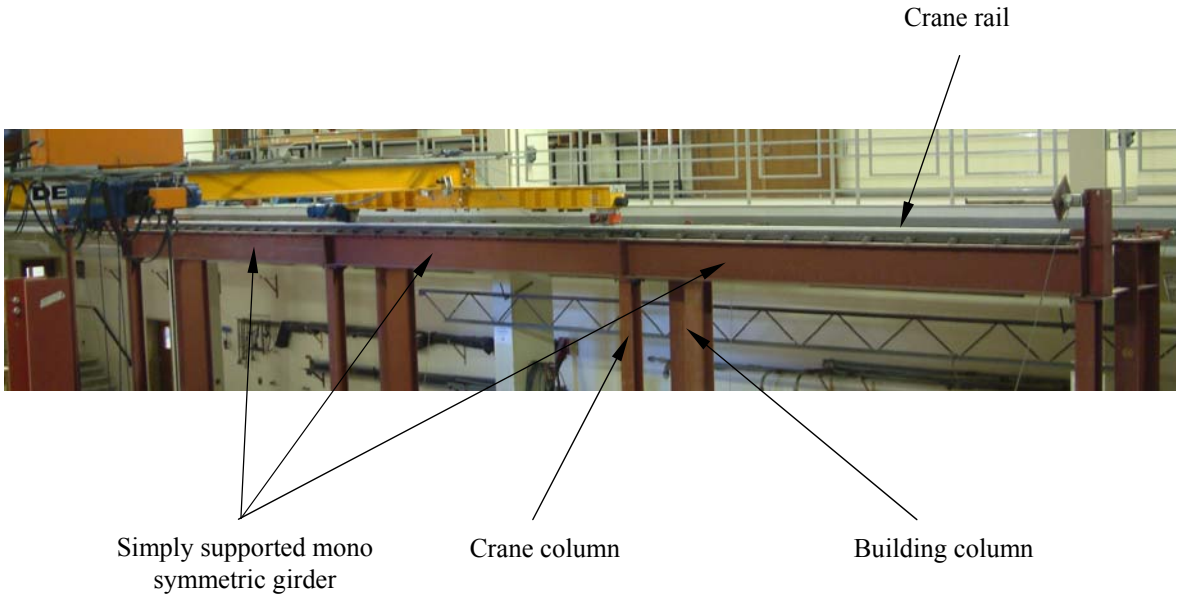

Figure 3.8.1 A close-up view of the experimental configuration of the continuous crane rail and the simply supported mono-symmetric girders supported on crane columns

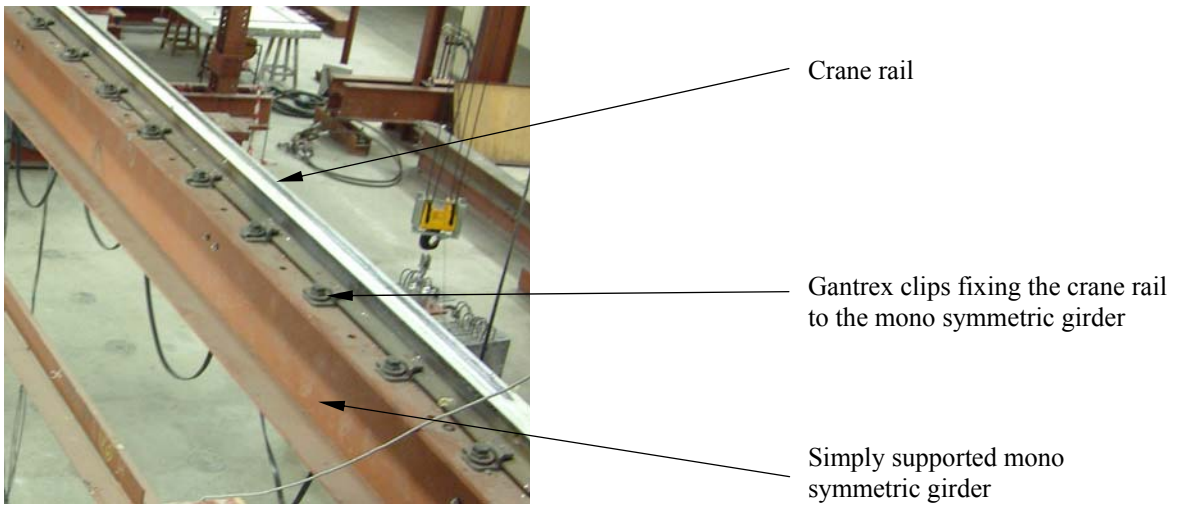

Figure 3.8.2 Close-up view of the experimental configuration of the mono symmetric girder, the crane rail and the gantrex clips. (The elastomeric pad is hidden between the girder and the rail).

The purpose of a previous study which was commissioned by the Institute of Structural Engineering at the University of Stellenbosch and conducted by Viljoen [1.3], to determine the local behaviour of a simply supported compound beam subjected to vertical and horizontal loading.

Thus, it was essential to have a fine mesh of the simply supported compound beam to accurately predict the local behaviour. Viljoen [1.3], used a total of 10 008 three-dimensional 20 node brick elements with an estimated 173 754 DOF to model the simply supported compound beam as shown in Figure 3.8.3. A shell model would have been much more efficient to analyse the simply supported compound beam.

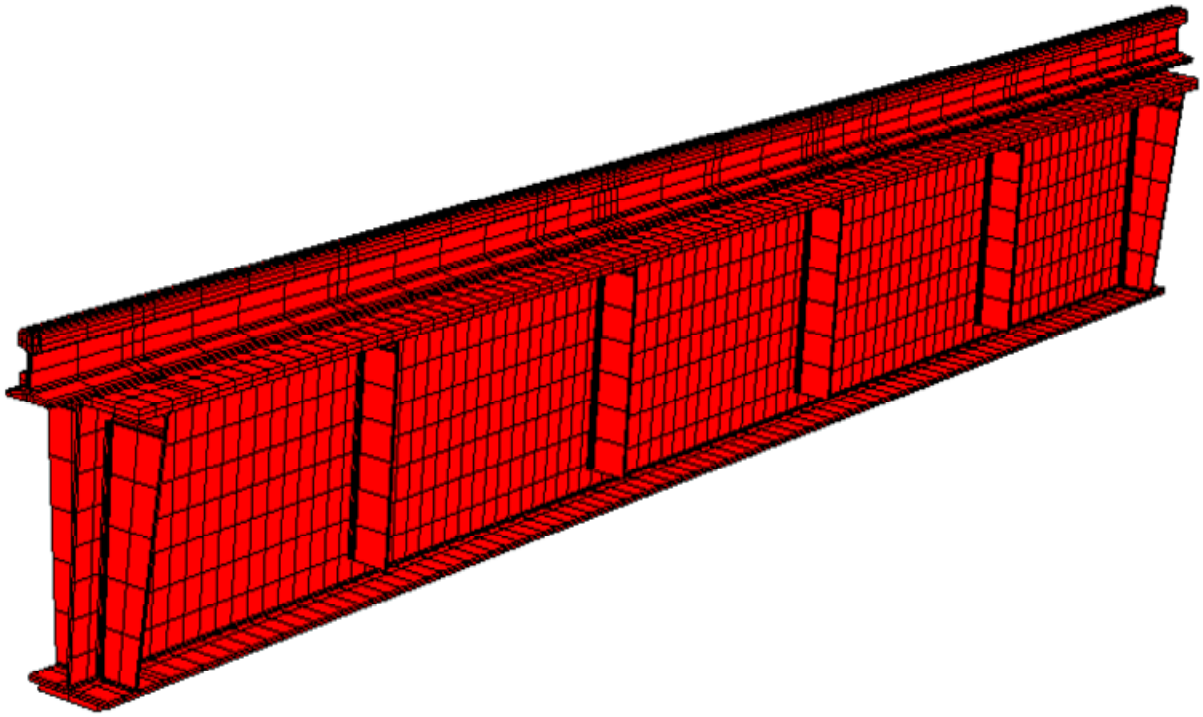

Figure 3.8.3 Viljoen's [1.3], FEA meshed model of the compound beam using three-dimensional 20-node brick elements

The focus of the current research is to determine the global behaviour of the experimental model numerically. Thus, it would be impractical to use Viljoen's [1.3], approach to model the compound beam with three dimensional 20-node brick elements as this would result in approximately 0.52 million DOF per 13 788mm length of beam. This is omitting the additional DOF to account for the holes, the gantrex clips and bolts. This necessitated the use of beam elements to model the compound beam sections.

Since the mono-symmetric girders are simply supported and the elastomeric pad and crane rail are continuous over the crane columns, it is not possible to model the compound beam entirely as a

continuous beam or with three simply supported beams.

The stiffness of the mono symmetric girders contributes approximately 94% towards the total stiffness of the compound beam. Since the girder's stiffness is dominant, the compound beam behaves similar to a simply supported beam, except near the beam ends. This is due to the stiffness contribution of the crane rails which are continuous over the crane columns, which changes the displacement and rotation profiles of the compound beam. The result of the compound beam is a change in boundary conditions for each girder segment. The boundary condition influences the response of the whole beam.

Combinations of long and short beams were used to model the compound beams to allow for the correct displacement and rotation profiles along the length of the beam to be achieved. The short beams of 596mm length were positioned above the crane columns between the long beams. The nodes of the ends of the short and long beams were rigidly connected using weld connectors to allow transfer of moments to occur between the beams. This resulted in a continuous beam consisting of long and short beams as depicted in Figure 3.8.4.

A set of experimental tests were performed by De Lange [1.6], to determine the vertical displacements when individual point loads were positioned at midspan of each span of the compound beam, respectively. The short beams' bending moment of inertia in the FEA model was adjusted until the correct displacement and rotation profiles were obtained, compared to the experimental results, while keeping the long beam's moment of inertia constant. The bending moments of inertia of the long and short beam are 352.2 x 10^6 mm^4 and 30 x 10^6 mm^4, respectively.

The long and short beams were modelled with 10 and 5 three dimensional three node shear flexible (Timeshenko) quadratic beam elements, respectively.

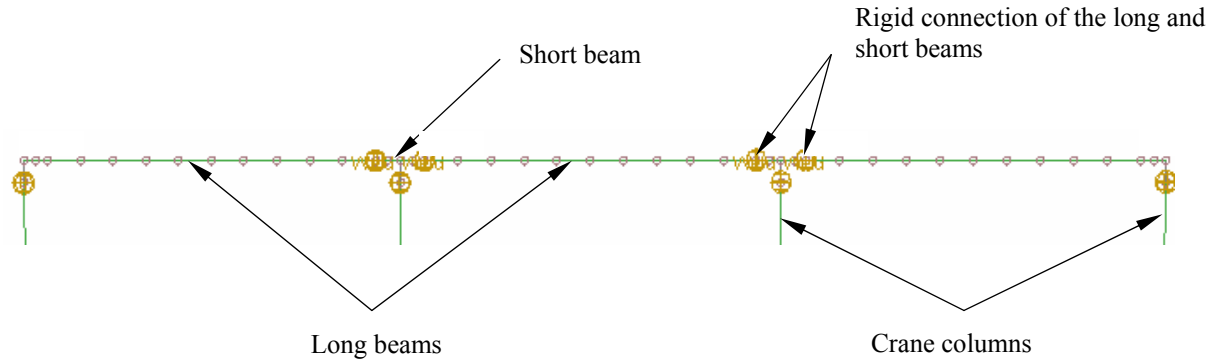

Figure 3.8.4 FEA representation of the crane columns, short and long beams with there respective connector elements

3.9 Compound Beams and Crane Rail Interaction

The purpose of the experimental mono-symmetric girders is to transfer the forces from the wheels to the crane columns. A close-up view of the girder, crane rail, and elastomeric pad is shown in figure 3.8.2.

The purposes of the FEA crane rails are

(i) to transfer the forces from the skis to the compound beams
(ii) act as wheel guides
(iii) provide the correct translations and rotations in all directions
(iv) to study global contact forces between the crane rail head and wheels when the crane travels on the crane rails.

The purpose of the FEA model is to determine the global response of the experimental crane and crane supporting structure when subjected to loading. The FEA model with the skis can accurately predict the contact forces between the skis and the crane rails. The current FEA model cannot accurately predict the contact stresses between the skis and the crane rails. The contact forces obtained from this model can be used as an input parameter in Perez-Winkler's [1.4], model to accurately obtain the contact stresses between the crane wheels and the crane rails. Thus, it would be impractical to model the crane rails with brick elements due to the large number of DOF which would be obtained. This would also lead to a computationally inefficient modelling of the crane rails. Therefore a better modelling of the crane rails was required.

The purposes of the crane rail are to transfer contact forces to the girder and also act as guides for the wheels. Thus, only the profile of the crane rail head was modelled to perform the above functions. The crane rail head was modelled with 8 node quadratic shell elements which were connected to the compound beam. The shell elements are pictorial only as the rigid links connect the ski contact nodes to the elements representing the compound beam / rail / resilient pad. The stiffness of the crane rail head has already been incorporated into the stiffness of the compound section. Thus, the crane rail head is merely to transfer forces, act as wheel guides and study contact forces between the wheels and the crane rail.

Figure 3.9.1 shows a cross section through the experimental mono-symmetric girder and crane rail. The elastomeric pad is intentionally omitted due to its very low Young's Modulus compared to steel. The compound section shown in Figure 3.9.1 was used to determine the elastic geometric properties of the compound beam which were assigned to the long beams.

Figure 3.9.2 shows a cross section through the compound beam and the channel shaped crane rail head's profile in the FEA model. A set of connectors are used to transfer the forces and displacements from the crane rail head's profile to the compound beam. To achieve this, a set of 5 nodes was created on the perimeter of the cross section at the end of each element length of the crane rail head profile as shown in Figure 3.9.3. These nodes are used to ensure that the crane rail head's profile acts as a rigid body. The longitudinal rotational DOF of the crane rail head's profile is independent of that of the corresponding compound beam's rotational DOF about Y axis.

The top and bottom flanges of the mono-symmetric girder are connected to the building columns to prevent complete rotation about the longitudinal (Y) axis. Thus, in the FEA model the compound girder and crane rail head is also prevented from rotation about the longitudinal axis by preventing rotation at the crane columns.

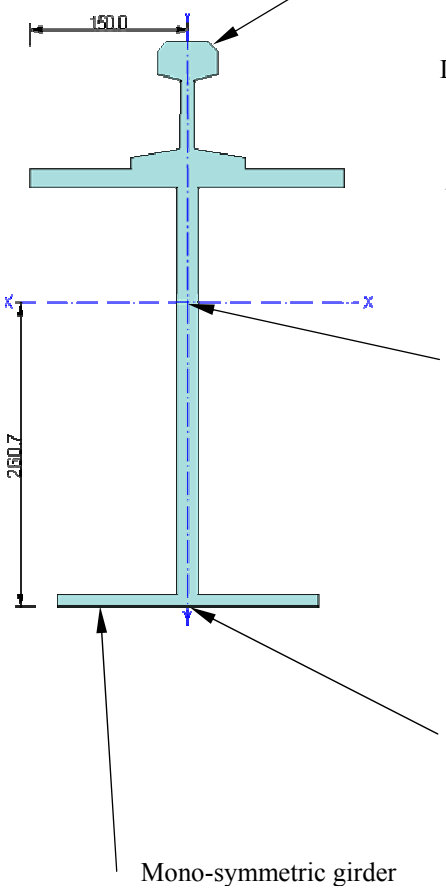

Figure 3.9.1 Experimental representation of the mono symmetric girder and crane rail head

Figure 3.9.2 FEA representation of the mono symmetric girder and crane rail head

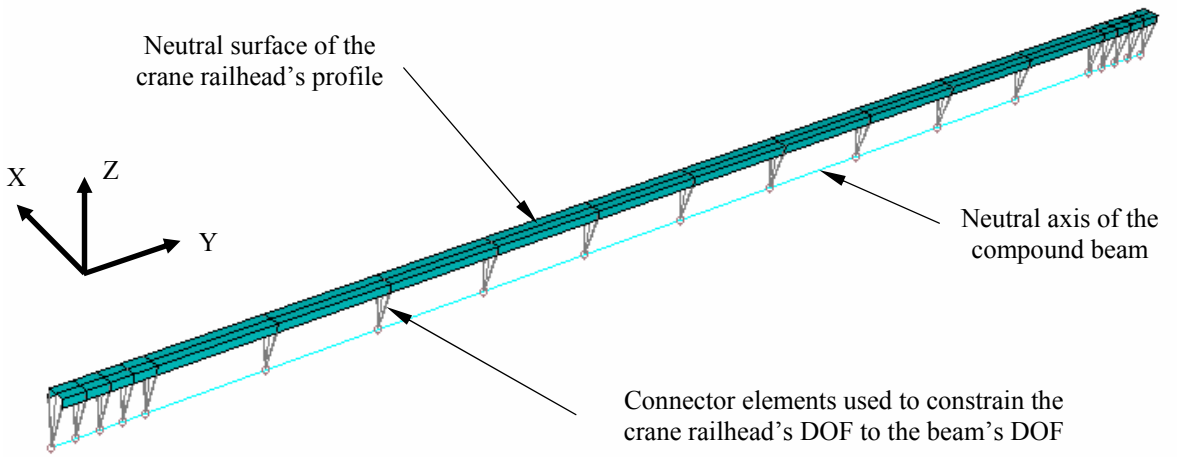

Figure 3.9.3 FEA representation of the crane railhead profile with its nodes constrained to the compound beam's nodes

3.10 Drive Motors for Longitudinal Motion of the Crane

In the experimental model the two back wheels are each driven by a 55kW electric motor, allowing the crane to attain longitudinal speeds of 0.55m/s. The purpose of these motors is to drive the wheels along the rails. Most modern cranes use electric motors which constantly adjust the torque to keep the speed of the wheels constant, even when the hoist load is eccentric. It is hence unlikely for skewing to occur if modern electric motors are used, the tolerances between the wheel flanges and crane rail head are adhered to, and the crane rails are set to within the required tolerances. Most modern cranes are equipped with a ramp-up and ramp-down function which increases or decreases the torque over a specified period of time. This function is crucial when investigating the impact of the crane into the end stops.

The purpose of the drive motors for longitudinal motion of the crane in the FEA model is to drive the crane causing it to move with constant acceleration or constant speed. The acceleration (propulsion) of the crane is modelled with an acceleration boundary condition applied to the nodes of the back skis and then deactivated at the moment of impact. The longitudinal movement of the crane together with the payload is then dependent on the boundary condition applied to the skis. It would be computationally too expensive to model the longitudinal wheels motors. The modelling of the motors is outside the scope of this research project.

3.11 Crane Columns

Figure 3.11.1 shows the mono-symmetric girders, the building columns, the foundation lever beams and the crane columns. The crane columns are 3 180mm tall and composed of $152 \times 152 \times 23$ H-sections with the weak axis oriented across the longitudinal direction of the girders. The purpose of the crane columns is to transfer the forces from the mono-symmetric girders to the foundation. The crane column experiences an axial deformation of 0.26mm when subjected to a load of 50kN (≅ 5-ton). The critical Euler buckling load for crane columns about its weak axis considerably exceeds the applied load. Thus it is unlikely that the crane columns will buckle under the applied forces.

The purpose of the crane columns in the FEA model is to transfer axial forces from the compound beams to the foundation. The crane columns are modelled with Euler-Bernoulli beam elements due to the anticipated low transverse shear deformations expected at the top of the crane columns and the low probability of buckling of the crane columns. The crane columns are modelled using 10 three dimensional two-node (Euler-Bernoulli) linear elements (B31) depicted in Figure 3.11.2. The horizontal lateral bracing system supporting the building columns will be removed in future research work to allow the structure to act as a portal frame. Thus, at this stage the horizontal lateral displacements of the building and crane columns could be significant. For this reason the crane columns were meshed into 10 elements.

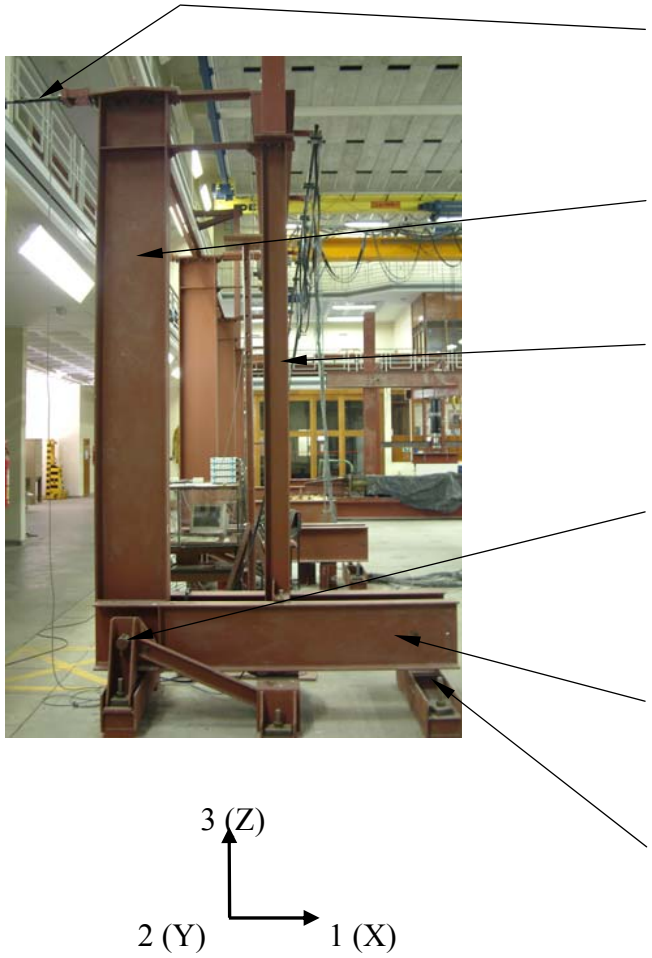

Figure 3.11.1 Experimental configuration of the building columns and the foundation lever beam

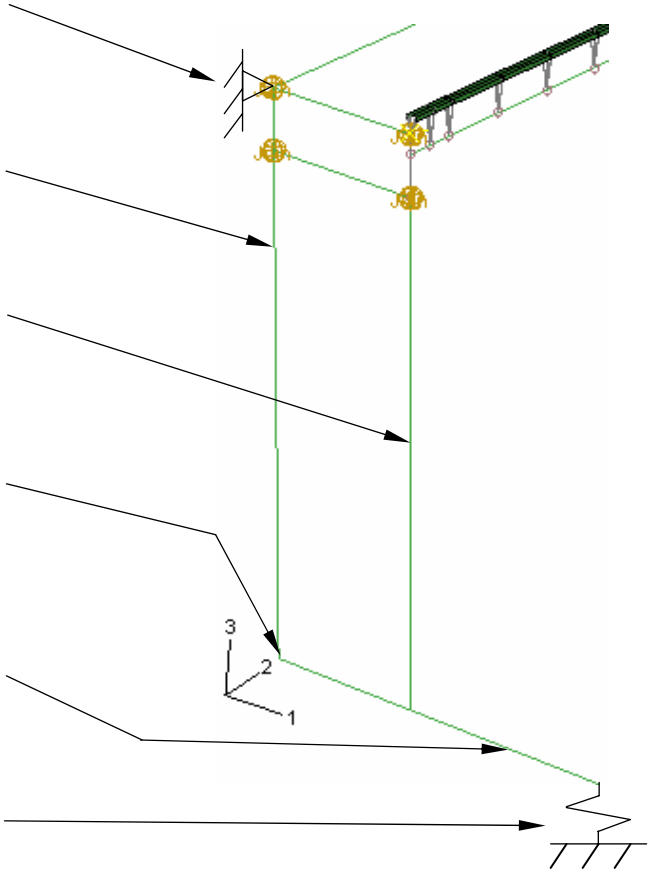

Figure 3.11.2 FEA representation of the building columns and the foundation lever beam

3.12 Building Columns and Foundation Lever Beams

Figure 3.11.1 shows the experimental configuration of the building columns and foundation lever beams. The building columns are 3 555mm tall and composed of $457 \times 191 \times 67$ I sections and oriented as shown in Figure 3.11.1. The building columns stiffness is approximately 24 times greater than the crane columns stiffness. The apexes of the crane columns are connected to the building columns to provide horizontal lateral stability to the crane columns.

The foundation lever beams are 2 200mm long and composed of $406 \times 140 \times 46$ I sections and oriented as shown in Figure 3.11.1. The foundation lever beams are rigidly connected at one end to the base of the building columns while connected to a vertical spring at its opposite end.

The building columns and foundation lever beams depicted in Figure 3.11.1 are usually not included in an industrial building. The above members were included in the experimental and FEA model to allow for the crane columns' stiffness adjustments about the strong axis. The purpose of the combined building columns and foundation lever beams which are hinged at the base of the building columns is to provide varying horizontal lateral stability to the crane columns depending on the stiffness of the vertical springs. For this research project the apexes of the building columns is restraint in the horizontal lateral direction, thus providing full lateral support to the crane columns.

The purpose of combining the building columns and the foundation lever beams in the FEA model is to provide horizontal lateral stability to the crane columns depending on the support at the apexes of the building columns and the stiffness of the vertical spring. The apexes of the building columns are restrained in the horizontal lateral direction thus eliminating the spring at the opposite end of the foundation lever beams.

The building columns will act in a similar manner to the crane columns and are thus modelled with 10 three dimensional two-node (Euler-Bernoulli) linear beam elements as depicted in Figure 3.11.2.

The foundation lever beams could experience large shear forces and bending moments depending on the spring stiffness. The foundation lever beams are thus modelled with 10 three dimensional three-node (Timeshenko) quadratic beam elements (B32) as depicted in Figure 3.11.2.

The intersection of the building columns and foundation lever beams are rigidly joined with a weld connector to allow the transfer of shear forces and bending moments between these members.

3.13 Horizontal Lateral Bracing System

The apexes of the building columns are horizontally laterally connected to the first floor of the laboratory with the horizontal lateral bracing struts composed of 20mm diameter steel rods, which are 600mm long as shown in Figure 3.11.1. The horizontal lateral bracing struts were designed to only transmit axial forces generated via the crane wheels through the crane rails to the horizontal lateral supports.

The horizontal lateral bracing system depicted in Figure 3.11.1 is usually not included in an industrial building. These members were included in the experimental and FEA model to prevent horizontal lateral displacement of the apexes of the building and crane columns. In future research work the horizontal lateral bracing system will be removed to determine the flexibility of the portal frame structure.

In the FEA model the horizontal lateral bracing system were modelled by restraining the apexes of the building columns as only the horizontal lateral reactions are important and not the strains within the bracing system. The horizontal lateral supports at the top of the apexes of the building columns may be omitted to study the effect on the horizontal lateral displacements of the crane rails by adjusting the stiffness of the vertical spring attached to the foundation lever beams.

3.14 Top and Bottom Horizontal Lateral Girder Bracing Struts

The top and bottom flanges of the girders are connected to the building columns, as shown in Figure 3.14.1, using horizontal lateral bracing struts, which are composed of double T-cross sections with cross sectional areas of 1.5×10^3 mm^2 and 600mm in length. The purpose of the horizontal lateral bracing struts is to transfers the horizontal lateral forces from the girders to the building columns.

The purpose of the horizontal lateral girder bracing struts in the FEA model is only to transfer the axial forces from the compound beams to the building columns. The horizontal lateral girder

bracing struts are modelled with 1 three dimensional two node linear truss elements (T3D2), since the horizontal lateral bracing struts are only required to transmit axial forces.

The connections of the girder flanges and building columns with the horizontal lateral bracing struts are modelled with join connectors, as these connectors can only transfer axial forces, as depicted in Figure 3.14.2.

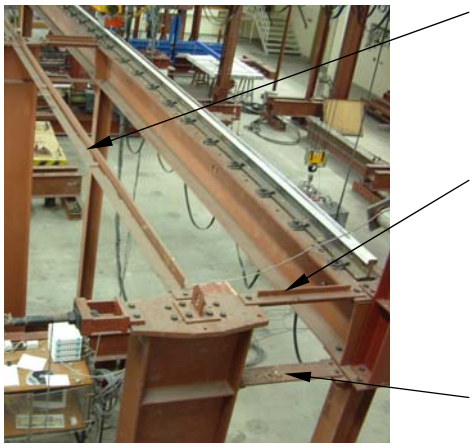

Figure 3.14.1 Experimental model of the horizontal lateral bracing struts and the top and bottom lateral bracing struts

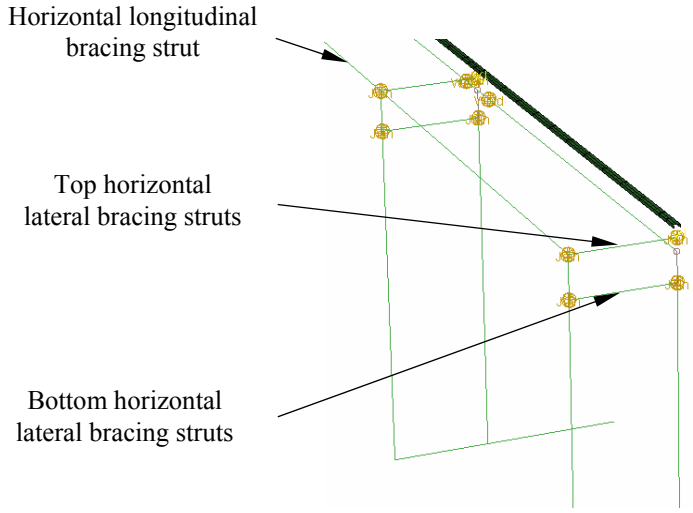

Figure 3.14.2 FEA representation of horizontal lateral bracing struts and the top and bottom bracing struts

3.15 Horizontal Longitudinal Bracing Struts

The apexes of the building columns are connected to each other with horizontal longitudinal bracing struts composed of 60 x 60 x 4mm angle sections which are 4 260mm long as shown in Figure 3.14.1. The purpose of the horizontal longitudinal bracing struts is to transfer only axial forces in a horizontal longitudinal direction between the building columns.

The horizontal longitudinal bracing struts act in a similar manner to the horizontal lateral bracing struts, except that these members are aligned in a horizontal longitudinal direction between the building columns. The horizontal longitudinal bracing struts are thus modelled with 1 three dimensional two node linear truss elements (T3D2).

3.16 Horizontal Longitudinal Bracing System

The apexes of two sets of crane and building columns are connected to an intricate horizontal longitudinal bracing system to prevent the supporting structure from swaying in the horizontal longitudinal direction as shown in Figure 3.16.1.

Since the horizontal longitudinal bracing system is merely to prevent the supporting structure from swaying and because the forces in these members are not relevant, the bracing system was omitted and replaced with horizontal longitudinal supports at the apexes of two sets of building and crane columns in the FEA model.

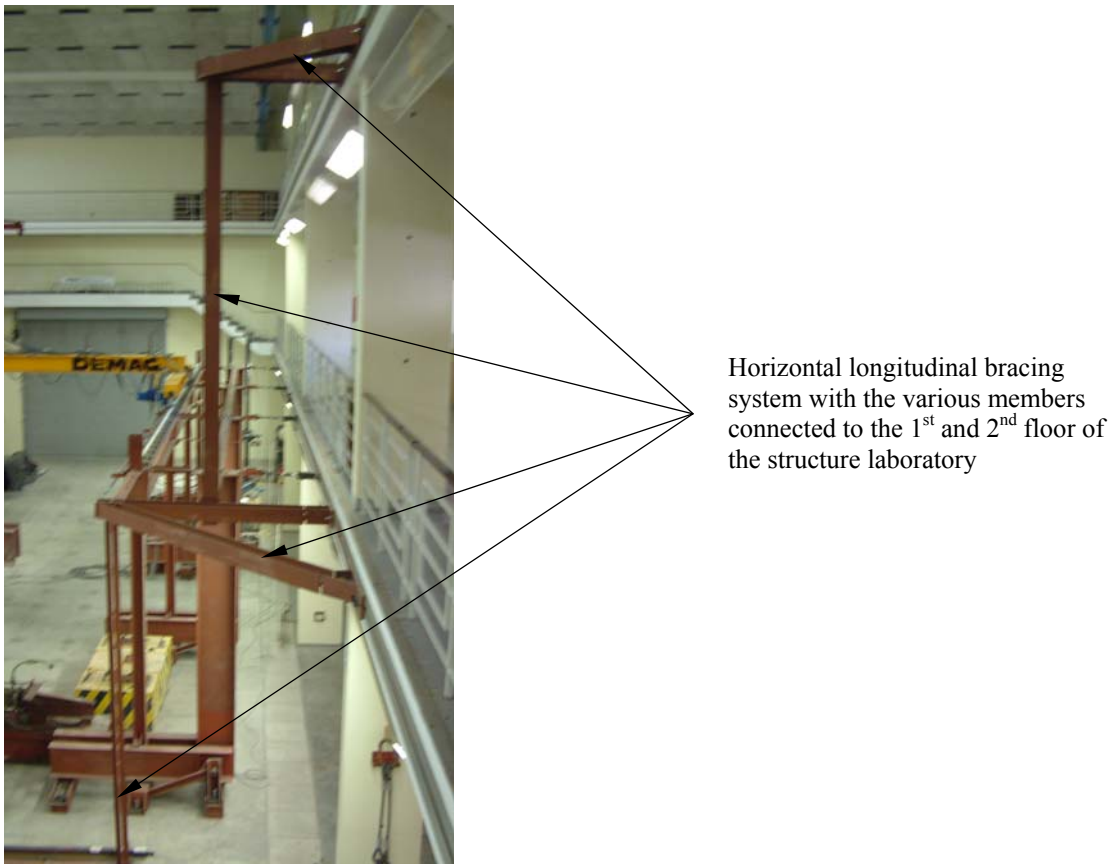

Figure 3.16.1 Experimental model of the horizontal longitudinal bracing system

3.17 Hoist Load (Payload) and Cable Configuration

A compact payload of approximately 5-ton (5128kg) was designed for the experimental tests, which consists of "in-fill" lead plates attached to the reinforced concrete cube as shown in Figure

3.17.1. The purpose of the lead plates is to reduce the overall size of the hoist load to 1.2 × 1.2 × 1.5m. In order to correctly represent the behaviour of the payload during impact, it was necessary to determine the adjusted centre of gravity as well as the rotational moments of inertia about the three axes, as these properties have a significant influence on the impact response, i.e. end buffer impact forces and natural frequencies. The compact payload was modelled using a lumped mass instead of modelling the payload using brick elements. The mass with the rotational moments of inertia were assigned to the centroid of the lumped mass in the FEA model as depicted in Figure 3.17.2. The payload was connected to the pulley by means of a rigid connector, which constrains the pulley's DOF to the hoist load's DOF.

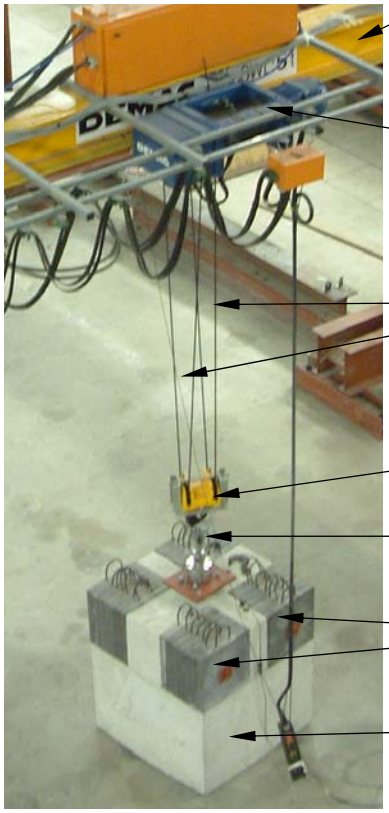

Figure 3.17.1
Experimental model of the compact (new) payload with cables

Figure 3.17.2
FEA representation of the compact payload with cable

Figure 3.17.1 also shows the experimental configuration of how the payload is connected to the crane bridge with two sets of 9.5mm diameter cables, a pulley system and two sets of hooks. The purpose of the cables is to transfer the forces from the payload to the crane bridge when the payload is hoisted.

It is essential that the cables are modelled correctly in the FEA model as this has a significant influence on the magnitude of the impact forces and the natural frequencies of the hoist load. Thus, the two sets of cables could not be modelled with a single cable in the FEA model. The horizontal longitudinal distance between the crane bridge and crab as well as the interaction between the pulley and cables must also be modelled correctly, as it influences the cable angles depending on the hoist load's height above ground level. For efficiency, the two sets of cables were condensed to form one cable running around the pulley as depicted in Figure 3.17.2. This was achieved by using the equivalent areas of the two cables. The cables are modelled as truss elements since no bending moment is transferred between the elements. An element length bias is applied to the cable to create small elements close to the pulley becoming larger towards the crane bridge. Thus, the cable is modelled with 45 three dimensional two node linear truss elements (T3D2) elements as depicted in Figure 3.17.2.

It is also important to compute the system's deformations induced by the deformed cable's configuration during impact. This is achieved using the Geometric Nonlinear capability in ABAQUS, which also accounts for large deflection theory.

3.18 Cable and Pulley Interaction

The pulley is able to rotate smoothly around the cables with minimal frictional resistance in the experimental configuration. During the experimental impact tests, the cables deformed from a normal "V" shape in Figure 3.17.2 to an oblique "V" shape as the pulley rotated and climbed along the cable.

To achieve the rotation and climbing effect of the pulley along the cable during the FEA simulations, the cable was required to be continuous around the pulley. Since the pulley rotates smoothly around the cable in the experimental configuration, the friction properties were omitted in the FEA model. A contact configuration which allows no separation between the pulley and the cable were also implemented in the FEA model.

3.19 Crane Buffers

The crane buffers consist of DPZ100 cellular plastic buffers, of 100mm length, 100mm diameter at its base and tapering to 95mm on the opposite end as shown in Figure 3.19.1. The buffers are made of cellular polyurethane material which exhibit excellent qualities with respect to elasticity, cushioning and energy absorption. The energy absorbed increases with the impact speed of the crane. This is due to the polytropic compression of the gasses in the cellular structure. The advantages of the buffers are, its use in adverse conditions, its ability to operate at temperatures between -20˚C and 80˚C and its resistance to most chemicals used in industrial applications.

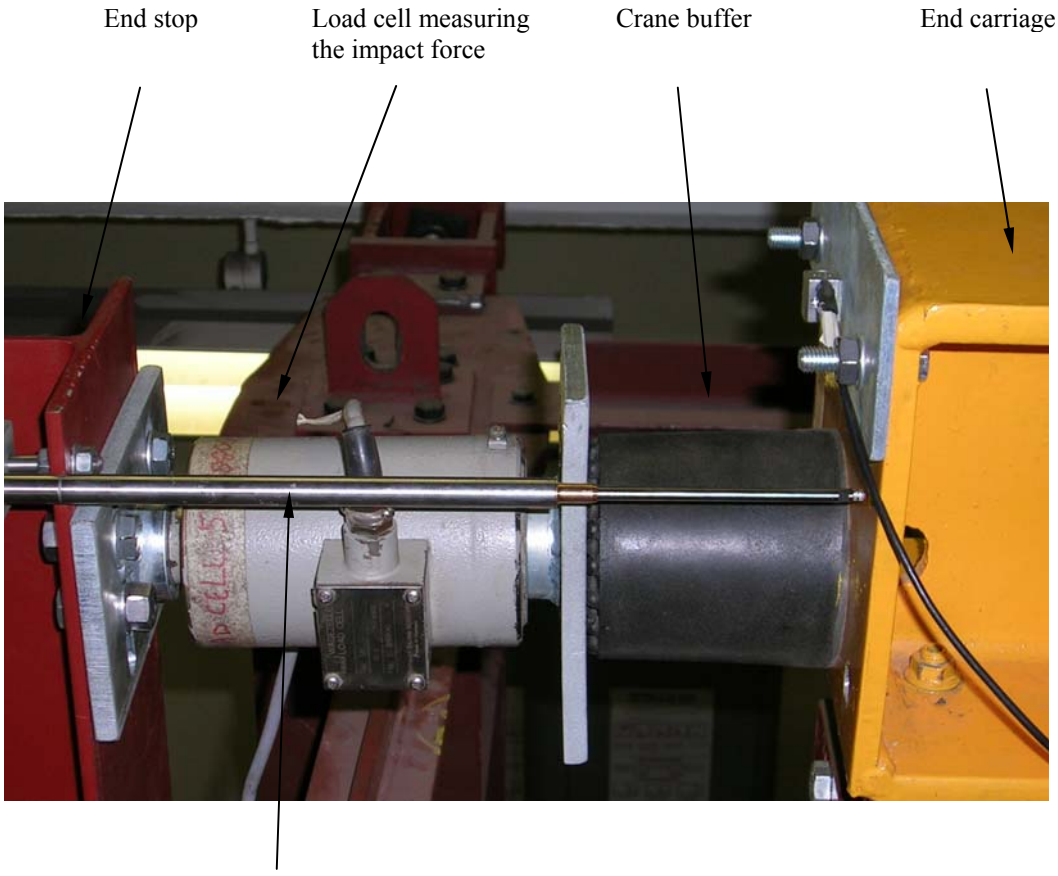

Figure 3.19.1 Experimental configuration of the crane buffer between the end carriage, the end stop and the load cell

The purpose of the crane end buffers is to absorb energy during impact thereby reducing the end buffer impact forces which the crane imposes on the end stops. The crane buffer's behaviour is similar to that of a spring during the compression and relaxation phases, except that springs have damping characteristics. Thus, for the spring elements to exhibit the characteristics of the cellular plastic buffers in the FEA model, the spring elements must be modelled with the appropriate elastic and damping properties.

3.19.1 Elastic Characteristics of the Crane End Buffers

No clarity was obtained from DEMAG whether the elastic characteristics of the end buffers were obtained for a constant deformation strain rate or whether the elastic characteristics were obtained for an initial velocity which decreases as the buffers are compressed. Due to this uncertainty, DEMAG's elastic curve of 0.55m/s was compared to the experimental data.

The representative impact force vs. displacement hysteresis' of the crane end buffers, LHS # 5 and RHS # 2, were obtained from the experimental tests and is presented in Figure 3.19.1.1. The lines joining the points of zero velocity of the hysteresis curves are superimposed on Figure 3.19.1.1.

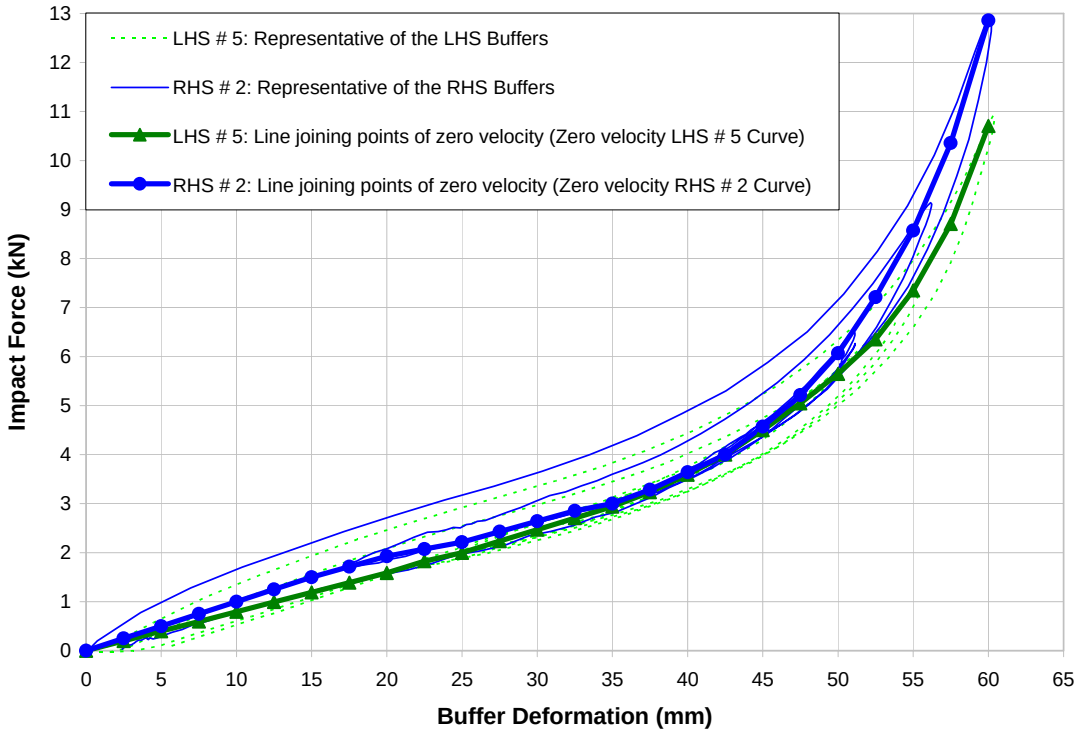

Figure 3.19.1.1 Comparison between the hysteresis curves of the end buffer impact response and the line joining the points of zero velocity on the hysteresis curves

DEMAG's elastic curve of 0.55m/s is compared to the representative experimental RHS and LHS zero velocity elastic curves presented in Figure 3.19.1.2. There is an extremely good correlation between the elastic characteristics of the DEMAG curve of 0.55m/s and the "zero velocity" LHS # 5's elastic curve presented in Figure 3.19.1.2. It can be concluded that the elastic characteristic curves supplied by DEMAG are obtained for a non constant strain rate.

The "zero velocity" LHS's elastic curve were chosen for the crane end buffers in the FEA model. The "zero velocity" LHS's elastic curve shown in Figure 3.19.1.2 were extrapolated from the trend line equation to obtain the force vs. displacement data beyond 60mm and is also shown on Figure 3.19.1.2. This was necessary as the maximum end buffer deformations during impact were expected to exceed 60mm.

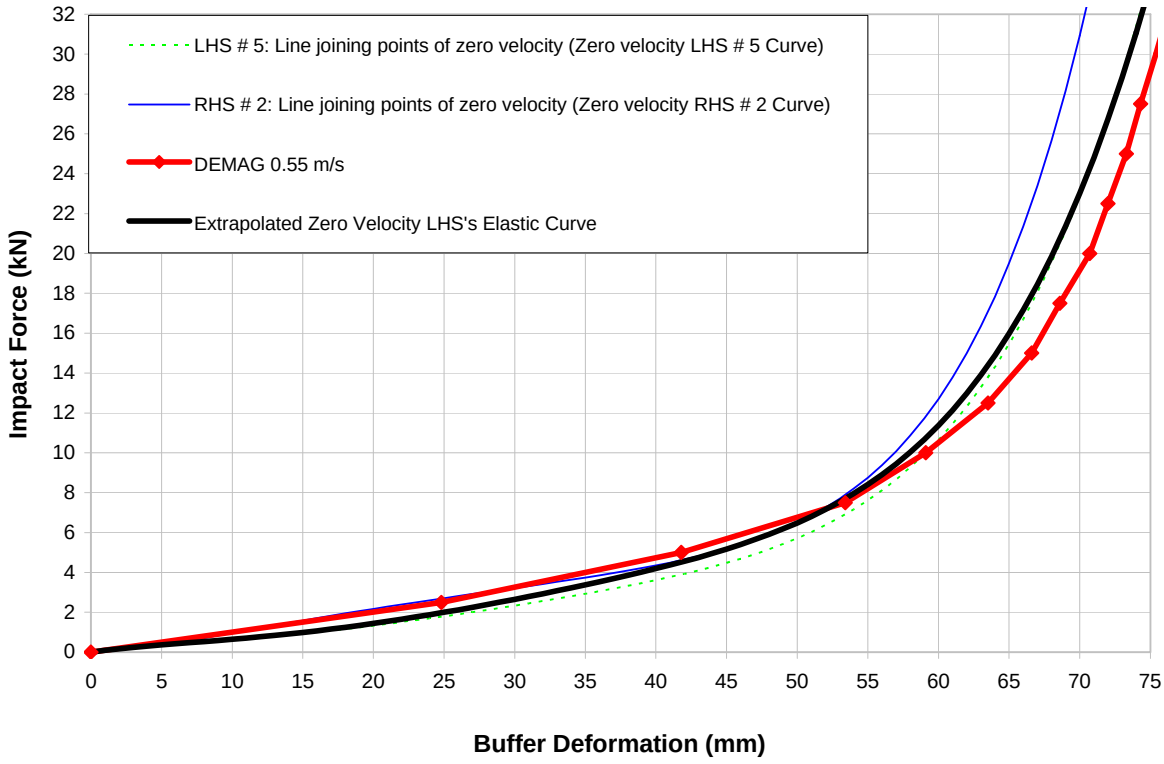

Figure 3.19.1.2 Comparison between DEMAG and the lines joining the points of zero velocity of the hysteresis curves' elastic characteristics

The experimental tests and FEA simulations consist of the three unique steps, namely, hoisting of the payload, an acceleration step and an impact step. During the acceleration step, the crane accelerates at 0.2m/s^2 for 2.75s over a distance of 756.25mm. Thus, the elastic properties of the spring must be adjusted to be inactive for the acceleration step, i.e. while the crane is being accelerated the spring compresses without resistance so that the spring can be in continuous contact

with the crane and the end stops. In the adjusted elastic spring element properties, the force remains zero until the spring element is compressed a distance of 756.25mm. The original and adjusted elastic spring element properties are presented in Figure 3.19.1.3.

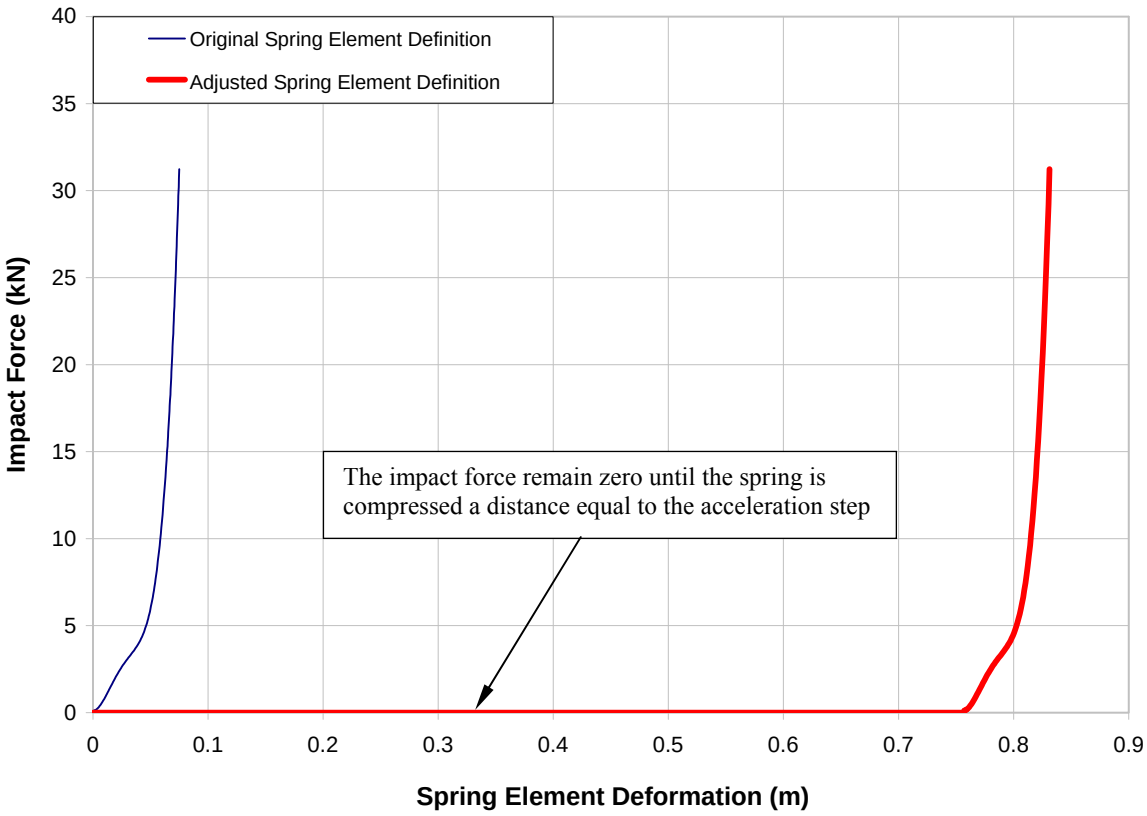

Figure 3.19.1.3 Comparison between original and adjusted FEA spring elastic characteristics

3.19.2 Damping Characteristics of the Crane End Buffers

The damping characteristics of the buffers are extremely important in determining the energy absorption and buffer forces during impact. Without the correct damping characteristics, it is impossible to correctly simulate the impact response during a collision between the crane and the end stops. Figure 3.19.2.1 shows the first cycle of the hysteresis curve of the impact force vs. end buffer deformation of the buffer LHS # 5. The extrapolated "zero velocity" LHS elastic curve is also superimposed on Figure 3.19.2.1. If no damping characteristics are specified, the loading and unloading cycle will follow the same path along the spring element's elastic curve.

The damping force for the loading cycle is the positive difference between the loading cycle of the hysteresis curve (top thin line in Figure 3.19.2.1) and the elastic curve at specific positions along

the loading cycle. If the unloading cycle is not specified, the return curve will follow the same path as the loading curve. Thus, it is imperative that the unloading damping characteristics also be specified. The damping force for the unloading cycle is the negative difference between the loading and unloading cycle of the hysteresis curve (top and bottom thin lines in Figure 3.19.2.1).

Table 3.19.2.1, presents the damping characteristics for the loading and unloading cycles, as obtained from the Figure 3.19.2.1.

Table 3.19.2.1 The damping characteristics for the loading and unloading cycles, as obtained from the Figure 3.19.2.1

Damping for the Loading Characteristics		
Damping Force (N)	Velocity (m/s)	Relative Position (mm)
0	0.550	0
783	0.500	16
957	0.458	32
826	0.385	41
783	0.355	43
696	0.294	47
652	0.227	50
739	0.149	53
695	0.083	54
609	0.006	55

Damping for the Unloading Characteristics	
Damping Force (N)	Velocity (m/s)
1347	-0.049
1303	-0.111
1303	-0.150
1260	-0.224
1217	-0.295
1130	-0.359
1087	-0.399
957	-0.431
739	-0.443

It is critical that the damping characteristics of the buffer in the FEA model are modelled correctly. Although obvious, if the damping characteristics of the buffers are incorrectly modelled this could lead to the end buffer forces being either under or over estimated. Therefore the damping characteristics of the end buffer during the hoisting, acceleration and impacts must be correctly modelled. The damping characteristics of the end buffers during the hoisting of the payload and the acceleration phase of the crane are zero. The damping of the end buffers are activated from the

moment the end buffers collide into the end stops and deactivated once the end buffers loose contact with the end stops. Thus a viscous damping model is not sufficient to describe the loading damping characteristics which are velocity, displacement and force dependent. The loading damping characteristics were modelled using the damping force, velocity and displacement data obtained from a representative experimental test.

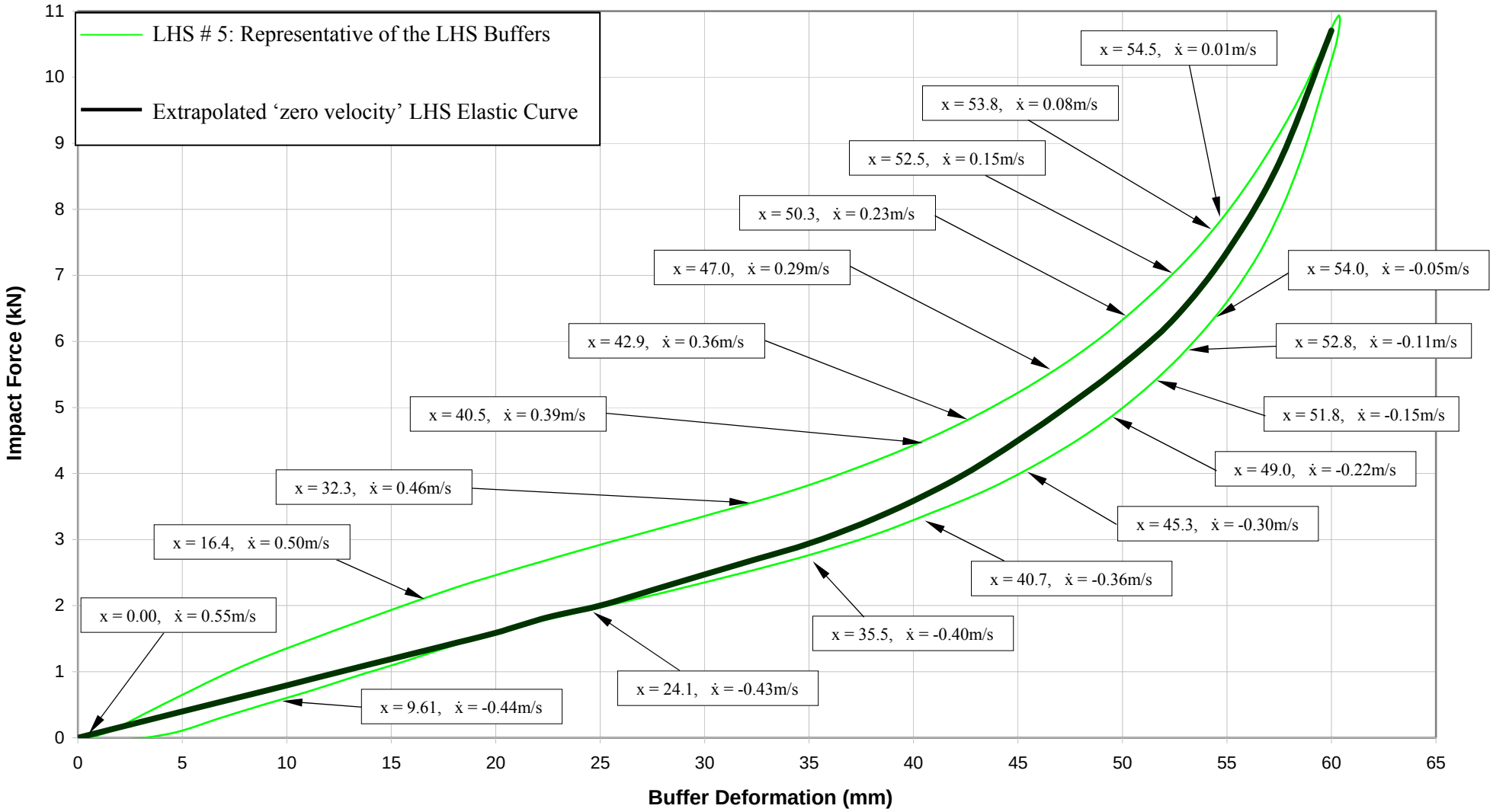

Figure 3.19.2.1 First cycle of the hysteresis curve of the impact force vs. end buffer deformation of the buffer LHS # 5

CHAPTER 4: FEA MODEL CALIBRATION

4.1 Introduction

Before any simulations could be conducted it was necessary to calibrate the FEA model to the experimental tests. All the experimental tests were performed by De Lange [1.6]. The purpose of this chapter is to explain how the FEA model was calibrated to the experimental tests.

Figure 4.1.1 presents the experimental end buffer impact force vs. time when the crane without payload collides into the end stops. For the above condition, only one impact is expected when the crane without payload collides into the end stops. Figure 4.1.1 clearly shows that two additional peaks follow the first peak. The additional peaks are due to the variably-adjusted step-down torque which is present in the drive motors for the longitudinal motion of the crane after the operator releases the longitudinal acceleration button at the moment of impact. The variably-adjusted step-down torque function allows the torque to be adjusted (increased or decreased) over a set period of time. The impact force response is also affected by the disc brakes which engage the moment the operator releases the longitudinal acceleration crane motor button. These experimental tests are here classified as "'Power-Off' with residual torque".

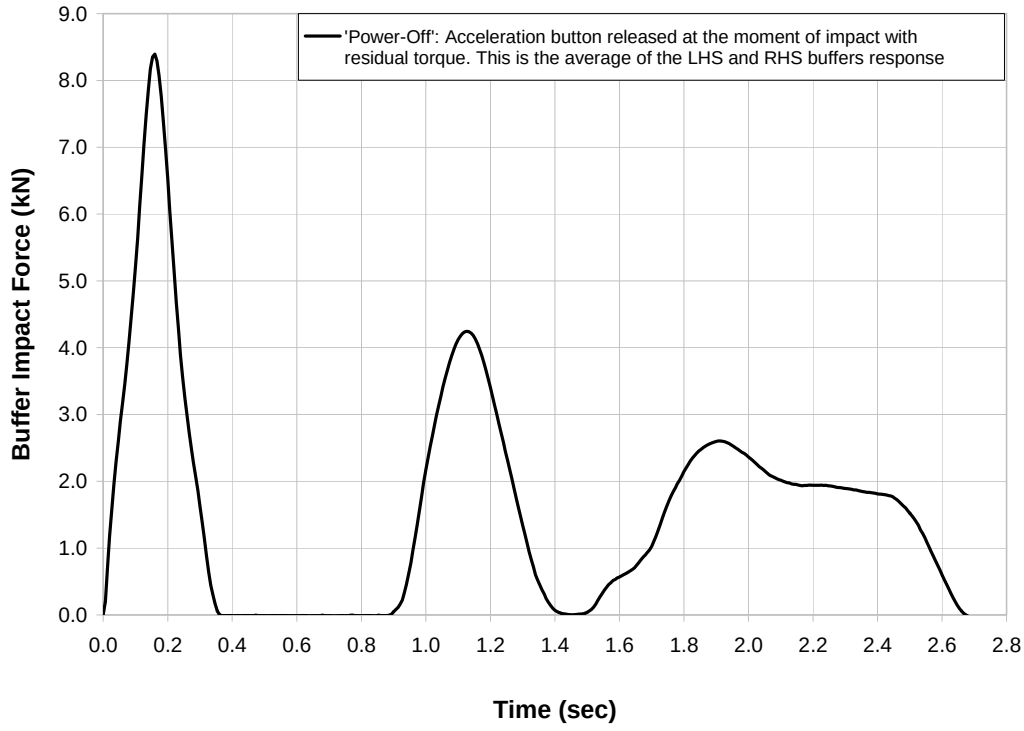

Figure 4.1.1 End buffer impact force response when the crane collides into the end stops for the "'Power-Off' with residual torque" tests without the payload attached.

The "'Power-Off' with residual torque" tests were compared with the same experimental configuration "Power-On" tests to determine the effect of the residual torque. The "Power-On" tests are defined when the crane collides into the end stops with the drive motors for the longitudinal motion of the crane fully engaged over a set period of time. Figure 4.1.2 presents the comparison of the experimental tests for the "'Power-Off' with residual torque" and "Power-On" conditions. The difference between the magnitudes of the first peaks is 7.3%, while the second peaks differ by 14.2%. This implies that the "'Power-Off' with residual torque" tests behave in a similar manner to that of the "Power-On" tests. Thus, the residual torque and the effect of the brake have a significant influence on the impact response.

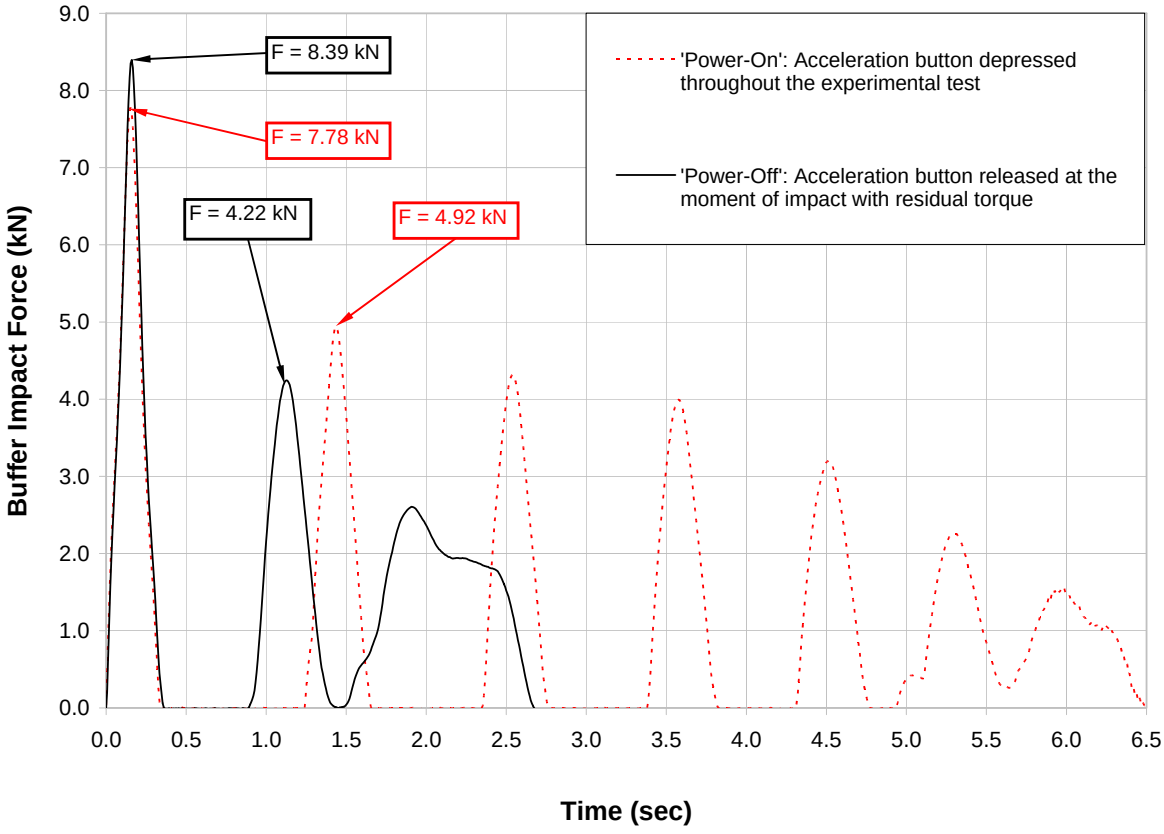

Figure 4.1.2 Comparison of the end buffer impact force response between the "'Power-Off' with residual torque" and "Power-On" experimental tests.

Another set of experimental tests were conducted by disengaging the residual torque function and disc brakes to eliminate their effect on the impact response. These tests are referred to as "'Power-Off' no residual torque". As expected only one impact occurs since there is no residual torque to drive the crane back into the end stops. As expected the first impact force is also 14.5% less than "'Power-Off' with residual torque". Figure 4.1.3 presents a comparison of the experimental

"'Power-Off' with residual torque", "'Power-Off' no residual torque" and "Power-On" tests.

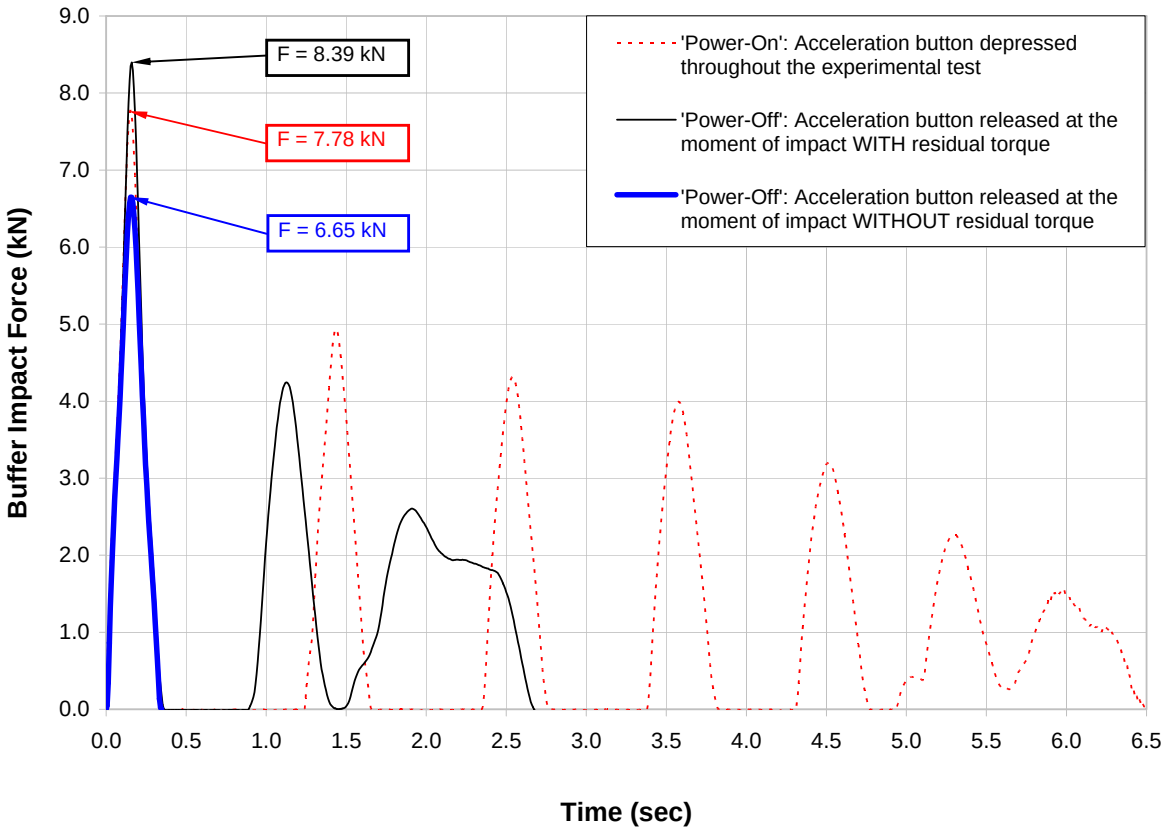

Figure 4.1.3 Comparison of the end buffer impact force response between the "'Power-Off' with residual torque", "Power-On" and "'Power-Off' without residual torque" experimental tests.

The FEA model was calibrated to the "'Power-Off' without residual torque" experimental tests to eliminate any uncertainty which the residual torque may cause.

4.2 Experimental Test Configurations

The experimental tests were repeated 3 times for each test configuration to reduce variance. All the experimental tests were performed under the following conditions:

(i) For the "'Power-Off' without residual torque" scenario, i.e. the end buffers collide with the end stops without any additional torque being transferred to the wheel and the disc brakes are disengaged from the moment of impact.

(ii) The crane accelerates at $0.2m/s^2$ over 2.75s to attain a speed of 0.55m/s.

(iii) The payload was symmetrically positioned on the crane bridge for the tests which required the payload.

(iv) The payload was at rest and in a stationary position at the start of the experimental tests (i.e. no vertical or horizontal oscillations of the payload).

(v) No horizontal longitudinal restraint was placed on the payload thus allowing the payload to oscillate during the acceleration and impact phases of the experimental tests.

(vi) No longitudinal misalignment of one of the end stops was considered for the basic experimental tests and FEA simulations.

4.3 FEA Model Calibration to Experimental Tests

4.3.1 Crane Impact without Payload Attached to the Crane Bridge: "'Power-Off' without residual torque"

The first set of experimental impact tests was performed on the crane without the payload while the crab was symmetrically positioned on the crane bridge, for the conditions stated in 4.2. The average of the three experimental impact force vs. time responses was obtained and is presented in figure 4.3.1.1.

The FEA simulations were obtained using the simplifications discussed in Chapter 3: Finite Element Modelling, by omitting all the irrelevant elements, i.e. payload, cables, pulley, etc. The FEA end buffer impact response simulation is superimposed on figure 4.3.1.1.

The FEA simulations yield an impact force of 6.6kN at 0.149s, while the experimental tests yield an impact force of 6.5kN at 0.153s. The difference between the impact forces is less than 2%, thus the FEA simulations provide a good correlation with the experimental response. The FEA simulation shows a better correlation for the compression phase of the end buffers compared to the relaxation phase of the end buffers.

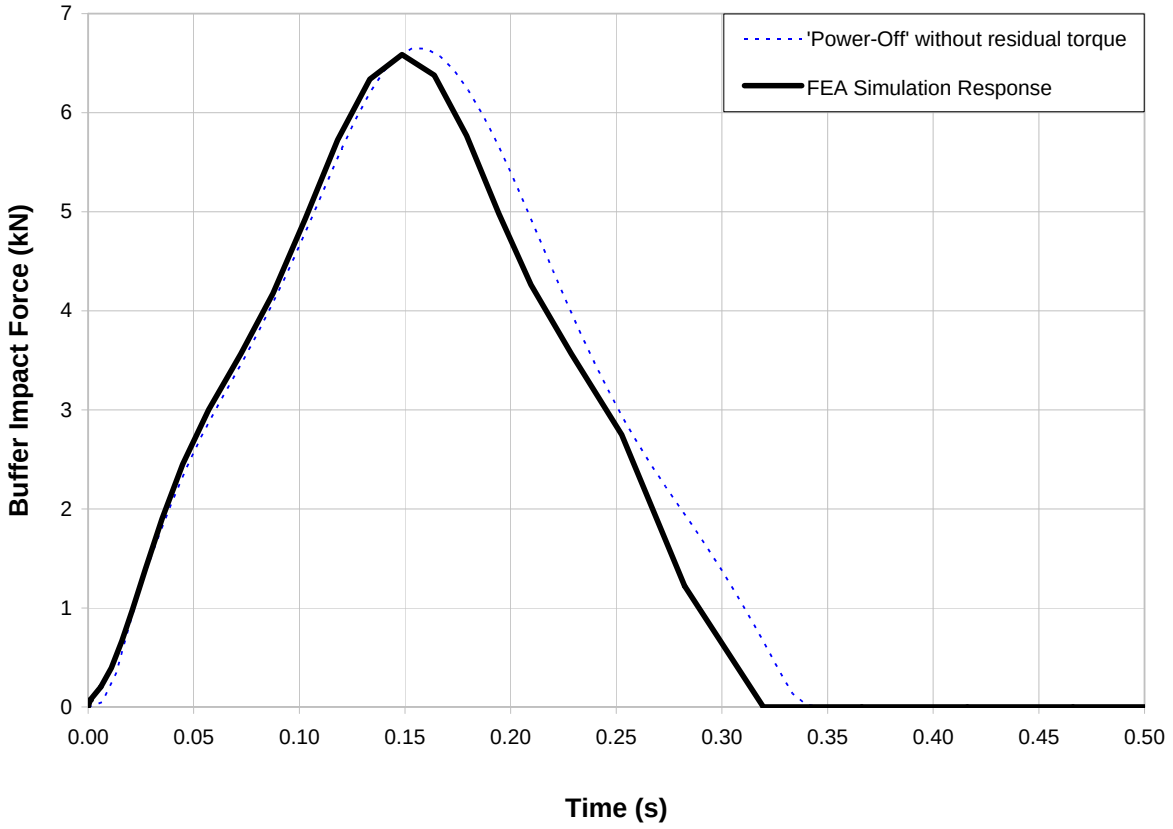

Figure 4.3.1.1 Comparison of the end buffer impact force response for the experimental "'Power-Off' without residual torque" and FEA simulation without payload is attached to the crane bridge

4.3.2 Crane Impact <u>with</u> Payload Hoisted to 0.15m above Ground Level: "'Power-Off' without residual torque"

The experimental tests were performed for the above configuration in conjunction with the conditions described in 4.2. The payload was hoisted to 0.15m above ground level, which resulted in the top surface of the payload being 3.22m below the crane bridge. The average of the three (3) experimental test responses for the "'Power-Off' without residual torque" is presented in figure 4.3.2.1. After the first impact the end buffers lose contact with the end stops for 0.42s before impacting the end stops for two consecutive collisions. The 2nd and 3rd impacts are due to the payload's inertia yanking the crane back into the end stops. The entire duration of the impact sequence is approximately 1,85s. The experimental responses resulted in three impacts which occur at 0.17s, 1.02s and 1.69s with magnitudes of 6.68kN, 4.47kN and 1.48kN respectively.

The FEA simulation of the experimental configuration is superimposed on figure 4.3.2.1. The FEA simulations follow the same trend as the experimental response with slight discrepancies. The FEA simulations resulted in three impacts which occur at 0.15s, 0.88s and 1.48s with magnitudes of 6.35kN, 4.43kN and 2.61kN, respectively.

In the FEA simulations the end buffers make contact with the end stops at 0.63s while in the experimental tests this occurs at 0.77s. The negative shift of 0.14s of the FEA simulations is carried throughout remaining response. The discrepancy could be due to a number of parameters which is tabulated and compared in Table 4.3.2.1.

Table 4.3.2.1 Comparison of the parameters which could substantially affect the impact response

Parameters	Experimental Configuration	FEA Configuration
Horizontal payload lag with respect to the crane bridge at the moment of impact	Not measured	Known Lag Angle = 0^0
Crab position on the crane bridge	At Midspan (1)	At Midspan
End stop misalignment of the end stops in relation to each other	No Misalignment (1)	No Misalignment
Crane supporting structure's flexibility during impact	Not Measured	Known from FEA simulations
Crane speed at the moment of impact	0.55m/s (1)	0.55m/s
Buffer's elastic characteristics	Identical for both buffers (1)	Identical for both buffers
Buffer's damping characteristics	Identical for both buffers (1)	Identical for both buffers
Release of the longitudinal acceleration button at the moment of impact	Done by operator, varies significantly	Exact, released at the moment of impact
Note: (1) The values of the experimental parameters are within the measurement tolerances applicable to the specific parameter		

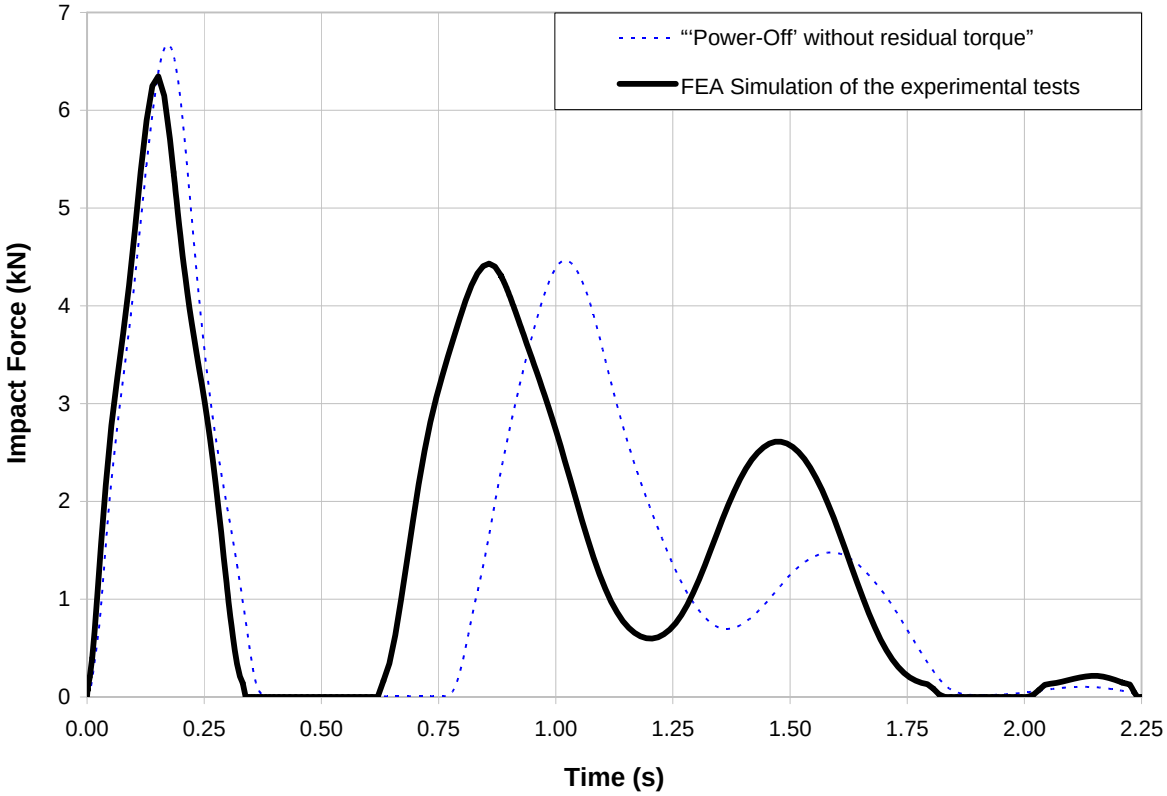

Figure 4.3.2.1 Comparison of the end buffer impact force response for the experimental "'Power-Off' without residual torque" tests and FEA simulation when the payload is 0.15m above ground level

4.3.3 Crane Impact with Payload Hoisted to 2.20m above Ground Level: "'Power-Off' without residual torque"

The experimental tests were performed for the above configuration in conjunction with the conditions described in 4.2. The payload was hoisted to 2.20m above ground level, , which resulted in the top surface of the payload being 1.37m below the crane bridge. The average of the three (3) experimental test responses for the "'Power-Off' without residual torque" is presented in figure 4.3.3.1. The end buffers stay in contact with the end stops for the entire duration of the impact tests. The entire duration of the impact lasts approximately 1.41s, almost a quarter of the time less compared to the tests when the payload is hoisted to 0.15m above ground level. The experimental responses resulted in three impacts which occur at 0.16s, 0.73s and 1.04s with magnitudes of 7.08kN, 2.74kN and 3.89kN, respectively. Surprisingly the second impact is smaller than the third impact. A possible reason for the above could be the cancellation of modes as the crane is propelled backward while the payload moves forward especially when the cables are shorter.

The FEA simulation of the experimental configuration is superimposed on figure 4.3.3.1. The FEA simulation predicts the first impact reasonably accurately, where after the FEA simulations deviates substantially from the experimental test responses. The FEA simulations resulted in three impacts which occur at 0.16s, 0.75s and 1.30s with magnitudes of 6.59kN, 6.88kN and 2.37kN respectively. In the FEA simulations the end buffers lose contact with the end stops for 0.12s after the first impact.

The magnitude and occurrence of the first peak in the experimental tests and FEA simulation shows a difference of +7.4% and 0%, respectively. The magnitude and occurrence of the second peak in the experimental tests and FEA simulation show a difference of +39.8% and 2.7%, respectively. The third peaks of the FEA simulation and the experimental tests have no correlation to each other.

Preliminary FEA simulations revealed that the payload lag, the crab position, the end stop misalignment, the crane supporting structure's flexibility, the crane speed, the buffer's elastic characteristics, the buffer's damping characteristics, the cable length and the release of the longitudinal acceleration button at the moment of impact have a significant influence on the impact response. The length of the cables plays a crucial role in the impact response, especially when the cables are short.

Together with the factors presented in Table 4.3.2.1, the modes of vibration, especially the lower modes, could also cause variations which could completely alter the response of the system. Modal Analysis and Modal Superposition were conducted and discussed in chapter 5 to determine whether any of the modes have a significant effect on the impact response. Similarly, a sensitivity analysis was conducted in chapter 6 to determine the effect on the impact response when the variables are adjusted.

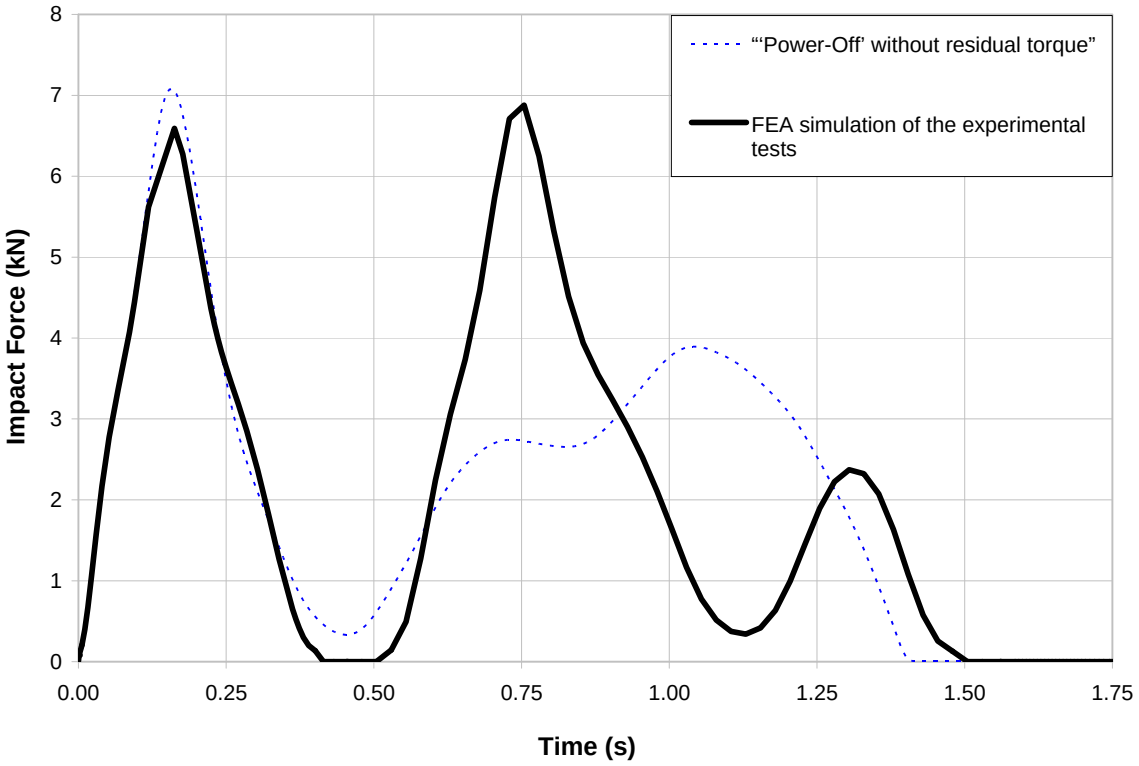

Figure 4.3.3.1 Comparison of the end buffer impact force response for the experimental complete "'Power-Off' without residual torque" and FEA simulation when the payload is 2.20m above ground level

4.3.4 Crane Impact without Payload: "Power-ON"

The experimental tests without payload and with "Power-ON" were performed in conjunction with the conditions described in 4.2. For these tests the two horizontal drive motors for the longitudinal motion of the crane which produce 55kW were engaged throughout the experimental tests. For safety reasons, the experimental tests were performed without the payload. These tests are referred to as "Power-On". The average of the three (3) "Power-On" experimental test responses is presented in figure 4.3.4.1.

The experimental tests were conducted over a period of 6.5s. The first impact force increases by 16.5% when the "Power-On" tests are compared to "'Power-Off' no residual torque". An interesting observation of the "Power-On" tests is that the time to the second peak is substantially delayed and occurs at approximately 1.45s from the start of the tests. The time to the second impact occurs at 1.02s and 0.75s when the payload is 0.15m and 2.20m above ground level. The delay in

the second impact could be as a result of the wheels losing traction with the railhead (spinning effect) and also the lifting of the driving wheels when the crane moves backward.

The FEA "Power-On" simulation without payload is superimposed on figure 4.3.4.1. The same FEA model used in section 4.3.1 will be used for the current FEA simulations, except that modifications need to be introduced for the constantly running electric motors. It is impossible to accurately simulate the spinning and loss of contact of the conventional experimental wheels due to the "skis" approach implemented in the FEA model. Thus, a simplification was introduced to model the loss of contact and spinning of the motorised conventional experimental wheels. The constantly running motors of 55 kW produces a force of 550N given the dimensions of the wheels. This force was applied to the back skis of the crane. A time dependent amplitude function was used together with the applied force to model the loss of contact and the spinning of the conventional wheels. During the forward motion of the crane the force amplitude was given a value of 550N. To account for the slipping and loss of contact of the conventional wheels the force amplitude during the reverse motion was adjusted and assigned a value of between 550×0.45 and 550×0.65. There is a good correlation between the experimental test responses and FEA simulation responses.

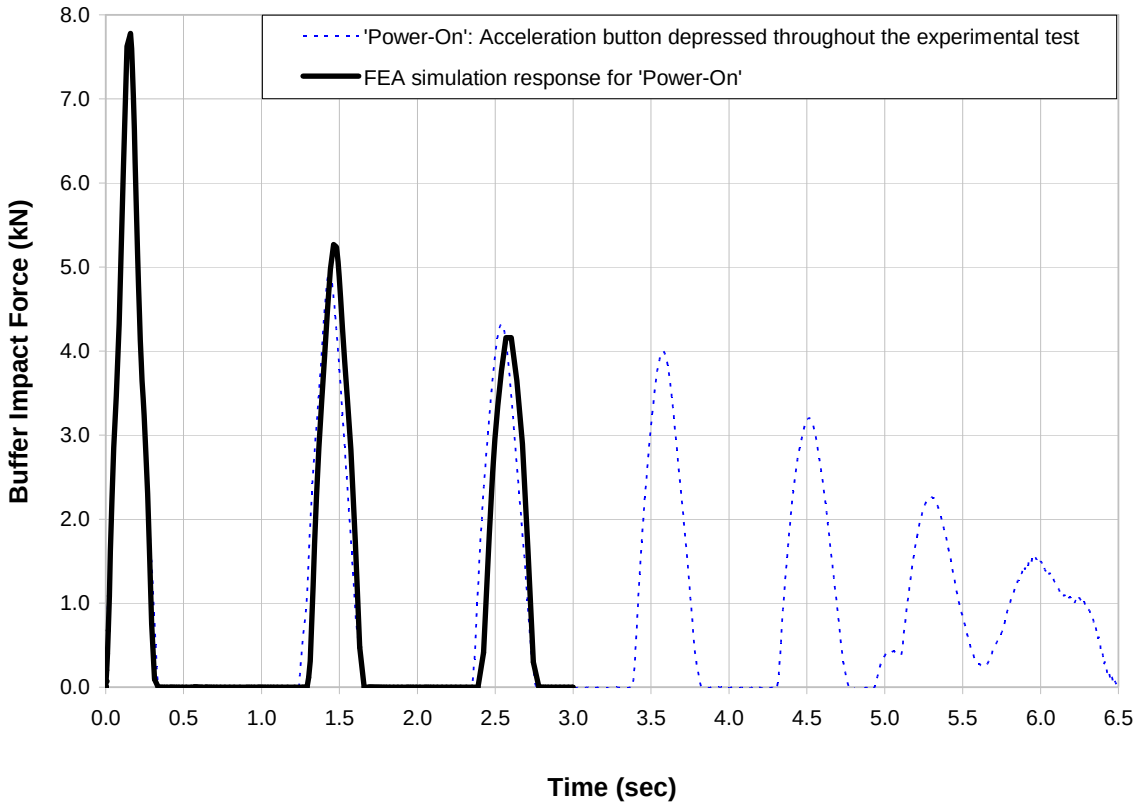

Figure 4.3.4.1 Comparison of the end buffer impact force response for the experimental "power-on" and FEA simulation without payload

4.4 Conclusion

Calibrating the FEA model to the experimental results proved more challenging than expected, especially when the payload was hoisted 2.20m above the ground. This was a result of the many complex phenomena as specified in Table 4.3.2.1, which has a significant influence on the impact response. The preliminary FEA simulations provided useful insight into the behaviour of the impact response when the parameters are adjusted.

An exact match could have been achieved through extensive “tweaking” of the FEA model. This was eventually abandoned as irrelevant since parameters obtained for the exact match would be for a particular situation only, i.e. the parameters would differ when the payload is positioned at different places. The effect of the varying the parameters in the FEA simulations responses is investigated in detail in the sensitivity study.

CHAPTER 5 : MODAL ANALYSIS AND MODAL SUPERPOSITION

5.1 Introduction

The initial FEA simulations yielded end buffer responses which were significantly different from the experimental test responses as the payload was hoisted closer to the crane bridge. To gain better insight into the response of the individual components of the FEA model, modal analysis and modal superposition were performed on only the crane with all relevant components with the payload. The modal analysis was used to determine the mode shapes which contribute significantly toward the horizontal longitudinal displacements of the crane buffers. The data from the modal analysis was used to perform the modal superposition to determine the effect of the various modes of vibration's contribution to the total response. The reason for using the modal analysis and modal superposition methods is to investigate whether the higher modes of vibration have a "chaotic" effect on the total response of the system.

5.1.1 Chaos Theory

Since "Chaos" theory is not part of the general vocabulary of civil engineering practioners it will be briefly explained. Chaos theory can be defined as the study of dynamic systems that shows a strong sensitivity to initial conditions, sometimes referred to as the butterfly effect.

The following is an example to illustrate the effect of small events on the total systems response. Consider a tennis ball being dropped onto an oscillating tennis racket. The response of the tennis ball will be very different depending on the position in which the tennis ball strikes the racket. The amplitude of the tennis ball will be amplified if the ball strikes the racket during the positive phase of an oscillation. The positive phase of an oscillation is when the racket moves toward the falling ball. The amplitude of the tennis ball will be reduced if the ball strikes the racket during the negative phase of an oscillation.

Thus, the frequency oscillations of the crane bridge are much greater compared to the payload's oscillations. The effect of the oscillatory position of the crane bridge, the position of the crane with relation to the payload, etc., can have a significant effect on the total response of the crane displacement and velocity responses.

5.2 Modal Analysis

5.2.1 Modal Analysis Theory

A brief review of the theory of modal analysis is presented.

The natural frequencies $(\boldsymbol{\omega})$ for a multiple undamped DOF system is given by equation 5.2.1.1,

$$\det \left| \overline{\overline{K}} - \omega^2 \times \overline{\overline{M}} \right| = 0 \qquad \textit{(5.2.1.1)}$$

where,

$\overline{\overline{M}}$ and $\overline{\overline{K}}$	are the nodal mass and stiffness matrices
ω's	are the natural frequencies

The linearised differential equation of motion for the FEM discretisation is presented in equation 5.2.1.2,

$$\overline{\overline{M}} \times \ddot{\overline{x}}(t) + \overline{\overline{C}} \times \dot{\overline{x}}(t) + \overline{\overline{K}} \times \overline{x}(t) = \overline{R}(t) \qquad \textit{(5.2.1.2)}$$

where,

$\overline{\overline{C}}$	is the damping matrix
$\overline{R}(t)$	is the consistent force vector
$\ddot{\overline{x}}(t)$, $\dot{\overline{x}}(t)$ and $\overline{x}(t)$	are the nodal acceleration, velocity and displacement vectors

The linearised nodal DOF in equation 5.2.1.2 are transformed to the linearised modal differential equation presented in equation 5.2.1.3,

$$\overline{\overline{M}}^* \times \ddot{\overline{y}}(t) + \overline{\overline{C}}^* \times \dot{\overline{y}}(t) + \overline{\overline{K}}^* \times \overline{y}(t) = \overline{R}^*(t) \qquad \textit{(5.2.1.3)}$$

where,

$\overline{\overline{M}}^*$, $\overline{\overline{C}}^*$ and $\overline{\overline{K}}^*$	are the modal mass, damping and stiffness matrices
$\overline{R}^*(t)$	is the modal force vector
$\ddot{\overline{y}}(t)$, $\dot{\overline{y}}(t)$ and $\overline{y}(t)$	are the modal acceleration, velocity and displacement vectors

To obtain the modal mass, modal damping and modal stiffness matrices, the mass, damping and stiffness matrices are pre-multiplied by the transpose of the mode shape matrix and post multiplied by the mode shape matrix as shown in equations 5.2.1.4, 5.2.1.5 and 5.2.1.6. This results in the modal mass and modal stiffness matrices being diagonalised, i.e. the matrices only have terms on the diagonal with all other non-diagonal terms being equal to zero. This allows the modes to be decoupled from each other, studied individually and combined when necessary. The modal force is obtained by pre-multiplying the transpose of the mode shape matrix with nodal force vector as presented in equation 5.2.1.7.

$$M^{*} = \Phi^{T} \times M \times \Phi \qquad (5.2.1.4)$$

$$C^{*} = \Phi^{T} \times C \times \Phi \qquad (5.2.1.5)$$

$$K^{*} = \Phi^{T} \times K \times \Phi \qquad (5.2.1.6)$$

$$R^{*}(t) = \Phi^{T} \times R(t) \qquad (5.2.1.7)$$

The relationship between the nodal DOF and the modal DOF is given by equation 5.2.1.8,

$$\bar{x}(t) = \bar{\bar{\Phi}} \times \bar{y}(t) \qquad (5.2.1.8)$$

Finally the reaction forces can be obtained from equation 5.2.1.7 which is presented in equation 5.2.1.9,

$$\bar{R}^{*}(t) = \Phi^{T}_{i\ (Left)} \times \bar{R}_{Left}(t) + \Phi^{T}_{i\ (Right)} \times \bar{R}_{Right}(t) \qquad (5.2.1.9)$$

5.2.2 Modal Analysis Results

The modal analysis was performed on the crane with the payload without the crane supporting structure as shown in Figures 5.2.2.1 and 5.2.2.2. The wheels were restrained against vertical translation, while all other DOF's were unrestrained. The Rotational Moment of Inertias (RMOI's) of the payload were determined and included in the modal analysis as the payload has significant rotation during impact.

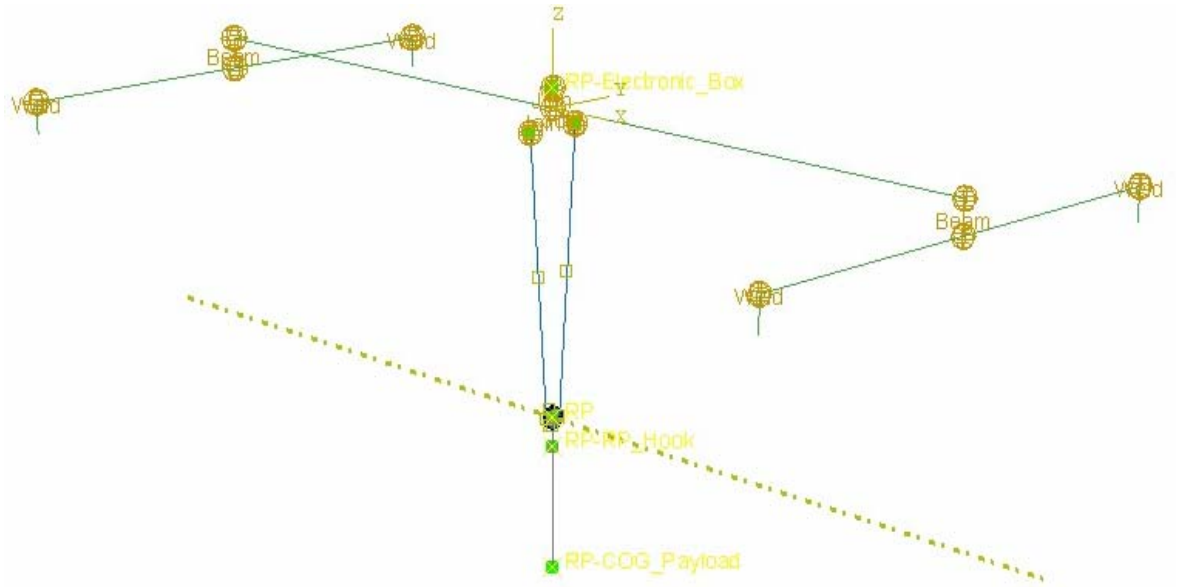

Figure 5.2.2.1 FEA representation of the crane with the payload hoisted 0.15m above GL

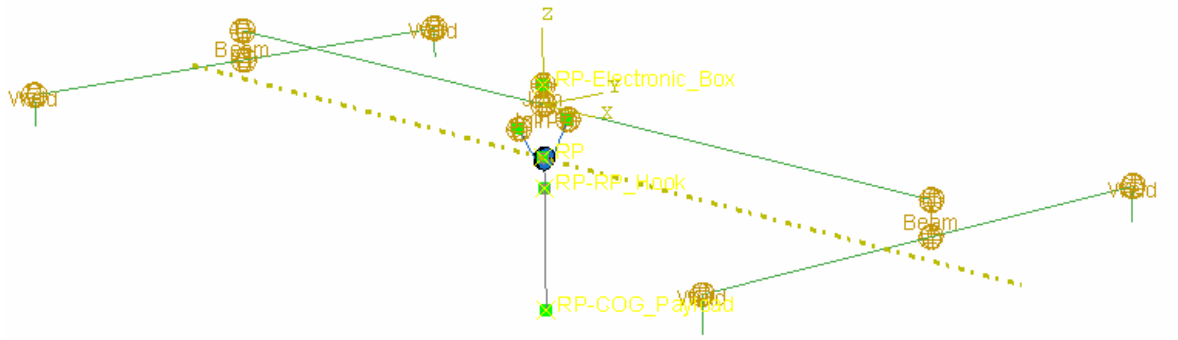

Figure 5.2.2.2 FEA representation of the crane with the payload hoisted 2.20m above GL

Tables 5.2.2.1 and 5.2.2.2 list the modal analysis results for the modes with significant longitudinal displacements for the given payload configuration when the payload is hoisted to 0.15m and 2.20m above ground level. The mode shapes, Φ_{LHS} and Φ_{RHS}, were interpreted from the modal analysis for the respective modes with the corresponding natural frequencies. Modal analysis results were obtained using ABAQUS.

Table 5.2.2.1 Modal analysis results when the payload is hoisted 0.15m above ground level

Mode #	Mode Description	Mode Shape Φ_{LHS} of End Carriage	Mode Shape Φ_{RHS} of End Carriage	Natural Frequency $\boldsymbol{\omega}$ (rad/sec)	Modal Mass $\mathbf{M}^*$ (kg)	Modal Stiffness $\mathbf{K}^*$ (kg.rad^2/sec^2)
1	Rigid Body: Horizontal Longitudinal	1.000	1.000	0	7227	0
2	Payload Oscillations	0.968	0.968	3.285	2684	28965
3	Hook + Half Sine Crane Bridge Oscillations	-0.417	-0.417	49.863	566	1406784
4	Pulley + Half Sine Crane Bridge Oscillations	0.110	0.110	111.09	125.3	1546449
5	Full SINE Bending of Crane Bridge	-0.216	-0.216	153.18	457.8	10741401

Table 5.2.2.2 Modal analysis results when the payload is hoisted 2.20m above ground level

Mode #	Mode Description	Mode Shape Φ_{LHS} of End Carriage	Mode Shape Φ_{RHS} of End Carriage	Natural Frequency $\boldsymbol{\omega}$ (rad/sec)	Modal Mass $\mathbf{M}^*$ (kg)	Modal Stiffness $\mathbf{K}^*$ (kg.rad^2/sec^2)
1	Rigid Body: Horizontal Longitudinal	1.000	1.000	0	7218	0
2	Payload Oscillations	0.972	0.972	4.916	2727	65904
3	Hook + Half Sine Crane Bridge Oscillations	-0.388	-0.388	49.124	925	2231842
4	Pulley + Half Sine Crane Bridge Oscillations	0.200	0.200	51.166	477	1247693

5.3 Modal Superposition

The modal analysis data (mode shapes, natural frequencies, modal masses and modal stiffness) with the 1st experimental impact force vs. time response was required to perform the modal superposition. The averages of the experimental impact force vs. time responses were obtained due to the variations in the 1st impact responses when the payload was hoisted 0.15m and 2.20m above ground level as presented in figure 5.3.1. The modal history responses were obtained using equation 5.2.1.3.

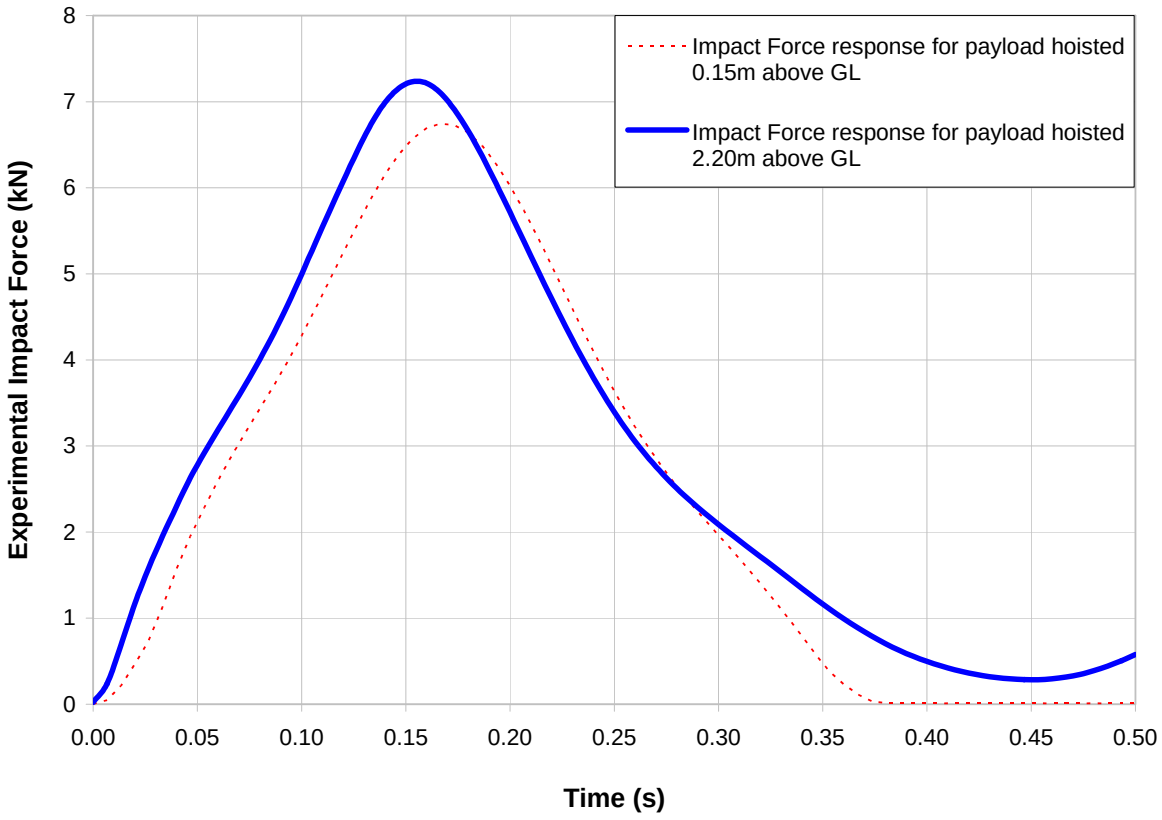

Figure 5.3.1 1st Experimental impact response when the payload is hoisted 0.15m and 2.20m above ground level.

The modal superposition method was performed using the Unit Impulse method and verified by the Direct Integration Method.

5.3.1 Modal Superposition by the Unit Impulse Method

For simplification, the load history of the impact responses shown in figure 5.3.1 can be approximated by an Impulse response. The magnitude of the impulse was obtained by determining the area under the force vs. time responses shown in Figure 5.3.1. The areas under the force vs. time responses are 1248.1Ns and 1409.0Ns for the 0.15m and 2.20m cases respectively. The impulse force is applied at the peak amplitude at t = 0.167s and t = 0.16s when the payload is hoisted 0.15m and 2.20m above ground level.

The displacement and velocity responses can be obtained from closed form solutions for each modal DOF. The displacement response for the Unit Impulse was obtained from Meirovitch [5.1] which is presented by equation 5.3.1.1. The velocity response was obtained by differentiation and is presented in equation 5.3.1.2.

The nodal loads must be transformed into the modal loads using equation 5.2.1.8. The rotational modes of vibration's responses are zero as the mode shapes have opposite signs and thus the impulse force equals zero.

$$x(t) = \frac{1}{m \times \omega_d} \times \left\{ e^{(-\xi \times \omega_n \times t)} \times \sin(\omega_d \times t) \right\} \qquad \begin{array}{l} \text{for } t>0, \\ \text{for } t<0, \quad x(t) = 0 \end{array} \qquad \textit{(5.3.1.1)}$$

$$\dot{x}(t) = \frac{d}{dt} \left\{ x(t) \right\}$$

$$\dot{x}(t) = \frac{1}{m \times \omega_d} \times \left\{ \begin{array}{l} -\xi \times \omega_n \times e^{(-\xi \times \omega_n \times t)} \times \sin(\omega_d \times t) \\ + \; e^{(-\xi \times \omega_n \times t)} \times \omega_d \times \cos(\omega_d \times t) \end{array} \right\} \qquad \begin{array}{l} \text{for } t>0, \\ \text{for } t<0, \quad x(t) = 0 \end{array} \qquad \textit{(5.3.1.2)}$$

where,

$x(t)$	is the displacement response for an impulse load at a particular time
m	is the modal mass at the corresponding frequency
ω_n	is the undamped natural frequency at the specific mode of vibration
ω_d	is the damped natural frequency at the specific mode of vibration
t	is the time when the response is required.

$\dot{x}(t)$ is the velocity response for an impulse load at a particular time

As mentioned earlier, the purpose of the Modal Analysis and Modal Superposition methods is to determine whether any of the modes of vibration have a chaotic effect on the displacement and velocity responses of the system. The displacement and velocity responses were determined for the modes of vibration shown in Table 5.2.2.1, excluding the rigid body motion of the crane, using equations 5.3.1.1 and 5.3.1.2. The rigid body motion's responses were excluded from the analysis since it would not have a chaotic effect on the system. The individual and superimposed displacement and velocity responses of the modes are presented in Figures 5.3.1.1 through 5.3.1.4 when the payload is hoisted 2.20m above ground level.

The only effect which the rigid body motion's responses would have on the system is to shift the responses and determine the position and maximum velocity of the system. Since this was not the aim of this section, it was ignored.

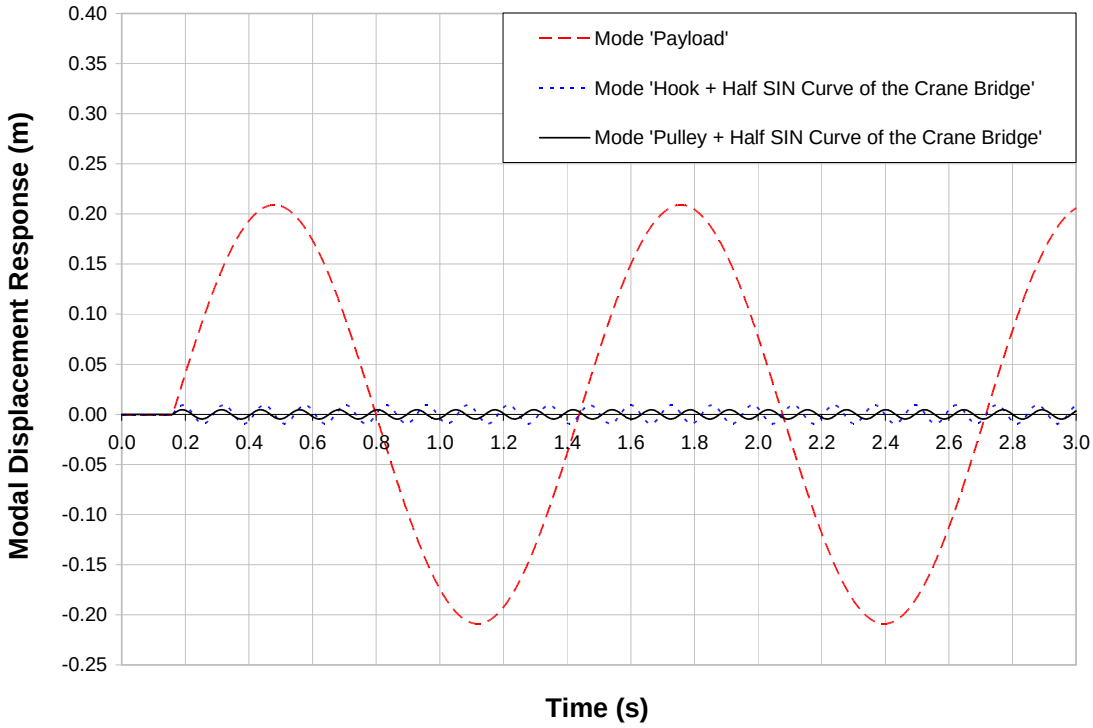

Figure 5.3.1.1 Displacement response of the individual modes of vibration when the payload is hoisted 2.20m above ground level by the Impulse method.

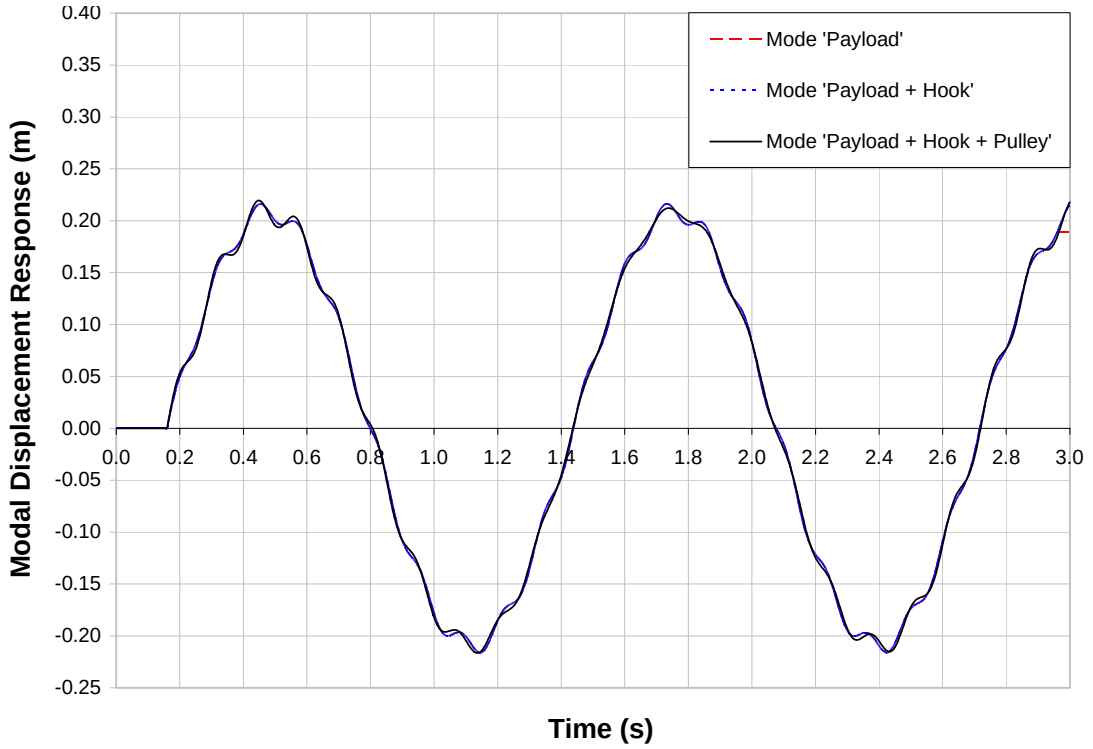

Figure 5.3.1.2 Displacement response of the combined modes of vibration when the payload is hoisted 2.20m above ground level by the Impulse method.

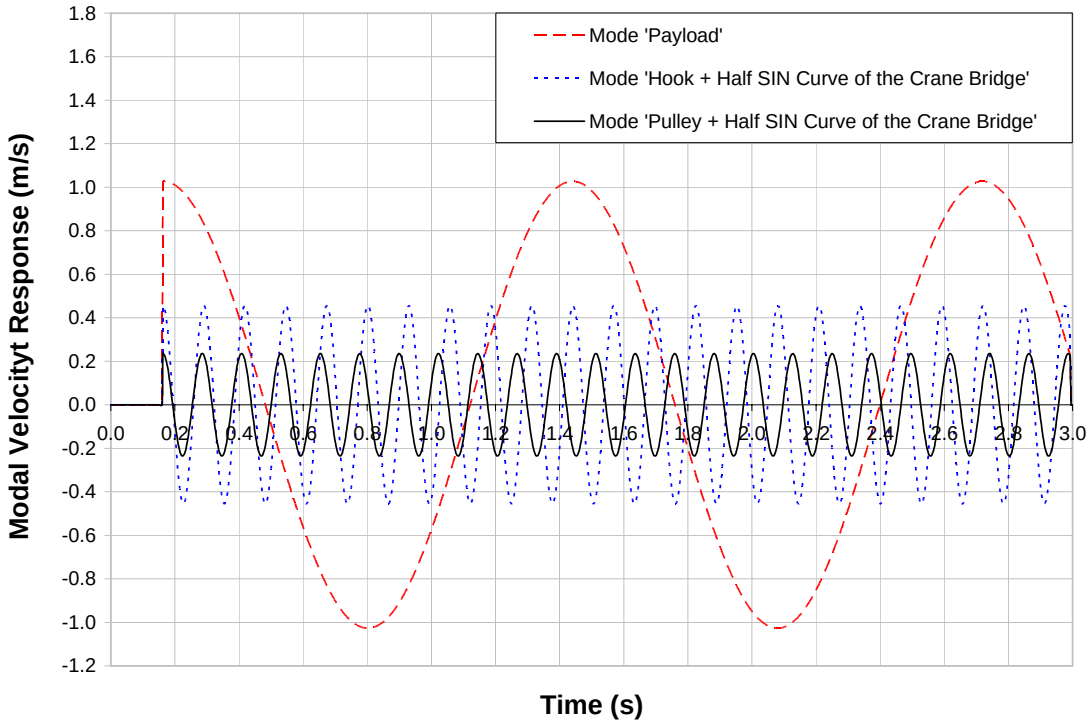

Figure 5.3.1.3 Velocity response of the individual modes of vibration when the payload is hoisted 2.20m above ground level by the Impulse method.

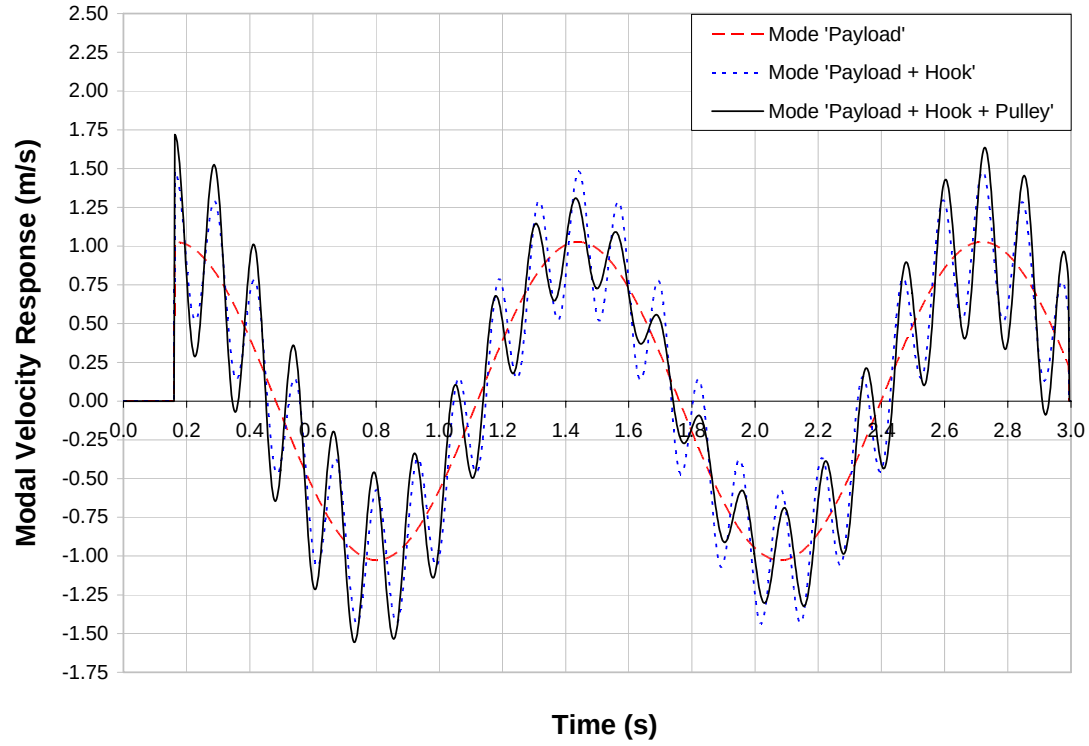

Figure 5.3.1.4 Velocity response of the combined modes of vibration when the payload is hoisted 2.20m above ground level by the Impulse method.

5.3.2 Modal Superposition by the Direct Integration Method

The higher modes of vibration do have a substantial influence on the impact response based on the results of the modal superposition by the Impulse method. The modal superposition by the Direct Integration method will be employed to verify that the higher modes of vibration do have a substantial influence on the impact response. The closed form solutions for the displacement and velocity responses of the Direct Integration method were obtained from Paz [5.2] as presented by equation 5.3.2.1 and 5.3.2.2. The advantage of the Direct Integration method is that it allows for the inclusion of the initial displacement, velocity and force before motion occurs. The solution is exact for an excitation function which is composed of linear segments and when the time steps, (Δt), are chosen such that it does not miss the peaks of the function.

$$x_{i+1} = A_1 \times x_i + B_1 \times \dot{x}_i + C_1 \times F_i + D_1 \times F_{i+1} \qquad (5.3.2.1)$$

$$\dot{x}_{i+1} = A_2 \times x_i + B_2 \times \dot{x}_i + C_2 \times F_i + D_2 \times F_{i+1} \qquad (5.3.2.2)$$

where,

$$A_1 = e^{(-\xi \times \omega_n \times t)} \times \left(\frac{\xi \times \omega_n}{\omega_d} \times \sin(\omega_d \times t) + \cos(\omega_d \times t) \right) \qquad (5.3.2.3)$$

$$B_1 = e^{(-\xi \times \omega_n \times t)} \times \left(\frac{1}{\omega_d} \times \sin(\omega_d \times t) \right) \qquad (5.3.2.4)$$

$$C_1 = \frac{1}{K} \times \left\{ e^{(-\xi \times \omega_n \times t)} \times \begin{bmatrix} \left(\frac{1 - 2 \times \xi^2}{\omega_d \times t} - \frac{\xi \times \omega_n}{\omega_d} \right) \times \sin(\omega_d \times t) \\ -\left(1 + \frac{2 \times \xi}{\omega_n \times t} \right) \times \cos(\omega_d \times t) \end{bmatrix} + \frac{2 \times \xi}{\omega_n \times t} \right\} \qquad (5.3.2.5)$$

$$D_1 = \frac{1}{K} \times \left\{ e^{(-\xi \times \omega_n \times t)} \times \begin{bmatrix} \frac{2 \times \xi^2 - 1}{\omega_d \times t} \times \sin(\omega_d \times t) \\ + \frac{2 \times \xi}{\omega_n \times t} \times \cos(\omega_d \times t) \end{bmatrix} + \left(1 - \frac{2 \times \xi}{\omega_n \times t} \right) \right\} \qquad (5.3.2.6)$$

$$A_2 = -e^{(-\xi \times \omega_n \times t)} \times \left(\frac{\omega_n^{\,2}}{\omega_d} \times \sin(\omega_d \times t) \right) \qquad (5.3.2.7)$$

$$B_2 = e^{(-\xi \times \omega_n \times t)} \times \left(\cos(\omega_d \times t) - \frac{\xi \times \omega_n}{\omega_d} \times \sin(\omega_d \times t) \right) \qquad (5.3.2.8)$$

$$C_2 = \frac{1}{K} \times \left\{ e^{(-\xi \times \omega_n \times t)} \times \left[\left(\frac{\omega_n^{\,2}}{\omega_d} + \frac{\omega_n \times \xi}{t \times \omega_d} \right) \times \sin(\omega_d \times t) + \frac{1}{t} \times \cos(\omega_d \times t) \right] - \frac{1}{t} \right\} \qquad (5.3.2.9)$$

$$D_2 = \frac{1}{K \times t} \times \left\{ e^{(-\xi \times \omega_n \times t)} \times \left[\frac{\omega_n \times \xi}{\omega_d} \times \sin(\omega_d \times t) + \cos(\omega_d \times t) \right] + 1 \right\} \qquad (5.3.2.10)$$

where,

x_i is the initial displacement

$\dot{x}_i$ is the initial velocity

x_{i+1} is the displacement at step t_{i+1}

$\dot{x}_{i+1}$ is the velocity at t_{i+1}

ω_n is the undamped natural frequency at the specific mode of vibration

ω_d is the damped natural frequency at the specific mode of vibration

t is the incremental time step

F_i is the initial force applied before motion occurs

F_{i+1} is the force applied at step t_{i+1}

A_1, B_1, C_1 and D_1 are constants of integration used for the displacement response

A_2, B_2, C_2 and D_2 are constants of integration used for the velocity response

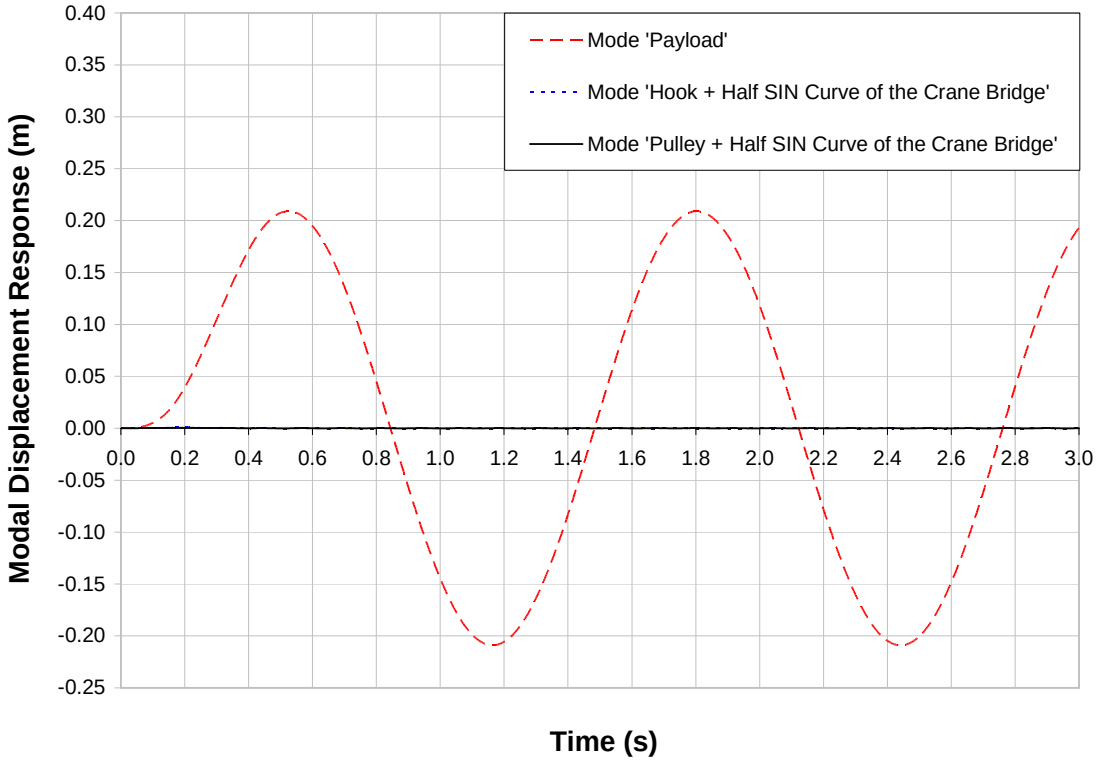

Figure 5.3.2.1 Displacement response of the individual modes of vibration when the payload is hoisted 2.20m above ground level by the Direct Integration method.

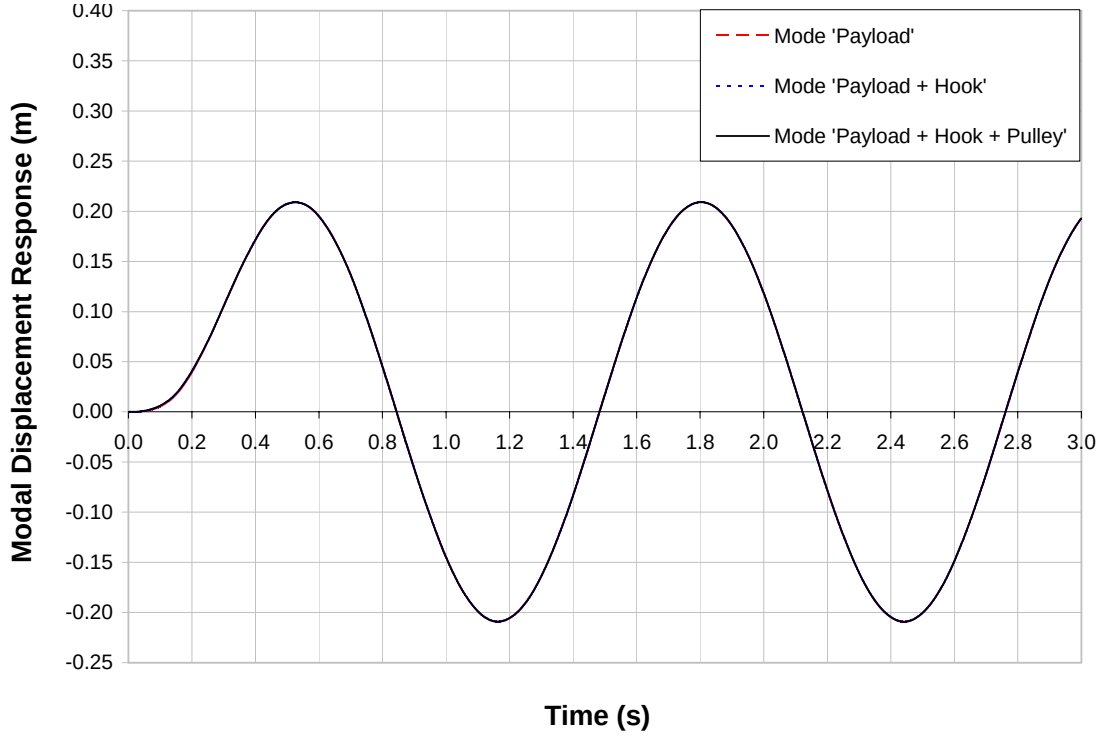

Figure 5.3.2.2 Displacement response of the combined modes of vibration when the payload is hoisted 2.20m above ground level by the Direct Integration method.

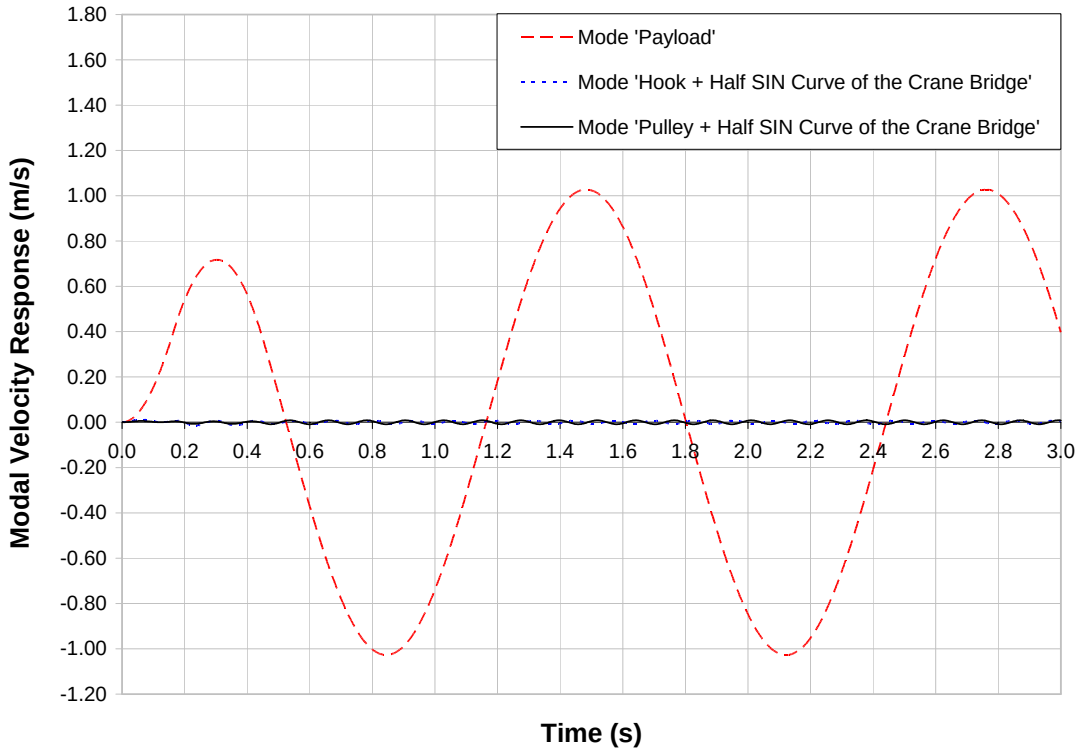

Figure 5.3.2.3 Velocity response of the individual modes of vibration when the payload is hoisted 2.20m above ground level by the Direct Integration method.

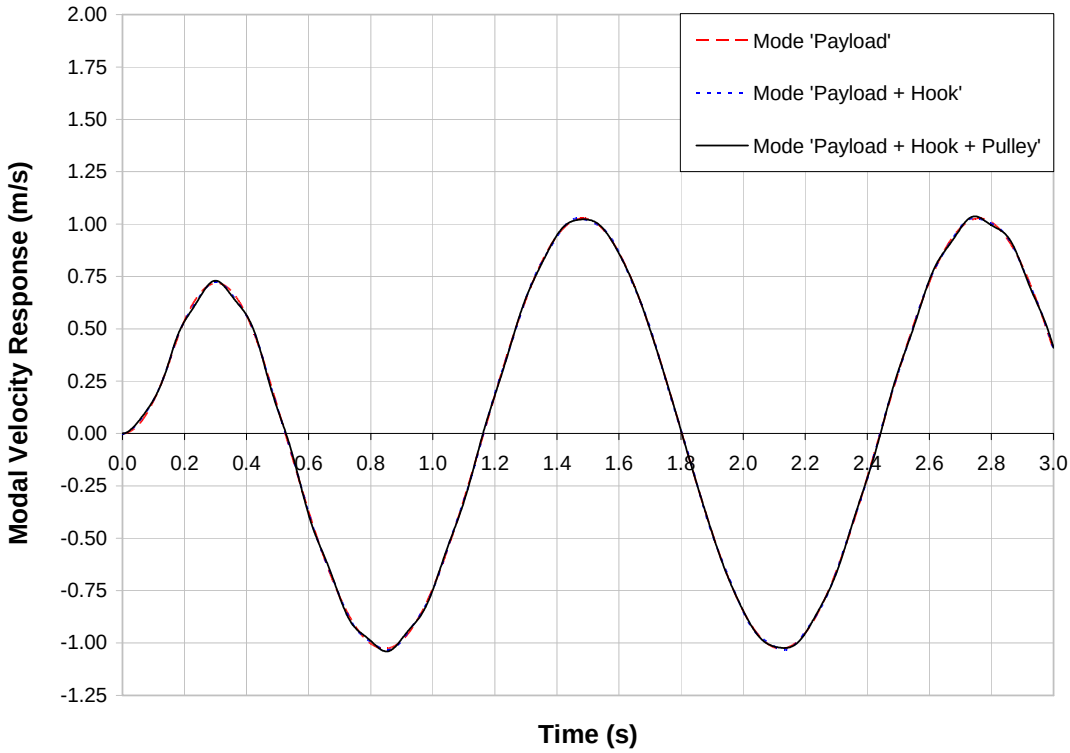

Figure 5.3.2.4 Velocity response of the combined modes of vibration when the payload is hoisted 2.20m above ground level by the Direct Integration method.

5.4 Comparison between the Responses of the Impulse and the Direct Integration Methods

Figures 5.4.1 and 5.4.2 presents the individual lower modes of vibration's displacement and velocity responses of the Impulse and Direct Integration methods. There exists a good correlation between the responses of the above methods except for a shift. This could be attributed to the time when the impulse is applied compared to the Direct Integration method where the force is applied from the start of the analysis. Thus, the Impulse method could be used when frequencies of the modes of vibration are low, as in the case of the rigid body and the payload. The choice of the Impulse method is predominantly due to its ease of implementation compared to the Direct Integration method.

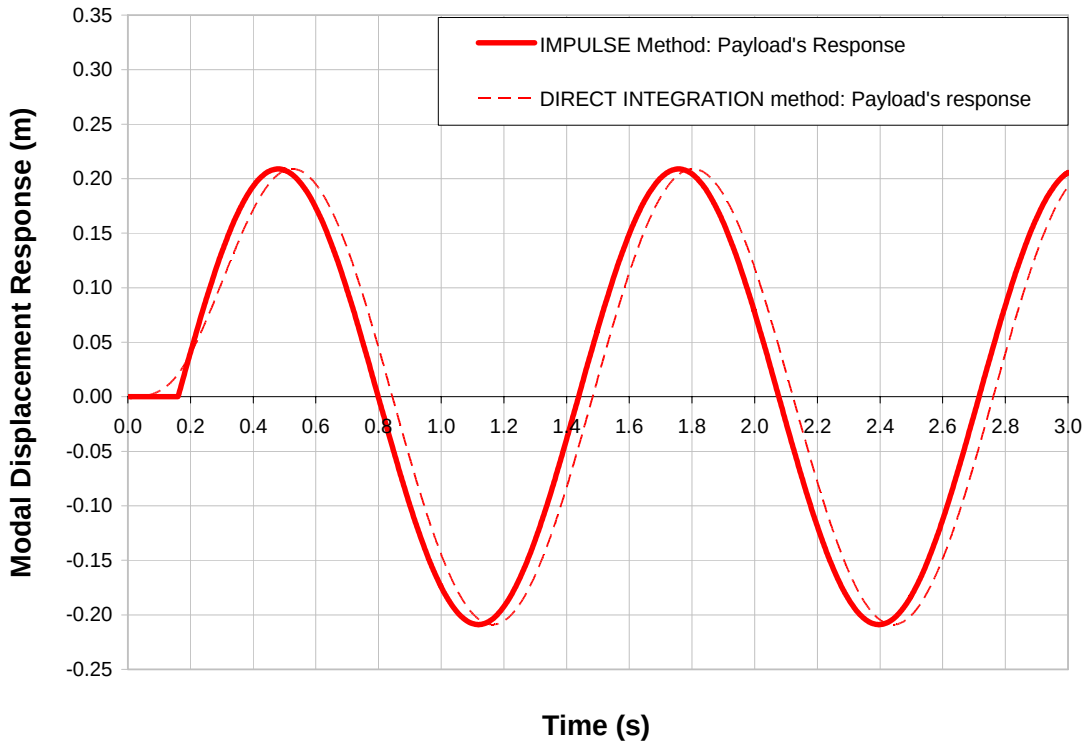

Figure 5.4.1 Comparison between the Impulse and the Direct Integration methods individual lower modes of vibration's **displacement responses** when the payload is hoisted **2.20m** above ground level

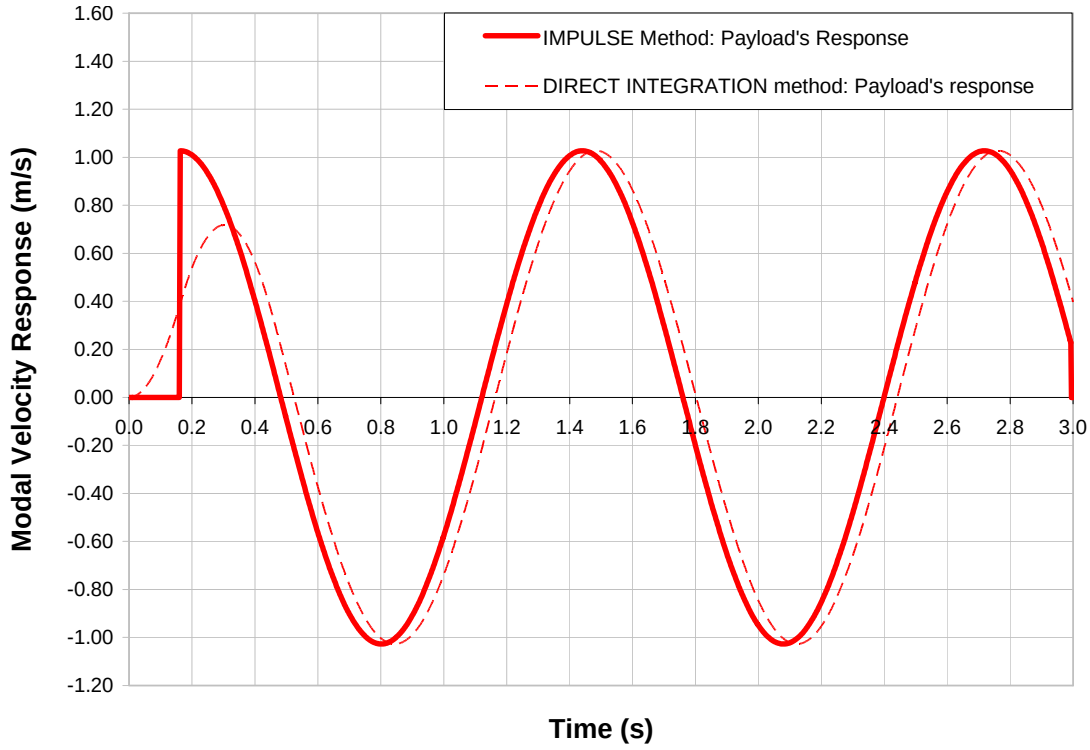

Figure 5.4.2 Comparison between the Impulse and the Direct Integration methods individual lower modes of vibration's **velocity responses** when the payload is hoisted **2.20m** above ground level

Figures 5.4.3 and 5.4.4 presents the individual higher modes of vibration's displacement and velocity responses of the Impulse and Direct Integration methods. There is visibly a remarkable difference between the responses obtained from the Impulse and Direct Integration methods. The Impulse method yields 41% greater displacement and velocity responses compared to the Direct Integration method.

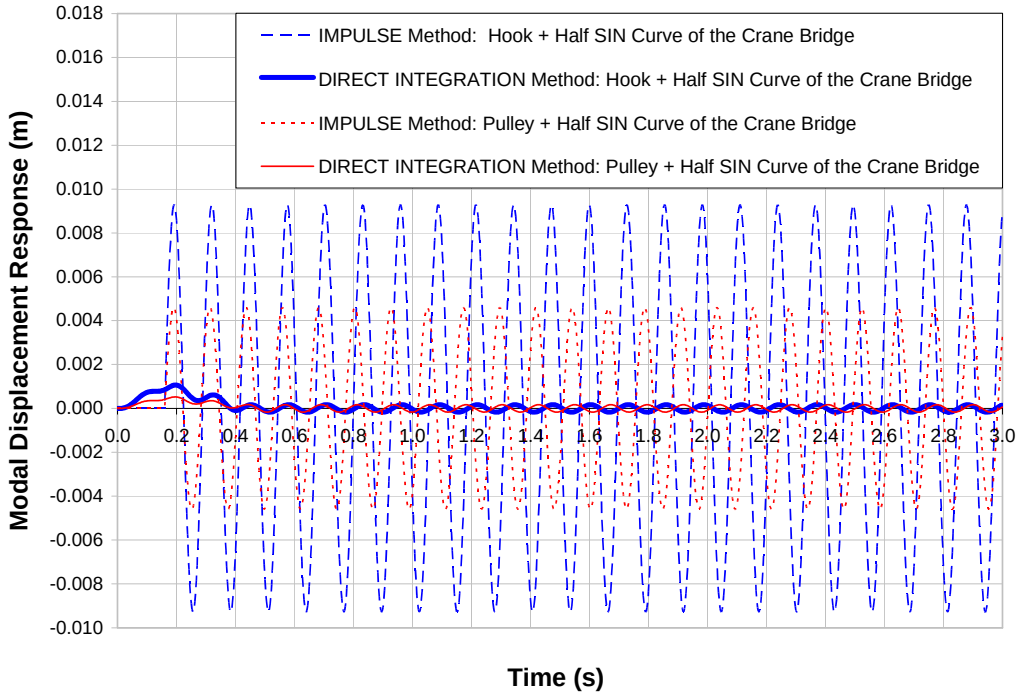

Figure 5.4.3 Comparison between the Impulse and the Direct Integration methods individual higher modes of vibration's **displacement responses** when the payload is hoisted **2.20m** above ground level

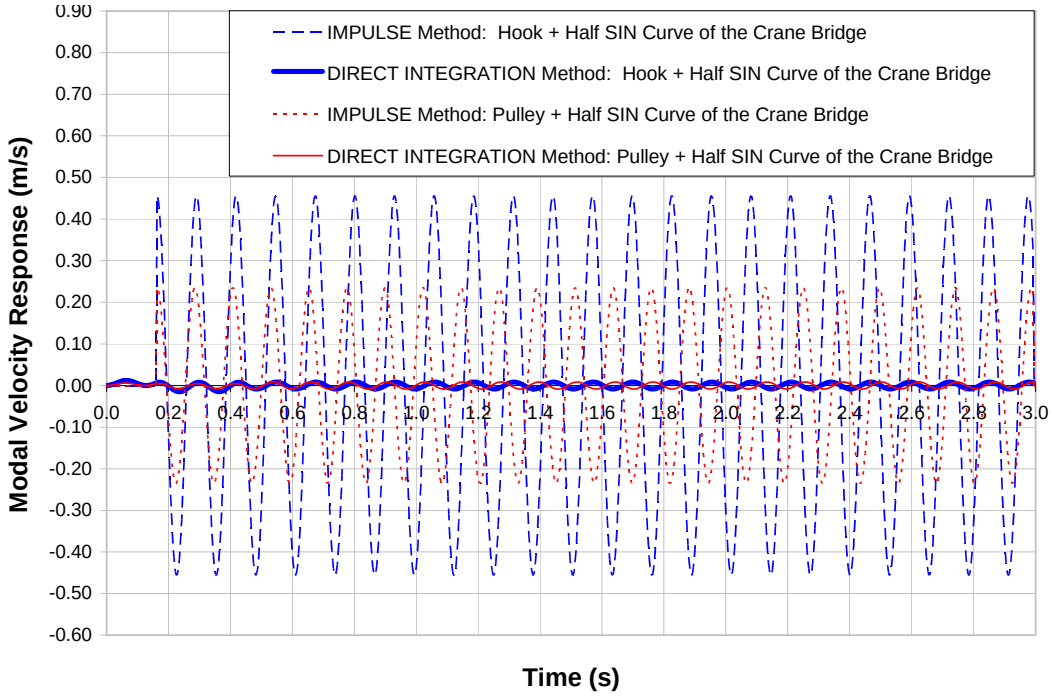

Figure 5.4.4 Comparison between the Impulse and the Direct Integration methods individual higher modes of vibration's **velocity responses** when the payload is hoisted **2.20m** above ground level

5.5 Conclusion

The displacement and velocity responses of the higher modes of vibration based upon the Impulse method are incorrect. The higher modes of vibration which are considered have approximately 4.5 oscillations over the period during which the 1st triangular load is applied. The Impulse method does not take this into account. From the above analysis, the Impulse method should be used when the frequency of the mode of vibration is small, i.e. less than one (1).

When the Direct Integration method is employed the higher modes of vibration do not contribute to a chaotic response of the system as initially suspected. Instead, the Modal Analysis and Modal Superposition show that it is predominantly the responses of the rigid body and payload which contribute to the response of the system.

The higher modes of vibration can be excluded from the total response of the system. Thus, the combined effect of the lower modes of vibration (rigid body and payload) would suffice to predict the starting position of the 2nd impact and its velocity intensity.

CHAPTER 6 : SENSITIVITY STUDY

6.1 Introduction

A sensitivity analysis was conducted on the parameters presented in Table 6.1.1 which have a significant effect on the impact response when the crane collides into the end stops. The base value and the range of variation for each parameter which was investigated are presented in Table 6.1.1. Table 6.1.2 presents another parameter which was simply turned on and off to determine the effect which it had on the impact response.

The FEA model which was developed in Chapter 3, was used to conduct the sensitivity analysis. The sensitivity analysis was conducted to determine the effect on the impact response by varying only the parameter under investigation while keeping all other parameters constant. The writer is aware that the parameters do not act individually. The parameter effects are presented individually to eliminate the confusion of combining several parameter responses simultaneously.

The FEA simulations will be presented for both the “Power-Off” and “Power-On” cases to show the effect on the impact response. For the FEA “Power-Off” simulations, no additional torque is transferred to the wheels from the moment of impact. For the FEA “Power-On” simulations, the motors transfer full torque to the wheels throughout the simulations, which are significantly affected by the slipping and lifting of the motorized crane wheels during impact. Similarly, the FEA simulations will be presented when the payload is hoisted to 0.15m and 2.20m above ground level to show the effect which the payload height above ground level has on the impact response.

A limited number of experimental tests were conducted due to the difficulty of adjusting and controlling the parameters presented in Tables 6.1 and 6.2. The base experimental tests were conducted for the following conditions:

(i) For the “Power-Off” case with the payload symmetrically positioned on the crane bridge and hoisted to 0.15m and 2.20m above ground level.

(ii) For the “Power-Off” case with residual torque (step down torque) with the payload symmetrically positioned on the crane bridge and hoisted to 0.15m and 2.20m above ground level.

(iii) For the “Power-On” case without the payload, while the crab was symmetrically positioned on the crane bridge.

Except for the velocity of the crane and position of the crab and payload, the rest of the parameters presented in Tables 6.1 and 6.2 were difficult to control experimentally. During the experimental tests, no measurements of these parameters were made. This resulted in relying on judgment when observing the video recording taken during the impact tests to determine the variance of some of these parameters.

Table 6.1.1 Parameters identified for the FEA sensitivity analysis which could have a significant effect on the impact response

Parameter (Variable)	Base value	Range of variation	Description of variation
Lag of the payload's Centre of Gravity (C.O.G.) with respect to the crane bridge.	0^0	$2.50^0 \pm$	• The base value of 0^0 is assumed when the payload is positioned directly below the crane bridge at the moment of impact. • A horizontal lag of 82mm ($1.25^0 \pm$) is observed in the FEA model when the crane accelerates at $0.2m/s^2$ when the C.O.G. of the payload is 3.75m below the neutral axis of the crane bridge. • The FEA simulations were conducted for a variance of 0^0, $1.25^0 \pm$ and twice the observed maximum lag, i.e. $2.50^0 \pm$
Crab and payload's eccentricity on the crane bridge	0m	3.39m ±	• The base value is assumed when the crab and payload is symmetrically positioned on the crane bridge. This occurs at a distance of 4.14m from either end of the crane bridge. The eccentricity will be measured from this position. • The FEA simulations were conducted with a variance of 0m, 1.695m ± and 3.39m ± from the midspan of the crane bridge.
End stop misalignment	0	150mm	• The base value is assumed when the line connecting the impact faces of the two end stops is exactly perpendicular to the direction of travel, i.e. 0mm between the faces of the two end stops. The misalignment is obtained when one of the end stops is horizontally longitudinally misaligned with respect to the other. • An expected normal misalignment could range between 25mm and 50mm. The worst case is when the wooden end block of 150mm at one side is removed from the crane supporting structure.

Table 6.1.1 (Continued) Parameters identified for the FEA sensitivity analysis which could have a significant effect on the impact response

Parameter (Variable)	Base value	Range of variation	Description of variation
Crane supporting flexibility	Rigid ≅0	Weak, Intermediate and Strong Spring	• The base value is assumed when the crane supporting structure is horizontally longitudinally braced, thus preventing horizontal longitudinal translation, i.e. ≅0. • The bracing system was replaced with horizontal longitudinal springs of which the stiffness can be adjusted to investigate the effect of the flexibility of the crane supporting. • The FEA simulations were conducted to determine the effect of a rigid, semi-flexible and flexible crane supporting system.
Crane speed at impact	0.55m/s	- 0.165m/s	• The base value is assumed as the maximum speed the crane can obtain when the payload is attached to the crane bridge, i.e. 0.55m/s. • The average speed as measured by the encoders differs by as much as 9% compared to the actual speed. The proposed SANS 10160 code stipulates that the crane speed could be reduced by 30% if the crane is fitted with automatic speed reducers. • The FEA simulations were conducted with a variance of 9% ± (0.05m/s ±) and -30% of the full rated speed of the crane $0.55 - 0.3 \times 0.55 = 0.385$m/s
Elastic buffer characteristics	Stiffness curve used in FEA	20% ±	• The base value is assumed as the unadjusted elastic buffer characteristic curve defined in Chapter 3.19. • Various factors affect the buffers elastic characteristics which should be taken into account. The FEA simulations were conducted with a variance of 20% ±.

Table 6.1.2 Parameters which can significantly affect the impact response when the crane collides with the end stop

Parameter (Variable)	Base value	Alternative	Description of variation
Buffers' damping characteristics	Damping determined as described in Chapter 3.19	Without damping	• The base buffer's damping characteristics properties are described in Chapter 3.19, (i.e. unadjusted buffer damping characteristics). • The buffers' damping characteristics are unknown and not supplied by the manufacturer. The FEA simulations were conducted without any buffer damping characteristics for this parameter.

6.2 The Effect of the Payload's Lag Angle on the Impact Response

6.2.1 Description of the Lag Angle model parameter setup

The visual assessment of the video recordings of the experimental impact tests indicates that the payload does sometimes lag behind the crane bridge at the moment of impact. In some cases the payload is ahead of the crane bridge at the moment of impact.

To study the effect of the individual parameters on the impact response all the parameters, except the parameter under investigation, were kept constant at there base values. The payload was given the same acceleration boundary conditions as the motorized crane wheels. This resulted in the payload being positioned directly below the crane bridge at the moment of impact and did not allow the payload to oscillate before impact. This position (0^0) of the payload was regarded as the base state for the payload lag parameter.

The FEA simulations yielded an 82mm (1.25^0) payload lag when the crane accelerates at $0.20m/s^2$ when the payload was hoisted to 0.15m above ground. The lag parameters were chosen as the base value 0^0, $\pm 1.25^0$ and $\pm 2.50^0$ with reference to the crane bridge.

Figure 6.2.1.1 shows a schematic presentation of the side elevation of the end carriage and payload with a negative lag, i.e. the payload lags behind the crane bridge at the moment of impact.

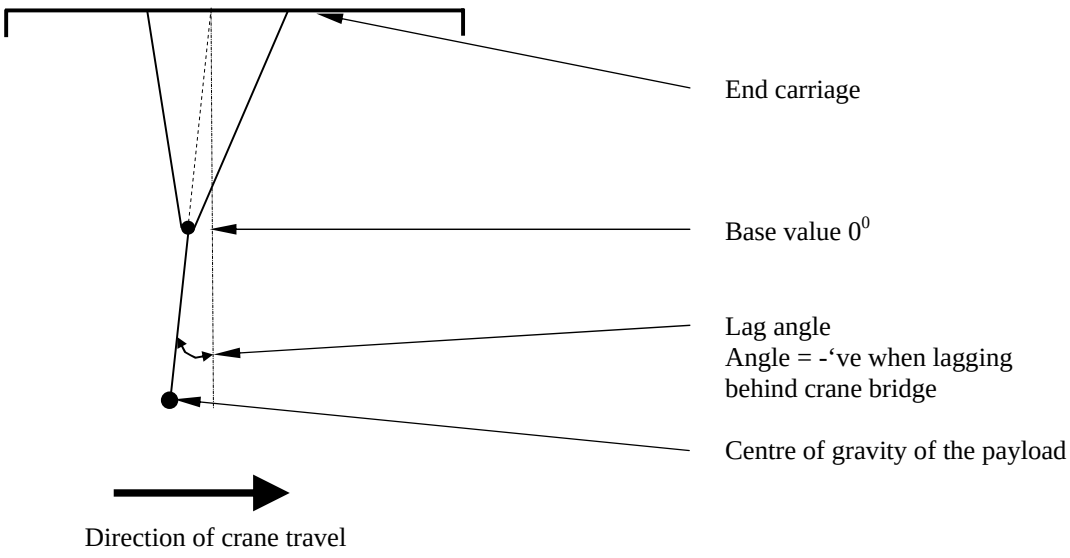

Figure 6.2.1.1 Schematic presentation of a negative payload lag

6.2.2 Interpretation of the FEA simulations

Figures 6.2.2.1 to 6.2.2.4 present the effect of the payload lag on the impact response, for the "Power-Off" and the "Power-On" FEA simulations when the payload is hoisted 0.15m and 2.20m above ground level. For enlargements of Figures 6.2.2.1 to 6.2.2.4 refer to Appendix A, "FEA Simulations of the Payload Lag". The tabular analysis of the magnitudes of the 1st and 2nd peaks as well as the percentage time difference between the peaks are presented in Tables 6.2.2.1 to 6.2.2.4.

6.2.2.1 Remarks when the payload is 0.15m above ground level

The responses obtained from the FEA simulations met the expectations.

When the negative payload lag angle increases the subsequent trends are apparent for the FEA "Power-Off" and "Power-On" simulations with respect to the base response:

- the 1st impact force decreases,
- the 2nd impact force increases and
- the time between the 1st and 2nd impact peaks decreases.

The opposite is true when the positive payload lag increases.

The significant information which can be extrapolated from the FEA "Power-Off" simulations with respect to the base responses is:

- The 1st impact force increases by 38% for a positive lag of 2.50^0.
- The 2nd impact force increases 32% for a negative lag of 2.50^0.
- The time difference between the impact peaks increases by 14% for a negative lag of 2.50^0.
- When full power "Power-On" is included in the FEA simulations, the maximum impact force increases from 8.79kN to 10.03kN, an increase of 14%.

6.2.2.2 Remarks when the payload is 2.20m above ground level

The trends when the payload is hoisted to 2.20m above ground level are similar to that when the payload is hoisted to 0.15m above ground level, except that there is only a small time difference between the impact peaks.

The significant information which can be extrapolated from the FEA “Power-Off” simulations with respect to the base responses are;

- The 1st impact force increases by 33% for a positive lag of 2.50^0.
- The 2nd impact force increases by 7% for a positive lag of 2.50^0.
- The time difference between the impact peaks increases by 3% for a negative lag of 2.50^0.
- When full power “Power-On” is included in the FEA simulations, the maximum impact force increases from 8.56kN to 9.92kN, an increase of 16%.

6.2.2.3 Conclusion

The differences in the periods between the peaks are more pronounced for the longer cable length as opposed to the shorter cable length. This is due to the longer cables creating a longer arc during its swinging action during impact. The maximum impact force of 10.03kN is obtained from varying this parameter. The maximum time difference between impacts varies by 14%.

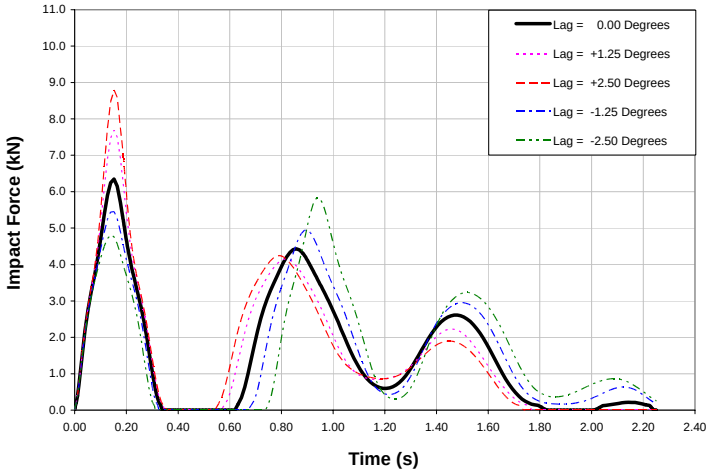

Figure 6.2.2.1 Lag Effect: Payload Bottom with "Power-OFF"

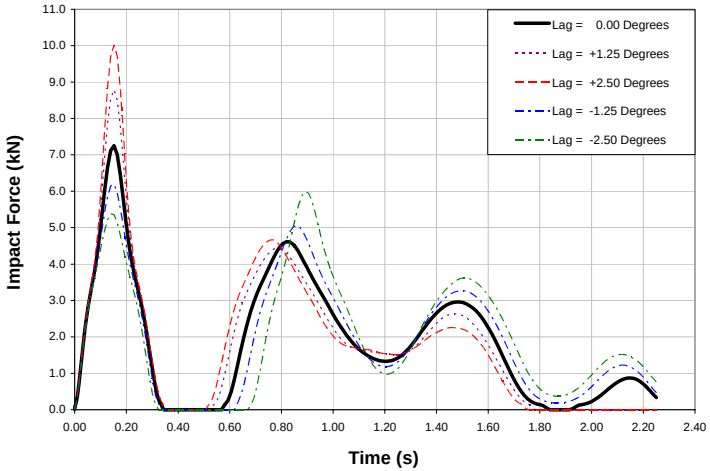

Figure 6.2.2.2 Lag Effect: Payload Bottom with "Power-ON"

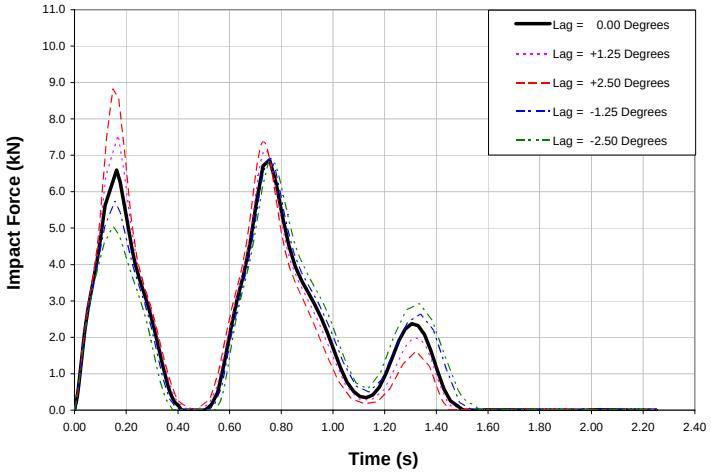

Figure 6.2.2.3 Lag Effect: Payload Top with "Power-OFF"

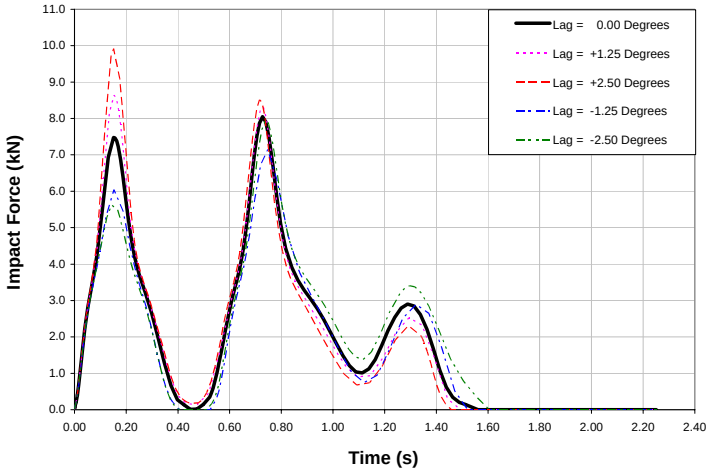

Figure 6.2.2.4 Lag Effect: Payload Top with "Power-ON"

Table 6.2.2.1 Comparison of the influence of the **Lag parameter** when the payload is hoisted **0.15m** above ground level with **"Power-OFF"**

Lag	1st Impact Force **(kN)**	2nd Impact Force **(kN)**	Time Difference between the 1st and 2nd peaks **(s)**	Difference of the 1st Impact Force w.r.t. Base Model **(%)**	Difference of the 2nd Impact Force w.r.t. Base Model **(%)**	Time difference between the 1st and 2nd peaks **(%)**
-2.50^0	4.81	5.83	0.81	-24	32	14
-1.25^0	5.45	4.95	0.75	-14	12	6
Base Model: 0^0	*6.35*	*4.43*	*0.71*	*N/A*	*N/A*	*N/A*
$+1.25^0$	7.69	4.15	0.67	21	-6	-6
$+2.50^0$	8.79	4.25	0.64	38	-4	-10

Table 6.2.2.2 Comparison of the influence of the **Lag parameter** when the payload is hoisted **0.15m** above ground level with **"Power-ON"**

Lag	1st Impact Force **(kN)**	2nd Impact Force **(kN)**	Time Difference between the 1st and 2nd peaks **(s)**	Difference of the 1st Impact Force w.r.t. Base Model **(%)**	Difference of the 2nd Impact Force w.r.t. Base Model **(%)**	Time difference between the 1st and 2nd peaks **(%)**
-2.50^0	5.38	5.99	0.75	-26	30	10
-1.25^0	6.19	5.06	0.70	-15	10	3
Base Model: 0^0	*7.26*	*4.61*	*0.68*	*N/A*	*N/A*	*N/A*
$+1.25^0$	8.79	4.44	0.62	21	-4	-9
$+2.50^0$	10.03	4.67	0.62	38	1	-9

Table 6.2.2.3 Comparison of the influence of the **Lag parameter** when the payload is hoisted **2.20m** above ground level with **"Power-OFF"**

Lag	1st Impact Force **(kN)**	2nd Impact Force **(kN)**	Time Difference between the 1st and 2nd peaks **(s)**	Difference of the 1st Impact Force w.r.t. Base Model **(%)**	Difference of the 2nd Impact Force w.r.t. Base Model **(%)**	Time difference between the 1st and 2nd peaks **(%)**
-2.50^0	5.54	6.84	0.60	-17	-1	3
-1.25^0	5.74	6.92	0.60	-14	1	3
Base Model: 0^0	*6.65*	*6.88*	*0.58*	*N/A*	*N/A*	*N/A*
$+1.25^0$	7.56	7.15	0.58	14	4	0
$+2.50^0$	8.56	7.38	0.56	29	7	-3

Table 6.2.2.4 Comparison of the influence of the **Lag parameter** when the payload is hoisted **2.20m** above ground level with **"Power-ON"**

Lag	1st Impact Force **(kN)**	2nd Impact Force **(kN)**	Time Difference between the 1st and 2nd peaks **(s)**	Difference of the 1st Impact Force w.r.t. Base Model **(%)**	Difference of the 2nd Impact Force w.r.t. Base Model **(%)**	Time difference between the 1st and 2nd peaks **(%)**
-2.50^0	5.63	7.96	0.60	-25	-1	3
-1.25^0	6.04	7.14	0.60	-19	-11	3
Base Model: 0^0	*7.48*	*8.05*	*0.58*	*N/A*	*N/A*	*N/A*
$+1.25^0$	8.64	8.31	0.58	16	3	0
$+2.50^0$	9.92	8.52	0.57	33	6	-2

6.3 The Effect of the Crab and Payload's Eccentricity on the Impact Response

6.3.1 Description of the Crab and Payload's Eccentricity model parameter setup

The crab is allowed to travel along the crane bridge and thus its position at the moment of impact can vary. Thus, this parameter needs to be investigated to determine whether its effect will be significant when impact occurs. The crab's eccentricity is the only parameter which will vary during the simulations. The crab is symmetrically positioned on the crane bridge for the base model, i.e. 4.14m from either end. The crab can attain a maximum eccentricity of 3.39m from the midspan of the crane bridge. To further investigate the crab eccentricity's effect another position midway between the above positions was investigated. The eccentricity is measured from the midspan of the crane bridge towards the end of the crane bridge.

Figure 6.3.1.1 shows a schematic presentation of the plan view of the end carriage and crab's eccentric positions.

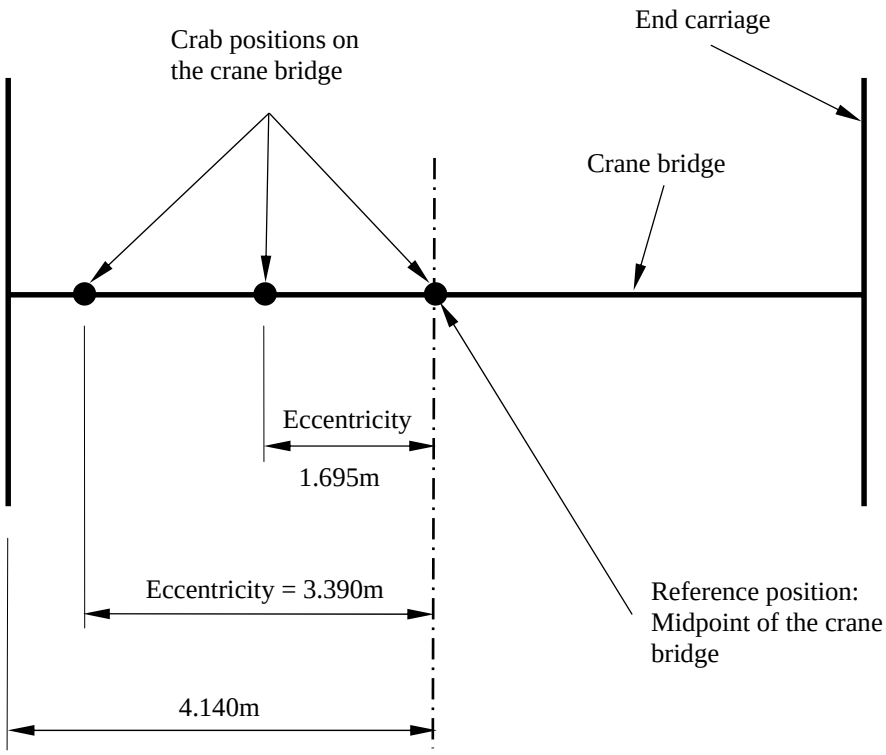

Figure 6.3.1.1 Schematic presentation of the plan view of the crab's eccentric positions

6.3.2 Interpretation of the FEA simulations

Figures 6.3.2.1 to 6.3.2.4 present the FEA simulations effect of the crab and payload's eccentricity on the impact response, for the "Power-Off" and the "Power-On" cases when the payload is 0.15m and 2.20m above ground level. For enlargements of Figures 6.3.2.1 to 6.3.2.4 refer to Appendix B, "FEA Crab and Payload's Eccentricity Responses". The tabular analyses of the magnitudes of the 1st and 2nd peaks as well as the time difference between the peaks are presented in Tables 6.3.2.1 to 6.3.2.4.

The responses obtained from the FEA simulations gave intuitive results. The end buffer impact response increases on the side to which the crab is eccentric and decreases for the opposite end buffer.

6.3.2.1 Remarks when the payload is 0.15m above ground level

As the eccentricity of the crab and payload increases the subsequent trends are apparent for the FEA "Power-Off" and "Power-On" simulations with respect to the base response:

- the 1st end buffer impact force increases on the side of the eccentricity, while the opposite end buffer impact force decreases.
- the 2nd end buffer impact force shows similar trends as the 1st impact forces
- the time differences between the 1st and 2nd peaks remain practically unchanged.

The significant information which can be extrapolated from the FEA "Power-Off" simulations with respect to the base responses is;

- The 1st impact force increases by 22% when the crab and payload is at its maximum eccentricity.
- The 2nd impact force increases by 31% when the crab and payload is at its maximum eccentricity.
- The time difference between the impact peaks decreases by 4% when the crab and payload is at its maximum eccentricity.
- When full power "Power-On" is included in the FEA simulations, the maximum impact force increases from 7.38kN to 8.85kN, an increase of 20%.

6.3.2.2 Remarks when the payload is 2.20m above ground level

The trends when the payload is hoisted to 2.20m above ground level are similar to that when the payload is hoisted to 0.15m above ground level.

The significant information which can be extrapolated from the FEA simulations with respect to the base responses is;

- The 1st impact force increases by 26% when the crab and payload is at its maximum eccentricity.
- The 2nd impact force increases by 18% when the crab and payload is positioned at an eccentricity = 1.695m.
- The time difference between the impact peaks increases by 5% when the crab and payload is positioned at an approximately eccentricity = 1.695m.
- When full power “Power-On” is included in the FEA simulations, the maximum impact force increases from 8.03kN to 9.39kN, an increase of 17%.

6.3.2.3 Conclusion

The maximum impact force of 9.39kN was obtained when the crab was positioned at its maximum eccentricity of 3.39m from the midpoint of the crane bridge when the payload is hoisted to 2.20m above ground level. The 1st and 2nd impact forces are affected by this parameter, while the period between the impact forces are almost unchanged. Thus, the impact response is affected by the position of the payload at the moment of impact.

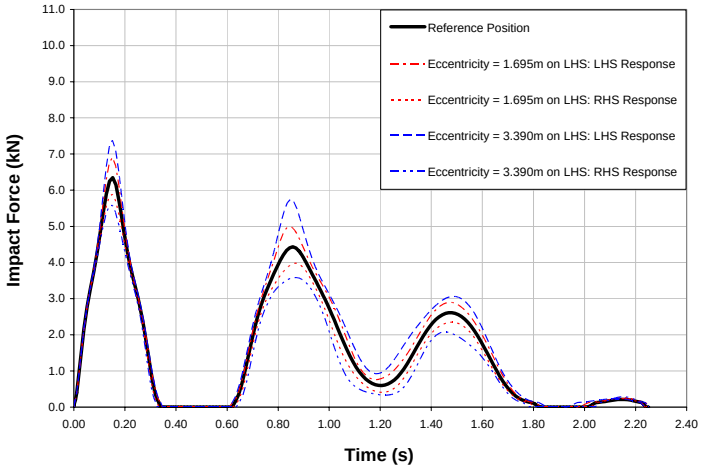

Figure 6.3.2.1 Crab Eccentricity Effect: Payload Bottom with "Power-OFF"

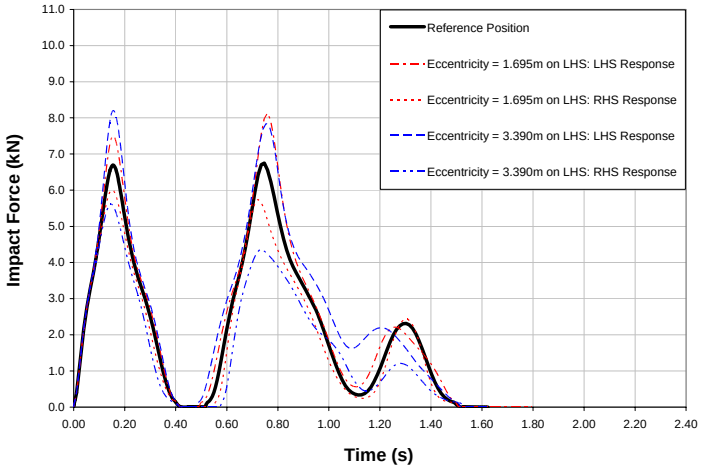

Figure 6.3.2.3 Crab Eccentricity Effect: Payload Top with "Power-OFF"

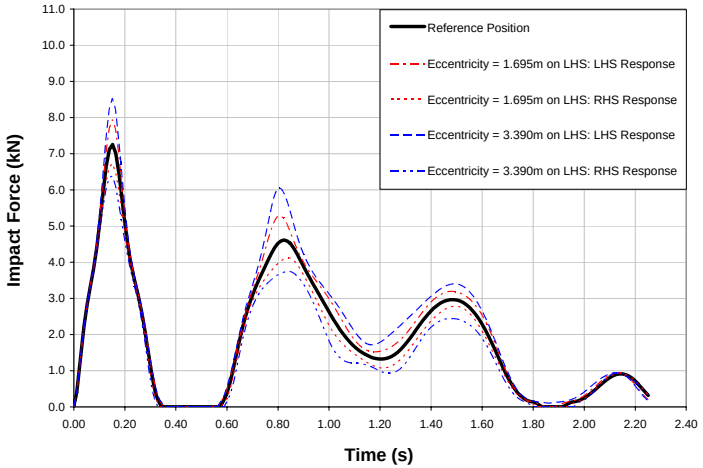

Figure 6.3.2.2 Crab Eccentricity Effect: Payload Bottom with "Power-ON"

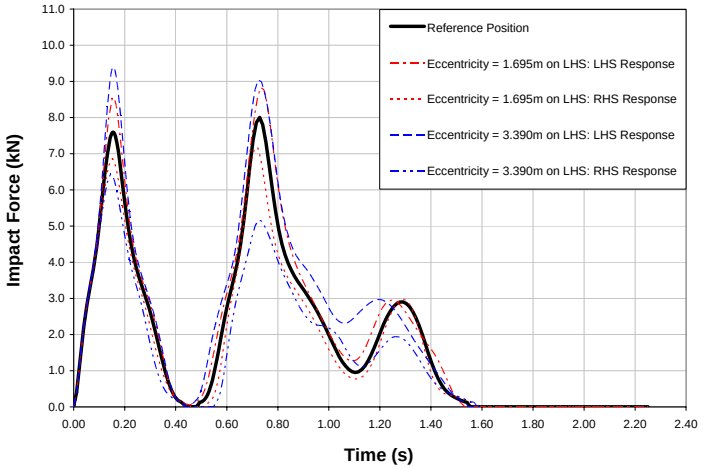

Figure 6.3.2.4 Crab Eccentricity Effect: Payload Top with "Power-ON"

Table 6.3.2.1 Comparison of the influence of the **Crab Eccentricity parameter** when the payload is hoisted **0.15m** above ground level with **"Power-OFF"**

Crab Eccentricity	1st Impact Force **(kN)**	2nd Impact Force **(kN)**	Time Difference between the 1st and 2nd peaks **(s)**	Difference of the 1st Impact Force w.r.t. Base Model **(%)**	Difference of the 2nd Impact Force w.r.t. Base Model **(%)**	Time difference between the 1st and 2nd peaks **(%)**
Base Model: Midpoint of crane bridge	*6.35*	*4.43*	*0.71*	*N/A*	*N/A*	*N/A*
Eccentricity = 1.695m from reference position	6.91	4.49	0.70	9	1	-1
Eccentricity = 3.390m from reference position	7.38	5.75	0.70	16	30	-1

Table 6.3.2 Comparison of the influence of the **Crab Eccentricity parameter** when the payload is hoisted **0.15m** above ground level with **"Power-ON"**

Crab Eccentricity	1st Impact Force **(kN)**	2nd Impact Force **(kN)**	Time Difference between the 1st and 2nd peaks **(s)**	Difference of the 1st Impact Force w.r.t. Base Model **(%)**	Difference of the 2nd Impact Force w.r.t. Base Model **(%)**	Time difference between the 1st and 2nd peaks **(%)**
Base Model: Midpoint of crane bridge	*7.26*	*4.61*	*0.68*	*N/A*	*N/A*	*N/A*
Eccentricity = 1.695m from reference position	7.94	5.28	0.65	9	15	-4
Eccentricity = 3.390m from reference position	8.85	6.05	0.65	22	31	-4

Table 6.3.2.3 Comparison of the influence of the **Crab Eccentricity parameter** when the payload is hoisted **2.20m** above ground level with **"Power-OFF"**

Crab Eccentricity	1st Impact Force **(kN)**	2nd Impact Force **(kN)**	Time Difference between the 1st and 2nd peaks **(s)**	Difference of the 1st Impact Force w.r.t. Base Model **(%)**	Difference of the 2nd Impact Force w.r.t. Base Model **(%)**	Time difference between the 1st and 2nd peaks **(%)**
Base Model: Midpoint of crane bridge	*6.65*	*6.88*	*0.58*	*N/A*	*N/A*	*N/A*
Eccentricity = 1.695m from reference position	7.49	8.13	0.61	13	18	5
Eccentricity = 3.390m from reference position	8.03	7.84	0.59	21	14	2

100

Table 6.3.2.4 Comparison of the influence of the **Crab Eccentricity parameter** when the payload is hoisted **2.20m** above ground level with **"Power-ON"**

Crab Eccentricity	1st Impact Force **(kN)**	2nd Impact Force **(kN)**	Time Difference between the 1st and 2nd peaks **(s)**	Difference of the 1st Impact Force w.r.t. Base Model **(%)**	Difference of the 2nd Impact Force w.r.t. Base Model **(%)**	Time difference between the 1st and 2nd peaks **(%)**
Base Model: Midpoint of crane bridge	*7.48*	*8.05*	*0.58*	*N/A*	*N/A*	*N/A*
Eccentricity = 1.695m from reference position	8.56	8.83	0.58	14	10	0
Eccentricity = 3.390m from reference position	9.39	9.04	0.57	26	12	-2

6.4 The Effect of the Crane Supporting Structure's Flexibility on the Impact Response

6.4.1 Description of the Crane Supporting Structure's Flexibility model parameter setup

All the codes and guidelines which were reviewed ignore the flexibility of the crane supporting structure. The codes assume that the crane supporting structure is rigid and does not deflect during impact. The base model was developed with a horizontal longitudinal bracing system at the top of the crane and building columns. This resulted in an extremely rigid system with minimal horizontal longitudinal deflection of the end stops. No experimental data was recorded for this parameter and thus makes comparison difficult with the FEA model. The researcher is of the opinion that the crane supporting structure does displace longitudinally during impact. This could be as a result of slipping at the connections of the various members and also the elasticity of the members.

To determine the effect of the crane supporting structure's flexibility, the horizontal longitudinal bracing system was removed and replaced with a spring in the FEA model. The weak spring was used to model a crane supporting structure with minimal resistance to horizontal longitudinal deflection. The intermediate spring was used to model a crane supporting structure with some resistance to horizontal longitudinal deflection. Finally the stiff spring was used to model a very rigid crane supporting structure, similar to the horizontal longitudinal bracing system. The spring stiffness for the weak, intermediate and stiff spring are 1.75×10^5 N/m, 1.75×10^6 N/m and 1.75×10^7 N/m respectively. The weak, intermediate and stiff spring resulted in a horizontal longitudinal displacement at the apex of the building columns of 22.9mm, 4.40mm and 0.50mm when the payload was hoisted to 0.15m above ground level for the FEA "Power-Off" simulations.

The horizontal longitudinal support at the apex of the crane and building columns were used in the base model to compare the responses of the weak, intermediate and stiff springs.

Figures 6.4.1.1 shows the schematic representation of the crane columns with the longitudinal bracing system, while Figure 6.4.1.2 shows the schematic representation of the crane columns with spring support.

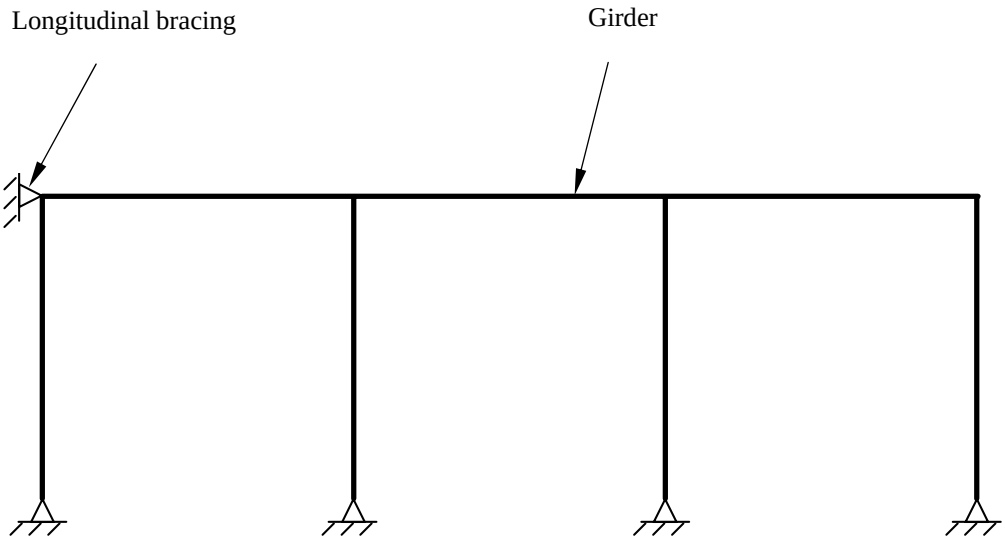

Figure 6.4.1.1 Schematic presentation of the side elevation of the crane columns with the horizontal longitudinal bracing system

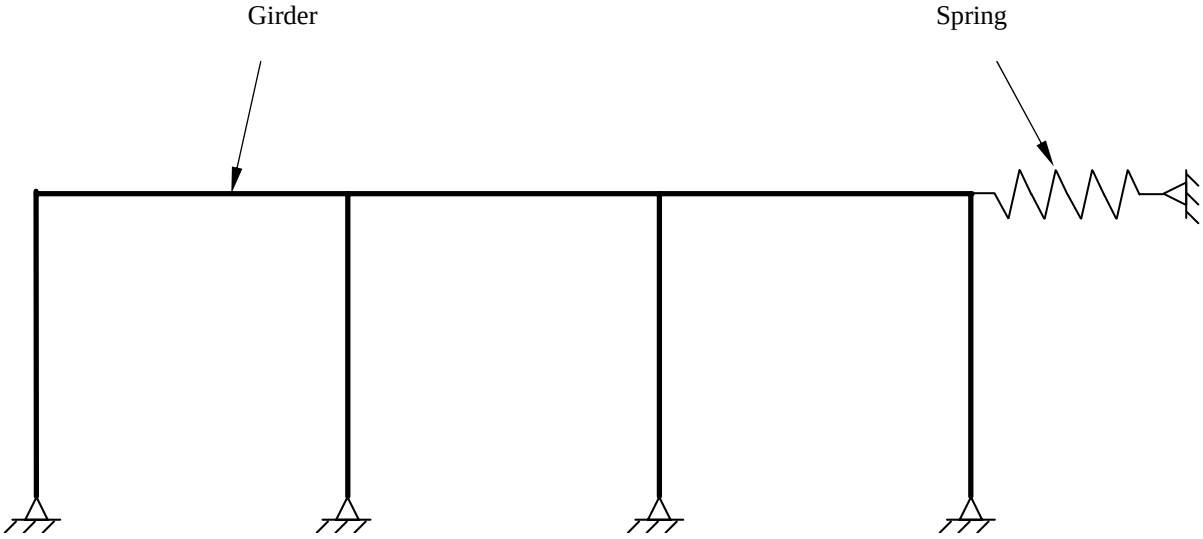

Figure 6.4.1.2 Schematic presentation of the side elevation of the crane columns with the horizontal longitudinal spring

6.4.2 Interpretation of the FEA simulations

Figures 6.4.2.1 to 6.4.2.4 present the FEA simulations effect of the crane supporting structure's flexibility on the impact response, for the "Power-Off" and the "Power-On" cases when the

payload is 0.15m and 2.20m above ground level. For enlargements of Figures 6.4.2.1 to 6.4.2.4 refer to Appendix C, "FEA Crane Supporting Structure's Flexibility Responses". The tabular analyses of the magnitudes of the 1st and 2nd peaks as well as the time difference between the peaks are presented in Tables 6.4.2.1 to 6.4.2.4.

The responses obtained from the FEA simulations are intuitive. As expected the crane supporting structure displaces significantly when the horizontal longitudinal bracing system is removed and replaced with a weak spring. The horizontal longitudinal displacement of the crane supporting structure decreases as the spring's stiffness increases.

6.4.2.1 Remarks when the payload is 0.15m above ground level

When the horizontal longitudinal bracing system is removed and as the spring stiffness decreases the subsequent trends are apparent for the FEA "Power-Off" and "Power-On" simulations with respect to the base response:

- the 1st impact force decreases
- the 2nd impact force increases
- the time differences between the 1st and 2nd peaks increases.

The significant information which can be extrapolated from the FEA "Power-Off" simulations with respect to the base responses is:

- The 1st impact force decreases by 31% when the horizontal bracing system is replaced by a weak spring.
- The 2nd impact force increases by 49% when the horizontal bracing system is replaced by a weak spring.
- The time difference between the impact peaks increases by 12% when the horizontal bracing system is replaced by a weak spring.
- When full power "Power-On" is included in the FEA simulations, the maximum impact force increases from 6.29kN to 7.65kN, an increase of 22% for the stiff elastic spring characteristics.

6.4.2.2 Remarks when the payload is 2.20m above ground level

The trends when the payload is hoisted to 2.20m above ground level are similar to that when the

payload is hoisted to 0.15m above ground level.

The significant information which can be extrapolated from the FEA simulations with respect to the base responses is:

- The 1st impact force decreases by 34% when the horizontal bracing system is replaced by a weak spring.
- The 2nd impact force increases by 14% when the horizontal bracing system is replaced by a weak spring.
- The time difference between the impact peaks increases by 34% when the horizontal bracing system is replaced by a weak spring.
- When full power "Power-On" is included in the FEA simulations, the maximum impact force increases from 7.84kN to 9.01kN, an increase of 15% for the weak elastic spring characteristics.

6.4.2.3 Conclusion

The maximum impact force of 9.01kN occurs at the 2nd impact when the crane supporting structure is fitted with a weak spring and the payload is hoisted to 2.20m above ground level. The 1st and 2nd impact forces as well as the period between the impact forces are significantly affected by this parameter. Thus, the impact response is affected by the position of the payload at the moment of impact.

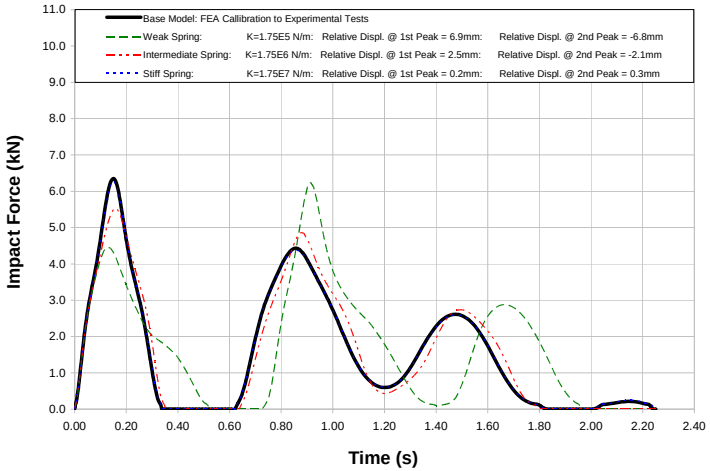

Figure 6.4.2.1 Crane Supporting Structure's Flexibility Effect: Payload Bottom - "Power-OFF"

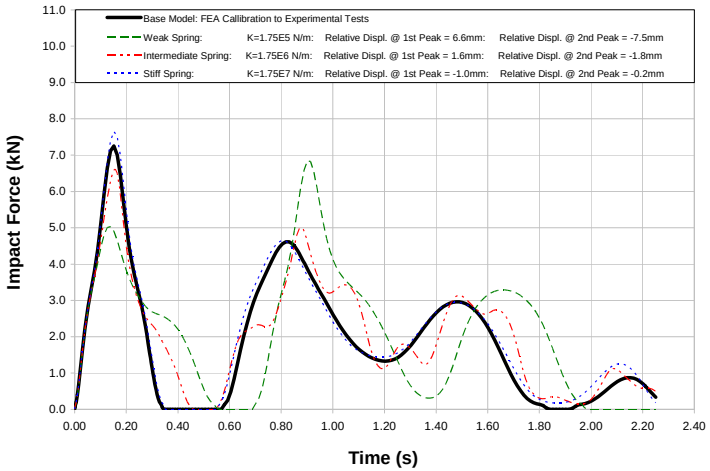

Figure 6.4.2.2 Crane Supporting Structure's Flexibility Effect: Payload Bottom - "Power-ON"

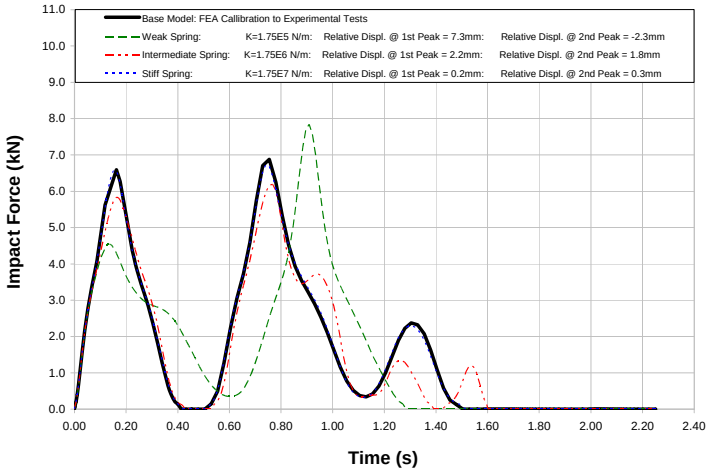

Figure 6.4.2.3 Crane Supporting Structure's Flexibility Effect: Payload Top - "Power-OFF"

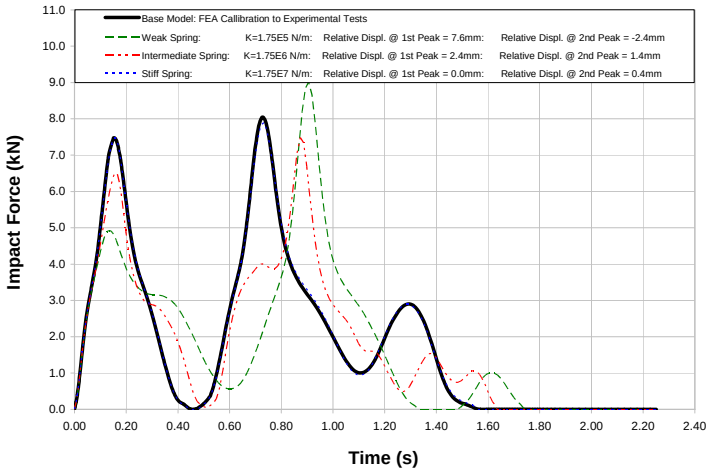

Figure 6.4.2.4 Crane Supporting Structure's Flexibility Effect: Payload Top - "Power-ON"

Table 6.4.2.1 Comparison of the influence of the **Crane Supporting Structure's Flexibility parameter** when the payload is hoisted **0.15m** above ground level with **"Power-OFF"**

Spring Type	1st Impact Force **(kN)**	2nd Impact Force **(kN)**	Time Difference between the 1st and 2nd peaks **(s)**	Difference of the 1st Impact Force w.r.t. Base Model **(%)**	Difference of the 2nd Impact Force w.r.t. Base Model **(%)**	Time difference between the 1st and 2nd peaks **(%)**
Base Model: Calibrated with Experimental model	*6.35*	*4.43*	*0.71*	*N/A*	*N/A*	*N/A*
Weak	4.46	6.25	0.79	-30	41	11
Intermediate	5.52	4.86	0.72	-13	10	1
Stiff	6.29	4.38	0.71	-1	-1	0

Table 6.4.2.2 Comparison of the influence of the **Crane Supporting Structure's Flexibility parameter** when the payload is hoisted **0.15m** above ground level with **"Power-ON"**

Spring Type	1st Impact Force **(kN)**	2nd Impact Force **(kN)**	Time Difference between the 1st and 2nd peaks **(s)**	Difference of the 1st Impact Force w.r.t. Base Model **(%)**	Difference of the 2nd Impact Force w.r.t. Base Model **(%)**	Time difference between the 1st and 2nd peaks **(%)**
Base Model: Calibrated with Experimental model	*7.26*	*4.61*	*0.68*	*N/A*	*N/A*	*N/A*
Weak	5.03	6.85	0.76	-31	49	12
Intermediate	6.62	5.01	0.72	-9	9	6
Stiff	7.65	4.65	0.66	5	1	-3

Table 6.4.2.3 Comparison of the influence of the **Crane Supporting Structure's Flexibility parameter** when the payload is hoisted **2.20m** above ground level with **"Power-OFF"**

Spring Type	1st Impact Force **(kN)**	2nd Impact Force **(kN)**	Time Difference between the 1st and 2nd peaks **(s)**	Difference of the 1st Impact Force w.r.t. Base Model **(%)**	Difference of the 2nd Impact Force w.r.t. Base Model **(%)**	Time difference between the 1st and 2nd peaks **(%)**
Base Model: Calibrated with Experimental model	*6.65*	*6.88*	*0.58*	*N/A*	*N/A*	*N/A*
Weak	4.55	7.84	0.78	-32	14	34
Intermediate	4.84	6.19	0.60	-27	-10	3
Stiff	6.58	6.74	0.59	-1	-2	2

Table 6.4.2.4 Comparison of the influence of the **Crane Supporting Structure's Flexibility parameter** when the payload is hoisted **2.20m** above ground level with **"Power-ON"**

Spring Type	1st Impact Force **(kN)**	2nd Impact Force **(kN)**	Time Difference between the 1st and 2nd peaks **(s)**	Difference of the 1st Impact Force w.r.t. Base Model **(%)**	Difference of the 2nd Impact Force w.r.t. Base Model **(%)**	Time difference between the 1st and 2nd peaks **(%)**
Base Model: Calibrated with Experimental model	*7.48*	*8.05*	*0.58*	*N/A*	*N/A*	*N/A*
Weak	4.92	9.01	0.77	-34	12	33
Intermediate	6.52	7.48	0.71	-13	-7	22
Stiff	7.48	7.90	0.57	0	-2	-2

6.5 The Effect of the Longitudinal Crane Travel Speed on the Impact Response

6.5.1 Description of the Crane Speed model parameter setup

The torque produced by the wheel motors of the crane is constantly adjusted to maintain a constant speed. This results in the crane speed being either slightly greater or less than the nominal speed of 0.55m/s. From the experimental data, the speed measured by the encoders on the motorized wheels differs by as much as ±0.05m/s from the calculated speed of the crane. Subsequently, the effect of the increase or decrease of the crane speed on the impact response was investigated. The speed of the crane was adjusted to 0.50m/s (- 9%) and 0.60m/s (+ 9%).

In addition, the proposed SANS 10160 code stipulates that the speed of the crane can be reduced by 30% if speed retarding mechanisms are installed on the crane and crane supporting structure. The reduced impact speed of 0.385m/s was also investigated.

The responses obtained from the FEA simulations are intuitive. The impact response increases as the speed of the crane increases. In the same manner as the speed of the crane decreases, so too does the impact response.

6.5.2 Interpretation of the FEA simulations

Figures 6.5.2.1 to 6.5.2.4 present the FEA simulations effect of the crane speed on the impact response, for the “Power-Off” and the “Power-On” cases when the payload is 0.15m and 2.20m above ground level. For enlargements of Figures 6.5.2.1 to 6.5.2.4 refer to Appendix D, “FEA Longitudinal Travel Crane Speed Responses”. The tabular analyses of the magnitudes of the 1st and 2nd peaks as well as the time difference between the peaks are presented in Tables 6.5.2.1 to 6.5.2.4.

6.5.2.1 Remarks when the payload is 0.15m above ground level

When the longitudinal crane travel speed decreases the subsequent trends are apparent for the FEA “Power-Off” and “Power-On” simulations with respect to the base response:

- the 1st impact force decreases
- the 2nd impact force decreases
- the time differences between the 1st and 2nd peaks remain relatively unaffected.

The reverse occurs when the longitudinal crane travel speed increases, except for the time difference between the peaks which remain relatively unchanged

- the 1st impact force increases
- the 2nd impact force increases

The significant information which can be extrapolated from the FEA "Power-Off" simulations with respect to the base responses is:

- The 1st impact force increases by 24% when the longitudinal crane speed increases by 0.05m/s (a 9% increase in the speed of the crane).
- The 2nd impact force increases by 53% when the longitudinal crane speed increases by 0.05m/s (a 9% increase in the speed of the crane).
- The time difference between the impact peaks decreases by 9% when the longitudinal crane speed decreases by 30% to 0.385m/s.
- When full power "Power-On" is included in the FEA simulations, the maximum impact force increases from 7.88kN to 8.97kN, an increase of 14%.
- When the speed of the crane is reduced by 30% to 0.385m/s, the 1st and 2nd peaks decrease by 46% and 41%, respectively. The time between the peaks yield a maximum difference of 9%.

6.5.2.2 Remarks when the payload is 2.20m above ground level

The impact response when the payload is hoisted 2.20m above ground level follows the same trend as when the payload is 0.15m above ground level.

- The 1st impact force increases by 25% when the longitudinal crane speed increases by 0.05m/s (a 9% increase in the speed of the crane).
- The 2nd impact force increases by 28% when the longitudinal crane speed increases by 0.05m/s (a 9% increase in the speed of the crane).
- The time difference between the impact peaks decreases by 3% when the longitudinal crane speed increases by 0.05m/s.
- When full power "Power-On" is included in the FEA simulations, the maximum impact

force increases from 8.30kN to 10.34kN, an increase of 25%. This is the occasional case when the maximum 2nd impact force is greater than the maximum 1st impact force.

- When the speed of the crane is reduced by 30% to 0.385m/s, the 1st and 2nd peaks decrease by 51% and 54% respectively. The time between the peaks yield a maximum difference of 2%.

6.5.2.3 Conclusion

The maximum impact force of 10.34kN occurs when the crane travels at 0.60m/s (a 9% increase in the speed of the crane) and the payload is hoisted 2.20m above ground level. The 1st and 2nd impact are significantly affected by this parameter, while the period between the impact forces are marginally affected. Thus, the impact response is affected by the longitudinal speed of the crane at the moment of impact.

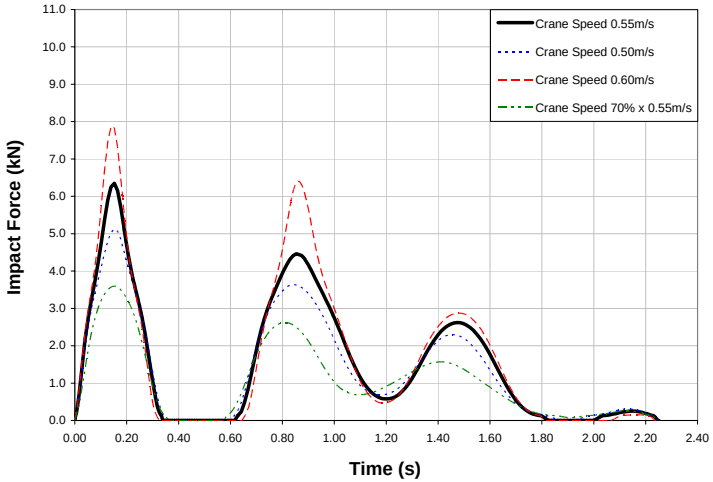

Figure 6.5.2.1 Effect of the Crane speed: Payload Bottom - "Power-OFF"

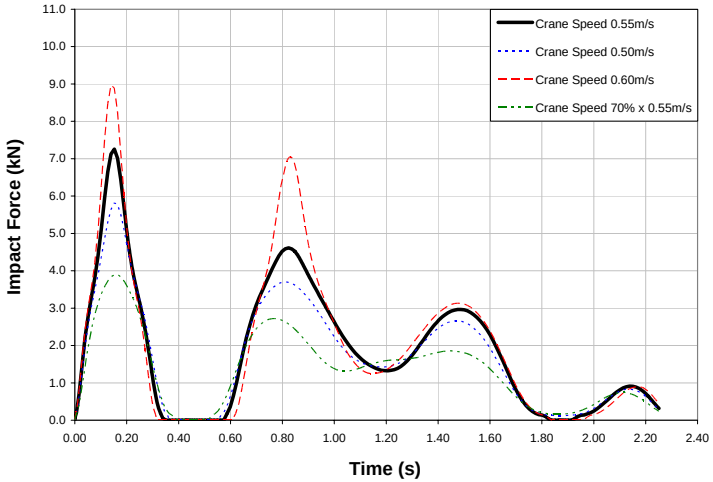

Figure 6.5.2.2 Effect of the Crane speed: Payload Bottom - "Power-ON"

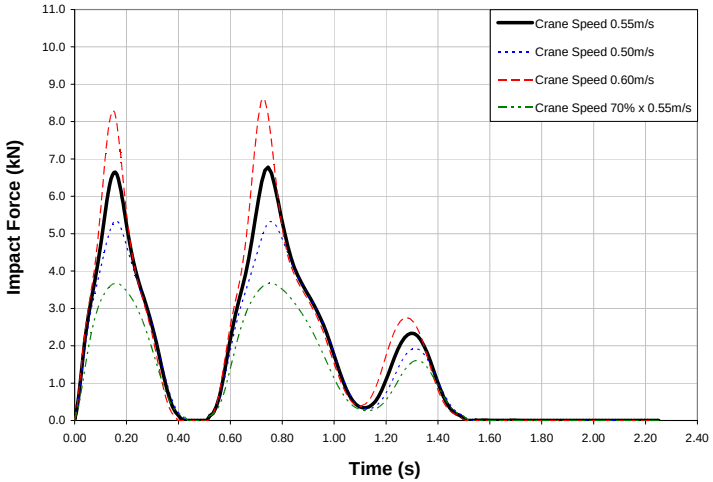

Figure 6.5.2.3 Effect of the Crane speed: Payload Top - "Power-OFF"

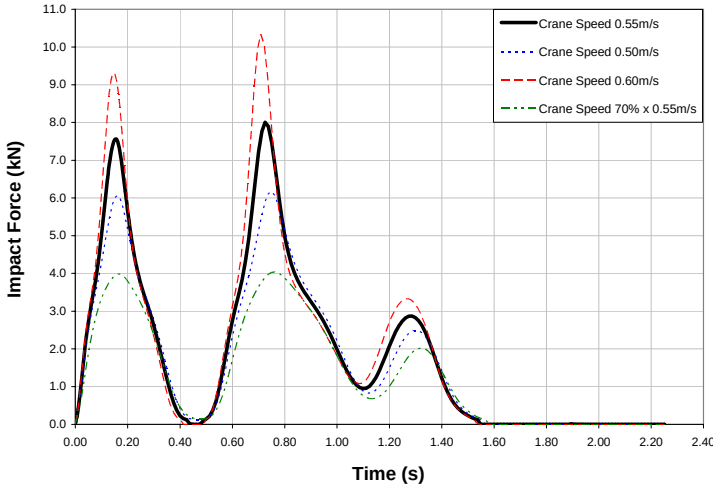

Figure 6.5.2.4 Effect of the Crane speed: Payload Top - "Power-ON"

Table 6.5.2.1 Comparison of the influence of the **Crane Speed parameter** when the payload is hoisted **0.15m** above ground level with **"Power-OFF"**

Crane Speed **(m/s)**	1st Impact Force **(kN)**	2nd Impact Force **(kN)**	Time Difference between the 1st and 2nd peaks **(s)**	Difference of the 1st Impact Force w.r.t. Base Model **(%)**	Difference of the 2nd Impact Force w.r.t. Base Model **(%)**	Time difference between the 1st and 2nd peaks **(%)**
70% x 0.55 = 0.385 (30% Decrease)	3.60	2.62	0.66	-43	-41	-7
0.50 (9% Decrease)	5.13	3.64	0.69	-19	-18	-3
Base Model: 0.55	*6.35*	*4.43*	*0.71*	*N/A*	*N/A*	*N/A*
0.60 (9% Increase)	7.88	6.41	0.72	24	45	1

Table 6.5.2.2 Comparison of the influence of the **Crane Speed parameter** when the payload is hoisted **0.15m** above ground level with **"Power-ON"**

Crane Speed **(m/s)**	1st Impact Force **(kN)**	2nd Impact Force **(kN)**	Time Difference between the 1st and 2nd peaks **(s)**	Difference of the 1st Impact Force w.r.t. Base Model **(%)**	Difference of the 2nd Impact Force w.r.t. Base Model **(%)**	Time difference between the 1st and 2nd peaks **(%)**
70% x 0.55 = 0.385 (30% Decrease)	3.90	2.72	0.62	-46	-41	-9
0.50 (9% Decrease)	5.82	3.70	0.66	-20	-20	-3
Base Model: 0.55	*7.26*	*4.61*	*0.68*	*N/A*	*N/A*	*N/A*
0.60 (9% Increase)	8.97	7.05	0.69	24	53	1

Table 6.5.2.3 Comparison of the influence of the **Crane Speed parameter** when the payload is hoisted **2.20m** above ground level with **"Power-OFF"**

Crane Speed **(m/s)**	1st Impact Force **(kN)**	2nd Impact Force **(kN)**	Time Difference between the 1st and 2nd peaks **(s)**	Difference of the 1st Impact Force w.r.t. Base Model **(%)**	Difference of the 2nd Impact Force w.r.t. Base Model **(%)**	Time difference between the 1st and 2nd peaks **(%)**
70% x 0.55 = 0.385 (30% Decrease)	3.67	3.68	0.59	-45	-47	2
0.50 (9% Decrease)	5.35	5.35	0.59	-20	-22	2
Base Model: 0.55	*6.65*	*6.88*	*0.58*	*N/A*	*N/A*	*N/A*
0.60 (9% Increase)	8.30	8.30	0.58	25	21	0

Table 6.5.2.4 Comparison of the influence of the **Crane Speed parameter** when the payload is hoisted **2.20m** above ground level with **"Power-ON"**

Crane Speed **(m/s)**	1st Impact Force **(kN)**	2nd Impact Force **(kN)**	Time Difference between the 1st and 2nd peaks **(s)**	Difference of the 1st Impact Force w.r.t. Base Model **(%)**	Difference of the 2nd Impact Force w.r.t. Base Model **(%)**	Time difference between the 1st and 2nd peaks **(%)**
70% x 0.55 = 0.385 (30% Decrease)	3.67	3.68	0.59	-51	-54	2
0.50 (9% Decrease)	6.06	6.17	0.59	-19	-23	2
Base Model: 0.55	*7.48*	*8.05*	*0.58*	*N/A*	*N/A*	*N/A*
0.60 (9% Increase)	9.31	10.34	0.56	24	28	-3

6.6 The Effect of the End Stop Misalignment on the Impact Response

6.6.1 Description of the End Stop Misalignment model parameter setup

As the length of the crane bridge increases the probability increases that the end stops will be misaligned. A 25mm misalignment of one of the end stops over an 8m length is barely noticeable. The researcher chose to misalign the left hand side end stop by 25mm and 50mm to study their effect on the impact response. Figure 6.6.1.1 presents the left hand side end stop misaligned.

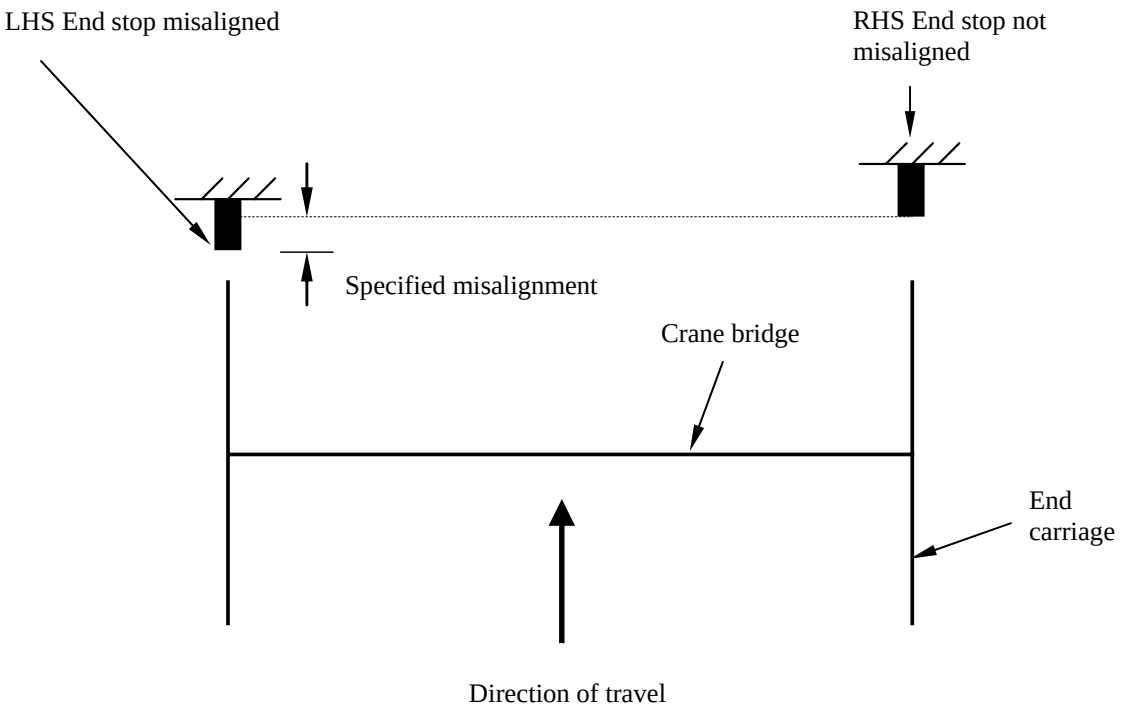

Figure 6.6.1.1 Schematic presentation of the plan view of a misaligned end stop

Additionally, one of the end stops could also be misaligned by as much as 150mm. This misalignment is due to the end block used to prevent the wheels from touching the angle plate shown in Figure 6.6.1.2 being omitted or falling from its position.

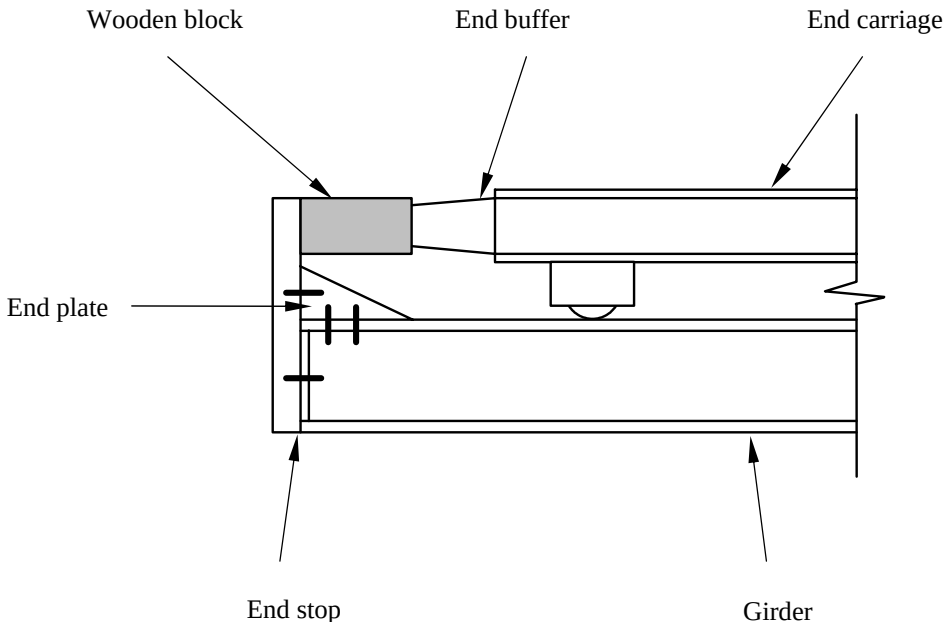

Figure 6.6.1.2 Schematic presentation of the side elevation showing the wooden block, end buffer and end stop

The acceleration boundary condition specified on the motorized wheels is deactivated at the moment of impact with the first (LHS) buffer. From this moment the impact response is dependent on the inertia of the crane and the payload.

6.6.2 Interpretation of the FEA simulations

Figures 6.6.2.1 to 6.6.2.4 present the FEA simulations effect of the crane supporting structure's flexibility on the impact response, for the "Power-Off" and the "Power-On" cases when the payload is 0.15m and 2.20m above ground level. For enlargements of Figures 6.6.2.1 to 6.6.2.4, refer to Appendix E, "FEA End Stop Eccentricity Responses". The tabular analyses of the magnitudes of the 1st and 2nd peaks as well as the time difference between the peaks are presented in Tables 6.6.2.1 to 6.6.2.4.

Surprisingly, the impact forces did not significantly increase as the end stop misalignment increased.

6.6.2.1 Remarks when the payload is 0.15m above ground level

As the end stop misalignment increases the subsequent trends are apparent for the FEA "Power-Off" and "Power-On" simulations with respect to the base response;

- the 1st impact force increases
- the 2nd impact force increases
- the time differences between the 1st and 2nd peaks increases.

The significant information which can be extrapolated from the FEA "Power-Off" simulations with respect to the base responses is:

- The 1st impact force increases by 33% when the LHS end stop is misaligned by 150mm.
- The 2nd impact force increases by 65% when the LHS end stop is misaligned by 150mm.
- The time difference between the impact peaks increases by 32% when the LHS end stop is misaligned by 50mm.
- The 1st impact force with "Power-Off" stabilizes at approximately 7.90kN and does not significantly increase as the end buffer's misalignment increases.
- When full power "Power-On" is included in the FEA simulations, the maximum impact force increases from 7.43kN to 9.69kN, an increase of 30%.

6.6.2.2 Remarks when the payload is 2.20m above ground level

The impact response when the payload is hoisted 2.20m above ground level follows the same trend as when the payload is 0.15m above ground level.

- The 1st impact force increases by 34% when the LHS end stop is misaligned by 50mm.
- The 2nd impact force increases by 37% when the LHS end stop is misaligned by 25mm.
- The time difference between the impact peaks increases by 34% when the LHS end stop is misaligned by 150mm.
- The 1st impact force with "Power-Off" stabilizes at approximately 8.92kN and does not significantly increase as the end buffer's misalignment increases.
- This is the occasional case when the maximum 2nd impact force is greater than the maximum 1st impact force.
- When full power "Power-On" is included in the FEA simulations, the maximum impact force increases from 9.41kN to 10.11kN, an increase of 7%.

6.6.2.3 Conclusion

The researcher expected the impact forces to increase significantly as the end stops misalignment increases. Possible reasons for the lower than expected impact forces are; the flexibility of the crane and skewing of the crane may cause side friction on the skis to have a clamping effect and act as a brake, resulting in the increasing end stop misalignment to have little further influence on the magnitude of the impact force. The impact response at the non misaligned side reduces rapidly as the misalignment increases. The impact forces at the non misaligned side yields no response when the end stop is misaligned to 150mm. The maximum impact force obtained for this parameter is 9.78kN.

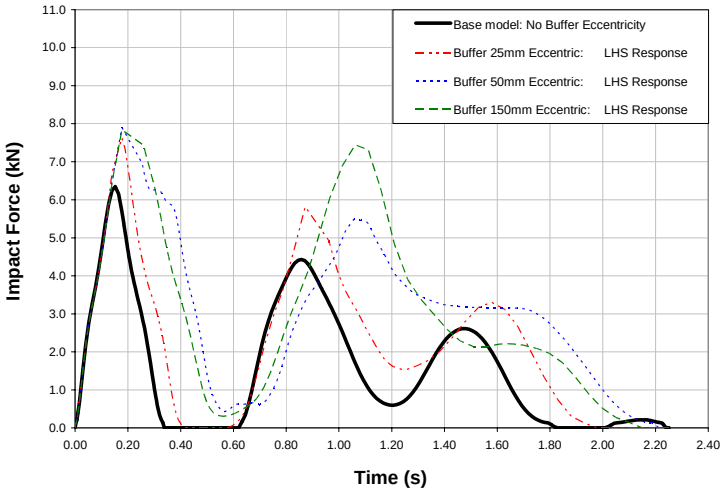

Figure 6.6.2.1 End Stop Misalignment Effect: Payload Bottom - "Power-OFF"

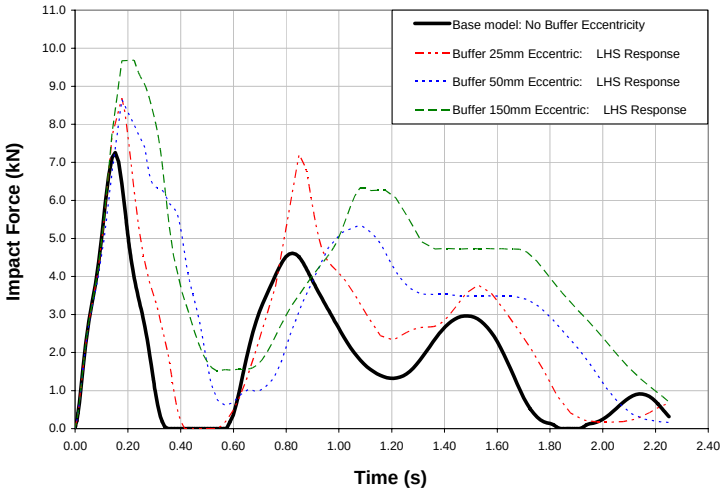

Figure 6.6.2.2 End Stop Misalignment Effect: Payload Bottom - "Power-ON"

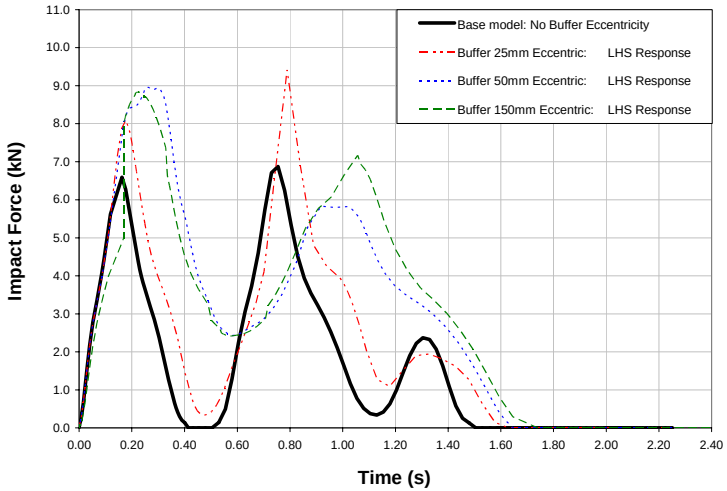

Figure 6.6.2.3 End Stop Misalignment Effect: Payload Top - "Power-OFF"

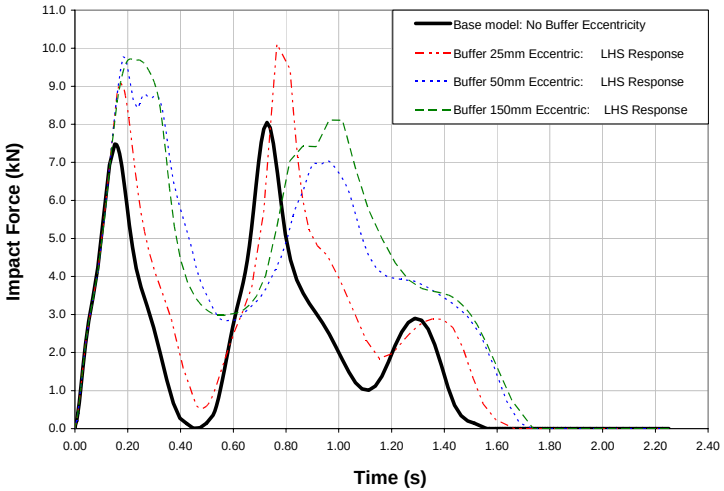

Figure 6.6.2.4 End Stop Misalignment Effect: Payload Top - "Power-ON"

Table 6.6.2.1 Comparison of the influence of an **End Stop Misalignment parameter** when the payload is hoisted **0.15m** above ground level with "**Power-OFF"**

Horizontal Misalignment of the LHS End Stop	1st Impact Force **(kN)**	2nd Impact Force **(kN)**	Time Difference between the 1st and 2nd peaks **(s)**	Difference of the 1st Impact Force w.r.t. Base Model **(%)**	Difference of the 2nd Impact Force w.r.t. Base Model **(%)**	Time difference between the 1st and 2nd peaks **(%)**
Base Model (≙0)	*6.35*	*4.43*	*0.71*	*N/A*	*N/A*	*N/A*
25mm	7.63	4.91	0.79	20	11	11
50mm	7.90	5.49	0.88	24	24	24
150mm	7.43	7.31	0.85	17	65	20

Table 6.6.2.2 Comparison of the influence of an **End Stop Misalignment parameter** when the payload is hoisted **0.15m** above ground level with **"Power-ON"**

Horizontal Misalignment of the LHS End Stop	1st Impact Force **(kN)**	2nd Impact Force **(kN)**	Time Difference between the 1st and 2nd peaks **(s)**	Difference of the 1st Impact Force w.r.t. Base Model **(%)**	Difference of the 2nd Impact Force w.r.t. Base Model **(%)**	Time difference between the 1st and 2nd peaks **(%)**
Base Model (≙0)	*7.26*	*4.61*	*0.68*	*N/A*	*N/A*	*N/A*
25mm	8.69	6.84	0.70	20	48	3
50mm	8.65	5.33	0.90	19	16	32
150mm	9.69	6.33	0.86	33	37	26

Table 6.6.2.3 Comparison of the influence of an **End Stop Misalignment parameter** when the payload is hoisted **2.20m** above ground level with **"Power-OFF"**

Horizontal Misalignment of the LHS End Stop	1st Impact Force **(kN)**	2nd Impact Force **(kN)**	Time Difference between the 1st and 2nd peaks **(s)**	Difference of the 1st Impact Force w.r.t. Base Model **(%)**	Difference of the 2nd Impact Force w.r.t. Base Model **(%)**	Time difference between the 1st and 2nd peaks **(%)**
Base Model (≙0)	*6.65*	*6.88*	*0.58*	*N/A*	*N/A*	*N/A*
25mm	8.09	9.41	0.61	22	37	5
50mm	8.92	5.83	0.61	34	-15	5
150mm	8.83	7.16	0.78	33	4	34

Table 6.6.2.4 Comparison of the influence of an **End Stop Misalignment parameter** when the payload is hoisted **2.20m** above ground level with **"Power-ON"**

Horizontal Misalignment of the LHS End Stop	1st Impact Force **(kN)**	2nd Impact Force **(kN)**	Time Difference between the 1st and 2nd peaks **(s)**	Difference of the 1st Impact Force w.r.t. Base Model **(%)**	Difference of the 2nd Impact Force w.r.t. Base Model **(%)**	Time difference between the 1st and 2nd peaks **(%)**
Base Model (≙0)	*7.48*	*8.05*	*0.58*	*N/A*	*N/A*	*N/A*
25mm	9.10	10.11	0.59	22	26	2
50mm	9.78	7.04	0.77	31	-13	33
150mm	9.72	8.11	0.75	30	1	29

6.7 Effect of the Elastic Buffer Characteristics on the Impact Response

6.7.1 Description of the Elastic Buffer Characteristics model parameter setup

The elastic characteristics are influenced by various factors such as, the age of the buffers, the temperature of the buffers, the environment conditions which the buffers are exposed to and the numbers of times the buffer collides with the end stops within a short period of time. To allow for these factors, the buffers characteristics were adjusted by 10% ± and 20% ± to determine their effect on the impact response. The elastic characteristics of both LHS and RHS buffer were adjusted. This was achieved by adjusting only the impact force and leaving the buffer deformation unchanged.

Figure 6.7.1.1 presents the graphical representation of the base and adjusted models' elastic characteristics curves.

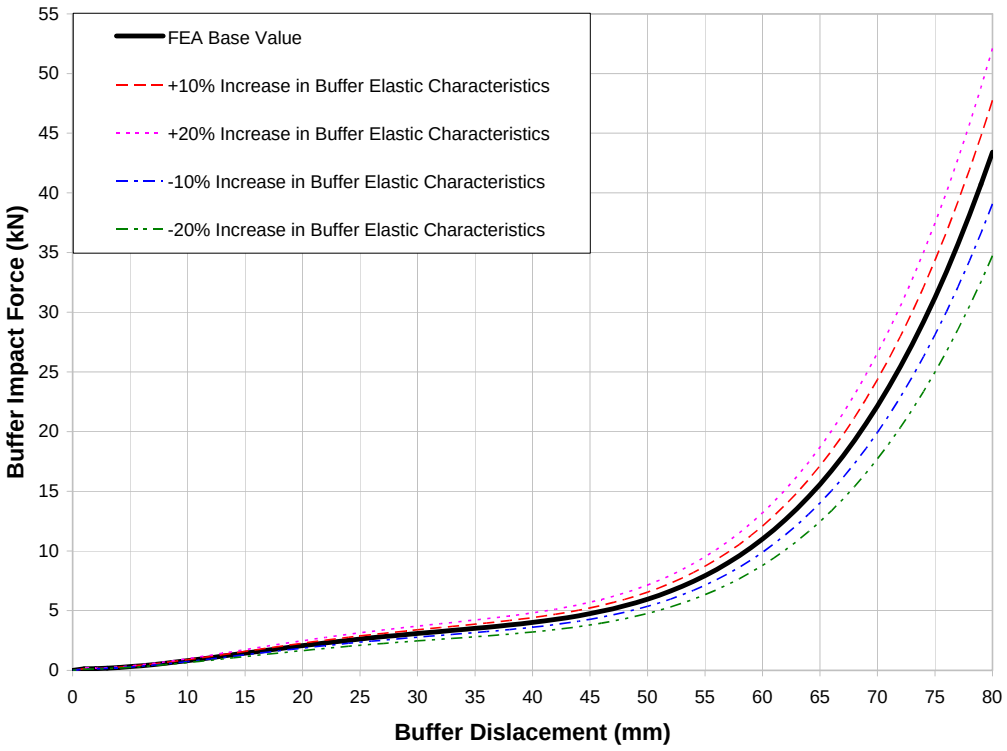

Figure 6.7.1.1 Graphical representation of the base and adjusted models' elastic characteristics curves.

6.7.2 Interpretation of the FEA simulations

Figures 6.7.2.1 to 6.7.2.4 present the FEA simulations effect of the crane supporting structure's flexibility on the impact response, for the "Power-Off" and the "Power-On" cases when the payload is 0.15m and 2.20m above ground level. For enlargements of Figures 6.7.2.1 to 6.7.2.4, refer to Appendix F, "FEA Elastic Buffer Characteristics Responses". The tabular analyses of the magnitudes of the 1st and 2nd peaks as well as the time difference between the peaks are presented in Tables 6.7.2.1 to 6.7.2.4.

6.7.2.1 Remarks when the payload is 0.15m above ground level

This parameter has a minimal effect on the force impact response. There are not any trends which are worth noting.

The significant information which can be extrapolated from the FEA "Power-Off" simulations with respect to the base responses are;

- The 1st impact force decreases by 4% when the buffer elastic characteristics are decreased by 20%.
- The 2nd impact force increases by 8% when the buffer elastic characteristics are increased by 20%.
- The time difference between the impact peaks increases by 4% when the buffer elastic characteristics are decreased by 20%.
- When full power "Power-On" is included in the FEA simulations, the maximum impact force increases from 6.38kN to 7.14kN, an increase of 12%.

6.7.2.2 Remarks when the payload is 2.20m above ground level

The impact response when the payload is hoisted 2.20m above ground level follows the same trend as when the payload is 0.15m above ground level.

- The 1st impact force increases by 6% when the buffer elastic characteristics are decreased by 20%.
- The 2nd impact force increases by 10% when the buffer elastic characteristics are decreased by 20%.
- The time difference between the impact peaks increases by 9% when the buffer elastic

characteristics are increased by 20%.

- When full power “Power-On” is included in the FEA simulations, the maximum impact force increases from 6.81kN to 7.92kN, an increase of 16%.

6.7.2.3 Conclusion

The maximum impact force of 7.92kN occurs when the payload is hoisted to 2.20m above ground level. This parameter has very little effect on the impact response. A greater difference in the impact forces was expected since the LHS buffer characteristics were adjusted by ±20%.

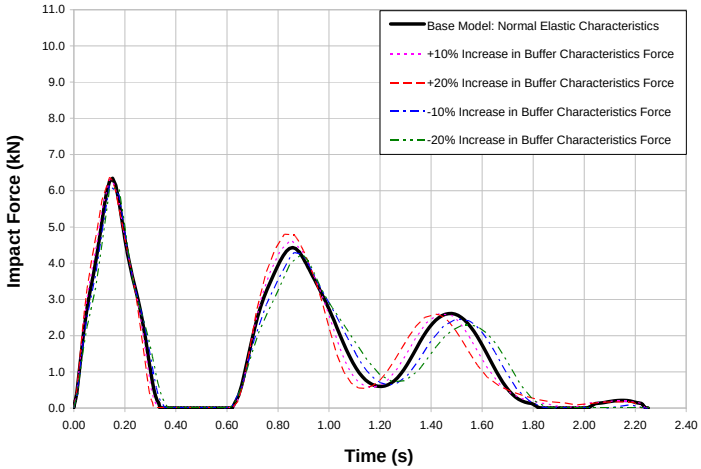

Figure 6.7.2.1 Elastic Characteristics Effect: Payload Bottom - "Power-OFF"

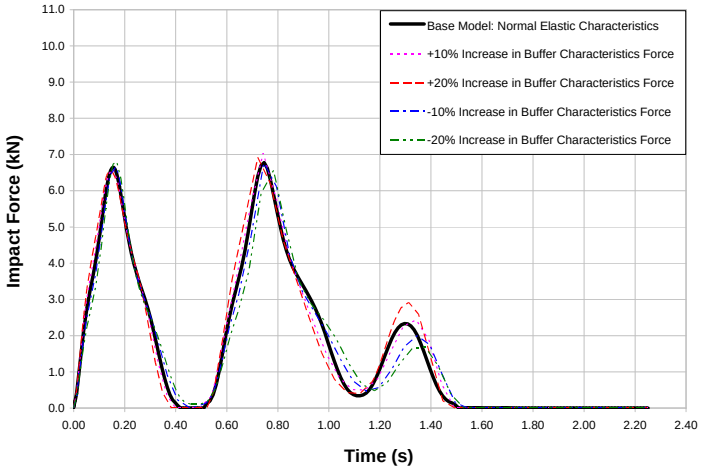

Figure 6.7.2.3 Elastic Characteristics Effect: Payload Top - "Power-OFF"

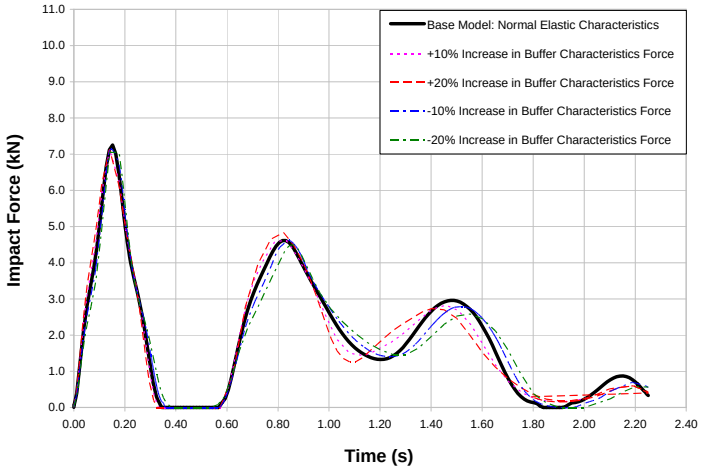

Figure 6.7.2.2 Elastic Characteristics Effect: Payload Bottom - "Power-ON"

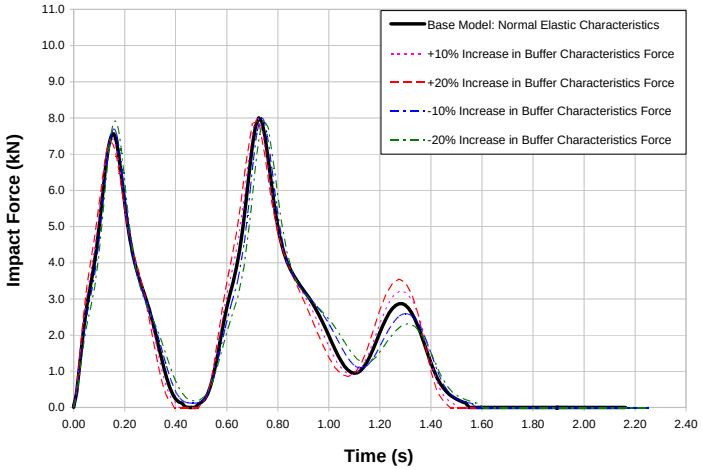

Figure 6.7.2.4 Elastic Characteristics Effect: Payload Top - "Power-ON"

Table 6.7.2.1 Comparison of the influence of the **Elastic Buffer parameter** when the payload is hoisted **0.15m** above ground level with **"Power-OFF"**

Elastic Characteristics of the Buffer	1st Impact Force **(kN)**	2nd Impact Force **(kN)**	Time Difference between the 1st and 2nd peaks **(s)**	Difference of the 1st Impact Force w.r.t. Base Model **(%)**	Difference of the 2nd Impact Force w.r.t. Base Model **(%)**	Time difference between the 1st and 2nd peaks **(%)**
+10% Force Increase	6.31	4.64	0.71	-1	5	0
+20% Force Increase	6.38	4.80	0.68	0	8	-4
Base Model	*6.35*	*4.43*	*0.71*	*N/A*	*N/A*	*N/A*
-10% Force Increase	6.16	4.29	0.72	-3	-3	1
-20% Force Increase	6.08	4.07	0.74	-4	-8	4

Table 6.7.2.2 Comparison of the influence of the **Elastic Buffer parameter** when the payload is hoisted **0.15m** above ground level with **"Power-ON"**

Elastic Characteristics of the Buffer	1st Impact Force **(kN)**	2nd Impact Force **(kN)**	Time Difference between the 1st and 2nd peaks **(s)**	Difference of the 1st Impact Force w.r.t. Base Model **(%)**	Difference of the 2nd Impact Force w.r.t. Base Model **(%)**	Time difference between the 1st and 2nd peaks **(%)**
+10% Force Increase	7.13	4.63	0.69	-2	0	1
+20% Force Increase	7.14	4.83	0.68	-2	5	0
Base Model	*7.26*	*4.61*	*0.68*	*N/A*	*N/A*	*N/A*
-10% Force Increase	7.09	4.62	0.70	-2	0	3
-20% Force Increase	7.05	4.50	0.68	-3	-2	0

Table 6.7.2.3 Comparison of the influence of the **Elastic Buffer parameter** when the payload is hoisted **2.20m** above ground level with **"Power-OFF"**

Elastic Characteristics of the Buffer	1st Impact Force **(kN)**	2nd Impact Force **(kN)**	Time Difference between the 1st and 2nd peaks **(s)**	Difference of the 1st Impact Force w.r.t. Base Model **(%)**	Difference of the 2nd Impact Force w.r.t. Base Model **(%)**	Time difference between the 1st and 2nd peaks **(%)**
+10% Force Increase	6.61	7.04	0.59	-1	2	2
+20% Force Increase	6.56	6.92	0.63	-1	1	9
Base Model	*6.65*	*6.88*	*0.58*	*N/A*	*N/A*	*N/A*
-10% Force Increase	6.66	6.77	0.58	0	-2	0
-20% Force Increase	6.81	7.57	0.62	2	10	7

Table 6.7.2.4 Comparison of the influence of the **Elastic Buffer parameter** when the payload is hoisted **2.20m** above ground level with **"Power-ON"**

Elastic Characteristics of the Buffer	1st Impact Force **(kN)**	2nd Impact Force **(kN)**	Time Difference between the 1st and 2nd peaks **(s)**	Difference of the 1st Impact Force w.r.t. Base Model **(%)**	Difference of the 2nd Impact Force w.r.t. Base Model **(%)**	Time difference between the 1st and 2nd peaks **(%)**
+10% Force Increase	7.43	8.04	0.57	-1	0	-2
+20% Force Increase	7.33	7.91	0.58	-2	-2	0
Base Model	*7.48*	*8.05*	*0.58*	*N/A*	*N/A*	*N/A*
-10% Force Increase	7.69	8.00	0.58	3	-1	0
-20% Force Increase	7.92	7.96	0.58	6	-1	0

6.8 Effect of the Buffer Damping Characteristics on the Impact Response

6.8.1 Description of the Buffer Damping Characteristics model parameter setup

The buffer damping characteristics are typically not supplied by the manufacturer and thus can only be determined experimentally. This creates a problem as the designer of the crane supporting structure has no indication of the energy absorption characteristics of the buffers. If the end buffers disintegrate during the 1st impact this will results in a loss of the buffer's elastic and damping characteristics for the consecutive impacts. Without the end buffer damping characteristics, the subsequent peaks could be significantly higher. The damping characteristics of the buffers were eliminated from the FEA simulations to determine the effect on the impact response. This results in the impact response loading and unloading along the same path, i.e. the elastic characteristics curve.

6.8.2 Interpretation of the FEA simulations

Figures 6.8.2.1 to 6.8.2.4 present the FEA simulations effect of the buffer damping characteristics on the impact response, for the "Power-Off" and the "Power-On" cases when the payload is 0.15m and 2.20m above ground level. For enlargements of Figures 6.8.2.1 to 6.8.2.4, refer to Appendix G, "FEA Buffer Damping Characteristic Responses". The tabular analyses of the magnitudes of the 1st and 2nd peaks as well as the time difference between the peaks are presented in Tables 6.8.2.1 to 6.8.2.4.

The damping characteristics as defined in Chapter 3 were used for the base model. This was compared to the FEA simulations when the damping characteristics were omitted.

The impact responses obtained from the FEA simulations are intuitive. The buffers act like springs when the buffer's damping characteristics are eliminated from the FEA simulations. The omission of the damping characteristics results in higher impact forces and also greater time differences between the peaks.

6.8.2.1 Remarks when the payload is 0.15m above ground level

When the damping characteristics are omitted from the FEA "Power-Off" and "Power-On" simulations, the following trends develop with respect to the base response:

- the 1st impact force increases
- the 2nd impact force increases
- the time difference between the 1st and 2nd peaks increases.

The significant information which can be extrapolated from the FEA "Power-Off" simulations with respect to the base responses is:

- The 1st impact force increases by 20%.
- The 2nd impact force increases by 211%.
- The time difference between the impact peaks increases by 17%.
- When full power "Power-On" is included in the FEA simulations, the maximum impact force increases from 13.03kN to 14.33kN, an increase of 10%.
- This is the occasional case when the maximum 2nd impact force is greater than the maximum 1st impact force.

6.8.2.2 Remarks when the payload is 2.20m above ground level

The impact response when the payload is hoisted 2.20m above ground level follows the same trend as when the payload is 0.15m above ground level.

The significant information which can be extrapolated from the FEA "Power-Off" simulations with respect to the base responses is:

- The 1st impact force increases by 20%.
- The 2nd impact force increases by 57%.
- The time difference between the impact peaks increases by 10%.
- When full power "Power-On" is included in the FEA simulations, the maximum impact force increases from 10.77kN to 12.48kN, an increase of 16%.
- This is the occasional case when the maximum 2nd impact force is greater than the maximum 1st impact force.

6.8.2.3 Conclusion

The maximum impact force of 14.33kN occurs when the payload is hoisted 0.15m above ground level. The 1st and 2nd impacts as well as the period between the peaks, are significantly affected by this parameter. Thus, the impact response is indeed affected by the buffer damping characteristics at the moment of impact.

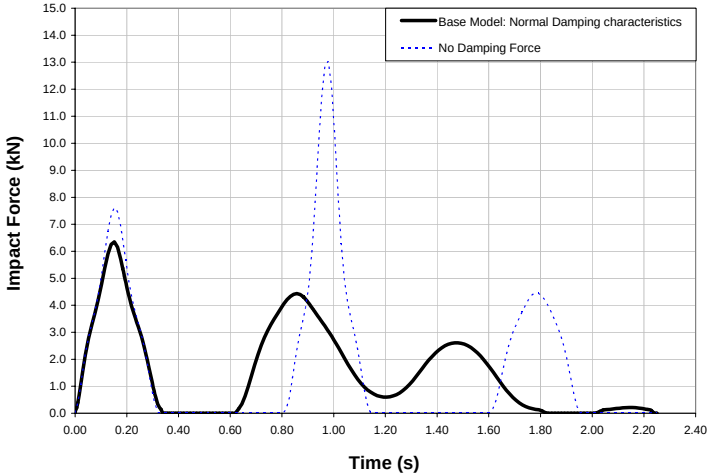

Figure 6.8.2.1 Damping Characteristics Effect: Payload Bottom - "Power-OFF"

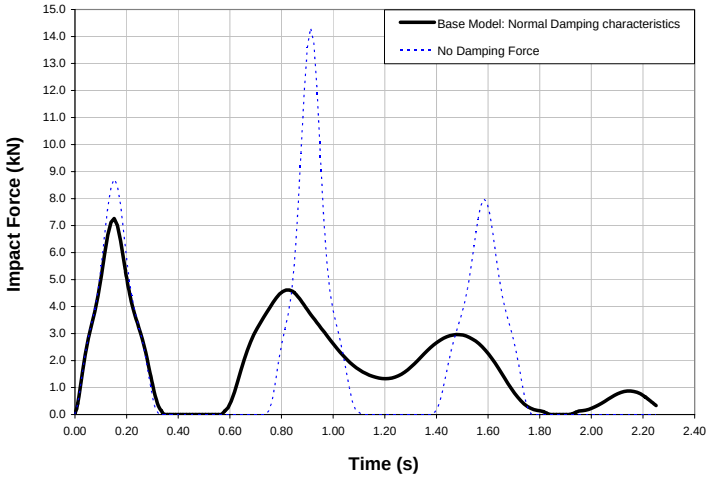

Figure 6.8.2.2 Damping Characteristics Effect: Payload Bottom - "Power-ON"

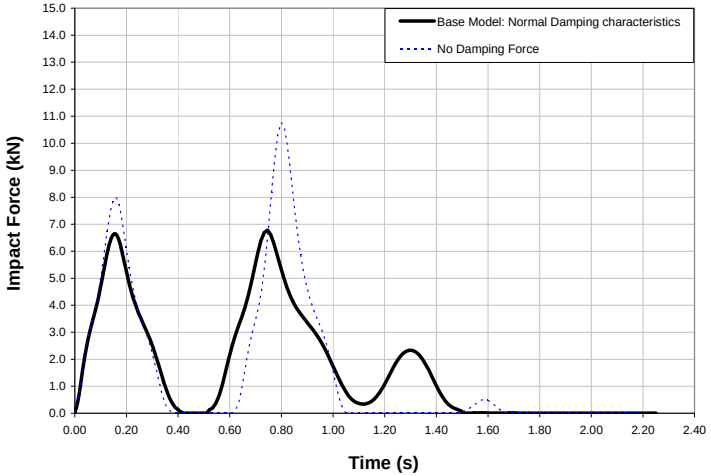

Figure 6.8.2.3 Damping Characteristics Effect: Payload Top - "Power-OFF"

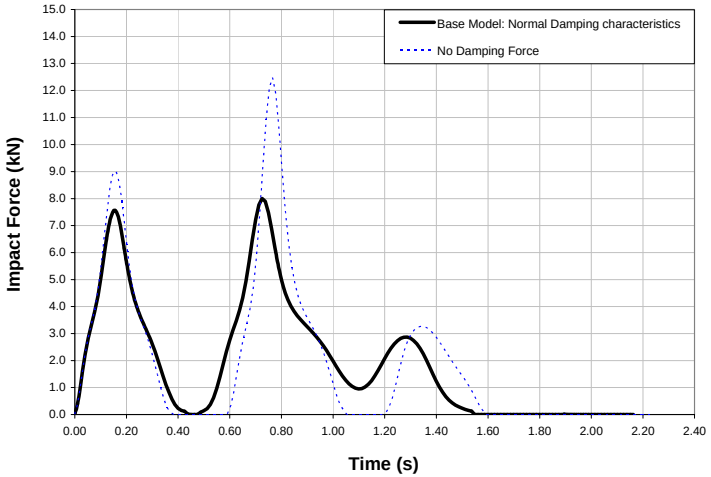

Figure 6.8.2.4 Damping Characteristics Effect: Payload Top - "Power-ON"

Table 6.8.2.1 Comparison of the influence of the **Buffer Damping parameter** when the payload is hoisted **0.15m** above ground level with **"Power-OFF"**

Damping Characteristics of the Buffers	1st Impact Force **(kN)**	2nd Impact Force **(kN)**	Time Difference between the 1st and 2nd peaks **(s)**	Difference of the 1st Impact Force w.r.t. Base Model **(%)**	Difference of the 2nd Impact Force w.r.t. Base Model **(%)**	Time difference between the 1st and 2nd peaks **(%)**
Base Model	*6.35*	*4.43*	*0.71*	*N/A*	*N/A*	*N/A*
No Damping	7.61	13.03	0.83	20	194	17

Table 6.8.2.2 Comparison of the influence of the **Buffer Damping parameter** when the payload is hoisted **0.15m** above ground level with **"Power-ON"**

Damping Characteristics of the Buffers	1st Impact Force **(kN)**	2nd Impact Force **(kN)**	Time Difference between the 1st and 2nd peaks **(s)**	Difference of the 1st Impact Force w.r.t. Base Model **(%)**	Difference of the 2nd Impact Force w.r.t. Base Model **(%)**	Time difference between the 1st and 2nd peaks **(%)**
Base Model	*7.26*	*4.61*	*0.68*	*N/A*	*N/A*	*N/A*
No Damping	8.71	14.33	0.76	20	211	12

Table 6.8.2.3 Comparison of the influence of the **Buffer Damping parameter** when the payload is hoisted **2.20m** above ground level with **"Power-OFF"**

Damping Characteristics of the Buffers	1st Impact Force **(kN)**	2nd Impact Force **(kN)**	Time Difference between the 1st and 2nd peaks **(s)**	Difference of the 1st Impact Force w.r.t. Base Model **(%)**	Difference of the 2nd Impact Force w.r.t. Base Model **(%)**	Time difference between the 1st and 2nd peaks **(%)**
Base Model	*6.65*	*6.88*	*0.58*	*N/A*	*N/A*	*N/A*
No Damping	7.99	10.77	0.64	20	57	10

Table 6.8.2.4 Comparison of the influence of the **Buffer Damping parameter** when the payload is hoisted **2.20m** above ground level with **"Power-ON"**

Damping Characteristics of the Buffers	1st Impact Force **(kN)**	2nd Impact Force **(kN)**	Time Difference between the 1st and 2nd peaks **(s)**	Difference of the 1st Impact Force w.r.t. Base Model **(%)**	Difference of the 2nd Impact Force w.r.t. Base Model **(%)**	Time difference between the 1st and 2nd peaks **(%)**
Base Model	*7.48*	*8.05*	*0.58*	*N/A*	*N/A*	*N/A*
No Damping	9.01	12.48	0.61	20	55	5

6.9 Summary of the Sensitivity Analysis

The maximum end buffer impact force for each parameter obtained from the FEA sensitivity analysis is presented in Table 6.9.1. Hereafter, the maximum end buffer impact force for each parameter obtained from the FEA sensitivity analysis will be referred to as the FEA impact forces. The FEA impact forces were obtained by adjusting one parameter at a time, while keeping the rest of the parameters constant. This results in the parameters acting individually and does not replicate reality. Therefore, the maximum force cannot simply be extracted from the FEA impact forces to obtain the maximum end buffer impact force which the crane will impose on the end buffers.

Table 6.9.1 Summary of the FEA impact forces

Parameter	Case (Scenario) where Maximum Impact Force Occurs	Occurrence of Max. Impact Force	Corresponding Base Impact Force (kN)	Maximum FEA Impact Force (kN)
Lag Angle	Payload Bottom with “Power-On”	1st	7.26	10.03
Crab and Payload Eccentricity	Payload Top with “Power-On”	1st	7.48	9.39
Crane Supporting Structure’s Flexibility	Payload Top with “Power-On”	2nd	8.05	9.01
Crane Impact Speed	Payload Top with “Power-On”	2nd	8.05	10.34
1 End Stop Misaligned	Payload Top with “Power-On”	2nd	8.05	10.11
Modified Buffer ‘s Elastic Characteristics	Payload Top with “Power-On”	2nd	8.05	8.04
Modified Buffer’s Damping Characteristics	Payload Bottom with “Power-On”	2nd	4.61	14.33

Figure 6.9.1 shows a selection of the impact responses of each parameter when varied. The responses of the parameters are superimposed with the base impact response when the payload is hoisted to 0.15m above ground level. Figure 6.9.1, shows that there is a significant difference in the magnitudes of the 1st and 2nd impact forces when compared to the base impact response. The time difference at 1st impact is insignificant, while the time difference at 2nd impact is significant.

This shows that the parameters do have a significant influence on the crane end buffer impact force response. This justifies the differences between the FEA and Experimental impact forces at calibration. Thus, the parameters can be tweaked in such a manner to produce FEA simulations which replicates the experimental impact force responses for the various cases. It is important to note that once the condition changes (i.e. payload height and "Power-Off / On", etc), the magnitude of the parameter's contribution will also be affected.

The FEA simulations were obtained by keeping parameters constant while only varying the parameter being investigated. This is not a true reflection of reality. The parameters were not combined in the FEA simulations since it is difficult to replicate the combined parameter effect experimentally to determine the maximum end buffer impact force. The maximum end buffer impact force is determined using a Constraint Optimization described in detail in chapter 7.

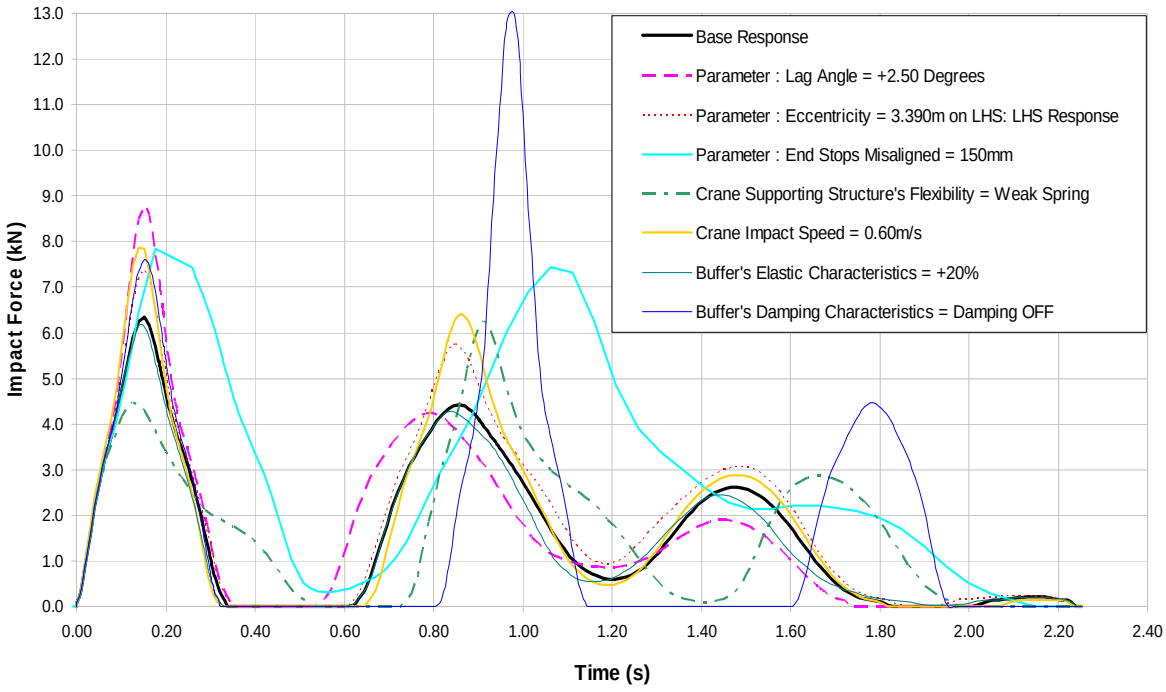

Figure 6.9.1 Selected impact force response of each parameter compared to base response when payload is hoisted to 0.15m above ground level

CHAPTER 7: ESTIMATION OF IMPACT FORCE DISTRIBUTION, COMPARISON WITH DESIGN CODES

7.1 Introduction

A constrained optimization technique was employed to determine the maximum end buffer impact force for a required level of reliability using the sensitivity of the force to the parameters.

In conclusion, the effectiveness of the codified SABS 0160 and the proposed SANS 10160 predicted end buffer impact forces will be assessed.

7.2 Estimation the Maximum End Buffer Impact Force using a Constraint Optimization Technique (Lagrange Multiplier Method)

7.2.1 Lagrange Multiplier Theory

The Lagrange Multiplier method, which is a Constraint Optimization technique, can be used to determine the extreme values (maxima or minima) of a function (**f**), subject to a constraint function (**g**). The Lagrange Multiplier method specifies that the gradients of the normal vectors of the optimization and constraint functions act in the same direction. The solution $\overline{x}$, verifies, as presented in equation 7.2.1.1,

$$\begin{aligned} &\overline{\nabla} f(\overline{x}) + \overline{\nabla} g(\overline{x}) \cdot \lambda = \overline{0} \\ &\textit{and} \\ &g(\overline{x}) = 0 \end{aligned} \qquad (7.2.1.1)$$

where,

f = Optimization function

g = Constraint function

λ = Factor lambda which equates ∇**f** and ∇**g**

The Lagrange Multiplier method will thus be used to determine parameters causing maximum end buffer impact force under the constraint of a given level of probability.

7.2.2 Optimization Function

The Normal (Gaussian) probability density function was chosen as the optimization function due to its simplicity and generality. The Normal probability density function can be used when the mean (μ) and standard deviation (σ) are known even when the other related parameters, such as skewness (γ_1), are not known. The Normal probability density function [7.2.2.1], is given by equation 7.2.2.1 as,

$$f(x) = \frac{1}{\sqrt{2\pi\sigma^2}} \times e^{-\frac{(x-\mu)^2}{2\sigma^2}} \qquad \text{for } -\infty < x < \infty \tag{7.2.2.1}$$

where,

$f(x)$ = Normal probability density function
x = Random variable
μ = Mean
σ = Standard deviation

From reliability analysis it is known that the "classical results" theorem [7.2.2.1] is used to transform the Normal probability density function presented in equation 7.2.2.1 to the optimization function which relates the parameters to a level of reliability which is presented in equation 7.2.2.2.a, given an optimum point $\bar{x}$ (known as the design point, the probability of exceedance is $\Phi(-\beta)$)

$$-\frac{1}{2}(\bar{x} - \bar{\mu})^T [\bar{\bar{C}}^{-1}] (\bar{x} - \bar{\mu}) = -\frac{1}{2}\beta^2 \tag{7.2.2.2.a}$$

where,

$[C^{-1}]_{ij} = \frac{1}{\sigma^2{}_{ij}}$

β = Reliability index

Hence the constraint equation $f(x)$, written in component notation is expressed by equation 7.2.2.2.b,

$$f(x) = -\frac{1}{2}\left(\sum_j^n \left(\sum_i^n (x_i - \mu_i)\,[\bar{\bar{C}}^{-1}]_{ij}\right)(x_j - \mu_j)\right) = -\frac{1}{2}\beta^2 \tag{7.2.2.2.b}$$

Since the $[C^{-1}]$ is a diagonal matrix, all the terms off the diagonal are zero. The only terms which are not zero are the terms on the diagonal which results in i = j. This allows equation 7.2.2.2.b to be rewritten as equation 7.2.2.2.c,

$$f(x) = -\frac{1}{2}\left(\sum_{i}^{n}\left(\sum_{i}^{n}(x_i - \mu_i)\,[\overline{\overline{C}}^{-1}]_{ii}\right)(x_i - \mu_i)\right) = -\frac{1}{2}\beta^2 \qquad (7.2.2.2.c)$$

If only the two parameters are considered per case (e.g. Payload Bottom with "Power-Off", etc.), then equation 7.2.2.2.c can be written as equation 7.2.2.2.d,

$$f(x) = -\frac{1}{2}\left((x_1 - \mu_1)\,[C^{-1}]_{11}\,(x_1 - \mu_1) + (x_2 - \mu_2)\,[C^{-1}]_{22}\,(x_2 - \mu_2)\right) = -\frac{1}{2}\beta^2 \qquad (7.2.2.2.d)$$

If the variable x is renamed to P, to associate P with the parameters, then equation 7.2.2.2.d can be written as 7.2.2.2.e,

$$f(P) = -\frac{1}{2}\left((P_1 - \mu_1)\,[C^{-1}]_{11}\,(P_1 - \mu_1) + (P_2 - \mu_2)\,[C^{-1}]_{22}\,(P_2 - \mu_2)\right) = -\frac{1}{2}\beta^2 \qquad (7.2.2.2.e)$$

Equation 7.2.2.2.e can be further simplified to yield equation 7.2.2.2.f as,

$$f(P) = -\frac{1}{2 \times \sigma_{11}^2} \times (P_1^2 - 2P_1 \times \mu_1 + \mu_1^2) - \frac{1}{2 \times \sigma_{22}^2} \times (P_2^2 - 2P_2 \times \mu_2 + \mu_2^2) = -\frac{1}{2}\beta^2 \qquad (7.2.2.2.f)$$

If we assume that the maximum impact force occurs when there is no mean, then equation 7.2.2.2.f can be written as equation 7.2.2.2.g,

$$f(P) = -\frac{P_1^2}{2 \times \sigma_{11}^2} - \frac{P_2^2}{2 \times \sigma_{22}^2} = -\frac{1}{2}\beta^2 \qquad (7.2.2.2.g)$$

7.2.2.1 Estimation of the Standard Deviations

Standard deviations were estimated for each parameter based upon engineering judgement. The standard deviations were obtained by reviewing video footage from experimental tests and FEA simulations are presented in Table 7.2.2.1.1.

Table 7.2.2.1.1 Estimated Standard Deviation for each parameter

Parameter	**Estimated Standard Deviation (σ)**
1. Lag Angle	0.022 Radians (1.25^0)
2. Crab & Payload Eccentricity	1.13 m
3. Crane Supporting Structures Flexibility	0.0025 m (2.5mm)
4. Crane Impact Speed	0.05 m/s
5. One (1) End Stop Misaligned	0.04125 m (41.25mm)
6. Buffer's Elastic Characteristics	20%
7. Buffer's Damping Characteristics	30%

7.2.3 Constraint Function

For a given level of probability one seeks the combination of parameters causing the larger force, hence **g** is the impact force, as a function of the parameters. Based on the data available from the FEM, **g** is modelled as a linear function as presented in equation 7.2.3.1.a,

$$g(P) = fo + \sum_{i=1}^{n} fp_i \cdot P_i \qquad (7.2.3.1.a)$$

where,

g(P) = Optimization function

fo = Base value impact force when the payload is symmetric and directly below the crane bridge at the moment of impact for the 4 different cases

fp_i = Change in force per parameter due to the selected number of standard deviation from the base impact force for the parameter

P_i = Parameter number

n = Number of parameters

Equation 7.3.3.1.a can be expanded for two variables and written as equation 7.2.3.1.b,

$$g(P) = fo + fp_1 \times P_1 + fp_2 \times P_2 \qquad (7.2.3.1.b)$$

7.2.3.1 Sensitivity of the Force to the Parameters

For each parameter, the gradient is computed to find an expression of g. The gradient is computed as the change in impact force to the change in parameter variation with respect to the base state. The gradients for the parameters show that the system is non-linear. Figure 7.2.3.1.1 presents the non-linear gradient response of the Lag Angle parameter. Figure 7.2.3.1.1 also presents a typical gradient response for all the other parameters. A linear gradient was however assumed for ease of computation, even though the impact force responses with respect to the change in parameter are non-linear.

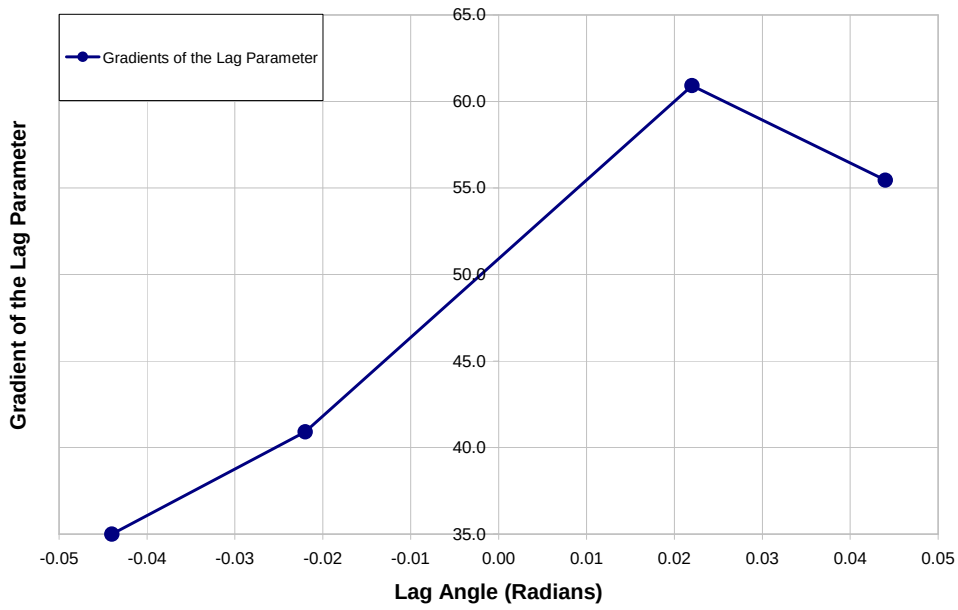

Figure 7.2.3.1.1 Gradient of the Lag Angle parameter

The change in force (fp_i) for each parameter from the base is obtained from equation 7.2.3.1.1,

$$fp_i = \frac{\partial f}{\partial P_i}\Delta P_i \qquad (7.2.3.1.1)$$

where,

fp_i = Change in force per parameter due to the selected number of standard deviation from the base impact force for the parameter

ΔP_i = Change in parameter

The change in force (fp_i) for each parameter for all the four cases, i.e. Payload Bottom "Power-Off", Payload Bottom "Power-On", Payload Top "Power-Off" and Payload Top "Power-On" for $\Delta P_i = 3\sigma_i$ (a change in parameter of three standard deviation) are presented in Table 7.2.3.1.1 for the 1st impact and Table 7.2.3.1.2 for the 2nd impact. The detailed calculations of the change in force for each parameter are presented in Annex H and I, "Change in Force per Parameter Calculations". Annexure H presents the detailed calculations for the 1st impact, while Annexure I present the detailed calculations for the 2nd impact.

Table 7.2.3.1.1 Change in force per parameter when the impact forces are 3σ from the base value for the 1st impact response

Parameter	**Payload Bottom "Power-Off" Change in Force (kN)**	**Payload Bottom "Power-On" Change in Force (kN)**	**Payload Top "Power-Off" Change in Force (kN)**	**Payload Top "Power-On" Change in Force (kN)**
Base Impact Force (f_O)	*6.35*	*7.26*	*6.65*	*7.48*
1. Lag Angle	3.17	3.69	2.50	3.56
2. Crab & Payload Ecc.	1.08	1.52	1.53	2.03
3. Crane Supporting Structures Flexibility	-2.66	-3.06	-2.63	-1.52
4. Crane Impact Speed	4.13	4.73	4.43	4.88
5. 1 End Stop Misaligned	3.69	4.17	4.85	5.19
6. Buffer's Elastic Characteristics	0.00	0.00	0.00	-0.01
7. Buffer's Damping Characteristics	1.13	1.31	1.21	1.38

Table 7.2.3.1.2 Change in force per parameter when the impact forces are 3σ from the base value for the 2nd impact response

Parameter	Payload Bottom "Power-Off"	Payload Bottom "Power-On"	Payload Top "Power-Off"	Payload Top "Power-On"
	Change in Force (kN)	**Change in Force (kN)**	**Change in Force (kN)**	**Change in Force (kN)**
Base Impact Force (f_O)	*4.43*	*4.61*	*6.88*	*8.05*
1. Lag Angle	-1.19	-0.96	0.38	1.09
2. Crab & Payload Ecc.	0.72	1.43	1.73	1.28
3. Crane Supporting Structures Flexibility	-1.48	-1.61	-2.96	-3.04
4. Crane Impact Speed	4.16	5.03	4.43	6.26
5. 1 End Stop Misaligned	2.46	4.75	3.39	2.58
6. Buffer's Elastic Characteristics	0.01	0.00	0.00	0.00
7. Buffer's Damping Characteristics	7.74	8.75	3.50	3.99

7.2.4 Solution Procedure of the Constraint Optimization Problem

The change in force of the Buffer's Elastic Characteristic adjustments are zero for all but two impact test cases as presented in Tables 7.2.3.1.1 and 7.2.3.1.2. This resulted in this parameter being ignored due to its insignificant contribution. This decreased the number of parameters used to determine the maximum end buffer impact force, using the Lagrange Multiplier method, from 7 to 6.

The Lagrange Multiplier method can now be used to determine the end buffer impact force once the constraint and optimization functions have been developed.

An example is used to illustrate the steps involved in determining the end buffer impact force for a required reliability index using the Lagrange Multiplier method. Three variables are considered; namely crane impact speed (P_4), end stop misalignment (P_5) and payload lag angle (P_1).

The 3 parameters used were chosen because these specific parameters yielded the largest values of the change in force per parameter as obtained from Table 7.2.3.1.1. The example is based on the Payload bottom with "Power-Off".

Step 1: Obtain the Optimization function, $f(\overline{P})$*, and the Constraint function,* $g(\overline{P})$

The optimization function $f(\overline{P})$ is obtained from equation 7.2.2.2.g, which is expanded for 3 parameters. The standard deviations of the respective parameters are obtained from Table 7.2.2.1.1. Upon substitution of the standard deviations were substituted into the expanded format of equation 7.2.2.2.g and simplified, thus yielding:

$$f(P) = -200P_4^{\,2} - 293.85P_5^{\,2} - 1033.06P_1^{\,2} = -\frac{1}{2}\beta^2$$

The constraint function $g(\overline{P})$ is obtained from equation 7.2.3.1.b, which is expanded for 3 parameters. The base impact force is obtained from Table 7.2.3.1.1, i.e. the base impact force for the Payload bottom with "Power-Off" case. The change in force per parameter fp_i is also obtained from Table 7.2.3.1.1. Upon substitution of the base impact force and change in force per parameter were substituted into the expanded format of equation 7.2.3.1.b and simplified, thus yielding:

$$g(P) = 6.35 + 4.13P_4 + 3.69P_5 + 3.17P_1$$

Step2: Determine the gradients of $f(\overline{P})$ *and* $g(\overline{P})$ *with respect to each parameter*

$$\frac{\partial f(P)}{\partial P_4} = -400.0P_4; \qquad \frac{\partial f(P)}{\partial P_5} = -587.7P_5; \qquad \frac{\partial f(P)}{\partial P_1} = -2066.1.6P_1$$

$$\frac{\partial g(P)}{\partial P_4} = 4.1; \qquad \frac{\partial g(P)}{\partial P_5} = 3.7; \qquad \frac{\partial g(P)}{\partial P_1} = 3.2$$

Step 3: Equate the gradients of each parameter to one another using the 1st line of equation 7.2.1.1 and determine lambda ($\boldsymbol{\lambda}$*)*

$$\overline{\nabla} f(\overline{x}) + \overline{\nabla} g(\overline{x}) \cdot \lambda = \overline{0}$$

$$-400.0P_4 = 4.1 \times \lambda \quad \Rightarrow \lambda = -97.6P_4$$
$$-587.7P_5 = 3.7 \times \lambda \quad \Rightarrow \lambda = -158.8P_5$$
$$-2066.1P_1 = 3.2 \times \lambda \quad \Rightarrow \lambda = -645.7P_1$$

Step 4: Equate the lambdas and express the parameters in terms of each other

$$-97.6P_4 = -158.8P_5 = -645.7P_1$$
$$P_5 = 0.614P_4$$
$$P_1 = 0.246P_5 = 0.151P_4$$

Step 5: Substitute the magnitude of the parameters into the optimization function, $f(\overline{P})$ *and find an expression for one of the parameters in terms the reliability index.*

$$f(P) = -200.0P_4^2 - 293.8P_5^2 - 1033.1P_1^2 = -\frac{1}{2}\beta^2$$
$$P_4 = \sqrt{\frac{-\frac{1}{2}\beta^2}{-536.4}}$$

Step 6: The magnitudes of the parameters can now be computed for various reliability indices.

	β = 1	**β = 2**	**β = 3**
$P_4 = \sqrt{\frac{-\frac{1}{2}\beta^2}{-3589.6}}$	0.0305	0.0432	0.0529
$P_5 = 0.614P_4$	0.0187	0.0265	0.0325
$P_1 = 0.151P_4$	0.0046	0.0065	0.0080

Step 7: The maximum end buffer impact force can now be computed by substituting the magnitudes of the parameters into the constraint function $g(\overline{P})$

	β = 1	**β = 2**	**β = 3**
Maximum End Buffer Impact Force	6.56 kN	6.65 kN	6.71 kN

7.2.5 Results of the Constraint Optimization Problem

The results of the constraint optimization problem for various levels of reliability are presented in Tables 7.2.5.1 and 7.2.5.2 for the "Power-Off" and "Power-On" conditions, respectively.

Table 7.2.5.1 Estimated maximum end buffer impact force from the 1st impact response

	Payload Bottom "Power-Off"	**Payload Bottom "Power-On"**	**Payload Top "Power-Off"**	**Payload Top "Power-On"**
Estimated maximum end buffer impact force for **β = 1**	7.64	9.05	8.44	9.83
Estimated maximum end buffer impact force for **β = 2**	8.93	10.83	10.23	12.19
Estimated maximum end buffer impact force for **β = 3**	10.22	12.62	12.03	**14.54**

Table 7.2.5.2 Estimated maximum end buffer impact force from the 2nd impact response

	Payload Bottom "Power-Off"	**Payload Bottom "Power-On"**	**Payload Top "Power-Off"**	**Payload Top "Power-On"**
Estimated maximum end buffer impact force for **β = 1**	1.96	1.51	9.11	9.95
Estimated maximum end buffer impact force for **β = 2**	-0.57	-1.59	11.35	11.85
Estimated maximum end buffer impact force for **β = 3**	-2.98	-4.69	13.58	13.75

The maximum end buffer impact force of 14.54kN occurs for the "Payload Top with Power-On" for the particular crane and crane supporting structure investigated, for various levels of the reliability index β. The detailed calculations of the end buffer impact forces for the various cases are presented in Annex J and K. Annex J, presents the detailed calculations for the 1st Impact, while Annex K presents the detailed calculations for the 2nd Impact.

The probability of exceedance is related to the reliability indices presented by equation 7.2.5.1 and is given for various reliability indices in Table 7.2.5.3,

$$P = \Phi(-\beta) \qquad (7.2.5.1)$$

Table 7.2.5.3 Level of Probability for various levels of reliability

β	Probability (%)
1	1.6×10^{-1}
2	2.3×10^{-2}
3	1.4×10^{-3}

Figure 7.3.5.1 presents the comparison of the various codified impact forces with the maximum estimated end buffer impact force for β = 1, 2 and 3.

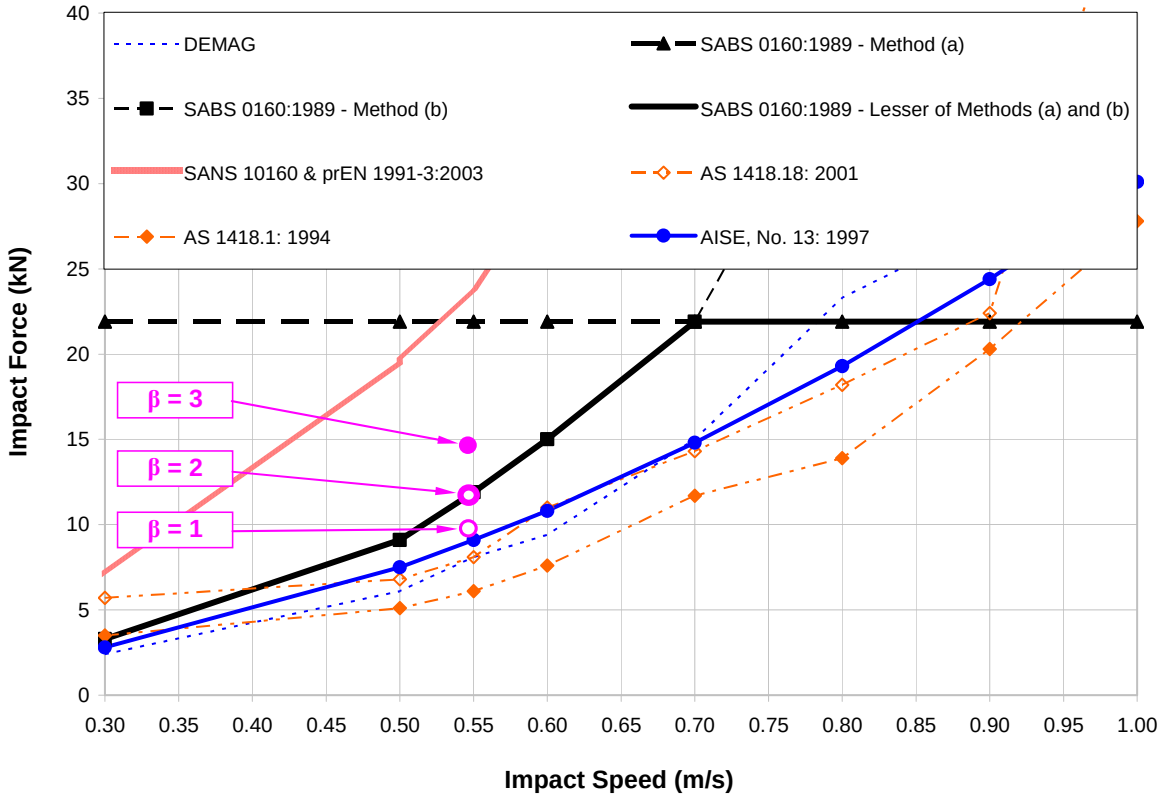

Figure 7.2.5.1 Comparison of the codified impact forces with the maximum end buffer impact force determined using the Lagrange Multiplier method.

From Figure 7.3.5.1, it can be concluded that SABS 0160 under estimates of the end buffer impact force by 18%, while SANS 10160 over estimates the end buffer impact force by 64% for a target reliability index of β = 3.

It can also be concluded that SABS 0160 corresponds to β = 2. The code therefore yields an impact force which has a probability of 2.3×10^{-2} of being exceeded.

CHAPTER 8: SUMMARY, CONCLUSIONS AND RECOMMENDATIONS

8.1 Summary

8.1.1 Literature Review and Problem Definition

In chapter 2, "*Literature Review and Problem Definition*", various codified estimates of the end buffer forces were determined and compared to each other. The estimated end buffer impact forces varied significantly due to the different design philosophies used by the various structural design codes of practice (design codes). Table 2.7.1 presents the criteria used by the various design codes for determining the end buffer impact forces. Generally, the design codes yielded comparable responses except for the proposed SANS 10160 and the EN 1991:3 codes which substantially over estimate the end buffer impact forces. Figure 8.1.1 presents the end buffer impact force response of the various design codes, as obtained from chapter 2, for an impact speed of 0.55m/s with the specific crane and crane supporting structure's configuration.

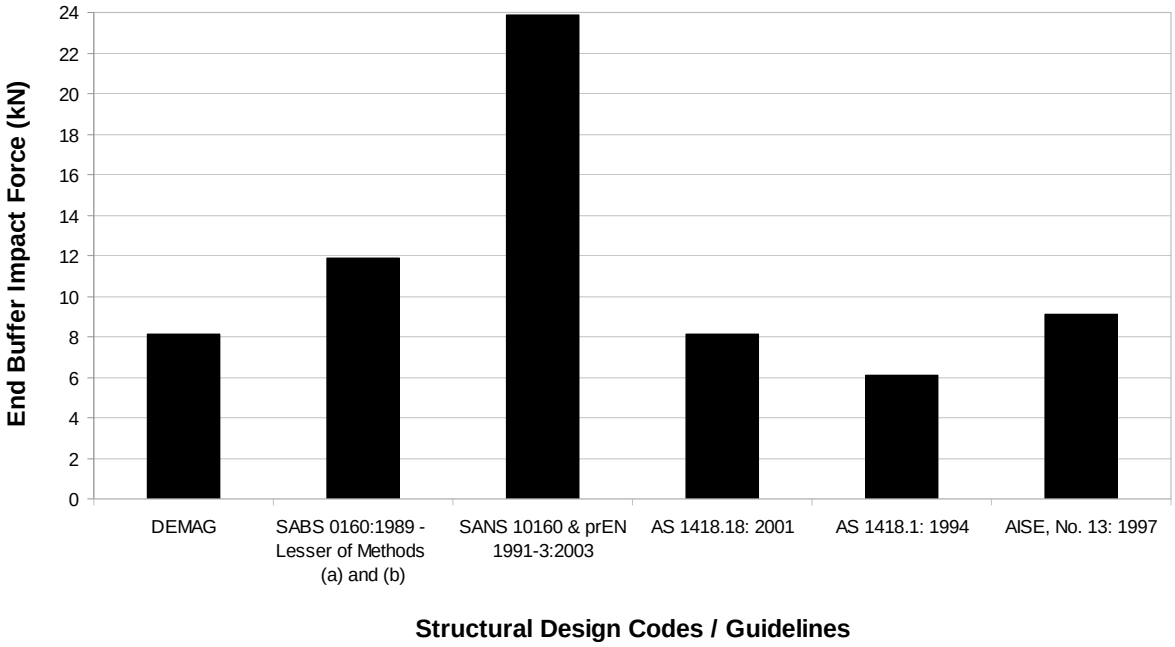

Figure 8.1 Comparison of the codified end buffer impact forces

In addition, the aims of the research project, as well as the methodologies which were used to achieve the aims, were clearly identified. The aims of the research project were:

(i) Identify the relevant physical parameters which have a significant effect on the end buffer impact response.

(ii) Develop a computationally efficient FEA model of the experimental 5-ton electric overhead travelling crane including the crane supporting structure, which could be used to determine the horizontal longitudinal forces, horizontal lateral forces and vertical wheel loads.

(iii) Determine the effect of the parameters on the end buffer impact forces through a FEA sensitivity study.

(iv) Determine the maximum end buffer impact force using the results of the FEA sensitivity study and the Lagrange Multiplier method.

(v) Develop a set of criteria which the designer should include in the FEA model to accurately simulate the end buffer impact response when the crane collides into the end stops.

The relevant physical parameters which the researcher considers to have a significant influence on the end buffer impact response and which should be considered in any FEA simulations are:

(i) The (horizontal) lag of the payload at the moment of impact

(ii) The eccentric position of the crab and payload on the crane bridge at the moment of impact

(iii) The crane supporting structure's flexibility

(iv) The speed of the crane at the moment of impact

(v) The elastic characteristics of the crane end buffers

(vi) The crane buffer's damping characteristics

(vii) The misalignment of the end stops

(viii) The height of the payload above ground level

(ix) Full power ("Power-On") activated during the impact

8.1.2 Finite Element Analysis Modelling

In chapter 3, "Finite *Element Analysis Modelling*", a computationally efficient FEA model of the entire experimental model was developed to determine the horizontal longitudinal forces, horizontal lateral forces and vertical wheel load forces for any condition. The end buffer impact forces could have been determined using the FEA simulations without modelling the entire crane supporting structure. The entire crane supporting structure was modelled to allow the investigation of the horizontal lateral forces and the vertical wheel load forces models.

Three dimensional quadratic beam elements were used to model the girders, beams and columns. Shell elements were used to model the railheads and the "skis" were used to model the conventional crane wheels. The cables were modelled with truss elements since no bending moment is transferred between the elements. The crab, hook, pulley and payload were modelled using lumped masses with its rotational moments of inertia assigned to its centre of gravity. The end buffers were modelled with non-linear spring elements with the appropriate elastic and damping characteristics assigned to the springs. The elastic characteristics (force vs. displacement) were obtained by joining the points of zero velocity of the hysteresis curve of the experimental impact analysis. The buffer's damping characteristics is a function of the force, the velocity and the displacement which were obtained as the difference between the end buffer's stiffness, loading and unloading curves. If no buffer damping is specified in the FEA model, the crane will load and unload along the elastic characteristics curve of the defined spring element.

The above simplifications resulted in a FEA model which has 1642 elements and 3391 nodes with approximately 20 350 DOF. The average impact analysis time including hoisting, acceleration and impact steps is approximately 20 minutes on a Pentium 4, 3 GHz ram desktop computer.

Figure 8.1.2 shows the complete FEA model together with all the constraints which were applied.

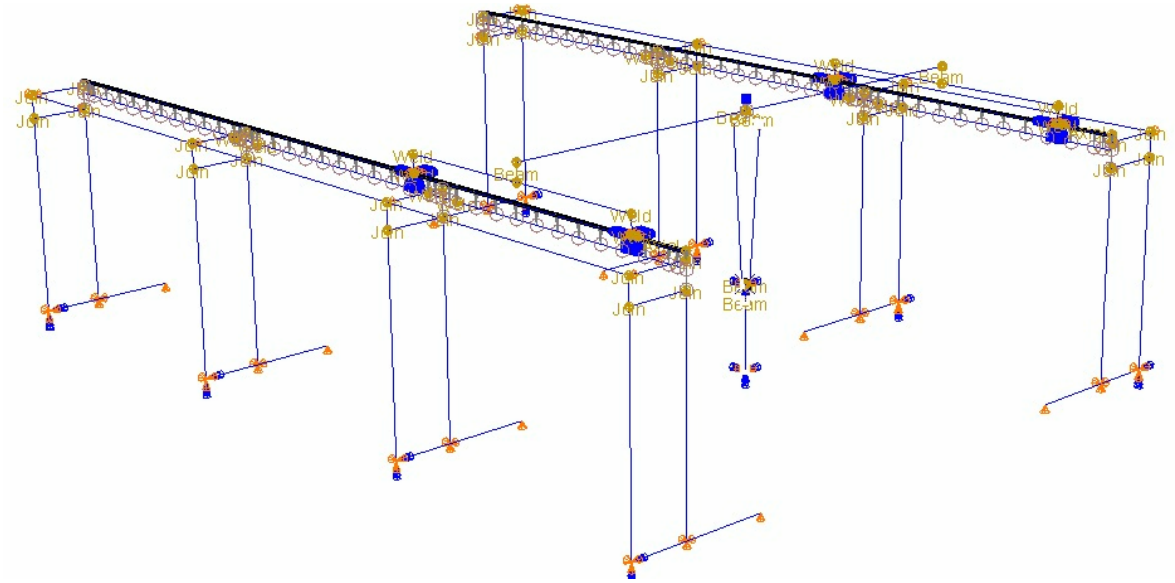

Figure 8.1.2 FEA model of the entire crane, payload and crane supporting structure

8.1.3 Model Calibration

In chapter 4, "*FEA Model Calibration*", the FEA model was calibrated to the basic experimental test results. The calibration was performed when the payload was hoisted 0.15m above the ground level. Figure 8.1.3.1 shows the average experimental response when the payload is 0.15m above ground level with "Power-OFF". Superimposed is the FEA response for the same conditions as the experimental model. The FEA model yielded acceptable end buffer impact forces, to within tolerances of 10% with the experimental model. The time difference of the relevant peaks yielded less acceptable results between the FEA and experimental models which are within 20% of each other.

The legend on Figure 8.1.3.1 shows the parameter values at the moment of impact. The FEA parameter values are known while some of the experimental parameter are unknown as they were not measured during the experimental tests. By adjusting the parameters in the FEA model, the FEA response can produce better correlations with the experimental response.

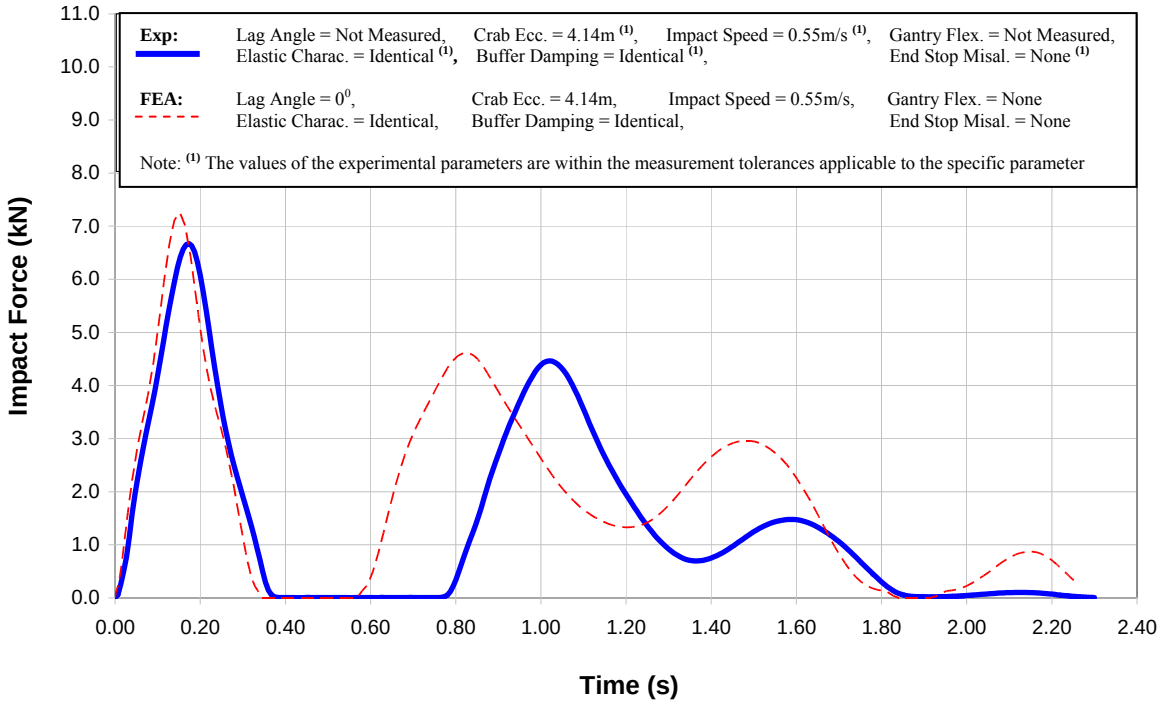

Figure 8.1.3.1 Calibrated FEA impact response to the experimental response when the payload is hoisted 0.15m above ground level with "Power-OFF"

Figure 8.1.3.2 presents the comparison between the FEA simulation response and experimental results when the payload is hoisted 2.20m above ground level.. Both the experimental tests and FEA simulations were conducted for the "Power-OFF" condition. The FEA response differs significantly from the experimental response after the 1st peak when the payload was hoisted 2.20m above ground level.

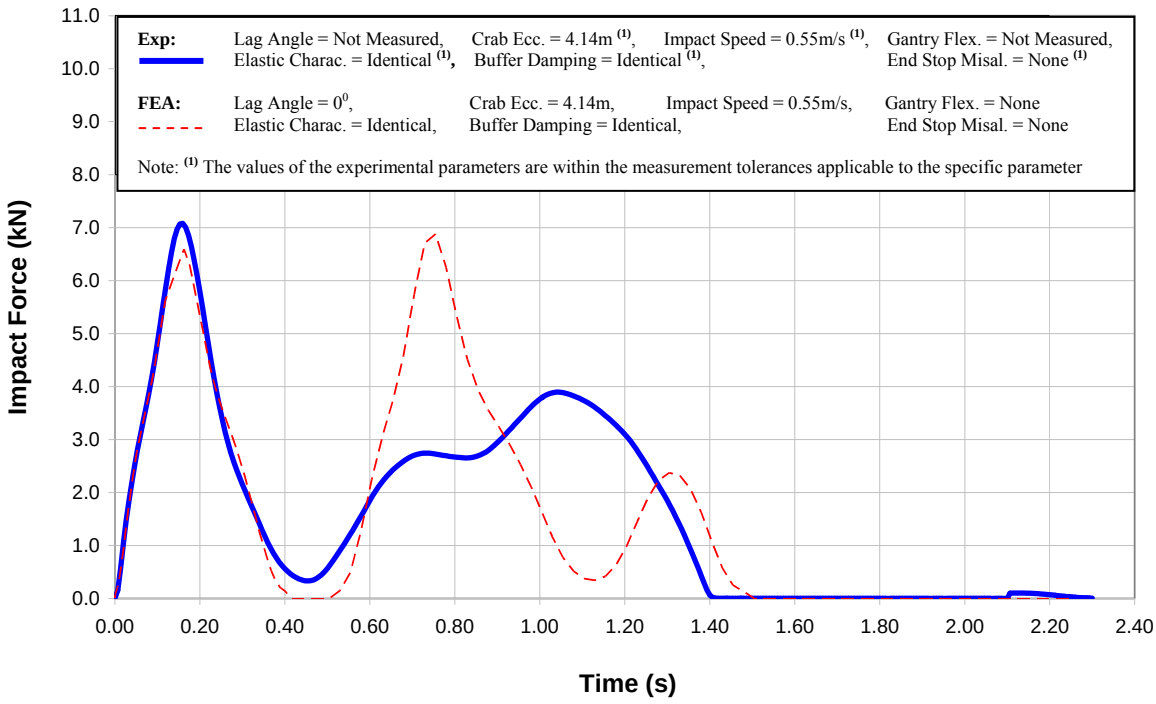

Figure 8.1.3.2 Comparison of the FEA impact response with the same calibrated data from the 0.15m payload case to the experimental response when the payload is hoisted 2.20m above ground level

No clear justification was found for the significant differences between the FEA and experimental responses after the 1st impact. The differences could be accounted to the higher modes of vibration or the parameters presented in section 8.1.1. After reviewing the experimental impact video clips the researcher discovered that the experimental parameters presented in section 8.1.1 were unknown. The effects of the various modes of vibration and the parameters on the end buffer impact response were investigated in chapter 5 and chapter 6 respectively, to clarify the differences between the responses.

8.1.4 Modal Analysis and Modal Superposition

In chapter 5, "*Modal Analysis and Modal Superposition*", the modal analysis and modal superposition methods were employed to investigate whether the various modes of vibration have a significant influence on the experimental impact response. The modal analysis was performed on the crane including the payload but without the crane supporting structure. The fundamental modes of vibration in both the 0.15m and 2.20m cases are the payload oscillation, the bending of the crane bridge and the rotation of the pulley on the cable.

A brief background into the modal superposition theory was presented. The Impulse and the Direct Integration methods were used to perform the modal superposition to determine the displacement and velocity responses of the various modes of vibration. Both methods were suitable for the lower modes of vibration and provided similar responses. The above methods yielded conflicting responses for the higher modes of vibration even though very small time increments ($\Delta t < T/10$) were used. The Impulse method for determining the responses of the higher modes of vibration is incorrect. The higher modes of vibration which were considered have approximately 4.5 oscillations over the time during which the 1st triangular load is applied. The Impulse method does not take this into account. The Integration method yielded the correct responses for the lower and higher modes of vibration.

The higher modes of vibration have a minimal effect on the displacement and velocity responses and can be ignored when performing the modal superposition.

8.1.5 Sensitivity Analysis

In chapter 6, "*Sensitivity Analysis*", the FEA model was used to conduct a parameter study on the variables listed in section 8.1.1. Each parameter was adjusted individually while the remaining parameters were kept constant. This was done to prevent confusion when the parameters acted simultaneously in a multi dimensional parameter study. The researcher acknowledges that the parameters do not work in isolation but collectively.

The FEA simulations were performed for each parameter when the payload was hoisted to 0.15m and to 2.20m above ground level as well as for "Power-Off" and "Power-On" cases.

8.1.5.1 Parameter: Lag Angle of the Payload

The horizontal payload lag has a distinct influence on the impact response when the crane collides into the end stops. Generally, the magnitude of the 1st peak increases and the magnitude of the 2nd peak decreases while the time difference between the peaks decreases as the positive lag angle increases. A positive lag is created when the payload is ahead of the crane bridge at the moment of impact. Generally, the reverse occurs for a negative increase in the payload's lag angle, i.e. the magnitude of the 1st peak decreases and the magnitude of the 2nd peak increases while the time difference between the peaks increases as the negative lag angle increases.

The maximum end buffer impact force of 10.03kN is obtained by varying this parameter between -2.50^0 and $+2.50^0$. The maximum time difference between impacts varies by 14%.

8.1.5.2 Parameter: Eccentricity of the Crab and Payload

The magnitudes of the impact forces are affected while the time difference between the impacts remains almost unchanged due to the eccentricity of the crab and the payload. The end buffer impact force increases as the crab and payload moves towards the particular side. The reverse occurs for the opposite end buffer impact force.

The maximum end buffer impact force of 9.39kN was obtained when the crab was positioned at its maximum eccentricity of 3.39m from the midpoint of the crane bridge. The maximum time difference between impacts varies by 5%.

8.1.5.3 Parameter: Crane Supporting Structure's Flexibility

The magnitudes and time difference between the peaks are affected by adjusting the spring stiffness when the longitudinal bracing system is removed. Generally a weak spring yields lower 1st impact forces, greater 2nd impact forces while the time difference between the peaks increases. As the spring becomes stiffer, i.e. the same as a bracing system, the 1st impact force increases, the 2nd impact force decreases and the time difference between the peaks also decreases.

The maximum impact force of 9.01kN occurs at 2nd impact which is obtained by varying this parameter from a stiff spring to a very weak spring. The maximum time difference between

impacts varies by 34%.

8.1.5.4 Parameter: Impact Speed of the Crane

The magnitudes of the 1st and 2nd impact forces are affected by adjusting the crane speed, while the time difference between the peaks is minimally affected. Generally, the impact force response increases as the crane speed increases. The reverse occurs when the crane speed is reduced.

The maximum end buffer impact force of 10.34kN is obtained by varying this parameter from 0.385 m/s (- 30%) to 0.60m/s (+ 9%). The maximum time difference between impacts varies by 9%.

8.1.5.5 Parameter: Misalignment of the End Stops

There was a marginal increase in the end buffer impact forces, as well as in the time difference between peaks, as the end stop misalignment increases. Contrary to the researcher's expectations, the end buffer impact forces did not increase as the end stop misalignment increases. This could be due to the crane bridge's flexibility as well as the skewing of the crane during impact. The magnitude of the 1st peak increases marginally while the 2nd peak is substantially affected by the end stop misalignment. The time difference between the peaks increases with an increase in the end stop misalignment.

The maximum impact force of 10.11kN is obtained by varying this parameter by 25mm, 50mm to 150mm. The maximum time difference between impacts varies by 34%.

8.1.5.6 Parameter: Modifying Buffer's Elastic Characteristics

The magnitudes of the peaks, as well as the time difference between the peaks, are marginally affected by adjusting the end buffer's elastic characteristics by ±10% and ±20%. This parameter could be ignored in future research work due to its insignificant effect.

The maximum end buffer impact force of 8.04kN is obtained by varying this parameter. The maximum time difference between impacts varies by 9%.

8.1.5.7 Parameter: Buffer's Damping Characteristics

When the buffer's damping characteristics are omitted, the FEA simulations yield a marginal increase in the 1st impact force, while the 2nd impact force is substantially affected. The time difference between the peaks is marginally affected by the omission of the buffer's damping characteristics. The 2nd impact force increases by a maximum of 211%, which occurs when the payload is hoisted 0.15m above ground level. This parameter yielded the most severe end buffer impact force.

The maximum impact force of 14.33kN is obtained when the buffer's damping characteristics are ignored. The maximum time difference between impacts varies by 17%.

8.1.6 Comparison between FEA Responses and the Codified End Buffer Impact Forces

In chapter 7, "*Comparison between the FEA Responses and the Codified End Buffer Impact Forces*", the FEA impact force and the Codified predictions are compared. The comparison shows that SABS 0160:1989 presents reasonable predictions, while the proposed SANS 10160 code is extremely conservative in its prediction of the end buffer impact force. The FEA impact force was obtained by adjusting one parameter at a time while keeping all the other parameters constant.

A Constraint Optimization Technique, namely, the Lagrange Multiplier method uses the contributions of each parameter to estimate the maximum end buffer impact force using the change in force per parameter for the various cases (e.g. Payload Bottom with "Power-Off", Payload Bottom with "Power-On", etc.). The change in force per parameter was obtained by estimating a reasonable standard deviation for each parameter and using the required reliability with the average gradient.

The estimated end buffer impact forces using the Lagrange Multiplier method were computed for various levels of reliability. Since the South African structural design codes of practice are calibrated for a reliability level of 3, the maximum end buffer impact force is determined for the same level of reliability. The maximum end buffer impact force of 14.54kN was obtained for the particular crane and crane supporting structure studied using a reliability level of 3.

Based on the analysis of the particular crane and crane supporting structure studied, the SABS

0160: 1990 underestimates the end buffer impact force by 18%, while the proposed SANS 10160 severely over estimates the end buffer impact force by 64%.

Figure 8.1.6.1 presents the comparison of the codified end buffer impact forces and the estimated maximum end buffer impact force using the Lagrange Multiplier method for an impact speed of 0.55m/s.

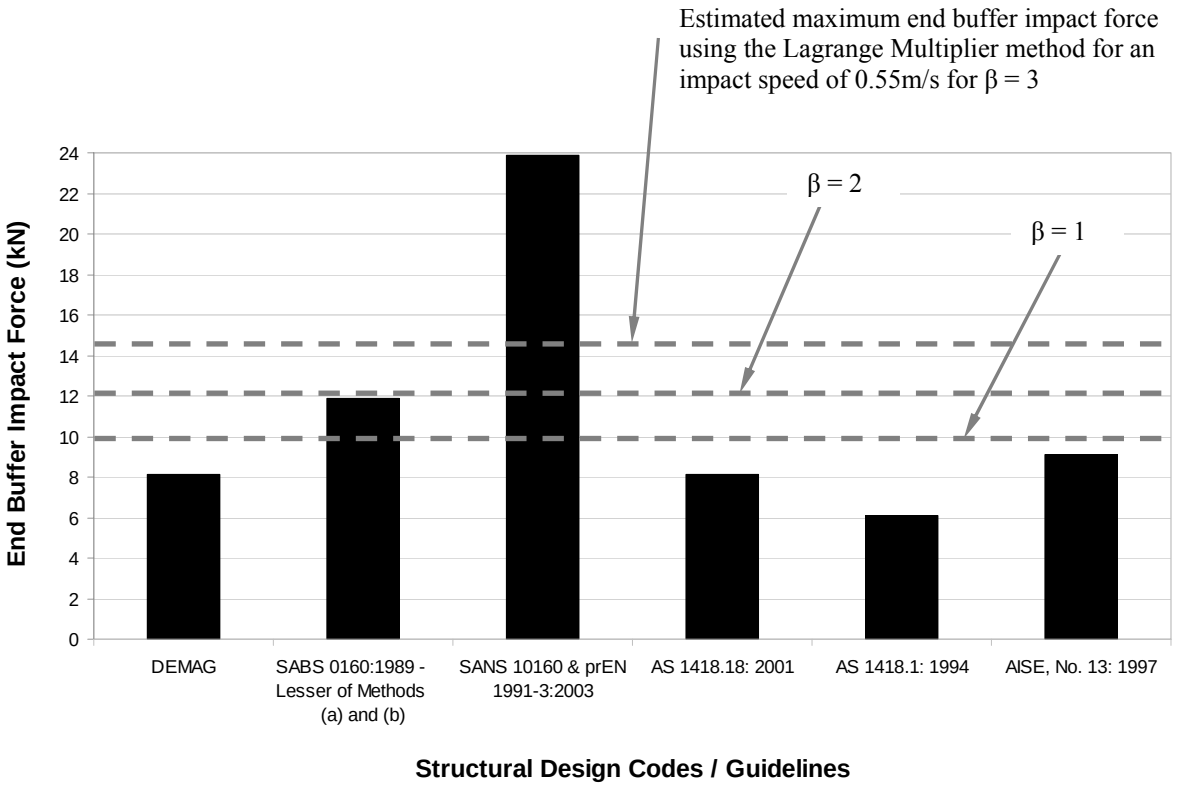

Figure 8.1.6.1 Comparison of the codified end buffer impact forces and the estimated maximum end buffer impact force using the Lagrange Multiplier method for an impact speed of 0.55m/s

8.2 Conclusions

The FEA collision simulations when the crane including the payload rams into the end stops is a complex topic, due to the many phenomena.

The aims of the research project into the end buffer impact forces were successfully achieved.

A computationally efficient FEA model of the entire experimental configuration was successfully

developed. The same FEA model was used to determine the horizontal lateral forces as well as the vertical wheel loads by McKenzie [1.8].

SABS 0160: 1989 underestimates the end buffer impact forces, while the proposed SANS 10160 is extremely conservative in its approach. The current SABS 0160: 1989 is calibrated to a reliability index of approximately 2.

The FEA simulations conducted in this research show that the parameters investigated do have a significant effect on the end buffer impact response.

From this investigation, the following can be concluded:

(i) Most codes ignore the effect of the payload on the impact force response if it is unrestrained (free to swing). The FEA simulations show that the horizontal longitudinal position of the payload at the moment of impact can increase the impact force by 38% for a minimal positive lag angle of 2.50^0 when the payload is in-front of the crane.

(ii) All codes also disregard the vertical position of the payload at the moment of impact. The FEA simulations show that vertical position of the payload at impact has a moderate effect on the 1st impact but a substantial effect on the 2nd impact.

(iii) Most codes do not specifically state how to account for the crab and payload eccentricity. The crab and payload's eccentricity causes a 26% increase in the end buffer impact force.

(iv) All codes are silent on the longitudinal flexibility of the crane supporting structure. A crane supporting structure which is longitudinally flexible will tend to yield greater 2nd impact forces than if the supporting structure is rigid. When the payload is hoisted to 2.20m above ground level the 2nd impact force exceeds the base impact force by a maximum of 14%.

(v) Most codes use the crane impact speed as a parameter to determine the impact force. The FEA simulations show that when the crane impact speed increases, the magnitudes of the impact response also increase. A 9% increase in the impact speed causes a 28% increase in the impact force when considering the 2nd peak where the maximum impact force occurs.

(vi) None of the codes specifically considers the misalignment of the end stops. The FEA simulations show that regardless of the magnitude of the misalignment, the 1st impact forces stabilize at 34% of the base impact force.

(vii) The adjustment of the elastic characteristics of the crane end buffers has an limited effect on the magnitude of the end buffer impact responses. A maximum of 10% increase in the impact force is obtained, which results from a secondary impact force and not the maximum impact force. Thus, this parameter could be disregarded from future investigations.

(viii) Most codes examined used the buffer's energy absorption characteristics to determine the crane end buffer impact force. None of the codes consider the failure (disintegration) of the buffers and the effects thereof. The FEA simulations show that in such a case the 2nd impact force is substantially greater than the base 1st and 2nd impact forces. The 2nd impact force increases by 211% when compared to the base response.

(ix) All codes disregard the effect of continuous power ("Power-On") transmitted to the wheels of the crane during impact. The "Power-On" condition increases the impact forces by approximately 16% compared to the "Power-Off" responses.

Thus, disregarding these effects can lead to substantially underestimating the end buffer impact forces, with potentially serious consequences.

8.3 Recommendations

The following aspects need to be further investigated to make a general statement on the efficiency of the SABS 0160:1989 and the proposed SANS 10160 codes of practice in determining the end buffer impact forces.

(i) Repeat the FEA simulations for different impact speeds.

(ii) Repeat the FEA simulations for various payload masses.

(iii) Repeat the FEA simulations for different crane bridge stiffness. The investigation

should also explore the effect of a double girder box crane bridge with various stiffnesses.

(iv) Repeat the FEA simulations for a combination of impact speeds, payload masses and different crane bridge stiffnesses.

(v) Determine the revised FEA impact forces and also determine the maximum end buffer impact force using the Lagrange Multiplier method by considering the additional parameters in (i) , (ii) and (iii).

(vi) The experimental investigations should be repeated and all relevant parameters presented in section 8.1.1 measured during the collision between the crane and the end stops.

(vii) Determine the effect of a liquid payload (for refineries) instead of the solid payload assumed in this research project.

(viii) From the FEA simulations, determine the critical values of the various parameters that cause the maximum end buffer impact force. Conduct experimental tests using the critical values of the various parameters to verify the maximum end buffer impact force obtained from the Constraint Optimization Technique.

(ix) Determine if the approximate period of the multiple impact peaks correspond to any modes (such as, the frequency of the swinging payload or the vibrating single DOF system formed by the mass of the crane and the stiffness of the buffers) of the crane or crane supporting structure.

REFERENCES

References: Chapter 1

1.1 Roswell, J.C., (1987), "*Crane Runway Systems*", Master's Degree Thesis, Department of Civil Engineering, University of Toronto

1.2 Barnard, Personal communication and crane support structure drawings

1.3 Viljoen, P, (2004), "*Investigation into the Top Flange and Web Deformation in a Crane Girder Panel*", Master's Degree Thesis, Department of Civil Engineering, University of Stellenbosch

1.4 Perez-Winkler, A.R., (2003), "*An investigation of Overhead Crane Wheel / rail / Girder Interaction*", Master's Degree Thesis, Department of Civil Engineering, University of Stellenbosch

1.5 Dymond, J.S., (2005), '*Reliability Based Codification for the Design of Overhead Travelling Crane Support Structures*", Doctorate Degree Dissertation, Department of Civil Engineering, University of Stellenbosch

1.6 De Lange, J.H., (2007), "*An Experimental Investigation into the Behaviour of a 5 Ton Electric Overhead Travelling Crane and its Supporting Structure*", Master's Degree Thesis, Department of Civil Engineering, University of Stellenbosch

1.7 Kohlhaas, S., (2004), "*Impact Forces on End Stops for Overhead Travelling Crane Support Structures*", Research Report**,** University of Stellenbosch

1.8 McKenzie, K., (2007), "*The Numerical Simulation of Wheel Loads on an Electric Overhead Travelling Crane Supporting Structure"*, Master's Degree Thesis, Department of Civil Engineering, University of Stellenbosch

References: Chapter 2

2.1 DEMAG, Personal Communiqué and *www.demag.com*

2.2 SABS 0160-1989 (as Amended 1989), "South African Standard: *Code of Practice for: The General Procedure And Loadings To Be Applied In The Design Of Buildings*", The Council of the South African Bureau of Standards, Clauses 5.7.6 and 5.7.7, Pages 95 to 100.

2.3 SANS 10160, Working document on SANS 10160, "South African National Standards 10160: *Basis Of Structural Design And Actions For Buildings And Industrial Structures, Section 10: Action Induced By Cranes and Machinery*", Personal Communication with a Member of the Working Group, Clause 10.2.12.1, Pages 1 to 26

2.4 prEN 1991-3:2003, European Standard 1991-3: EUROCODE 1 – "*Actions On Structures, Part 3: Actions Induced By Cranes and Machinery*", European Committee for Standardisation, CEN / TC250 / SC1, Clause 2.11.1, Pages 1 to 44.

2.5 AS 1418.18:2001, Australian Standard, **"***Cranes (Including Hoists and Winches), Part 18: Crane Runways and Monorails*", Appendix B, Page 41

2.6 AS 1418.1: 1994, "Standards Australia AS 1418.1 -1994: *Cranes (Including Hoists and Winches), Part 1: General Requirements*", 3rd Edition, Clause 4.7.5, Pages 24 to 26.

2.7 AISE Technical Report 6, October 2000, "*Specification for Electric Overhead Travelling Cranes for Steel Mill Service*", *Clause 3.8, Pages 48 and 49*

2.8 Lobov N.A., (1976), "C*alculation Of Dynamic Loads On An Overhead Travelling Crane During Its Movement*", Russian Engineering Journal, Volume 56, Issue 1, Pages 44 to 48.

2.9 Lobov, N. A., (1982), "*Loads Of An Overhead Travelling Crane caused By Transverse And Rotatory Motions Of The Bridge Girder*", Soviet Engineering Research, Volume 62, Issue 6, Pages 31 to 35.

2.10 Lobov N.A., (1984), "*Overhead Travelling Crane Loads When Track-Wheel Flanges Contact The Rails*", Soviet Engineering Research, Volume 64, Issue 7, Pages 22 to 26.

2.11 Lobov N.A., (1986), "*Loads On An Overhead Travelling Crane When It Moves With A Constant Skew Setting Of The Girder*", Soviet Engineering Research, Volume 66, Issue 12, Pages 13 to 17.

2.12 Karmakar. R. and Mukherjee A., (1990), "*Dynamics of Electric Overhead Travelling Cranes, A Bond Graph Approach*", Journal of Mechanical Machines Theory, Volume 25, No. 1, Pages 29 to 39.

2.13 Grigor'ev Yu. M. and Romashchenko V.A., (1975), "*Increased Stability Of An Overhead Travelling Crane Fitted With Taper Wheels Mounted The Inverse Cone Method*", Russian Engineering Journal, Volume 55, Issue. 5, Pages 39 to 42.

References: Chapter 3

3.1 ABAQUS, Personal Communiqué and *www.abaqus.com*

3.2 http://www.roymech.co.uk/Useful_Tables/Tribology/co_of_frict.htm

References: Chapter 5

5.1 Meirovitch, L, (2001), "*Fundamentals Of Vibrations*", 1st Edition, McGraw-Hill International Edition, ISBN 0-07-041345-2, Pages 158 to 162.

5.2 Paz, M, (1997), "*Structural Dynamics: Theory and Computation*", 4th Edition, Chapman and Hall, ISBN 0-412-07461-3, Pages 110 to 114.

References: Chapter 7

7.3.1 Larson, R., Hostetler, R. and Edwards, B., (1995), "*Calculus, Early Transcendental Functions*", 1st Edition, D.C. Heath and Company, ISBN 0-669-39349-5, Pages 914 to 919.

7.3.2.1 Montgomery, D. and Runger, G., (2002), "*Applied Statistics and Probability for Engineers*", 3rd Edition, John Wiley and Sons, ISBN 0-471-38181-0, Pages 109 to 112.

ANNEX A: FEA Simulations of the Payload Lag

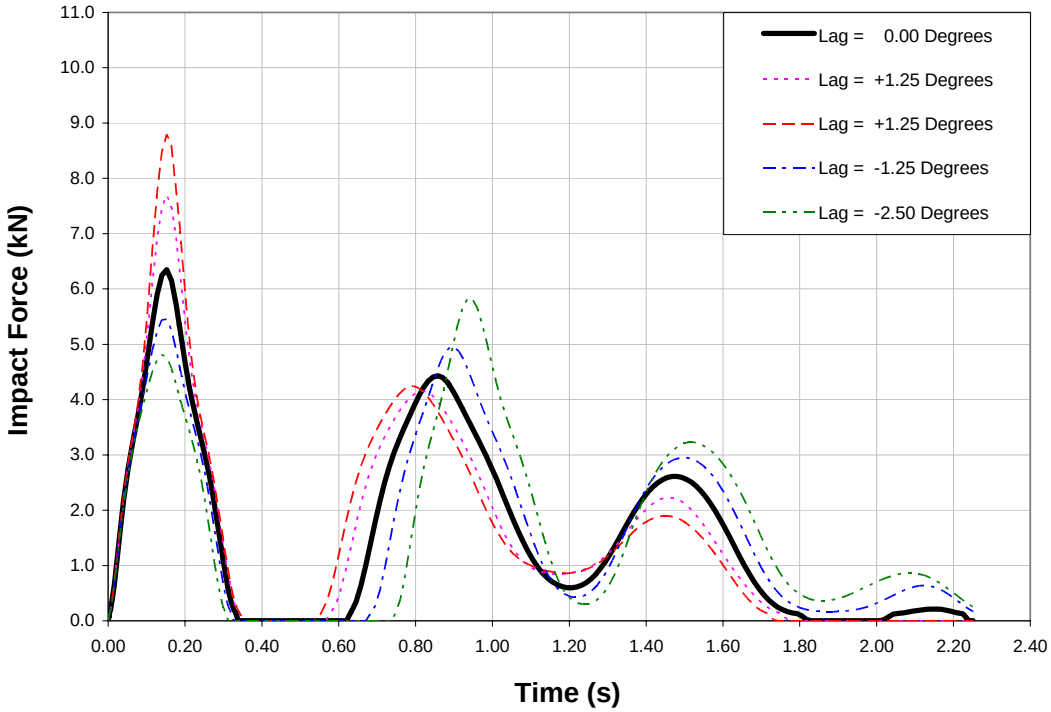

Figure A1 Lag Effect: Payload Bottom with "Power-OFF"

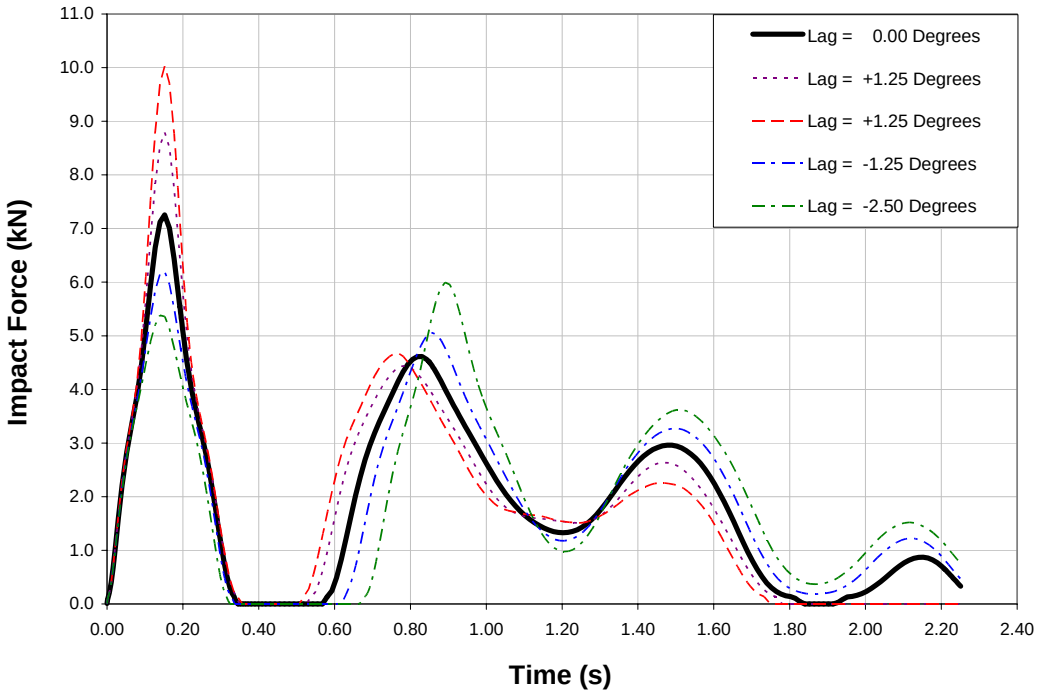

Figure A2 Lag Effect: Payload Bottom with "Power-ON"

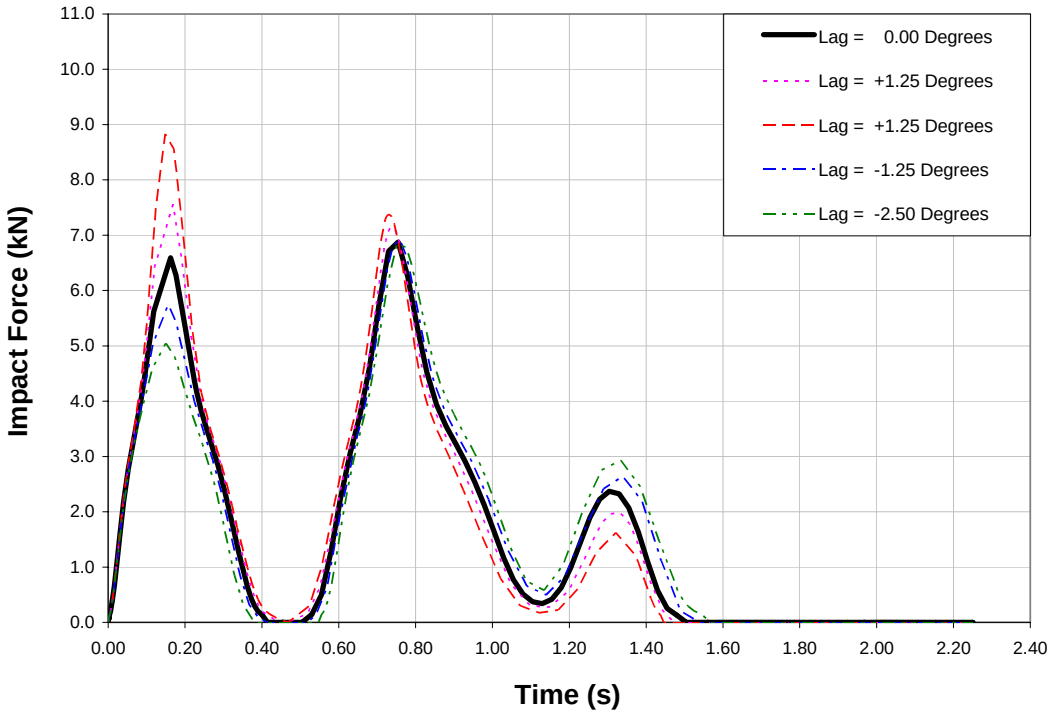

Figure A3 Lag Effect: Payload Top with "Power-OFF"

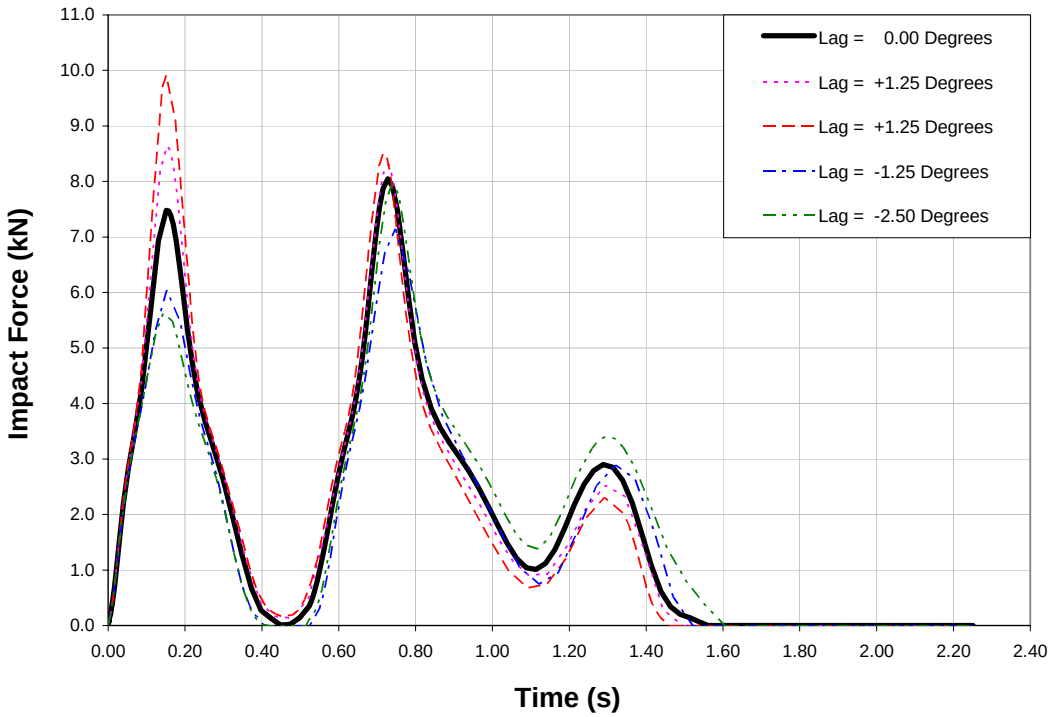

Figure A4 Lag Effect: Payload Top with "Power-ON

ANNEX B: FEA Crab and Payload's Eccentricity Responses

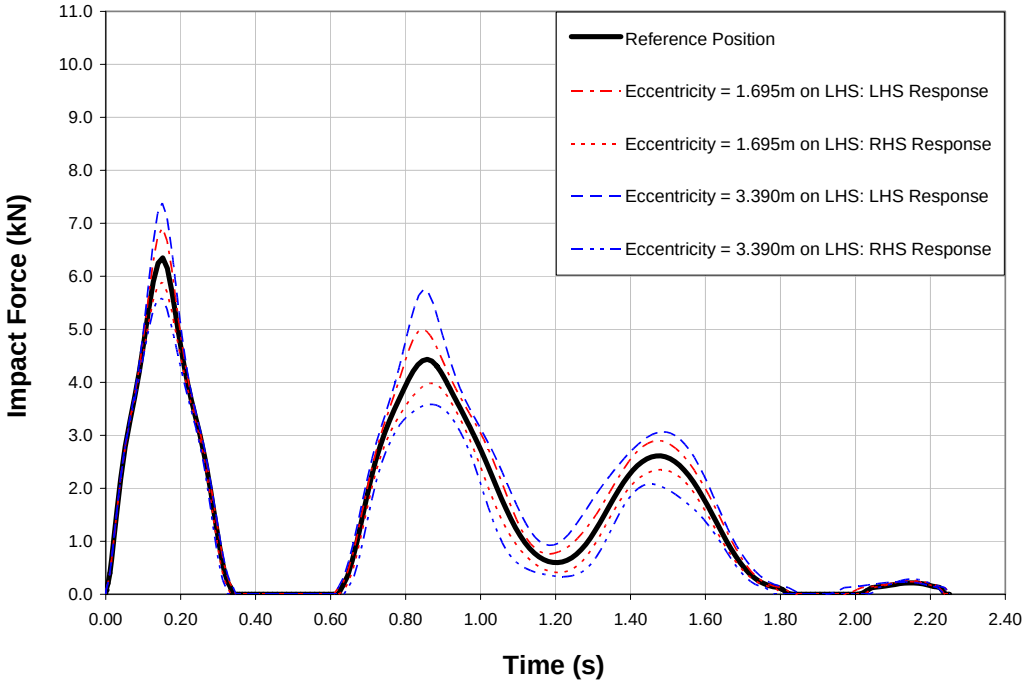

Figure B1 Crab Eccentricity Effect: Payload Bottom with "Power-OFF"

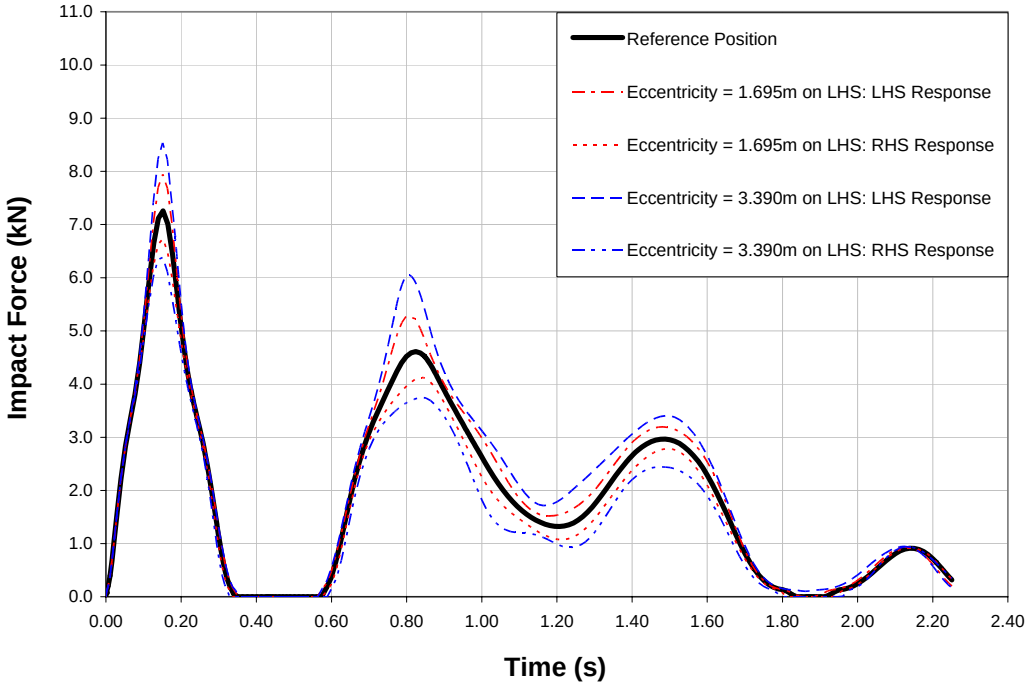

Figure B2 Crab Eccentricity Effect: Payload Bottom with "Power-ON"

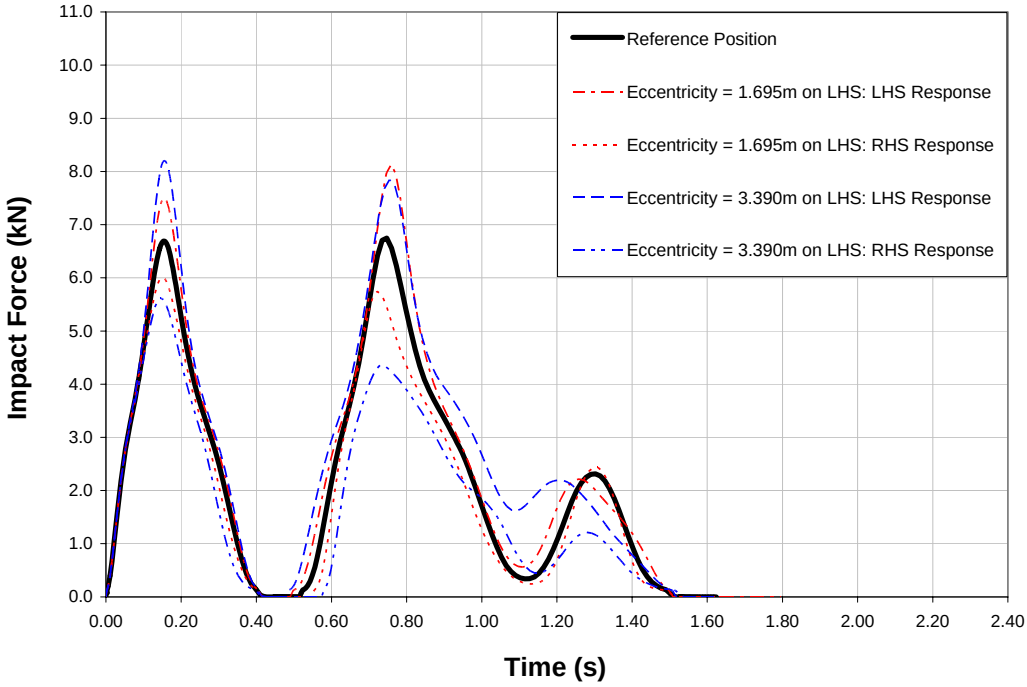

Figure B3 Crab Eccentricity Effect: Payload Top with "Power-OFF"

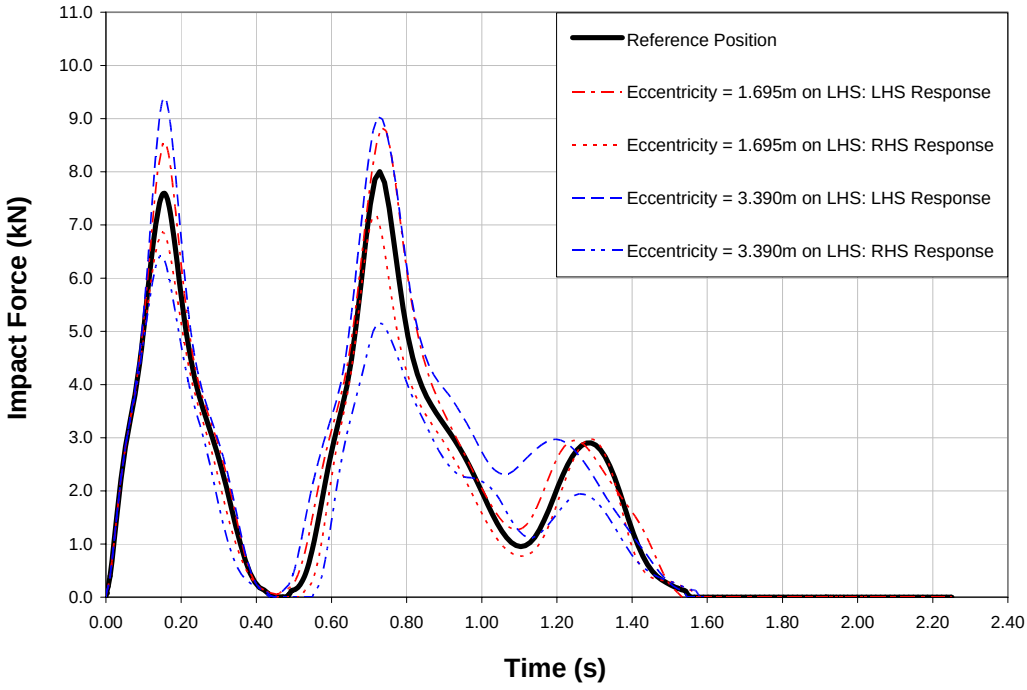

Figure B4 Crab Eccentricity Effect: Payload Top with "Power-ON"

ANNEX C: FEA Crane Supporting Structure's Flexibility Responses

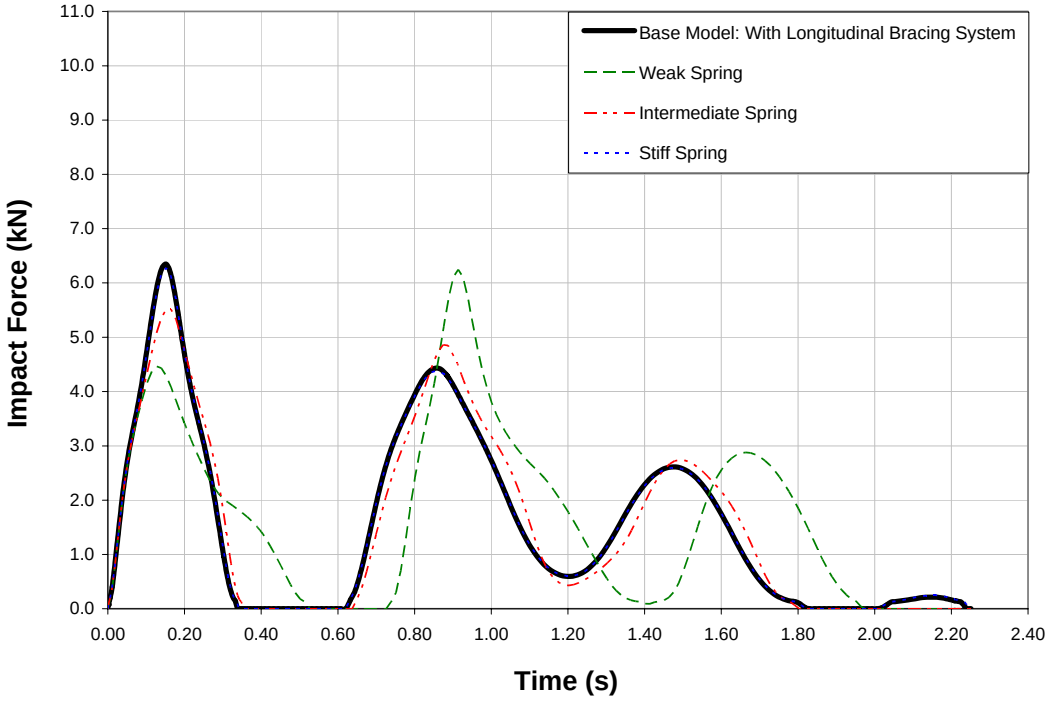

Figure C1 Crane Supporting Structure's Flexibility Effect: Payload Bottom - "Power-OFF"

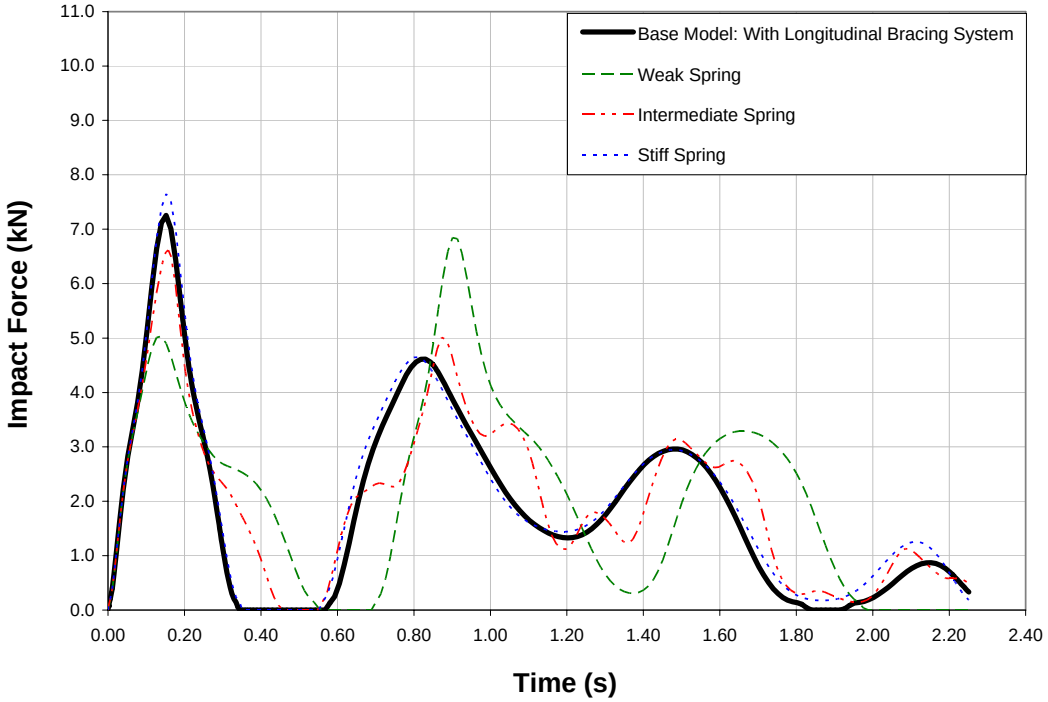

Figure C2 Crane Supporting Structure's Flexibility Effect: Payload Bottom - "Power-ON"

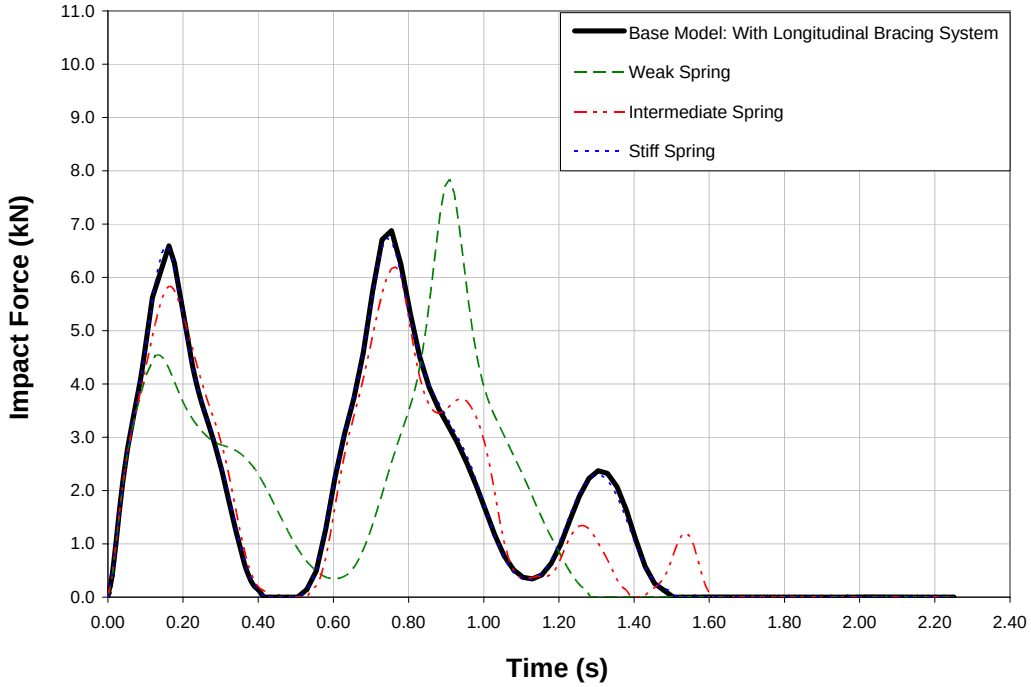

Figure C3 Crane Supporting Structure's Flexibility Effect: Payload Top - "Power-OFF"

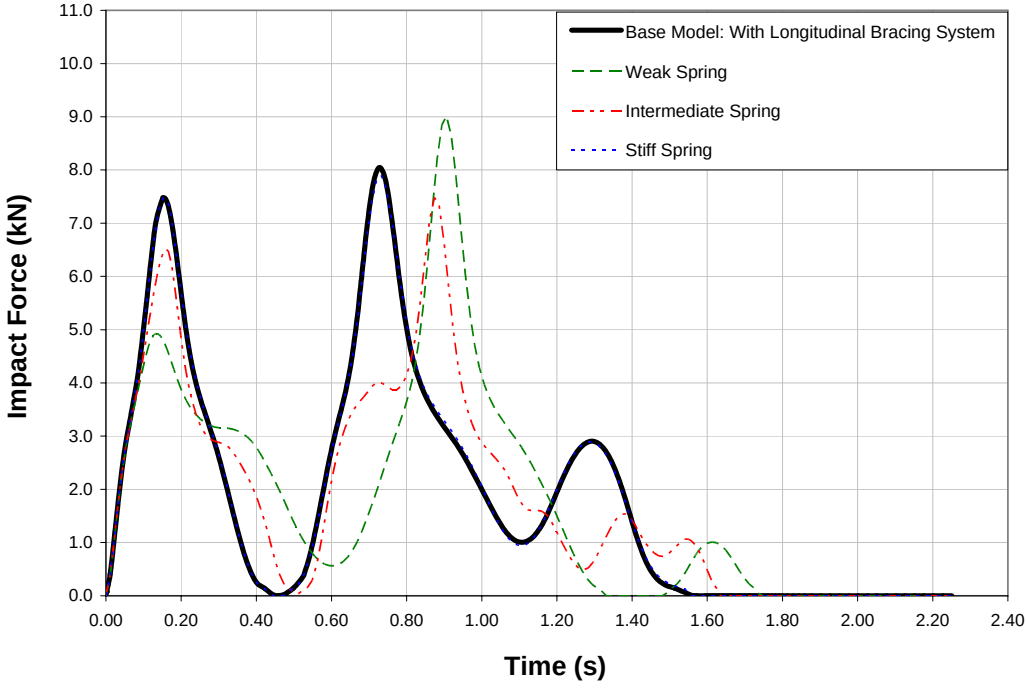

Figure C4 Crane Supporting Structure's Flexibility Effect: Payload Top - "Power-ON"

ANNEX D: FEA Longitudinal Travel Crane Speed Responses

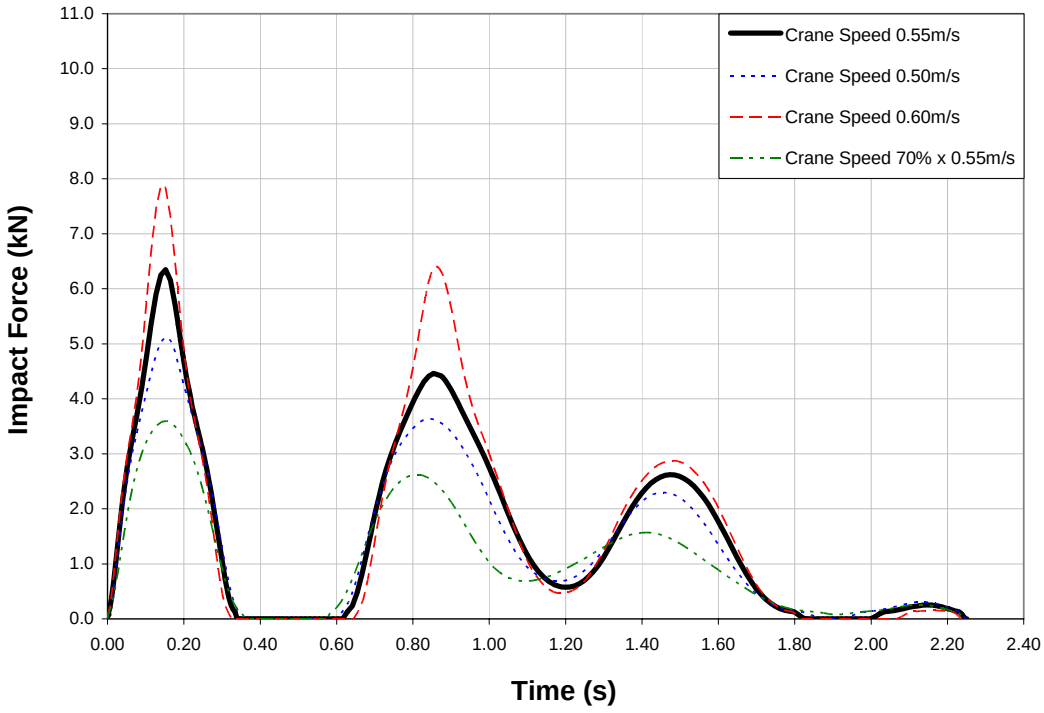

Figure D1 Effect of the Crane speed: Payload Bottom - “Power-OFF”

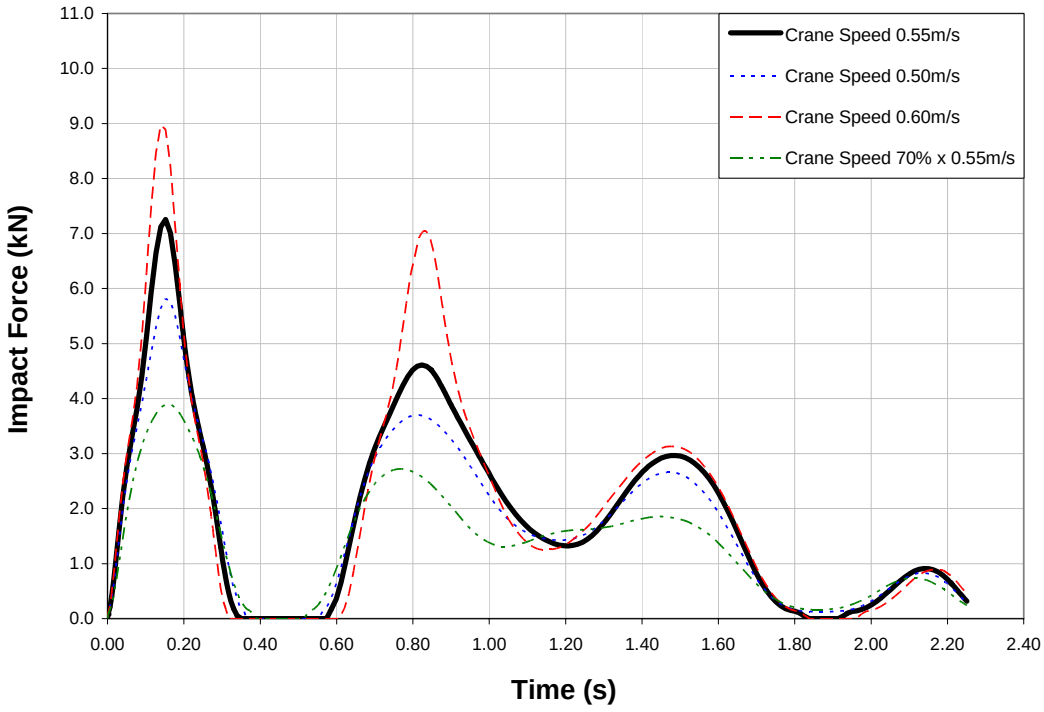

Figure D2 Effect of the Crane speed: Payload Bottom - “Power-ON”

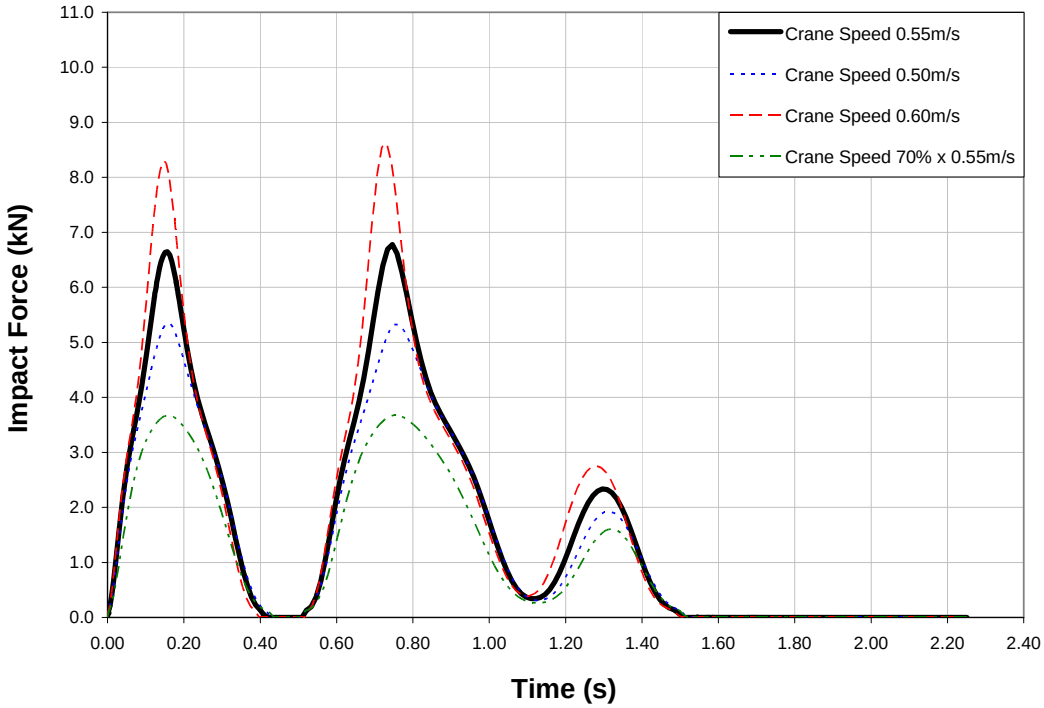

Figure D3 Effect of the Crane speed: Payload Top - “Power-OFF”

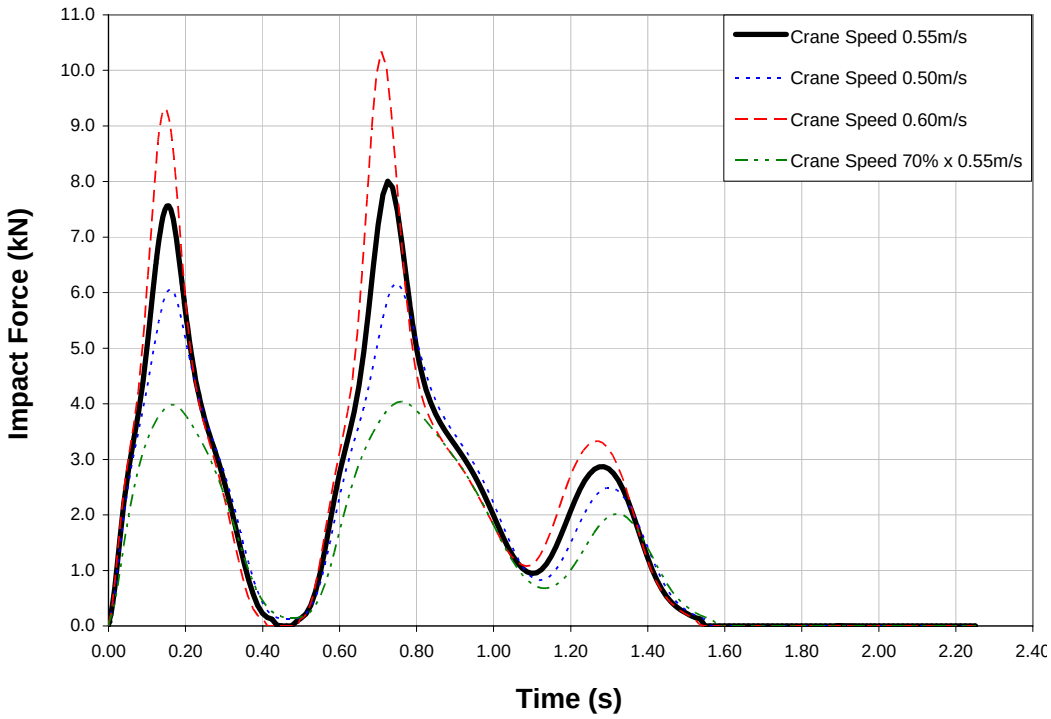

Figure D4 Effect of the Crane speed: Payload Top - “Power-ON”

ANNEX E: FEA End Stop Eccentricity Responses

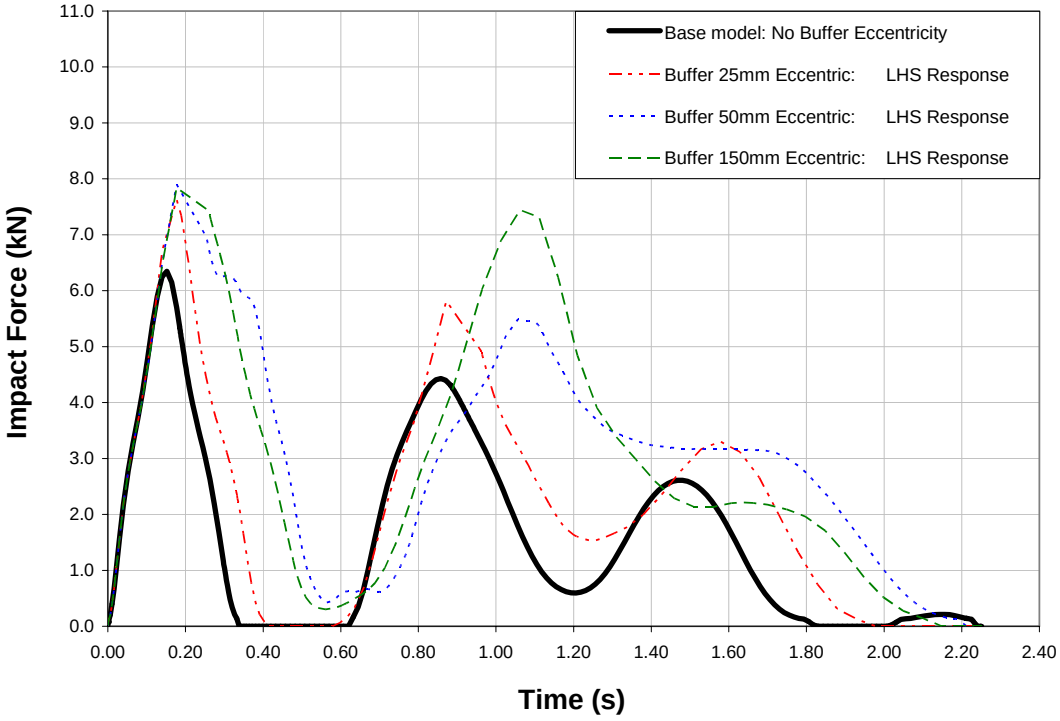

Figure E1 End Stop Misalignment Effect: Payload Bottom - "Power-OFF"

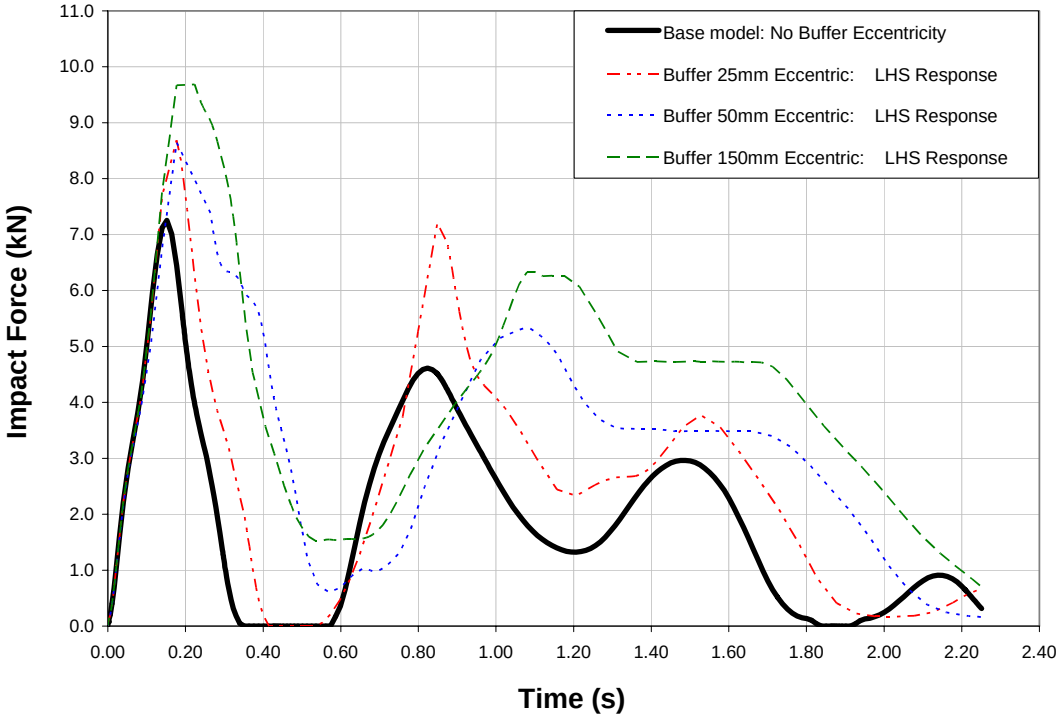

Figure E2 End Stop Misalignment Effect: Payload Bottom - "Power-ON"

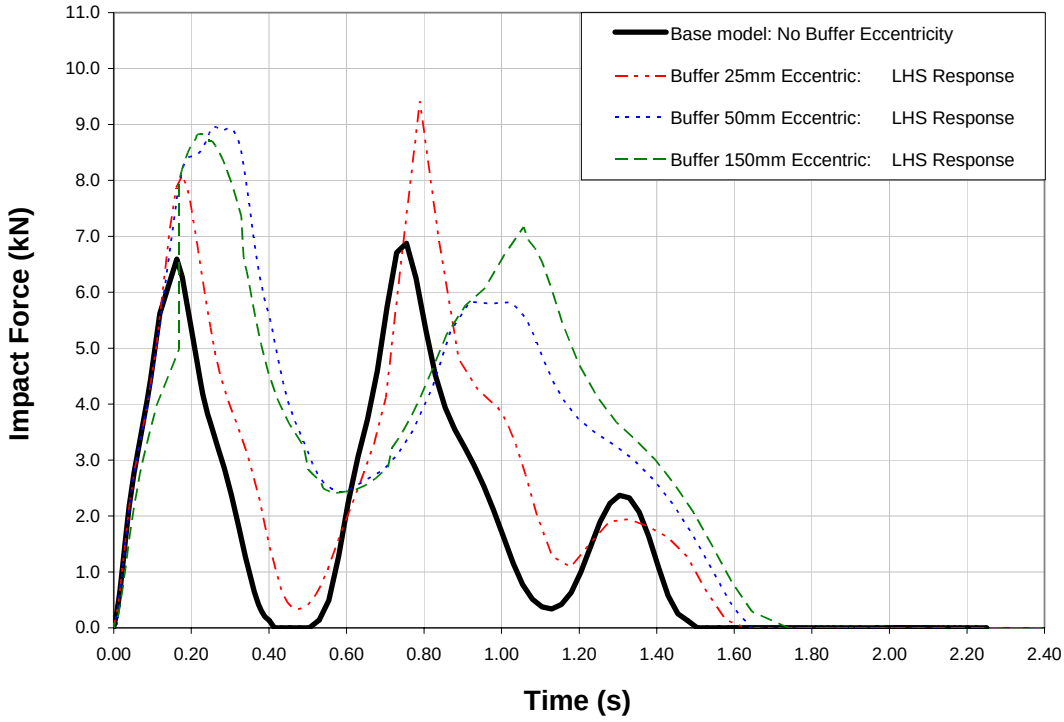

Figure E3 End Stop Misalignment Effect: Payload Top - "Power-OFF"

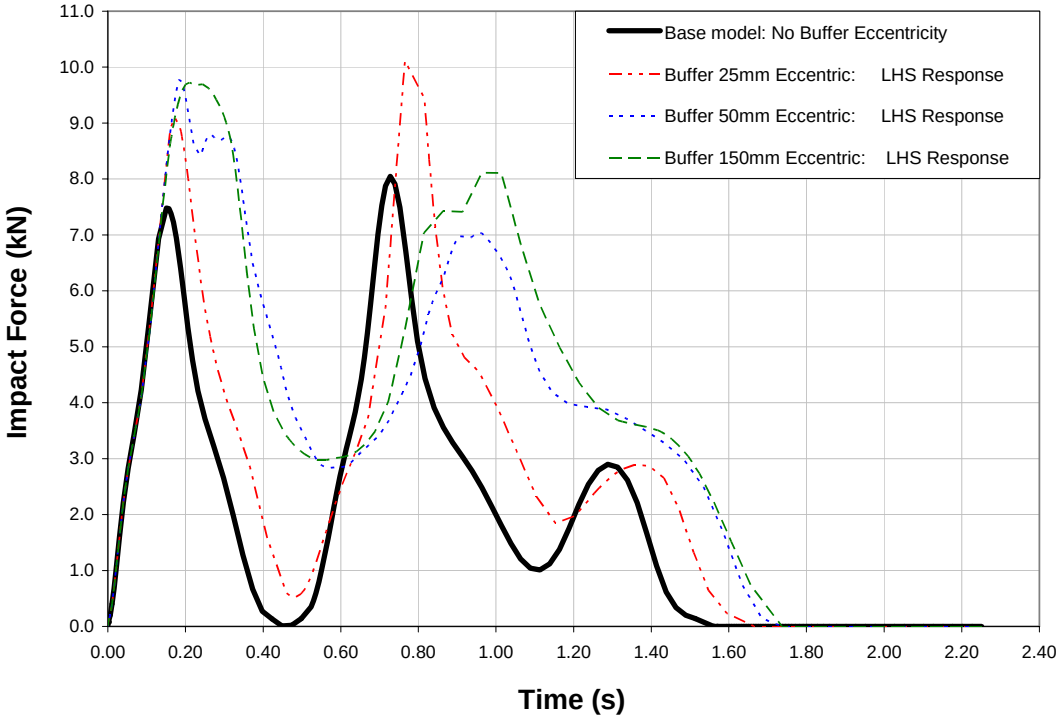

Figure E4 End Stop Misalignment Effect: Payload Top - "Power-ON"

ANNEX F: FEA Elastic Buffer Characteristics Responses

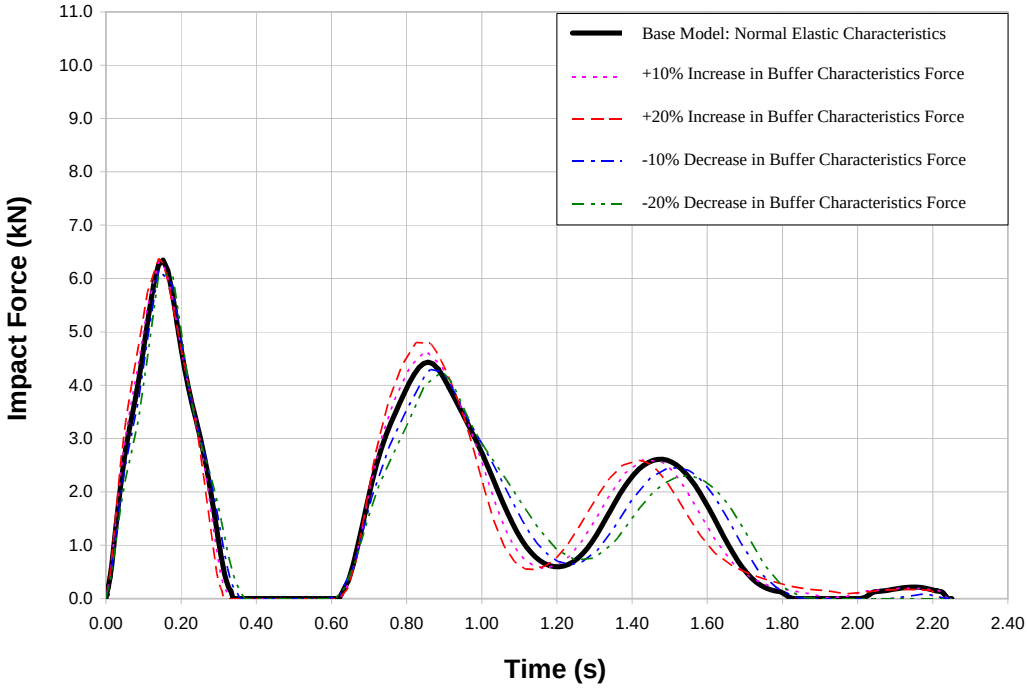

Figure F1 Elastic Characteristics Effect: Payload Bottom - “Power-OFF”

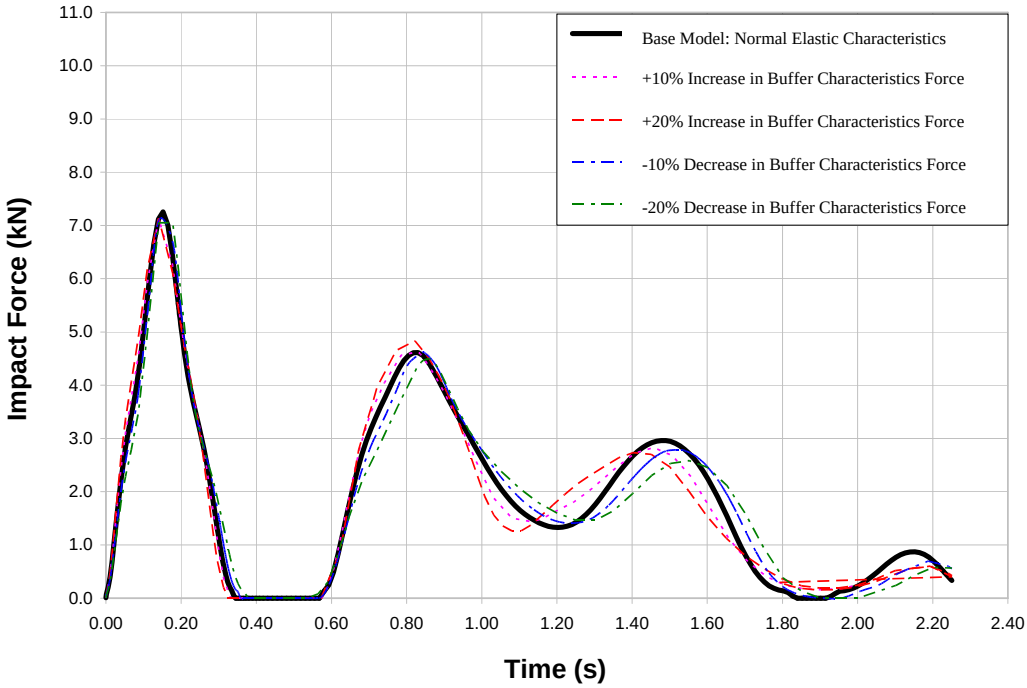

Figure F2 Elastic Characteristics Effect: Payload Bottom - “Power-ON”

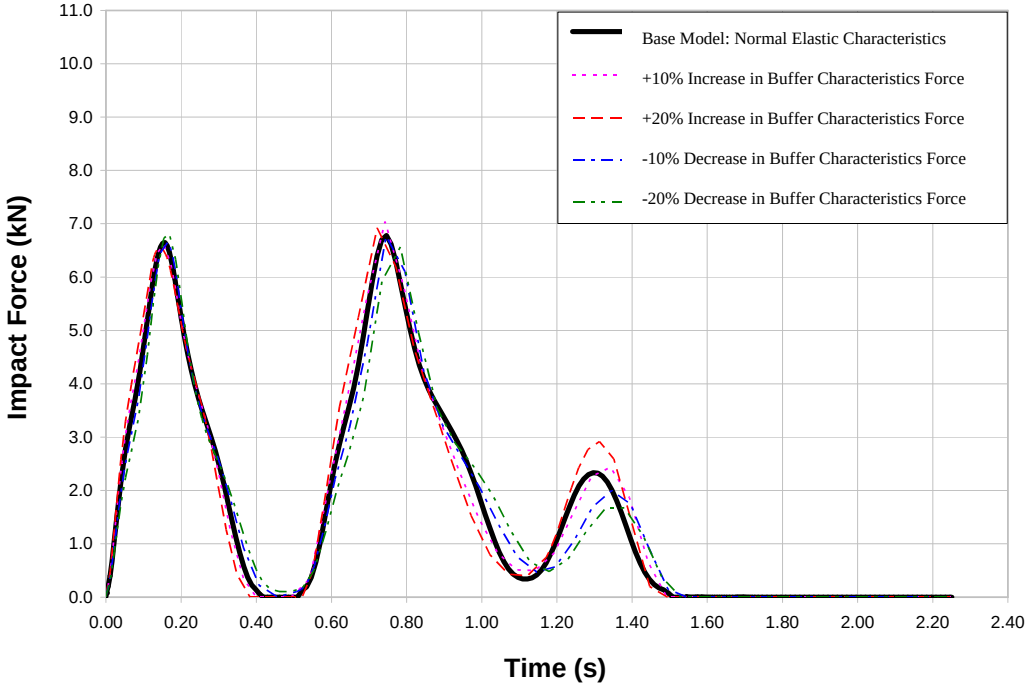

Figure F3 Elastic Characteristics Effect: Payload Top - “Power-OFF”

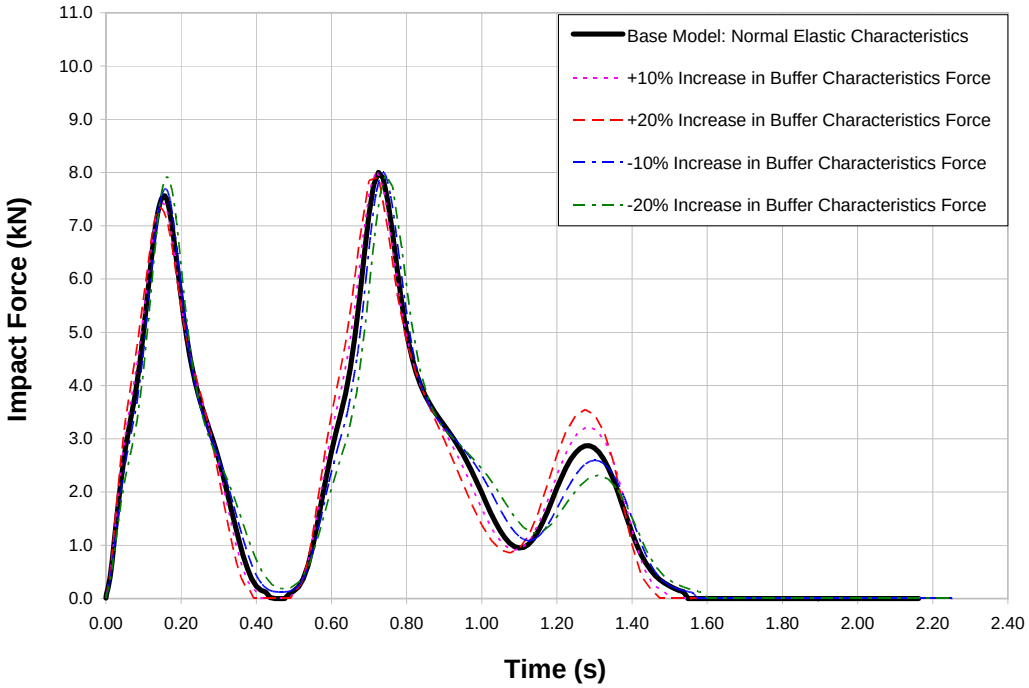

Figure F4 Elastic Characteristics Effect: Payload Top - “Power-ON”

ANNEX G: FEA Buffer Damping Characteristic Responses

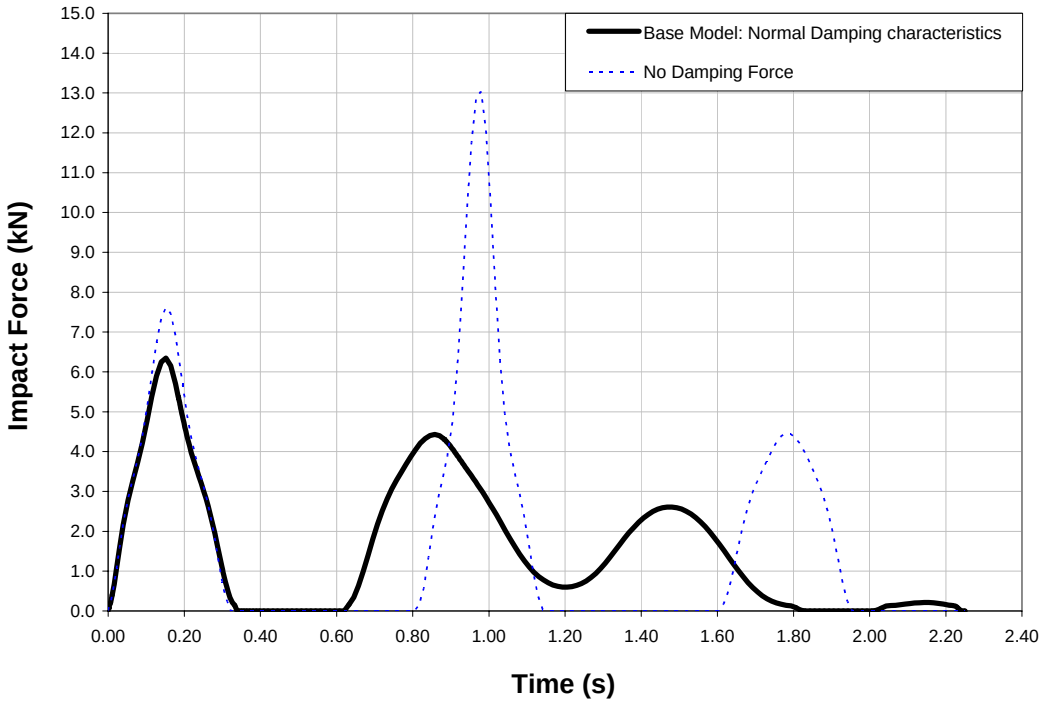

Figure G1 Damping Characteristics Effect: Payload Bottom - “Power-OFF”

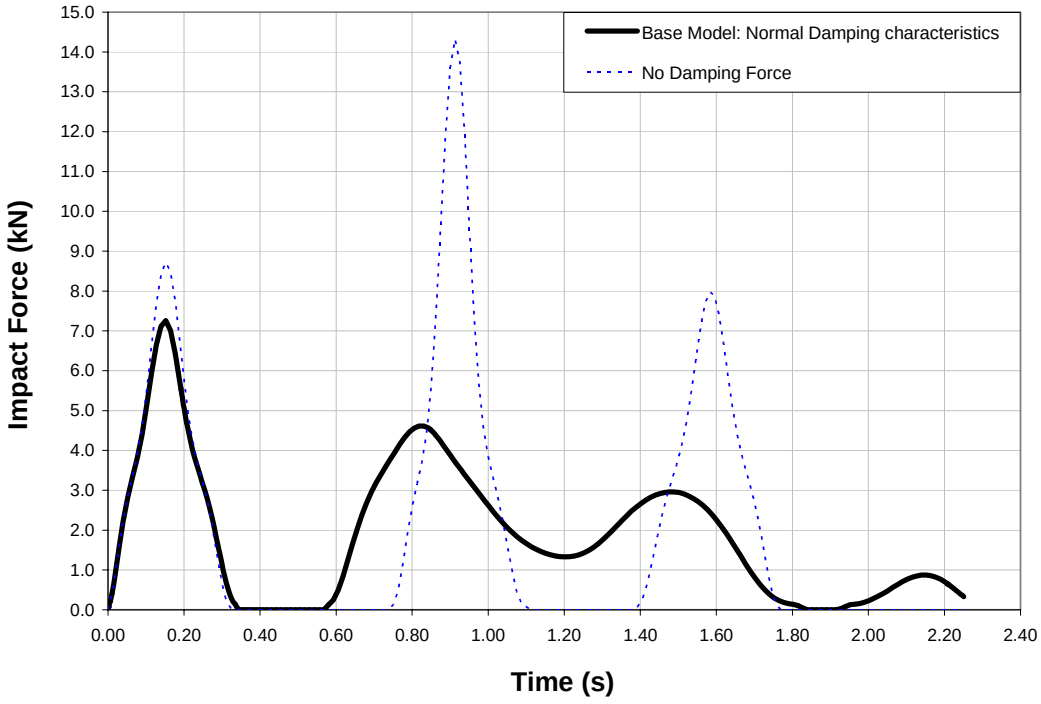

Figure G2 Damping Characteristics Effect: Payload Bottom - “Power-ON”

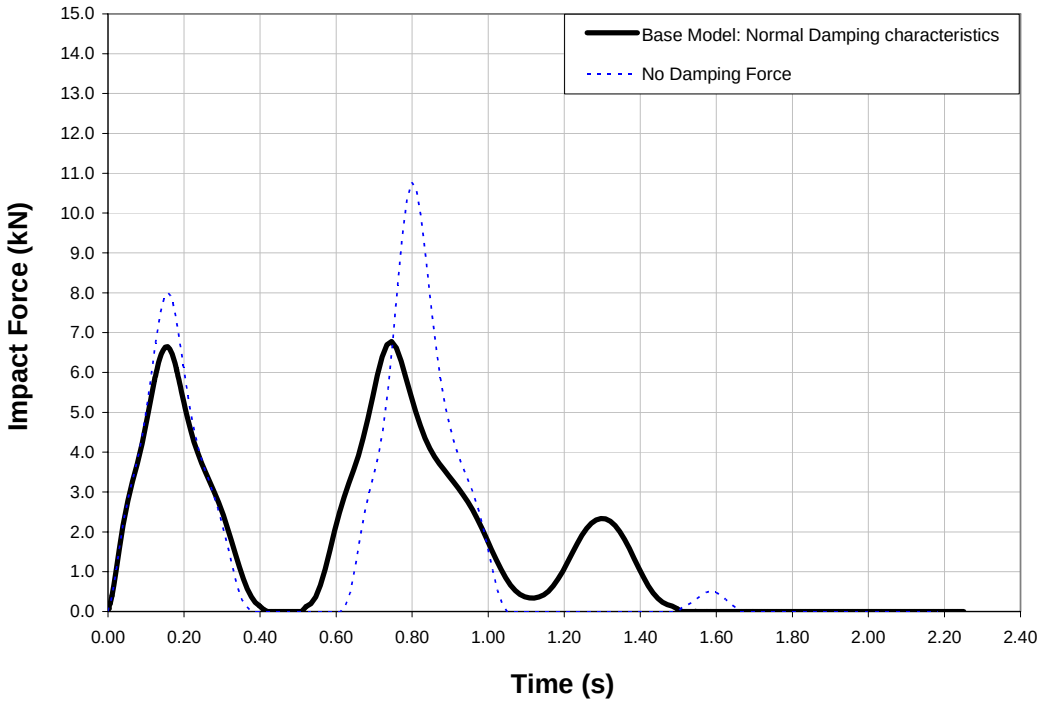

Figure G3 Damping Characteristics Effect: Payload Top - “Power-OFF”

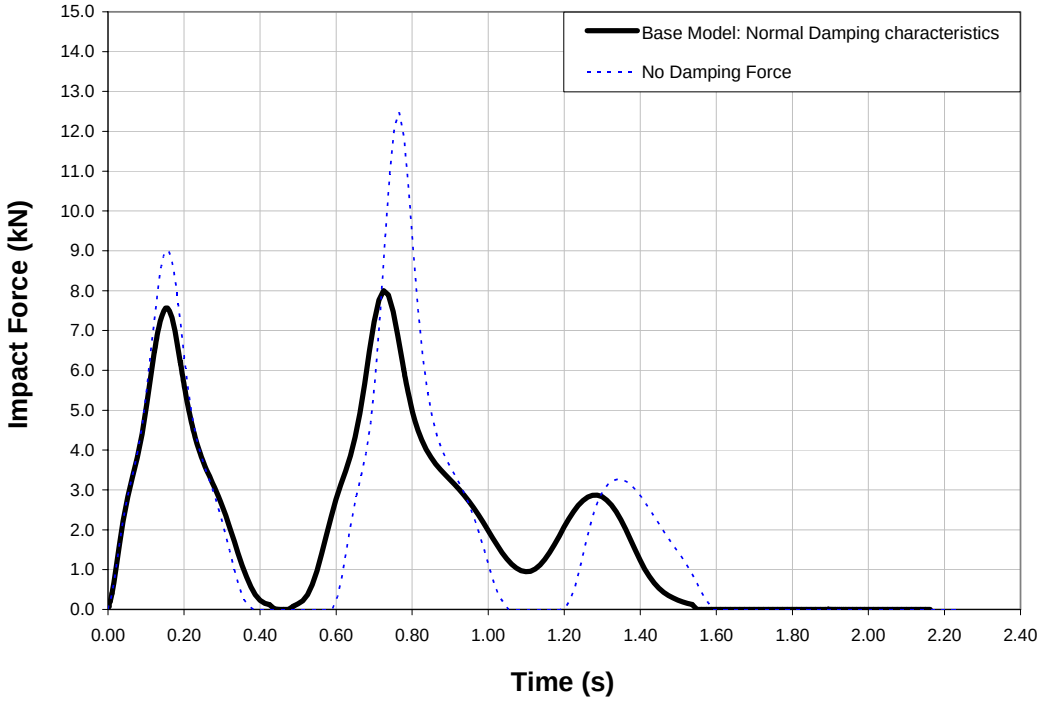

Figure G4 Damping Characteristics Effect: Payload Top - “Power-ON”

Annex H1: Parameter = Horizontal Lag Angle

1 rad = (360/(2π)) = 57.3^0 **1σ = 1.25^0 = 1.25 / 57.3 = 0.022 radians**

Lag Parameter: Power-Off: Payload = Bottom

Base Value Impact Force = fo = 6.35 kN
Base Value Impact Angle = 0 Radians

Lag Angle	FEA Impact Force	V (Gradient)	ΔP	Gradient x ΔP
-0.044	4.81	35.00	-0.044	-1.54
-0.022	5.45	40.91	-0.022	-0.90
0.022	7.69	60.91	0.022	1.34
0.044	8.79	55.45	0.044	2.44

NB: Normal lag of 1.25^0 occurs when crane transverses during normal travel, thus 1 σ = 1.25^0 = 0.022 radians.

Appr. value of the parameter resulting in 1 Standard Deviation = 0.022 Radians

From literature 1 Standard Deviation (σ) = 68.27%. Thus all impacts will occur within 1 σ.
To be conservative lets use 3 Standard Deviations, i.e. 99.73% of all impacts will occur within 3 σ
Use Standard Deviations = 3
Thus ΔP = Parameter @ 1 σ * 3 = 0.066

Average V (Gradient) = 48.07
V * ΔP = 3.17 (Change in Force per Parameter)
fo + V.(ΔP) = 9.52

Lag Parameter: Power-Off: Payload = Top

Base Value Impact Force = fo = 6.65 kN
Base Value Impact Angle = 0 Radians

Lag Angle	FEA Impact Force	V (Gradient)	ΔP	Gradient x ΔP
-0.044	5.54	25.23	-0.044	-1.11
-0.022	5.74	41.36	-0.022	-0.91
0.022	7.56	41.36	0.022	0.91
0.044	8.56	43.41	0.044	1.91

NB: Normal lag of 1.25^0 occurs when crane transverses during normal travel, thus 1 σ = 1.25^0 = 0.022 radians.

Appr. value of the parameter resulting in 1 Standard Deviation = 0.022 Radians

From literature 1 Standard Deviation (σ) = 68.27%. Thus all impacts will occur within 1 σ.
To be conservative lets use 3 Standard Deviations, i.e. 99.73% of all impacts will occur within 3 σ
Use Standard Deviations = 3
Thus ΔP = Parameter @ 1 σ * 3 = 0.066

Average V (Gradient) = 37.84
V * ΔP = 2.50 (Change in Force per Parameter)
fo + V.(ΔP) = 9.15

Lag Parameter: Power-On: Payload = Bottom

Base Value Impact Force = fo = 7.26 kN
Base Value Impact Angle = 0 Radians

Lag Angle	FEA Impact Force	V (Gradient)	ΔP	Gradient x ΔP
-0.044	5.38	42.73	-0.044	-1.88
-0.022	6.19	48.64	-0.022	-1.07
0.022	8.79	69.55	0.022	1.53
0.044	10.03	62.95	0.044	2.77

NB: Normal lag of 1.25^0 occurs when crane transverses during normal travel, thus 1 σ = 1.25^0 = 0.022 radians.

Appr. value of the parameter resulting in 1 Standard Deviation = 0.022 Radians

From literature 1 Standard Deviation (σ) = 68.27%. Thus all impacts will occur within 1 σ.
To be conservative lets use 3 Standard Deviations, i.e. 99.73% of all impacts will occur within 3 σ
Use Standard Deviations = 3
Thus ΔP = Parameter @ 1 σ * 3 = 0.066

Average V (Gradient) = 55.97
V * ΔP = 3.69 (Change in Force per Parameter)
fo + V.(ΔP) = 10.95

Lag Parameter: Power-On: Payload = Top

Base Value Impact Force = fo = 7.48 kN
Base Value Impact Angle = 0 Radians

Lag Angle	FEA Impact Force	V (Gradient)	ΔP	Gradient x ΔP
-0.04	5.63	42.05	-0.044	-1.85
-0.02	6.04	65.45	-0.022	-1.44
0.02	8.64	52.73	0.022	1.16
0.04	9.92	55.45	0.044	2.44

NB: Normal lag of 1.25^0 occurs when crane transverses during normal travel, thus 1 σ = 1.25^0 = 0.022 radians.

Appr. value of the parameter resulting in 1 Standard Deviation = 0.022 Radians

From literature 1 Standard Deviation (σ) = 68.27%. Thus all impacts will occur within 1 σ.
To be conservative lets use 3 Standard Deviations, i.e. 99.73% of all impacts will occur within 3 σ
Use Standard Deviations = 3
Thus ΔP = Parameter @ 1 σ * 3 = 0.066

Average V (Gradient) = 53.92
V * ΔP = 3.56 (Change in Force per Parameter)
fo + V.(ΔP) = 11.04

Annex H2: Parameter = Crab and Payload Eccentricity

Crab Eccentricity Parameter: Power-Off: Payload = Bottom

Base Value Impact Force = fo = 6.35 kN
Base Value Eccentricity = 0 m

Eccentricity Distance (m)	FEA Impact Force	V (Gradient)	ΔP	Gradient x ΔP
1.695	6.91	0.33	1.70	0.56
3.390	7.38	0.30	3.39	1.03

NB: A maximum eccentricity occurs at 3.39m from midpsan. Thus 3 σ = 3.39m. Thus 1 σ = 1.130m

Appr. value of the parameter resulting in 1 Standard Deviation = 1.13 m

From literature 1 Standard Deviation (**σ**) = 68.27%. Thus all impacts will occur within 1 **σ**.
To be conservative lets use **3** Standard Deviations, i.e. **99.73**% of all impacts will occur within **3 σ**
Use Standard Deviations = 3
Thus ΔP = Parameter @ 1 **σ** * 3 = **3.39**

Average V (Gradient) = 0.32
V * ΔP = 1.08 (Change in Force per Parameter)
fo + V.(ΔP) = 7.43

Crab Eccentricity Parameter: Power-Off: Payload = Top

Base Value Impact Force = fo = 6.65 kN
Base Value Eccentricity = 0 m

Eccentricity Distance (m)	FEA Impact Force	V (Gradient)	ΔP	Gradient x ΔP
1.695	7.49	0.50	1.70	0.84
3.390	8.03	0.41	3.39	1.38

NB: A maximum eccentricity occurs at 3.39m from midpsan. Thus 3s = 3.39m. Thus 1 s = 1.130m

Appr. value of the parameter resulting in 1 Standard Deviation = 1.13 m

From literature 1 Standard Deviation (**σ**) = 68.27%. Thus all impacts will occur within 1 **σ**.
To be conservative lets use **3** Standard Deviations, i.e. **99.73**% of all impacts will occur within **3 σ**
Use Standard Deviations = 3
Thus ΔP = Parameter @ 1 **σ** * 3 = **3.39**

Average V (Gradient) = 0.45
V * ΔP = 1.53 (Change in Force per Parameter)
fo + V.(ΔP) = 8.18

Crab Eccentricity Parameter: Power-On: Payload = Bottom

Base Value Impact Force = fo = 7.26 kN
Base Value Eccentricity = 0 m

Eccentricity Distance (m)	FEA Impact Force	V (Gradient)	ΔP	Gradient x ΔP
1.595	7.94	0.43	1.60	0.68
3.390	8.85	0.47	3.39	1.59

NB: A maximum eccentricity occurs at 3.39m from midpsan. Thus 3s = 3.39m. Thus 1 s = 1.130m

Appr. value of the parameter resulting in 1 Standard Deviation = 1.13 m

From literature 1 Standard Deviation (**σ**) = 68.27%. Thus all impacts will occur within 1 **σ**.
To be conservative lets use **3** Standard Deviations, i.e. **99.73**% of all impacts will occur within **3 σ**
Use Standard Deviations = 3
Thus ΔP = Parameter @ 1 **σ** * 3 = **3.39**

Average V (Gradient) = 0.45
V * ΔP = 1.52 (Change in Force per Parameter)
fo + V.(ΔP) = 8.78

Crab Eccentricity Parameter: Power-On: Payload = Top

Base Value Impact Force = fo = 7.48 kN
Base Value Eccentricity = 0 m

Eccentricity Distance (m)	FEA Impact Force	V (Gradient)	ΔP	Gradient x ΔP
1.695	8.56	0.64	1.70	1.08
3.390	9.38	0.56	3.39	1.90

NB: A maximum eccentricity occurs at 3.39m from midpsan. Thus 3s = 3.39m. Thus 1 s = 1.130m

Appr. value of the parameter resulting in 1 Standard Deviation = 1.13 m

From literature 1 Standard Deviation (**σ**) = 68.27%. Thus all impacts will occur within 1 **σ**.
To be conservative lets use **3** Standard Deviations, i.e. **99.73**% of all impacts will occur within **3 σ**
Use Standard Deviations = 3
Thus ΔP = Parameter @ 1 **σ** * 3 = **3.39**

Average V (Gradient) = 0.60
V * ΔP = 2.03 (Change in Force per Parameter)
fo + V.(ΔP) = 9.51

Annex H3: Parameter = Crane Supporting Structure's Flexibility

Gantry Flexibility Parameter: Power-Off: Payload = Bottom

Base Value Impact Force = fo = 6.35 kN
Base Value Spring Displacement = 0.0000 m

Relative δ w.r.t. base value(mm)	FEA Impact Force	V (Gradient)	ΔP	Gradient x ΔP
0.0069	4.46	-272.310	0.01	-1.89
0.0025	5.52	-336.079	0.00	-0.83
0.0002	6.29	-374.135	0.00	-0.06

NB: Assume Gantry Flexibility equal to Displacement = 2.5mm, thus 1 σ = 2.5mm = 0.0025m

Appr. value of the parameter resulting in 1 Standard Deviation = 2.50E-03 m

From literature 1 Standard Deviation (**σ**) = 68.27%. Thus all impacts will occur within 1 **σ**.
To be conservative lets use **3** Standard Deviations, i.e. **99.73**% of all impacts will occur within **3 σ**
Use Standard Deviations = 3
Thus ΔP = Parameter @ 1 **σ** * 3 = **0.008**

Average V (Gradient) = -355.107
V * ΔP = -2.66 (Change in Force per Parameter)
fo + V.(ΔP) = 3.69

Gantry Flexibility Parameter: Power-Off: Payload = Top

Base Value Impact Force = fo = 6.65 kN
Base Value Spring Displacement = 0.0000 m

Relative δ w.r.t. base value(mm)	FEA Impact Force	V (Gradient)	ΔP	Gradient x ΔP
0.0073	4.55	-289.388	0.01	-2.10
0.0022	5.84	-365.079	0.00	-0.81
0.0002	6.58	-394.041	0.00	-0.07

NB: Assume Gantry Flexibility equal to Displacement = 2.5mm, thus 1 s = 2.5mm = 0.0025m

Appr. value of the parameter resulting in 1 Standard Deviation = 2.50E-03 m

From literature 1 Standard Deviation (**σ**) = 68.27%. Thus all impacts will occur within 1 **σ**.
To be conservative lets use **3** Standard Deviations, i.e. **99.73**% of all impacts will occur within **3 σ**
Use Standard Deviations = 3
Thus ΔP = Parameter @ 1 **σ** * 3 = **0.008**

Average V (Gradient) = -379.560
V * ΔP = -2.85 (Change in Force per Parameter)
fo + V.(ΔP) = 3.80

Gantry Flexibility Parameter: Power-On: Payload = Bottom

Base Value Impact Force = fo = 7.26 kN
Base Value Spring Displacement = 0.0000 m

Relative δ w.r.t. base value(mm)	FEA Impact Force	V (Gradient)	ΔP	Gradient x ΔP
0.0066	5.03	-339.051	0.01	-2.23
0.0016	6.62	-405.506	0.00	-0.64
-0.0010	7.65	-409.774	0.00	0.39

NB: Assume Gantry Flexibility equal to Displacement = 2.5mm, thus 1 s = 2.5mm = 0.0025m

Appr. value of the parameter resulting in 1 Standard Deviation = 2.50E-03 m

From literature 1 Standard Deviation (**σ**) = 68.27%. Thus all impacts will occur within 1 **σ**.
To be conservative lets use **3** Standard Deviations, i.e. **99.73**% of all impacts will occur within **3 σ**
Use Standard Deviations = 3
Thus ΔP = Parameter @ 1 **σ** * 3 = **0.008**

Average V (Gradient) = -407.640
V * ΔP = -3.06 (Change in Force per Parameter)
fo + V.(ΔP) = 4.20

Gantry Flexibility Parameter: Power-On: Payload = Top

Base Value Impact Force = fo = 7.48 kN
Base Value Spring Displacement = 0.0000 m

Relative δ w.r.t. base value(mm)	FEA Impact Force	V (Gradient)	ΔP	Gradient x ΔP
0.0076	4.92	-337.934	0.01	-2.56
0.0024	6.52	-405.145	0.00	-0.96
0.0000	7.48	0.000	0.00	0.00

NB: Assume Gantry Flexibility equal to Displacement = 2.5mm, thus 1 s = 2.5mm = 0.0025m

Appr. value of the parameter resulting in 1 Standard Deviation = 2.50E-03 m

From literature 1 Standard Deviation (**σ**) = 68.27%. Thus all impacts will occur within 1 **σ**.
To be conservative lets use **3** Standard Deviations, i.e. **99.73**% of all impacts will occur within **3 σ**
Use Standard Deviations = 3
Thus ΔP = Parameter @ 1 **σ** * 3 = **0.008**

Average V (Gradient) = -202.573
V * ΔP = -1.52 (Change in Force per Parameter)
fo + V.(ΔP) = 5.96

Annex H4: Parameter = Crane Impact Speed

Crane Travel Parameter: Power-Off: Payload = Bottom

Base Value Impact Force = fo = 6.35 kN
Base Value Longitudinal Crane Speed = 0.55 m/s

Long. Crane Speed (m/s)	FEA Impact Force	V (Gradient)	ΔP	Gradient x ΔP
0.375	3.60	15.71	-0.18	-2.75
0.500	5.13	24.40	-0.05	-1.22
0.600	7.88	30.60	0.05	1.53

NB: Encorder Crane Speed can vary by ±0.05m/s compared to actual long crane speed, thus 1 σ = 0.05m/s

Appr. value of the parameter resulting in 1 Standard Deviation = 0.05 m/s

From literature 1 Standard Deviation (σ) = 68.27%. Thus all impacts will occur within 1 σ.
To be conservative lets use 3 Standard Deviations, i.e. 99.73% of all impacts will occur within 3 σ
Use Standard Deviations = 3
Thus ΔP = Parameter @ 1 σ * 3 = 0.15

Average V (Gradient) = 27.50
V * ΔP = 4.13 (Change in Force per Parameter)
fo + V.(ΔP) = **10.48**

Crane Travel Parameter: Power-Off: Payload = Top

Base Value Impact Force = fo = 6.65 kN
Base Value Longitudinal Crane Speed = 0.55 m/s

Long. Crane Speed (m/s)	FEA Impact Force	V (Gradient)	ΔP	Gradient x ΔP
0.375	3.67	17.03	-0.18	-2.98
0.500	5.35	26.00	-0.05	-1.30
0.600	8.30	33.00	0.05	1.65

NB: Encorder Crane Speed can vary by ±0.05m/s compared to actual long crane speed, thus 1 σ = 0.05m/s

Appr. value of the parameter resulting in 1 Standard Deviation = 0.05 m/s

From literature 1 Standard Deviation (σ) = 68.27%. Thus all impacts will occur within 1 σ.
To be conservative lets use 3 Standard Deviations, i.e. 99.73% of all impacts will occur within 3 σ
Use Standard Deviations = 3
Thus ΔP = Parameter @ 1 σ * 3 = 0.15

Average V (Gradient) = 29.50
V * ΔP = 4.43 (Change in Force per Parameter)
fo + V.(ΔP) = **11.08**

Crane Travel Parameter: Power-On: Payload = Bottom

Base Value Impact Force = fo = 7.26 kN
Base Value Longitudinal Crane Speed = 0.55 m/s

Long. Crane Speed (m/s)	FEA Impact Force	V (Gradient)	ΔP	Gradient x ΔP
0.375	3.90	19.20	-0.18	-3.36
0.500	5.82	28.80	-0.05	-1.44
0.600	8.97	34.20	0.05	1.71

NB: Encorder Crane Speed can vary by ±0.05m/s compared to actual long crane speed, thus 1 σ = 0.05m/s

Appr. value of the parameter resulting in 1 Standard Deviation = 0.05 m/s

From literature 1 Standard Deviation (σ) = 68.27%. Thus all impacts will occur within 1 σ.
To be conservative lets use 3 Standard Deviations, i.e. 99.73% of all impacts will occur within 3 σ
Use Standard Deviations = 3
Thus ΔP = Parameter @ 1 σ * 3 = 0.15

Average V (Gradient) = 31.50
V * ΔP = 4.73 (Change in Force per Parameter)
fo + V.(ΔP) = **11.99**

Crane Travel Parameter: Power-On: Payload = Top

Base Value Impact Force = fo = 7.48 kN
Base Value Longitudinal Crane Speed = 0.55 m/s

Long. Crane Speed (m/s)	FEA Impact Force	V (Gradient)	ΔP	Gradient x ΔP
0.375	3.67	21.77	-0.18	-3.81
0.500	6.06	28.40	-0.05	-1.42
0.600	9.31	36.60	0.05	1.83

NB: Encorder Crane Speed can vary by ±0.05m/s compared to actual long crane speed, thus 1 σ = 0.05m/s

Appr. value of the parameter resulting in 1 Standard Deviation = 0.05 m/s

From literature 1 Standard Deviation (σ) = 68.27%. Thus all impacts will occur within 1 σ.
To be conservative lets use 3 Standard Deviations, i.e. 99.73% of all impacts will occur within 3 σ
Use Standard Deviations = 3
Thus ΔP = Parameter @ 1 σ * 3 = 0.15

Average V (Gradient) = 32.50
V * ΔP = 4.88 (Change in Force per Parameter)
fo + V.(ΔP) = **12.36**

Annex H5: Parameter = End Stops Misaligned

End Stop Misalignment Parameter: Power-Off: Payload = Bottom

Base Value Impact Force = fo = 6.35 kN
Base Value End Stop Misalignment = 0 mm

1 End Stop Misaligned (m)	FEA Impact Force	V (Gradient)	ΔP	Gradient x ΔP
0.025	7.63	51.20	0.03	1.28
0.050	7.90	31.00	0.05	1.55
0.150	7.43	7.20	0.15	1.08

*NB: Assume 0.5% end stop misalignment = 0.05% * 8250 = 41.25mm, thus 1 σ = 41.25mm*

Appr. value of the parameter resulting in 1 Standard Deviation = 0.04125 m

From literature 1 Standard Deviation (σ) = 68.27%. Thus all impacts will occur within 1 σ.
To be conservative lets use 3 Standard Deviations, i.e. 99.73% of all impacts will occur within 3 σ
Use Standard Deviations = 3
Thus ΔP = Parameter @ 1 σ * 3 = 0.12

Average V (Gradient) = 29.80
V * ΔP = 3.69 (Change in Force per Parameter)
fo + V.(ΔP) = 10.04

End Stop Misalignment Parameter: Power-Off: Payload = Top

Base Value Impact Force = fo = 6.65 kN
Base Value End Stop Misalignment = 0 mm

1 End Stop Misaligned (m)	FEA Impact Force	V (Gradient)	ΔP	Gradient x ΔP
0.025	8.09	57.60	0.03	1.44
0.050	8.92	45.40	0.05	2.27
0.150	8.83	14.53	0.15	2.18

*NB: Assume 0.5% end stop misalignment = 0.05% * 8250 = 41.25mm, thus 1 σ = 41.25mm*

Appr. value of the parameter resulting in 1 Standard Deviation = 0.04 m

From literature 1 Standard Deviation (σ) = 68.27%. Thus all impacts will occur within 1 σ.
To be conservative lets use 3 Standard Deviations, i.e. 99.73% of all impacts will occur within 3 σ
Use Standard Deviations = 3
Thus ΔP = Parameter @ 1 σ * 3 = 0.12

Average V (Gradient) = 39.18
V * ΔP = 4.85 (Change in Force per Parameter)
fo + V.(ΔP) = 11.50

End Stop Misalignment Parameter: Power-On: Payload = Bottom

Base Value Impact Force = fo = 7.26 kN
Base Value End Stop Misalignment = 0 mm

1 End Stop Misaligned (m)	FEA Impact Force	V (Gradient)	ΔP	Gradient x ΔP
0.025	8.69	57.20	0.03	1.43
0.050	8.65	27.80	0.05	1.39
0.150	9.69	16.20	0.15	2.43

*NB: Assume 0.5% end stop misalignment = 0.05% * 8250 = 41.25mm, thus 1 σ = 41.25mm*

Appr. value of the parameter resulting in 1 Standard Deviation = 0.04 m

From literature 1 Standard Deviation (σ) = 68.27%. Thus all impacts will occur within 1 σ.
To be conservative lets use 3 Standard Deviations, i.e. 99.73% of all impacts will occur within 3 σ
Use Standard Deviations = 3
Thus ΔP = Parameter @ 1 σ * 3 = 0.12

Average V (Gradient) = 33.73
V * ΔP = 4.17 (Change in Force per Parameter)
fo + V.(ΔP) = 11.43

End Stop Misalignment Parameter: Power-On: Payload = Top

Base Value Impact Force = fo = 7.48 kN
Base Value End Stop Misalignment = 0 mm

1 End Stop Misaligned (mm)	FEA Impact Force	V (Gradient)	ΔP	Gradient x ΔP
0.025	9.10	64.80	0.03	1.62
0.050	9.78	46.00	0.05	2.30
0.150	9.72	14.93	0.15	2.24

*NB: Assume 0.5% end stop misalignment = 0.05% * 8250 = 41.25mm, thus 1 σ = 41.25mm*

Appr. value of the parameter resulting in 1 Standard Deviation = 0.04 m

From literature 1 Standard Deviation (σ) = 68.27%. Thus all impacts will occur within 1 σ.
To be conservative lets use 3 Standard Deviations, i.e. 99.73% of all impacts will occur within 3 σ
Use Standard Deviations = 3
Thus ΔP = Parameter @ 1 σ * 3 = 0.12

Average V (Gradient) = 41.91
V * ΔP = 5.19 (Change in Force per Parameter)
fo + V.(ΔP) = 12.67

Annex H6: Parameter = Buffer's Elastic Characteristics

Elastic Buffer Characteristic Parameter: Power-Off: Payload = Bottom

Base Value Impact Force = fo = 6.35 kN
Base Value % Difference in the Elastic Char. = 0 %

% Difference	FEA Impact Force	V (Gradient)	ΔP	Gradient x ΔP
10.00	6.31	0.00	10.00	-0.04
20.00	6.38	0.00	20.00	0.03
-10.00	6.16	0.02	-10.00	-0.19
-20.00	6.08	0.01	-20.00	-0.27

NB: Assume that the elastic buffer characteristics can vary by 20%, thus 1 σ = 20%.

Appr. value of the parameter resulting in 1 Standard Deviation = 0.2

From literature 1 Standard Deviation (σ) = 68.27%. Thus all impacts will occur within 1 σ.
To be conservative lets use 3 Standard Deviations, i.e. 99.73% of all impacts will occur within 3 σ
Use Standard Deviations = 3
Thus ΔP = Parameter @ 1 σ * 3 = 0.6

Average V (Gradient) = 0.01
V * ΔP = 0.00 (Change in Force per Parameter)
fo + V.(ΔP) = 6.35

Elastic Buffer Characteristic Parameter: Power-Off: Payload = Top

Base Value Impact Force = fo = 6.65 kN
Base Value % Difference in the Elastic Char. = 0 %

% Difference	FEA Impact Force	V (Gradient)	ΔP	Gradient x ΔP
10.00	6.61	0.00	10.00	-0.04
20.00	6.56	0.00	20.00	-0.09
-10.00	6.66	0.00	-10.00	0.01
-20.00	6.81	-0.01	-20.00	0.16

NB: Assume that the elastic buffer characteristics can vary by 20%, thus 1 σ = 20%.

Appr. value of the parameter resulting in 1 Standard Deviation = 0.2

From literature 1 Standard Deviation (σ) = 68.27%. Thus all impacts will occur within 1 σ.
To be conservative lets use 3 Standard Deviations, i.e. 99.73% of all impacts will occur within 3 σ
Use Standard Deviations = 3
Thus ΔP = Parameter @ 1 σ * 3 = 0.6

Average V (Gradient) = 0.00
V * ΔP = 0.00 (Change in Force per Parameter)
fo + V.(ΔP) = 6.65

Elastic Buffer Characteristic Parameter: Power-On: Payload = Bottom

Base Value Impact Force = fo = 7.26 kN
Base Value % Difference in the Elastic Char. = 0 %

% Difference	FEA Impact Force	V (Gradient)	ΔP	Gradient x ΔP
10.00	7.13	-0.01	10.00	-0.13
20.00	7.14	-0.01	20.00	-0.12
-10.00	7.09	0.02	-10.00	-0.17
-20.00	7.05	0.01	-20.00	-0.21

NB: Assume that the elastic buffer characteristics can vary by 20%, thus 1 σ = 20%.

Appr. value of the parameter resulting in 1 Standard Deviation = 0.2

From literature 1 Standard Deviation (σ) = 68.27%. Thus all impacts will occur within 1 σ.
To be conservative lets use 3 Standard Deviations, i.e. 99.73% of all impacts will occur within 3 σ
Use Standard Deviations = 3
Thus ΔP = Parameter @ 1 σ * 3 = 0.6

Average V (Gradient) = 0.00
V * ΔP = 0.00 (Change in Force per Parameter)
fo + V.(ΔP) = 7.26

Elastic Buffer Characteristic Parameter: Power-On: Payload = Top

Base Value Impact Force = fo = 7.48 kN
Base Value % Difference in the Elastic Char. = 0 %

% Difference	FEA Impact Force	V (Gradient)	ΔP	Gradient x ΔP
10.00	7.43	-0.01	10.00	-0.05
20.00	7.33	-0.01	20.00	-0.15
-10.00	7.69	-0.02	-10.00	0.21
-20.00	7.92	-0.02	-20.00	0.44

NB: Assume that the elastic buffer characteristics can vary by 20%, thus 1 σ = 20%.

Appr. value of the parameter resulting in 1 Standard Deviation = 0.2

From literature 1 Standard Deviation (σ) = 68.27%. Thus all impacts will occur within 1 σ.
To be conservative lets use 3 Standard Deviations, i.e. 99.73% of all impacts will occur within 3 σ
Use Standard Deviations = 3
Thus ΔP = Parameter @ 1 σ * 3 = 0.6

Average V (Gradient) = -0.01
V * ΔP = -0.01 (Change in Force per Parameter)
fo + V.(ΔP) = 7.47

Annex H7: Parameter = Buffer's Damping Characteristics

Buffer Damping Charactcteristic Parameter: Power-Off: Payload = Bottom

Base Value Impact Force = fo = 6.35 kN **0 = ON**
Base Value Damping Buffer Char. (ON) = 0 ON **1 = OFF**

Damping (ON / OFF)	FEA Impact Force	V (Gradient)	ΔP	Gradient x ΔP
1	7.61	1.26	1.00	1.26

NB: Assume Buffer damping Characteristics can vary by 30%, thus 1 σ = 30%

Appr. value of the parameter resulting in 1 Standard Deviation = 0.30

From literature 1 Standard Deviation (σ) = 68.27%. Thus all impacts will occur within 1 σ.
To be conservative lets use 3 Standard Deviations, i.e. 99.73% of all impacts will occur within 3 σ
Use Standard Deviations = 3
Thus ΔP = Parameter @ 1 σ * 3 = 0.90

Average V (Gradient) = 1.26
V * ΔP = 1.13 (Change in Force per Parameter)
fo + V.(ΔP) = 7.48

Buffer Damping Charactcteristic Parameter: Power-Off: Payload = Top

Base Value Impact Force = fo = 6.65 kN **0 = ON**
Base Value Damping Buffer Char. (ON) = 0 ON **1 = OFF**

Damping (ON / OFF)	FEA Impact Force	V (Gradient)	ΔP	Gradient x ΔP
1	7.99	1.34	1.00	1.34

NB: Assume Buffer damping Characteristics can vary by 30%, thus 1 σ = 30%

Appr. value of the parameter resulting in 1 Standard Deviation = 0.30

From literature 1 Standard Deviation (σ) = 68.27%. Thus all impacts will occur within 1 σ.
To be conservative lets use 3 Standard Deviations, i.e. 99.73% of all impacts will occur within 3 σ
Use Standard Deviations = 3
Thus ΔP = Parameter @ 1 σ * 3 = 0.90

Average V (Gradient) = 1.34
V * ΔP = 1.21 (Change in Force per Parameter)
fo + V.(ΔP) = 7.86

Buffer Damping Charactcteristic Parameter: Power-On: Payload = Bottom

Base Value Impact Force = fo = 7.26 kN **0 = ON**
Base Value Damping Buffer Char. (ON) = 0 ON **1 = OFF**

Damping (ON / OFF)	FEA Impact Force	V (Gradient)	ΔP	Gradient x ΔP
1	8.71	1.45	1.00	1.45

NB: Assume Buffer damping Characteristics can vary by 30%, thus 1 σ = 30%

Appr. value of the parameter resulting in 1 Standard Deviation = 0.30

From literature 1 Standard Deviation (σ) = 68.27%. Thus all impacts will occur within 1 σ.
To be conservative lets use 3 Standard Deviations, i.e. 99.73% of all impacts will occur within 3 σ
Use Standard Deviations = 3
Thus ΔP = Parameter @ 1 σ * 3 = 0.90

Average V (Gradient) = 1.45
V * ΔP = 1.31 (Change in Force per Parameter)
fo + V.(ΔP) = 8.57

Buffer Damping Charactcteristic Parameter: Power-On: Payload = Top

Base Value Impact Force = fo = 7.48 kN **0 = ON**
Base Value Damping Buffer Char. (ON) = 0 ON **1 = OFF**

Damping (ON / OFF)	FEA Impact Force	V (Gradient)	ΔP	Gradient x ΔP
1	9.01	1.53	1.00	1.53

NB: Assume Buffer damping Characteristics can vary by 30%, thus 1 σ = 30%

Appr. value of the parameter resulting in 1 Standard Deviation = 0.30

From literature 1 Standard Deviation (σ) = 68.27%. Thus all impacts will occur within 1 σ.
To be conservative lets use 3 Standard Deviations, i.e. 99.73% of all impacts will occur within 3 σ
Use Standard Deviations = 3
Thus ΔP = Parameter @ 1 σ * 3 = 0.90

Average V (Gradient) = 1.53
V * ΔP = 1.38 (Change in Force per Parameter)
fo + V.(ΔP) = 8.86

Annex I1: Parameter = Horizontal Lag Angle

1 rad = (360/(2π)) = 57.3^0 **1σ = 1.25^0 = 1.25 / 57.3 = 0.022 radians**

Lag Parameter: Power-Off: Payload = Bottom

Base Value Impact Force = fo = 4.43 kN
Base Value Impact Angle = 0 Radians

Lag Angle	FEA Impact Force	V (Gradient)	ΔP	Gradient x ΔP
-0.044	5.83	-31.82	-0.044	1.40
-0.022	4.95	-23.64	-0.022	0.52
0.022	4.15	-12.73	0.022	-0.28
0.044	4.25	-4.09	0.044	-0.18

NB: Normal lag of 1.25^0 occurs when crane transverses during normal travel, thus 1 σ = 1.25^0 = 0.022 radians.

Appr. value of the parameter resulting in 1 Standard Deviation = 0.022 Radians

From literature 1 Standard Deviation (σ) = 68.27%. Thus all impacts will occur within 1 σ.
To be conservative lets use 3 Standard Deviations, i.e. 99.73% of all impacts will occur within 3 σ
Use Standard Deviations = 3
Thus ΔP = Parameter @ 1 σ * 3 = 0.066

Average V (Gradient) = -18.07
V * ΔP = -1.19 (Change in Force per Parameter)
fo + V.(ΔP) = 3.24

Lag Parameter: Power-Off: Payload = Top

Base Value Impact Force = fo = 6.88 kN
Base Value Impact Angle = 0 Radians

Lag Angle	FEA Impact Force	V (Gradient)	ΔP	Gradient x ΔP
-0.044	6.84	0.91	-0.044	-0.04
-0.022	6.92	-1.82	-0.022	0.04
0.022	7.15	12.27	0.022	0.27
0.044	7.38	11.36	0.044	0.50

NB: Normal lag of 1.25^0 occurs when crane transverses during normal travel, thus 1 σ = 1.25^0 = 0.022 radians.

Appr. value of the parameter resulting in 1 Standard Deviation = 0.022 Radians

From literature 1 Standard Deviation (σ) = 68.27%. Thus all impacts will occur within 1 σ.
To be conservative lets use 3 Standard Deviations, i.e. 99.73% of all impacts will occur within 3 σ
Use Standard Deviations = 3
Thus ΔP = Parameter @ 1 σ * 3 = 0.066

Average V (Gradient) = 5.68
V * ΔP = 0.38 (Change in Force per Parameter)
fo + V.(ΔP) = 7.26

Lag Parameter: Power-On: Payload = Bottom

Base Value Impact Force = fo = 4.61 kN
Base Value Impact Angle = 0 Radians

Lag Angle	FEA Impact Force	V (Gradient)	ΔP	Gradient x ΔP
-0.044	5.99	-31.36	-0.044	1.38
-0.022	5.06	-20.45	-0.022	0.45
0.022	4.44	-7.73	0.022	-0.17
0.044	4.67	1.36	0.044	0.06

NB: Normal lag of 1.25^0 occurs when crane transverses during normal travel, thus 1 σ = 1.25^0 = 0.022 radians.

Appr. value of the parameter resulting in 1 Standard Deviation = 0.022 Radians

From literature 1 Standard Deviation (σ) = 68.27%. Thus all impacts will occur within 1 σ.
To be conservative lets use 3 Standard Deviations, i.e. 99.73% of all impacts will occur within 3 σ
Use Standard Deviations = 3
Thus ΔP = Parameter @ 1 σ * 3 = 0.066

Average V (Gradient) = -14.55
V * ΔP = -0.96 (Change in Force per Parameter)
fo + V.(ΔP) = 3.65

Lag Parameter: Power-On: Payload = Top

Base Value Impact Force = fo = 8.05 kN
Base Value Impact Angle = 0 Radians

Lag Angle	FEA Impact Force	V (Gradient)	ΔP	Gradient x ΔP
-0.04	7.96	2.05	-0.044	-0.09
-0.02	7.14	41.36	-0.022	-0.91
0.02	8.31	11.82	0.022	0.26
0.04	8.52	10.68	0.044	0.47

NB: Normal lag of 1.25^0 occurs when crane transverses during normal travel, thus 1 σ = 1.25^0 = 0.022 radians.

Appr. value of the parameter resulting in 1 Standard Deviation = 0.022 Radians

From literature 1 Standard Deviation (σ) = 68.27%. Thus all impacts will occur within 1 σ.
To be conservative lets use 3 Standard Deviations, i.e. 99.73% of all impacts will occur within 3 σ
Use Standard Deviations = 3
Thus ΔP = Parameter @ 1 σ * 3 = 0.066

Average V (Gradient) = 16.48
V * ΔP = 1.09 (Change in Force per Parameter)
fo + V.(ΔP) = 9.14

Annex I2: Parameter = Crab and Payload Eccentricity

Crab Eccentricity Parameter: Power-Off: Payload = Bottom

Base Value Impact Force = fo = 4.43 kN
Base Value Eccentricity = 0 m

Eccentricity Distance (m)	FEA Impact Force	V (Gradient)	ΔP	Gradient x ΔP
1.695	4.49	0.04	1.70	0.06
3.390	5.75	0.39	3.39	1.32

NB: A maximum eccentricity occurs at 3.39m from midpsan. Thus 3 σ = 3.39m. Thus 1 σ = 1.130m

Appr. value of the parameter resulting in 1 Standard Deviation = 1.13 m

From literature 1 Standard Deviation (**σ**) = 68.27%. Thus all impacts will occur within 1 **σ**.
To be conservative lets use **3** Standard Deviations, i.e. **99.73**% of all impacts will occur within **3 σ**
Use Standard Deviations = 3
Thus ΔP = Parameter @ 1 **σ** * 3 = **3.39**

Average V (Gradient) = 0.21
V * ΔP = 0.72 (Change in Force per Parameter)
fo + V.(ΔP) = **5.15**

Crab Eccentricity Parameter: Power-Off: Payload = Top

Base Value Impact Force = fo = 6.88 kN
Base Value Eccentricity = 0 m

Eccentricity Distance (m)	FEA Impact Force	V (Gradient)	ΔP	Gradient x ΔP
1.695	8.13	0.74	1.70	1.25
3.390	7.84	0.28	3.39	0.96

NB: A maximum eccentricity occurs at 3.39m from midpsan. Thus 3s = 3.39m. Thus 1 s = 1.130m

Appr. value of the parameter resulting in 1 Standard Deviation = 1.13 m

From literature 1 Standard Deviation (**σ**) = 68.27%. Thus all impacts will occur within 1 **σ**.
To be conservative lets use **3** Standard Deviations, i.e. **99.73**% of all impacts will occur within **3 σ**
Use Standard Deviations = 3
Thus ΔP = Parameter @ 1 **σ** * 3 = **3.39**

Average V (Gradient) = 0.51
V * ΔP = 1.73 (Change in Force per Parameter)
fo + V.(ΔP) = **8.61**

Crab Eccentricity Parameter: Power-On: Payload = Bottom

Base Value Impact Force = fo = 4.61 kN
Base Value Eccentricity = 0 m

Eccentricity Distance (m)	FEA Impact Force	V (Gradient)	ΔP	Gradient x ΔP
1.595	5.28	0.42	1.60	0.67
3.390	6.05	0.42	3.39	1.44

NB: A maximum eccentricity occurs at 3.39m from midpsan. Thus 3s = 3.39m. Thus 1 s = 1.130m

Appr. value of the parameter resulting in 1 Standard Deviation = 1.13 m

From literature 1 Standard Deviation (**σ**) = 68.27%. Thus all impacts will occur within 1 **σ**.
To be conservative lets use **3** Standard Deviations, i.e. **99.73**% of all impacts will occur within **3 σ**
Use Standard Deviations = 3
Thus ΔP = Parameter @ 1 **σ** * 3 = **3.39**

Average V (Gradient) = 0.42
V * ΔP = 1.43 (Change in Force per Parameter)
fo + V.(ΔP) = **6.04**

Crab Eccentricity Parameter: Power-On: Payload = Top

Base Value Impact Force = fo = 8.05 kN
Base Value Eccentricity = 0 m

Eccentricity Distance (m)	FEA Impact Force	V (Gradient)	ΔP	Gradient x ΔP
1.695	8.83	0.46	1.70	0.78
3.390	9.04	0.29	3.39	0.99

NB: A maximum eccentricity occurs at 3.39m from midpsan. Thus 3s = 3.39m. Thus 1 s = 1.130m

Appr. value of the parameter resulting in 1 Standard Deviation = 1.13 m

From literature 1 Standard Deviation (**σ**) = 68.27%. Thus all impacts will occur within 1 **σ**.
To be conservative lets use **3** Standard Deviations, i.e. **99.73**% of all impacts will occur within **3 σ**
Use Standard Deviations = 3
Thus ΔP = Parameter @ 1 **σ** * 3 = **3.39**

Average V (Gradient) = 0.38
V * ΔP = 1.28 (Change in Force per Parameter)
fo + V.(ΔP) = **9.33**

Annex I3: Parameter = Crane Supporting Structure's Flexibility

Gantry Flexibility Parameter: Power-Off: Payload = Bottom

Base Value Impact Force = fo = 4.43 kN
Base Value Spring Displacement = 0.0000 m

Relative δ w.r.t. base value(mm)	FEA Impact Force	V (Gradient)	ΔP	Gradient x ΔP
-0.0068	6.25	-266.503	-0.01	1.82
-0.0021	4.86	-207.254	0.00	0.43
0.0003	4.38	-187.958	0.00	-0.05

NB: Assume Gantry Flexibility equal to Displacement = 2.5mm, thus 1 σ = 2.5mm = 0.0025m

Appr. value of the parameter resulting in 1 Standard Deviation = 2.50E-03 m

From literature 1 Standard Deviation (**σ**) = 68.27%. Thus all impacts will occur within 1 **σ**.
To be conservative lets use **3** Standard Deviations, i.e. **99.73**% of all impacts will occur within **3 σ**
Use Standard Deviations = 3
Thus ΔP = Parameter @ 1 **σ** * 3 = **0.008**

Average V (Gradient) = -197.606
V * ΔP = -1.48 (Change in Force per Parameter)
fo + V.(ΔP) = **2.95**

Gantry Flexibility Parameter: Power-Off: Payload = Top

Base Value Impact Force = fo = 6.88 kN
Base Value Spring Displacement = 0.0000 m

Relative δ w.r.t. base value(mm)	FEA Impact Force	V (Gradient)	ΔP	Gradient x ΔP
-0.0023	7.84	-408.736	0.00	0.96
0.0018	6.19	-387.283	0.00	-0.69
0.0003	6.74	-402.919	0.00	-0.14

NB: Assume Gantry Flexibility equal to Displacement = 2.5mm, thus 1 s = 2.5mm = 0.0025m

Appr. value of the parameter resulting in 1 Standard Deviation = 2.50E-03 m

From literature 1 Standard Deviation (**σ**) = 68.27%. Thus all impacts will occur within 1 **σ**.
To be conservative lets use **3** Standard Deviations, i.e. **99.73**% of all impacts will occur within **3 σ**
Use Standard Deviations = 3
Thus ΔP = Parameter @ 1 **σ** * 3 = **0.008**

Average V (Gradient) = -395.101
V * ΔP = -2.96 (Change in Force per Parameter)
fo + V.(ΔP) = **3.92**

Gantry Flexibility Parameter: Power-On: Payload = Bottom

Base Value Impact Force = fo = 4.61 kN
Base Value Spring Displacement = 0.0000 m

Relative δ w.r.t. base value(mm)	FEA Impact Force	V (Gradient)	ΔP	Gradient x ΔP
-0.0075	6.85	-300.304	-0.01	2.24
-0.0018	5.01	-221.940	0.00	0.40
-0.0002	4.65	-206.225	0.00	0.04

NB: Assume Gantry Flexibility equal to Displacement = 2.5mm, thus 1 s = 2.5mm = 0.0025m

Appr. value of the parameter resulting in 1 Standard Deviation = 2.50E-03 m

From literature 1 Standard Deviation (**σ**) = 68.27%. Thus all impacts will occur within 1 **σ**.
To be conservative lets use **3** Standard Deviations, i.e. **99.73**% of all impacts will occur within **3 σ**
Use Standard Deviations = 3
Thus ΔP = Parameter @ 1 **σ** * 3 = **0.008**

Average V (Gradient) = -214.082
V * ΔP = -1.61 (Change in Force per Parameter)
fo + V.(ΔP) = **3.00**

Gantry Flexibility Parameter: Power-On: Payload = Top

Base Value Impact Force = fo = 8.05 kN
Base Value Spring Displacement = 0.0000 m

Relative δ w.r.t. base value(mm)	FEA Impact Force	V (Gradient)	ΔP	Gradient x ΔP
-0.0024	9.01	-403.482	0.00	0.96
0.0014	7.48	-405.427	0.00	-0.57
0.0004	7.90	-404.612	0.00	-0.15

NB: Assume Gantry Flexibility equal to Displacement = 2.5mm, thus 1 s = 2.5mm = 0.0025m

Appr. value of the parameter resulting in 1 Standard Deviation = 2.50E-03 m

From literature 1 Standard Deviation (**σ**) = 68.27%. Thus all impacts will occur within 1 **σ**.
To be conservative lets use **3** Standard Deviations, i.e. **99.73**% of all impacts will occur within **3 σ**
Use Standard Deviations = 3
Thus ΔP = Parameter @ 1 **σ** * 3 = **0.008**

Average V (Gradient) = -405.019
V * ΔP = -3.04 (Change in Force per Parameter)
fo + V.(ΔP) = **5.01**

Annex I4: Parameter = Crane Impact Speed

Crane Travel Parameter: Power-Off: Payload = Bottom

Base Value Impact Force = fo = 4.43 kN
Base Value Longitudinal Crane Speed = 0.55 m/s

Long. Crane Speed (m/s)	FEA Impact Force	V (Gradient)	ΔP	Gradient x ΔP
0.375	2.62	10.34	-0.18	-1.81
0.500	3.64	15.80	-0.05	-0.79
0.600	6.41	39.60	0.05	1.98

NB: Encorder Crane Speed can vary by ±0.05m/s compared to actual long crane speed, thus 1 σ = 0.05m/s

Appr. value of the parameter resulting in 1 Standard Deviation = 0.05 m/s

From literature 1 Standard Deviation (σ) = 68.27%. Thus all impacts will occur within 1 σ.
To be conservative lets use **3** Standard Deviations, i.e. **99.73**% of all impacts will occur within **3 σ**
Use Standard Deviations = 3
Thus ΔP = Parameter @ 1 σ * 3 = **0.15**

Average V (Gradient) = 27.70
V * ΔP = 4.16 (Change in Force per Parameter)
fo + V.(ΔP) = **8.59**

Crane Travel Parameter: Power-Off: Payload = Top

Base Value Impact Force = fo = 6.88 kN
Base Value Longitudinal Crane Speed = 0.55 m/s

Long. Crane Speed (m/s)	FEA Impact Force	V (Gradient)	ΔP	Gradient x ΔP
0.375	3.68	18.29	-0.18	-3.20
0.500	5.35	30.60	-0.05	-1.53
0.600	8.30	28.40	0.05	1.42

NB: Encorder Crane Speed can vary by ±0.05m/s compared to actual long crane speed, thus 1 σ = 0.05m/s

Appr. value of the parameter resulting in 1 Standard Deviation = 0.05 m/s

From literature 1 Standard Deviation (σ) = 68.27%. Thus all impacts will occur within 1 σ.
To be conservative lets use **3** Standard Deviations, i.e. **99.73**% of all impacts will occur within **3 σ**
Use Standard Deviations = 3
Thus ΔP = Parameter @ 1 σ * 3 = **0.15**

Average V (Gradient) = 29.50
V * ΔP = 4.43 (Change in Force per Parameter)
fo + V.(ΔP) = **11.31**

Crane Travel Parameter: Power-On: Payload = Bottom

Base Value Impact Force = fo = 4.61 kN
Base Value Longitudinal Crane Speed = 0.55 m/s

Long. Crane Speed (m/s)	FEA Impact Force	V (Gradient)	ΔP	Gradient x ΔP
0.375	2.72	10.80	-0.18	-1.89
0.500	3.70	18.20	-0.05	-0.91
0.600	7.05	48.80	0.05	2.44

NB: Encorder Crane Speed can vary by ±0.05m/s compared to actual long crane speed, thus 1 σ = 0.05m/s

Appr. value of the parameter resulting in 1 Standard Deviation = 0.05 m/s

From literature 1 Standard Deviation (σ) = 68.27%. Thus all impacts will occur within 1 σ.
To be conservative lets use **3** Standard Deviations, i.e. **99.73**% of all impacts will occur within **3 σ**
Use Standard Deviations = 3
Thus ΔP = Parameter @ 1 σ * 3 = **0.15**

Average V (Gradient) = 33.50
V * ΔP = 5.03 (Change in Force per Parameter)
fo + V.(ΔP) = **9.64**

Crane Travel Parameter: Power-On: Payload = Top

Base Value Impact Force = fo = 8.05 kN
Base Value Longitudinal Crane Speed = 0.55 m/s

Long. Crane Speed (m/s)	FEA Impact Force	V (Gradient)	ΔP	Gradient x ΔP
0.375	3.68	24.97	-0.18	-4.37
0.500	6.17	37.60	-0.05	-1.88
0.600	10.34	45.80	0.05	2.29

NB: Encorder Crane Speed can vary by ±0.05m/s compared to actual long crane speed, thus 1 σ = 0.05m/s

Appr. value of the parameter resulting in 1 Standard Deviation = 0.05 m/s

From literature 1 Standard Deviation (σ) = 68.27%. Thus all impacts will occur within 1 σ.
To be conservative lets use **3** Standard Deviations, i.e. **99.73**% of all impacts will occur within **3 σ**
Use Standard Deviations = 3
Thus ΔP = Parameter @ 1 σ * 3 = **0.15**

Average V (Gradient) = 41.70
V * ΔP = 6.26 (Change in Force per Parameter)
fo + V.(ΔP) = **14.31**

Annex I5: Parameter = End Stops Misaligned

End Stop Misalignment Parameter: Power-Off: Payload = Bottom

Base Value Impact Force = fo = 4.43 kN
Base Value End Stop Misalignment = 0 mm

1 End Stop Misaligned (m)	FEA Impact Force	V (Gradient)	ΔP	Gradient x ΔP
0.025	4.91	19.20	0.03	0.48
0.050	5.49	21.20	0.05	1.06
0.150	7.31	19.20	0.15	2.88

*NB: Assume 0.5% end stop misalignment = 0.05% * 8250 = 41.25mm, thus 1 σ = 41.25mm*

Appr. value of the parameter resulting in 1 Standard Deviation = 0.04125 m

From literature 1 Standard Deviation (σ) = 68.27%. Thus all impacts will occur within 1 σ.
To be conservative lets use 3 Standard Deviations, i.e. 99.73% of all impacts will occur within 3 σ
Use Standard Deviations = 3
Thus ΔP = Parameter @ 1 σ * 3 = 0.12

Average V (Gradient) = 19.87
V * ΔP = 2.46 (Change in Force per Parameter)
fo + V.(ΔP) = **6.89**

End Stop Misalignment Parameter: Power-Off: Payload = Top

Base Value Impact Force = fo = 6.88 kN
Base Value End Stop Misalignment = 0 mm

1 End Stop Misaligned (m)	FEA Impact Force	V (Gradient)	ΔP	Gradient x ΔP
0.025	9.41	101.20	0.03	2.53
0.050	5.83	-21.00	0.05	-1.05
0.150	7.16	1.87	0.15	0.28

*NB: Assume 0.5% end stop misalignment = 0.05% * 8250 = 41.25mm, thus 1 σ = 41.25mm*

Appr. value of the parameter resulting in 1 Standard Deviation = 0.04 m

From literature 1 Standard Deviation (σ) = 68.27%. Thus all impacts will occur within 1 σ.
To be conservative lets use 3 Standard Deviations, i.e. 99.73% of all impacts will occur within 3 σ
Use Standard Deviations = 3
Thus ΔP = Parameter @ 1 σ * 3 = 0.12

Average V (Gradient) = 27.36
V * ΔP = 3.39 (Change in Force per Parameter)
fo + V.(ΔP) = **10.27**

End Stop Misalignment Parameter: Power-On: Payload = Bottom

Base Value Impact Force = fo = 4.61 kN
Base Value End Stop Misalignment = 0 mm

1 End Stop Misaligned (m)	FEA Impact Force	V (Gradient)	ΔP	Gradient x ΔP
0.025	6.84	89.20	0.03	2.23
0.050	5.33	14.40	0.05	0.72
0.150	6.33	11.47	0.15	1.72

*NB: Assume 0.5% end stop misalignment = 0.05% * 8250 = 41.25mm, thus 1 σ = 41.25mm*

Appr. value of the parameter resulting in 1 Standard Deviation = 0.04 m

From literature 1 Standard Deviation (σ) = 68.27%. Thus all impacts will occur within 1 σ.
To be conservative lets use 3 Standard Deviations, i.e. 99.73% of all impacts will occur within 3 σ
Use Standard Deviations = 3
Thus ΔP = Parameter @ 1 σ * 3 = 0.12

Average V (Gradient) = 38.36
V * ΔP = 4.75 (Change in Force per Parameter)
fo + V.(ΔP) = **9.36**

End Stop Misalignment Parameter: Power-On: Payload = Top

Base Value Impact Force = fo = 8.05 kN
Base Value End Stop Misalignment = 0 mm

1 End Stop Misaligned (mm)	FEA Impact Force	V (Gradient)	ΔP	Gradient x ΔP
0.025	10.11	82.40	0.03	2.06
0.050	7.04	-20.20	0.05	-1.01
0.150	8.11	0.40	0.15	0.06

*NB: Assume 0.5% end stop misalignment = 0.05% * 8250 = 41.25mm, thus 1 σ = 41.25mm*

Appr. value of the parameter resulting in 1 Standard Deviation = 0.04 m

From literature 1 Standard Deviation (σ) = 68.27%. Thus all impacts will occur within 1 σ.
To be conservative lets use 3 Standard Deviations, i.e. 99.73% of all impacts will occur within 3 σ
Use Standard Deviations = 3
Thus ΔP = Parameter @ 1 σ * 3 = 0.12

Average V (Gradient) = 20.87
V * ΔP = 2.58 (Change in Force per Parameter)
fo + V.(ΔP) = **10.63**

Annex I6: Parameter = Buffer's Elastic Characteristics

Elastic Buffer Characteristic Parameter: Power-Off: Payload = Bottom

Base Value Impact Force = fo = 4.43 kN
Base Value % Difference in the Elastic Char. = 0 %

% Difference	FEA Impact Force	V (Gradient)	ΔP	Gradient x ΔP
10.00	4.64	0.02	10.00	0.21
20.00	4.8	0.02	20.00	0.37
-10.00	4.29	0.01	-10.00	-0.14
-20.00	4.07	0.02	-20.00	-0.36

NB: Assume that the elastic buffer characteristics can vary by 20%, thus 1 σ = 20%.

Appr. value of the parameter resulting in 1 Standard Deviation = 0.2

From literature 1 Standard Deviation (σ) = 68.27%. Thus all impacts will occur within 1 σ.
To be conservative lets use 3 Standard Deviations, i.e. 99.73% of all impacts will occur within 3 σ
Use Standard Deviations = 3
Thus ΔP = Parameter @ 1 σ * 3 = 0.6

Average V (Gradient) = 0.02
V * ΔP = 0.01 (Change in Force per Parameter)
fo + V.(ΔP) = **4.44**

Elastic Buffer Characteristic Parameter: Power-Off: Payload = Top

Base Value Impact Force = fo = 6.88 kN
Base Value % Difference in the Elastic Char. = 0 %

% Difference	FEA Impact Force	V (Gradient)	ΔP	Gradient x ΔP
10.00	7.04	0.02	10.00	0.16
20.00	6.92	0.00	20.00	0.04
-10.00	6.77	0.01	-10.00	-0.11
-20.00	7.57	-0.03	-20.00	0.69

NB: Assume that the elastic buffer characteristics can vary by 20%, thus 1 σ = 20%.

Appr. value of the parameter resulting in 1 Standard Deviation = 0.2

From literature 1 Standard Deviation (σ) = 68.27%. Thus all impacts will occur within 1 σ.
To be conservative lets use 3 Standard Deviations, i.e. 99.73% of all impacts will occur within 3 σ
Use Standard Deviations = 3
Thus ΔP = Parameter @ 1 σ * 3 = 0.6

Average V (Gradient) = 0.00
V * ΔP = 0.00 (Change in Force per Parameter)
fo + V.(ΔP) = **6.88**

Elastic Buffer Characteristic Parameter: Power-On: Payload = Bottom

Base Value Impact Force = fo = 4.61 kN
Base Value % Difference in the Elastic Char. = 0 %

% Difference	FEA Impact Force	V (Gradient)	ΔP	Gradient x ΔP
10.00	4.63	0.00	10.00	0.02
20.00	4.83	0.01	20.00	0.22
-10.00	4.62	0.00	-10.00	0.01
-20.00	4.5	0.01	-20.00	-0.11

NB: Assume that the elastic buffer characteristics can vary by 20%, thus 1 σ = 20%.

Appr. value of the parameter resulting in 1 Standard Deviation = 0.2

From literature 1 Standard Deviation (σ) = 68.27%. Thus all impacts will occur within 1 σ.
To be conservative lets use 3 Standard Deviations, i.e. 99.73% of all impacts will occur within 3 σ
Use Standard Deviations = 3
Thus ΔP = Parameter @ 1 σ * 3 = 0.6

Average V (Gradient) = 0.00
V * ΔP = 0.00 (Change in Force per Parameter)
fo + V.(ΔP) = **4.61**

Elastic Buffer Characteristic Parameter: Power-On: Payload = Top

Base Value Impact Force = fo = 8.05 kN
Base Value % Difference in the Elastic Char. = 0 %

% Difference	FEA Impact Force	V (Gradient)	ΔP	Gradient x ΔP
10.00	8.04	0.00	10.00	-0.01
20.00	7.91	-0.01	20.00	-0.14
-10.00	8.00	0.01	-10.00	-0.05
-20.00	7.96	0.00	-20.00	-0.09

NB: Assume that the elastic buffer characteristics can vary by 20%, thus 1 σ = 20%.

Appr. value of the parameter resulting in 1 Standard Deviation = 0.2

From literature 1 Standard Deviation (σ) = 68.27%. Thus all impacts will occur within 1 σ.
To be conservative lets use 3 Standard Deviations, i.e. 99.73% of all impacts will occur within 3 σ
Use Standard Deviations = 3
Thus ΔP = Parameter @ 1 σ * 3 = 0.6

Average V (Gradient) = 0.00
V * ΔP = 0.00 (Change in Force per Parameter)
fo + V.(ΔP) = **8.05**

Annex I7: Parameter = Buffer's Damping Characteristics

Buffer Damping Charactcteristic Parameter: Power-Off: Payload = Bottom

Base Value Impact Force = fo = 4.43 kN **0 = ON**
Base Value Damping Buffer Char. (ON) = 0 ON **1 = OFF**

Damping (ON / OFF)	FEA Impact Force	V (Gradient)	ΔP	Gradient x ΔP
1	13.03	8.60	1.00	8.60

NB: Assume Buffer damping Characteristics can vary by 30%, thus 1 σ = 30%

Appr. value of the parameter resulting in 1 Standard Deviation = 0.30

From literature 1 Standard Deviation (σ) = 68.27%. Thus all impacts will occur within 1 σ.
To be conservative lets use **3** Standard Deviations, i.e. **99.73**% of all impacts will occur within **3 σ**
Use Standard Deviations = 3
Thus ΔP = Parameter @ 1 σ * 3 = **0.90**

Average V (Gradient) = 8.60
V * ΔP = 7.74 (Change in Force per Parameter)
fo + V.(ΔP) = **12.17**

Buffer Damping Charactcteristic Parameter: Power-Off: Payload = Top

Base Value Impact Force = fo = 6.88 kN **0 = ON**
Base Value Damping Buffer Char. (ON) = 0 ON **1 = OFF**

Damping (ON / OFF)	FEA Impact Force	V (Gradient)	ΔP	Gradient x ΔP
1	10.77	3.89	1.00	3.89

NB: Assume Buffer damping Characteristics can vary by 30%, thus 1 σ = 30%

Appr. value of the parameter resulting in 1 Standard Deviation = 0.30

From literature 1 Standard Deviation (σ) = 68.27%. Thus all impacts will occur within 1 σ.
To be conservative lets use **3** Standard Deviations, i.e. **99.73**% of all impacts will occur within **3 σ**
Use Standard Deviations = 3
Thus ΔP = Parameter @ 1 σ * 3 = **0.90**

Average V (Gradient) = 3.89
V * ΔP = 3.50 (Change in Force per Parameter)
fo + V.(ΔP) = **10.38**

Buffer Damping Charactcteristic Parameter: Power-On: Payload = Bottom

Base Value Impact Force = fo = 4.61 kN **0 = ON**
Base Value Damping Buffer Char. (ON) = 0 ON **1 = OFF**

Damping (ON / OFF)	FEA Impact Force	V (Gradient)	ΔP	Gradient x ΔP
1	14.33	9.72	1.00	9.72

NB: Assume Buffer damping Characteristics can vary by 30%, thus 1 σ = 30%

Appr. value of the parameter resulting in 1 Standard Deviation = 0.30

From literature 1 Standard Deviation (σ) = 68.27%. Thus all impacts will occur within 1 σ.
To be conservative lets use **3** Standard Deviations, i.e. **99.73**% of all impacts will occur within **3 σ**
Use Standard Deviations = 3
Thus ΔP = Parameter @ 1 σ * 3 = **0.90**

Average V (Gradient) = 9.72
V * ΔP = 8.75 (Change in Force per Parameter)
fo + V.(ΔP) = **13.36**

Buffer Damping Charactcteristic Parameter: Power-On: Payload = Top

Base Value Impact Force = fo = 8.05 kN **0 = ON**
Base Value Damping Buffer Char. (ON) = 0 ON **1 = OFF**

Damping (ON / OFF)	FEA Impact Force	V (Gradient)	ΔP	Gradient x ΔP
1	12.48	4.43	1.00	4.43

NB: Assume Buffer damping Characteristics can vary by 30%, thus 1 σ = 30%

Appr. value of the parameter resulting in 1 Standard Deviation = 0.30

From literature 1 Standard Deviation (σ) = 68.27%. Thus all impacts will occur within 1 σ.
To be conservative lets use **3** Standard Deviations, i.e. **99.73**% of all impacts will occur within **3 σ**
Use Standard Deviations = 3
Thus ΔP = Parameter @ 1 σ * 3 = **0.90**

Average V (Gradient) = 4.43
V * ΔP = 3.99 (Change in Force per Parameter)
fo + V.(ΔP) = **12.04**

Payload Bottom: Power OFF **1st Impact Response**

Use 7 Variables

Parameter	Parameter #	Parameter Force Variance (PFV) @ 3σ	σ	i =
Lag Angle	DP1	3.17	0.02200	1
Crab and Payload Eccentricity	DP2	1.08	1.13000	2
Gantry Flexibility	DP3	-2.66	0.00250	3
Crane Impact Speed	DP4	4.13	0.05000	4
One End Stop Misaligned	DP5	3.69	0.04125	5
Buffer's Damping Characteristics	DP6	1.13	0.30000	6
Buffer's Elastic Characteristics	DP7	0.00	0.20000	7

Ignore Parameter 7, since its Parameter Force Variance is approximately 0.

Base Impact Force = 6.35 kN

Constraint Equation

g(DP) = Base Impact Force	PFV * DP1	PFV * DP2	PFV * DP3	PFV * DP4	PFV * DP5	PFV * DP6

∇	DP1	g(DP) =	3.173
∇	DP2	g(DP) =	1.075
∇	DP3	g(DP) =	-2.663
∇	DP4	g(DP) =	4.125
∇	DP5	g(DP) =	3.688
∇	DP6	g(DP) =	1.134

Constraint Equation: ***Assuming μ = 0***

$$f(DP) = -\frac{DP_1^2}{2\times\sigma_{11}^2} - \frac{DP_2^2}{2\times\sigma_{22}^2} - \frac{DP_3^2}{2\times\sigma_{33}^2} - \frac{DP_4^2}{2\times\sigma_{44}^2} - \frac{DP_5^2}{2\times\sigma_{55}^2} - \frac{DP_6^2}{2\times\sigma_{66}^2} = -\frac{1}{2}\beta^2$$

General Equation

	$DP1^2$	$DP2^2$	$DP3^2$	$DP4^2$	$DP5^2$	$DP6^2$
f(DP) =	-1033.058	-0.392	-80000.000	-200.000	-293.848	-5.556

∇	DP1	f(DP) =	-2066.116
∇	DP2	f(DP) =	-0.783
∇	DP3	f(DP) =	-160000.000
∇	DP4	f(DP) =	-400.000
∇	DP5	f(DP) =	-587.695
∇	DP6	f(DP) =	-11.111

Lagrange Multiplier Method: ***∇f(DP) = λ * ∇γ(DP)***

i =	∇_{DPi} f(DP)		∇_{DPi} g(DP)		
	DPi *				
1	-2066.116	= λ *	3.17	λ =	-651.258 DP1
2	-0.783	= λ *	1.08	λ =	-0.729 DP2
3	-160000.000	= λ *	-2.66	λ =	60075.780 DP3
4	-400.000	= λ *	4.13	λ =	-96.970 DP4
5	-587.695	= λ *	3.69	λ =	-159.364 DP5
6	-11.111	= λ *	1.13	λ =	-9.798 DP6

Equate λ's

DP1	DP2	DP3	DP4	DP5	DP6
-651.258	-0.729	60075.780	-96.970	-159.364	-9.798

DP2	=	893.96056 DP1			
DP3	=	-0.00001 DP2	=	-0.011 DP1	
DP4	=	-619.53148 DP3	=	6.716 DP1	
DP5	=	0.60848 DP4	=	4.087 DP1	
DP6	=	16.26470 DP5	=	66.467 DP1	

Substitute into Constraint Equation

Bottom term squared

-352446.858 DP1 **= -0.5* β^2**

For β= 1		
DP1	=	0.00119
DP2	=	1.06477
DP3	=	-0.00001
DP4	=	0.00800
DP5	=	0.00487
DP6	=	0.07917
Maximum Impact Force		
g(DP) =	**7.64 kN**	

For β= 2		
DP1	=	0.00238
DP2	=	2.12954
DP3	=	-0.00003
DP4	=	0.01600
DP5	=	0.00973
DP6	=	0.15833
Maximum Impact Force		
g(DP) =	**8.93 kN**	

For β= 3		
DP1	=	0.00357
DP2	=	3.19432
DP3	=	-0.00004
DP4	=	0.02400
DP5	=	0.01460
DP6	=	0.23750
Maximum Impact Force		
g(DP) =	**10.22 kN**	

Payload Bottom: Power ON **1st Impact Response**

Use 7 Variables

Parameter	Parameter #	Parameter Force Variance (PFV) @ 3σ	σ	i =
Lag Angle	DP1	3.69	0.02200	1
Crab and Payload Eccentricity	DP2	1.52	1.13000	2
Gantry Flexibility	DP3	-3.06	0.00250	3
Crane Impact Speed	DP4	4.73	0.05000	4
One End Stop Misaligned	DP5	4.17	0.04125	5
Buffer's Damping Characteristics	DP6	1.31	0.30000	6
Buffer's Elastic Characteristics	DP7	0.00	0.20000	7

Ignore Parameter 7, since its Parameter Force Variance is approximately 0.

Base Impact Force = 7.26 kN

Constraint Equation

g(DP) = Base Impact Force	PFV * DP1	PFV * DP2	PFV * DP3	PFV * DP4	PFV * DP5	PFV * DP6

∇	DP1	g(DP) =	3.694
∇	DP2	g(DP) =	1.518
∇	DP3	g(DP) =	-3.057
∇	DP4	g(DP) =	4.725
∇	DP5	g(DP) =	4.175
∇	DP6	g(DP) =	1.305

Constraint Equation: ***Assuming μ = 0***

$$f(DP) = -\frac{DP_1^2}{2\times\sigma_{11}^2} - \frac{DP_2^2}{2\times\sigma_{22}^2} - \frac{DP_3^2}{2\times\sigma_{33}^2} - \frac{DP_4^2}{2\times\sigma_{44}^2} - \frac{DP_5^2}{2\times\sigma_{55}^2} - \frac{DP_6^2}{2\times\sigma_{66}^2} = -\frac{1}{2}\beta^2$$

General Equation

	DP1²	DP2²	DP3²	DP4²	DP5²	DP6²
f(DP) =	-1033.058	-0.392	-80000.000	-200.000	-293.848	-5.556

∇	DP1	f(DP) =	-2066.116
∇	DP2	f(DP) =	-0.783
∇	DP3	f(DP) =	-160000.000
∇	DP4	f(DP) =	-400.000
∇	DP5	f(DP) =	-587.695
∇	DP6	f(DP) =	-11.111

Lagrange Multiplier Method: ***∇f(DP) = λ * ∇g(DP)***

i =	∇_{DPi} f(DP)		∇_{DPi} g(DP)		
	DPi *				
1	-2066.116	= λ *	3.69	λ =	-559.355 DP1
2	-0.783	= λ *	1.52	λ =	-0.516 DP2
3	-160000.000	= λ *	-3.06	λ =	52333.757 DP3
4	-400.000	= λ *	4.73	λ =	-84.656 DP4
5	-587.695	= λ *	4.17	λ =	-140.782 DP5
6	-11.111	= λ *	1.31	λ =	-8.514 DP6

Equate λ's

DP1	DP2	DP3	DP4	DP5	DP6
-559.355	-0.516	52333.757	-84.656	-140.782	-8.514

DP2	=	1083.95400 DP1			
DP3	=	-0.00001 DP2	=	-0.011 DP1	
DP4	=	-618.19251 DP3	=	6.607 DP1	
DP5	=	0.60133 DP4	=	3.973 DP1	
DP6	=	16.53486 DP5	=	65.696 DP1	

Substitute into Constraint Equation

Bottom term squared

-498471.704 DP1 **= -0.5* β²**

For β= 1		
DP1	=	0.00100
DP2	=	1.08561
DP3	=	-0.00001
DP4	=	0.00662
DP5	=	0.00398
DP6	=	0.06580
Maximum Impact Force		
g(DP) =	**9.05 kN**	

For β= 2		
DP1	=	0.00200
DP2	=	2.17123
DP3	=	-0.00002
DP4	=	0.01323
DP5	=	0.00796
DP6	=	0.13159
Maximum Impact Force		
g(DP) =	**10.83 kN**	

For β= 3		
DP1	=	0.00300
DP2	=	3.25684
DP3	=	-0.00003
DP4	=	0.01985
DP5	=	0.01194
DP6	=	0.19739
Maximum Impact Force		
g(DP) =	**12.62 kN**	

Payload TOP Power OFF **1st Impact Response**

Use 7 Variables

Parameter	Parameter #	Parameter Force Variance (PFV) @ 3σ	σ	i =
Lag Angle	DP1	2.50	0.02200	1
Crab and Payload Eccentricity	DP2	1.53	1.13000	2
Gantry Flexibility	DP3	-2.85	0.00250	3
Crane Impact Speed	DP4	4.43	0.05000	4
One End Stop Misaligned	DP5	4.85	0.04125	5
Buffer's Damping Characteristics	DP6	1.21	0.30000	6
Buffer's Elastic Characteristics	DP7	0.00	0.20000	7
			-0.00263	

Ignore Parameter 7, since its Parameter Force Variance is approximately 0.

Base Impact Force = 6.65 kN

Constraint Equation

g(DP) = Base Impact Force	PFV * DP1	PFV * DP2	PFV * DP3	PFV * DP4	PFV * DP5	PFV * DP6

∇	DP1	g(DP) =	2.498
∇	DP2	g(DP) =	1.530
∇	DP3	g(DP) =	-2.847
∇	DP4	g(DP) =	4.425
∇	DP5	g(DP) =	4.848
∇	DP6	g(DP) =	1.206

Constraint Equation: ***Assuming μ = 0***

$$f(DP) = -\frac{DP_1^2}{2\times\sigma_{11}^2} - \frac{DP_2^2}{2\times\sigma_{22}^2} - \frac{DP_3^2}{2\times\sigma_{33}^2} - \frac{DP_4^2}{2\times\sigma_{44}^2} - \frac{DP_5^2}{2\times\sigma_{55}^2} - \frac{DP_6^2}{2\times\sigma_{66}^2} = -\frac{1}{2}\beta^2$$

General Equation

	$DP1^2$	$DP2^2$	$DP3^2$	$DP4^2$	$DP5^2$	$DP6^2$
f(DP) =	-1033.058	-0.392	-80000.000	-200.000	-293.848	-5.556

∇	DP1	f(DP) =	-2066.116
∇	DP2	f(DP) =	-0.783
∇	DP3	f(DP) =	-160000.000
∇	DP4	f(DP) =	-400.000
∇	DP5	f(DP) =	-587.695
∇	DP6	f(DP) =	-11.111

Lagrange Multiplier Method: ***∇f(DP) = λ * ∇γ(DP)***

i =	∇_{DPi} f(DP)		∇_{DPi} g(DP)		
	DPi *				
1	-2066.116	= λ *	2.50	λ =	-827.274 DP1
2	-0.783	= λ *	1.53	λ =	-0.512 DP2
3	-160000.000	= λ *	-2.85	λ =	56205.445 DP3
4	-400.000	= λ *	4.43	λ =	-90.395 DP4
5	-587.695	= λ *	4.85	λ =	-121.218 DP5
6	-11.111	= λ *	1.21	λ =	-9.213 DP6

Equate λ's

DP1	DP2	DP3	DP4	DP5	DP6
-827.274	-0.512	56205.445	-90.395	-121.218	-9.213

DP2	=	1616.20877	DP1		
DP3	=	-0.00001	DP2	=	-0.015 DP1
DP4	=	-621.77273	DP3	=	9.152 DP1
DP5	=	0.74573	DP4	=	6.825 DP1
DP6	=	13.15700	DP5	=	89.792 DP1

Substitute into Constraint Equation

Bottom term squared

-1099120.761 DP1 **$= -0.5 * \beta^2$**

	For β= 1	
DP1	=	0.00067
DP2	=	1.09008
DP3	=	-0.00001
DP4	=	0.00617
DP5	=	0.00460
DP6	=	0.06056
Maximum Impact Force		
g(DP) =	**8.44 kN**	

	For β= 2	
DP1	=	0.00135
DP2	=	2.18017
DP3	=	-0.00002
DP4	=	0.01235
DP5	=	0.00921
DP6	=	0.12112
Maximum Impact Force		
g(DP) =	**10.23 kN**	

	For β= 3	
DP1	=	0.00202
DP2	=	3.27025
DP3	=	-0.00003
DP4	=	0.01852
DP5	=	0.01381
DP6	=	0.18169
Maximum Impact Force		
g(DP) =	**12.03 kN**	

Payload TOP Power ON **1st Impact Response**

Use 7 Variables

Parameter	Parameter #	Parameter Force Variance (PFV) @ 3σ	σ	i =
Lag Angle	DP1	3.56	0.02200	1
Crab and Payload Eccentricity	DP2	2.03	1.13000	2
Gantry Flexibility	DP3	-1.52	0.00250	3
Crane Impact Speed	DP4	4.88	0.05000	4
One End Stop Misaligned	DP5	5.19	0.04125	5
Buffer's Damping Characteristics	DP6	1.38	0.30000	6
Buffer's Elastic Characteristics	DP7	-0.01	0.20000	7

Ignore Parameter 7, since its Parameter Force Variance is approximately 0.

Base Impact Force = 7.48 kN

Constraint Equation

g(DP) = Base Impact Force	PFV * DP1	PFV * DP2	PFV * DP3	PFV * DP4	PFV * DP5	PFV * DP6

∇	DP1	g(DP) =	3.559
∇	DP2	g(DP) =	2.030
∇	DP3	g(DP) =	-1.519
∇	DP4	g(DP) =	4.875
∇	DP5	g(DP) =	5.187
∇	DP6	g(DP) =	1.377

Constraint Equation: ***Assuming μ = 0***

$$f(DP) = -\frac{DP_1^2}{2\times\sigma_{11}^2} - \frac{DP_2^2}{2\times\sigma_{22}^2} - \frac{DP_3^2}{2\times\sigma_{33}^2} - \frac{DP_4^2}{2\times\sigma_{44}^2} - \frac{DP_5^2}{2\times\sigma_{55}^2} - \frac{DP_6^2}{2\times\sigma_{66}^2} = -\frac{1}{2}\beta^2$$

General Equation

	DP1²	DP2²	DP3²	DP4²	DP5²	DP6²
f(DP) =	-1033.058	-0.392	-80000.000	-200.000	-293.848	-5.556

∇	DP1	f(DP) =	-2066.116
∇	DP2	f(DP) =	-0.783
∇	DP3	f(DP) =	-160000.000
∇	DP4	f(DP) =	-400.000
∇	DP5	f(DP) =	-587.695
∇	DP6	f(DP) =	-11.111

Lagrange Multiplier Method: ***∇f(DP) = λ * ∇γ(DP)***

i =	∇_{DPi} f(DP)		∇_{DPi} g(DP)		
	DPi *				
1	-2066.116	= λ *	3.56	λ =	-580.573 DP1
2	-0.783	= λ *	2.03	λ =	-0.386 DP2
3	-160000.000	= λ *	-1.52	λ =	105312.007 DP3
4	-400.000	= λ *	4.88	λ =	-82.051 DP4
5	-587.695	= λ *	5.19	λ =	-113.312 DP5
6	-11.111	= λ *	1.38	λ =	-8.069 DP6

Equate λ's

DP1	DP2	DP3	DP4	DP5	DP6
-580.573	-0.386	105312.007	-82.051	-113.312	-8.069

DP2	=	1504.90846 DP1			
DP3	=	0.00000 DP2	=	-0.006 DP1	
DP4	=	-1283.49008 DP3	=	7.076 DP1	
DP5	=	0.72412 DP4	=	5.124 DP1	
DP6	=	14.04281 DP5	=	71.950 DP1	

Substitute into Constraint Equation

Bottom term squared

-934338.632 DP1 **= -0.5* β²**

For β= 1		
DP1	=	0.00073
DP2	=	1.10089
DP3	=	0.00000
DP4	=	0.00518
DP5	=	0.00375
DP6	=	0.05263
Maximum Impact Force		
g(DP) =	**9.83 kN**	

For β= 2		
DP1	=	0.00146
DP2	=	2.20177
DP3	=	-0.00001
DP4	=	0.01035
DP5	=	0.00750
DP6	=	0.10527
Maximum Impact Force		
g(DP) =	**12.19 kN**	

For β= 3		
DP1	=	0.00219
DP2	=	3.30266
DP3	=	-0.00001
DP4	=	0.01553
DP5	=	0.01124
DP6	=	0.15790
Maximum Impact Force		
g(DP) =	**14.54 kN**	

Payload Bottom: Power OFF **2nd Impact Response**

Use 7 Variables

Parameter	Parameter #	Parameter Force Variance (PFV) @ 3σ	σ	i =
Lag Angle	DP1	-1.19	0.02200	1
Crab and Payload Eccentricity	DP2	0.72	1.13000	2
Gantry Flexibility	DP3	-1.48	0.00250	3
Crane Impact Speed	DP4	4.16	0.05000	4
One End Stop Misaligned	DP5	2.46	0.04125	5
Buffer's Damping Characteristics	DP6	7.74	0.30000	6
Buffer's Elastic Characteristics	DP7	0.01	0.20000	7

Ignore Parameter 7, since its Parameter Force Variance is approximately 0.

Base Impact Force = 4.43 kN

Constraint Equation

g(DP) = Base Impact Force	PFV * DP1	PFV * DP2	PFV * DP3	PFV * DP4	PFV * DP5	PFV * DP6

∇	DP1	g(DP) =	-1.193
∇	DP2	g(DP) =	0.720
∇	DP3	g(DP) =	-1.482
∇	DP4	g(DP) =	4.155
∇	DP5	g(DP) =	2.459
∇	DP6	g(DP) =	7.740

Constraint Equation: ***Assuming μ = 0***

$$f(DP) = -\frac{DP_1^2}{2\times\sigma_{11}^2} - \frac{DP_2^2}{2\times\sigma_{22}^2} - \frac{DP_3^2}{2\times\sigma_{33}^2} - \frac{DP_4^2}{2\times\sigma_{44}^2} - \frac{DP_5^2}{2\times\sigma_{55}^2} - \frac{DP_6^2}{2\times\sigma_{66}^2} = -\frac{1}{2}\beta^2$$

General Equation

	$DP1^2$	$DP2^2$	$DP3^2$	$DP4^2$	$DP5^2$	$DP6^2$
f(DP) =	-1033.058	-0.392	-80000.000	-200.000	-293.848	-5.556

∇	DP1	f(DP) =	-2066.116
∇	DP2	f(DP) =	-0.783
∇	DP3	f(DP) =	-160000.000
∇	DP4	f(DP) =	-400.000
∇	DP5	f(DP) =	-587.695
∇	DP6	f(DP) =	-11.111

Lagrange Multiplier Method: $\nabla f(DP) = \lambda * \nabla g(DP)$

i =	∇_{DPi} f(DP) DPi *	= λ *	∇_{DPi} g(DP)		
1	-2066.116	= λ *	-1.19	λ =	1732.592 **DP1**
2	-0.783	= λ *	0.72	λ =	-1.088 **DP2**
3	-160000.000	= λ *	-1.48	λ =	107959.006 **DP3**
4	-400.000	= λ *	4.16	λ =	-96.270 **DP4**
5	-587.695	= λ *	2.46	λ =	-239.046 **DP5**
6	-11.111	= λ *	7.74	λ =	-1.436 **DP6**

Equate λ's

DP1	DP2	DP3	DP4	DP5	DP6
1732.592	-1.088	107959.006	-96.270	-239.046	-1.436

DP2	=	**-1592.88944 DP1**			
DP3	=	**-0.00001 DP2**	=	**0.016 DP1**	
DP4	=	**-1121.42417 DP3**	=	**-17.997 DP1**	
DP5	=	**0.40272 DP4**	=	**-7.248 DP1**	
DP6	=	**166.51960 DP5**	=	**-1206.923 DP1**	

Substitute into Constraint Equation

Bottom term squared

-9167387.343 DP1 **= -0.5* β^2**

For β= 1		
DP1	=	0.00023
DP2	=	-0.37200
DP3	=	0.00000
DP4	=	-0.00420
DP5	=	-0.00169
DP6	=	-0.28187
Maximum Impact Force g(DP) =		**1.96 kN**

For β= 2		
DP1	=	0.00047
DP2	=	-0.74401
DP3	=	0.00001
DP4	=	-0.00841
DP5	=	-0.00339
DP6	=	-0.56373
Maximum Impact Force g(DP) =		**-0.51 kN**

For β= 3		
DP1	=	0.00070
DP2	=	-1.11601
DP3	=	0.00001
DP4	=	-0.01261
DP5	=	-0.00508
DP6	=	-0.84560
Maximum Impact Force g(DP) =		**-2.98 kN**

Payload Bottom: Power ON **2nd Impact Response**

Use 7 Variables

Parameter	Parameter #	Parameter Force Variance (PFV) @ 3σ	σ	i =
Lag Angle	DP1	-0.96	0.02200	1
Crab and Payload Eccentricity	DP2	1.43	1.13000	2
Gantry Flexibility	DP3	-1.61	0.00250	3
Crane Impact Speed	DP4	5.03	0.05000	4
One End Stop Misaligned	DP5	4.75	0.04125	5
Buffer's Damping Characteristics	DP6	8.75	0.30000	6
Buffer's Elastic Characteristics	DP7	0.00	0.20000	7

Ignore Parameter 7, since its Parameter Force Variance is approximately 0.

Base Impact Force = 4.61 kN

Constraint Equation

g(DP) = Base Impact Force	PFV * DP1	PFV * DP2	PFV * DP3	PFV * DP4	PFV * DP5	PFV * DP6

∇	DP1	g(DP) =	-0.960
∇	DP2	g(DP) =	1.432
∇	DP3	g(DP) =	-1.606
∇	DP4	g(DP) =	5.025
∇	DP5	g(DP) =	4.747
∇	DP6	g(DP) =	8.748

Constraint Equation: ***Assuming μ = 0***

$$f(DP) = -\frac{DP_1^2}{2\times\sigma_{11}^2} - \frac{DP_2^2}{2\times\sigma_{22}^2} - \frac{DP_3^2}{2\times\sigma_{33}^2} - \frac{DP_4^2}{2\times\sigma_{44}^2} - \frac{DP_5^2}{2\times\sigma_{55}^2} - \frac{DP_6^2}{2\times\sigma_{66}^2} = -\frac{1}{2}\beta^2$$

General Equation

	$DP1^2$	$DP2^2$	$DP3^2$	$DP4^2$	$DP5^2$	$DP6^2$
f(DP) =	-1033.058	-0.392	-80000.000	-200.000	-293.848	-5.556

∇	DP1	f(DP) =	-2066.116
∇	DP2	f(DP) =	-0.783
∇	DP3	f(DP) =	-160000.000
∇	DP4	f(DP) =	-400.000
∇	DP5	f(DP) =	-587.695
∇	DP6	f(DP) =	-11.111

Lagrange Multiplier Method: $\nabla f(DP) = \lambda * \nabla g(DP)$

i =	∇_{DPi} f(DP) DPi *	= λ *	∇_{DPi} g(DP)		
1	-2066.116	= λ *	-0.96	λ =	2152.204 DP1
2	-0.783	= λ *	1.43	λ =	-0.547 DP2
3	-160000.000	= λ *	-1.61	λ =	99650.214 DP3
4	-400.000	= λ *	5.03	λ =	-79.602 DP4
5	-587.695	= λ *	4.75	λ =	-123.817 DP5
6	-11.111	= λ *	8.75	λ =	-1.270 DP6

Equate λ's

DP1	DP2	DP3	DP4	DP5	DP6
2152.204	-0.547	99650.214	-79.602	-123.817	-1.270

DP2	=	-3935.36675 DP1			
DP3	=	-0.00001 DP2	=	0.022 DP1	
DP4	=	-1251.85581 DP3	=	-27.037 DP1	
DP5	=	0.64290 DP4	=	-17.382 DP1	
DP6	=	97.48323 DP5	=	-1694.473 DP1	

Substitute into Constraint Equation

Bottom term squared

-22251723.291 DP1 **= -0.5* β^2**

For β= 1		
DP1	=	0.00015
DP2	=	-0.58991
DP3	=	0.00000
DP4	=	-0.00405
DP5	=	-0.00261
DP6	=	-0.25400
Maximum Impact Force		
g(DP) =	**1.51 kN**	

For β= 2		
DP1	=	0.00030
DP2	=	-1.17983
DP3	=	0.00001
DP4	=	-0.00811
DP5	=	-0.00521
DP6	=	-0.50800
Maximum Impact Force		
g(DP) =	**-1.59 kN**	

For β= 3		
DP1	=	0.00045
DP2	=	-1.76974
DP3	=	0.00001
DP4	=	-0.01216
DP5	=	-0.00782
DP6	=	-0.76201
Maximum Impact Force		
g(DP) =	**-4.69 kN**	

Payload TOP: Power OFF **2nd Impact Response**

Use 7 Variables

Parameter	Parameter #	Parameter Force Variance (PFV) @ 3σ	σ	i =
Lag Angle	DP1	0.38	0.02200	1
Crab and Payload Eccentricity	DP2	1.73	1.13000	2
Gantry Flexibility	DP3	-2.96	0.00250	3
Crane Impact Speed	DP4	4.43	0.05000	4
One End Stop Misaligned	DP5	3.39	0.04125	5
Buffer's Damping Characteristics	DP6	3.50	0.30000	6
Buffer's Elastic Characteristics	DP7	0.00	0.20000	7

Ignore Parameter 7, since its Parameter Force Variance is approximately 0.

Base Impact Force = 6.88 kN

Constraint Equation

g(DP) = Base Impact Force	PFV * DP1	PFV * DP2	PFV * DP3	PFV * DP4	PFV * DP5	PFV * DP6

∇	**DP1**	**g(DP) =**	**0.375**
∇	**DP2**	**g(DP) =**	**1.730**
∇	**DP3**	**g(DP) =**	**-2.963**
∇	**DP4**	**g(DP) =**	**4.425**
∇	**DP5**	**g(DP) =**	**3.385**
∇	**DP6**	**g(DP) =**	**3.501**

Constraint Equation: ***Assuming μ = 0***

$$f(DP) = -\frac{DP_1^2}{2\times\sigma_{11}^2} - \frac{DP_2^2}{2\times\sigma_{22}^2} - \frac{DP_3^2}{2\times\sigma_{33}^2} - \frac{DP_4^2}{2\times\sigma_{44}^2} - \frac{DP_5^2}{2\times\sigma_{55}^2} - \frac{DP_6^2}{2\times\sigma_{66}^2} = -\frac{1}{2}\beta^2$$

General Equation

	$DP1^2$	$DP2^2$	$DP3^2$	$DP4^2$	$DP5^2$	$DP6^2$
f(DP) =	-1033.058	-0.392	-80000.000	-200.000	-293.848	-5.556

∇	**DP1**	**f(DP) =**	**-2066.116**
∇	**DP2**	**f(DP) =**	**-0.783**
∇	**DP3**	**f(DP) =**	**-160000.000**
∇	**DP4**	**f(DP) =**	**-400.000**
∇	**DP5**	**f(DP) =**	**-587.695**
∇	**DP6**	**f(DP) =**	**-11.111**

Lagrange Multiplier Method: $\nabla f(DP) = \lambda * \nabla g(DP)$

i =	∇_{DPi} f(DP) DPi *	= λ *	∇_{DPi} g(DP)		
1	-2066.116	= λ *	0.38	λ =	-5509.642 **DP1**
2	-0.783	= λ *	1.73	λ =	-0.453 **DP2**
3	-160000.000	= λ *	-2.96	λ =	53994.674 **DP3**
4	-400.000	= λ *	4.43	λ =	-90.395 **DP4**
5	-587.695	= λ *	3.39	λ =	-173.605 **DP5**
6	-11.111	= λ *	3.50	λ =	-3.174 **DP6**

Equate λ's

DP1	DP2	DP3	DP4	DP5	DP6
-5509.642	-0.453	53994.674	-90.395	-173.605	-3.174

DP2	**=**	**12171.00275**	**DP1**			
DP3	**=**	**-0.00001**	**DP2**	**=**	**-0.102**	**DP1**
DP4	**=**	**-597.31608**	**DP3**	**=**	**60.950**	**DP1**
DP5	**=**	**0.52070**	**DP4**	**=**	**31.737**	**DP1**
DP6	**=**	**54.70109**	**DP5**	**=**	**1736.033**	**DP1**

Substitute into Constraint Equation

Bottom term squared

-75789273.220 DP1 **= -0.5* β^2**

	For β= 1	
DP1	=	0.00008
DP2	=	0.98857
DP3	=	-0.00001
DP4	=	0.00495
DP5	=	0.00258
DP6	=	0.14101
Maximum Impact Force g(DP) =	**9.11 kN**	

	For β= 2	
DP1	=	0.00016
DP2	=	1.97714
DP3	=	-0.00002
DP4	=	0.00990
DP5	=	0.00516
DP6	=	0.28201
Maximum Impact Force g(DP) =	**11.35 kN**	

	For β= 3	
DP1	=	0.00024
DP2	=	2.96571
DP3	=	-0.00002
DP4	=	0.01485
DP5	=	0.00773
DP6	=	0.42302
Maximum Impact Force g(DP) =	**13.58 kN**	

Payload TOP: Power ON **2nd Impact Response**

Use 7 Variables

Parameter	Parameter #	Parameter Force Variance (PFV) @ 3σ	σ	i =
Lag Angle	DP1	1.09	0.02200	1
Crab and Payload Eccentricity	DP2	1.28	1.13000	2
Gantry Flexibility	DP3	-3.04	0.00250	3
Crane Impact Speed	DP4	6.26	0.05000	4
One End Stop Misaligned	DP5	2.58	0.04125	5
Buffer's Damping Characteristics	DP6	3.99	0.30000	6
Buffer's Elastic Characteristics	DP7	0.00	0.20000	7

Ignore Parameter 7, since its Parameter Force Variance is approximately 0.

Base Impact Force = 8.05 kN

Constraint Equation

g(DP) = Base Impact Force	PFV * DP1	PFV * DP2	PFV * DP3	PFV * DP4	PFV * DP5	PFV * DP6

∇	**DP1**	**g(DP) =**	**1.088**
∇	**DP2**	**g(DP) =**	**1.275**
∇	**DP3**	**g(DP) =**	**-3.038**
∇	**DP4**	**g(DP) =**	**6.255**
∇	**DP5**	**g(DP) =**	**2.582**
∇	**DP6**	**g(DP) =**	**3.987**

Constraint Equation: ***Assuming μ = 0***

$$f(DP) = -\frac{DP_1^2}{2\times\sigma_{11}^2} - \frac{DP_2^2}{2\times\sigma_{22}^2} - \frac{DP_3^2}{2\times\sigma_{33}^2} - \frac{DP_4^2}{2\times\sigma_{44}^2} - \frac{DP_5^2}{2\times\sigma_{55}^2} - \frac{DP_6^2}{2\times\sigma_{66}^2} = -\frac{1}{2}\beta^2$$

General Equation

	$DP1^2$	$DP2^2$	$DP3^2$	$DP4^2$	$DP5^2$	$DP6^2$
f(DP) =	-1033.058	-0.392	-80000.000	-200.000	-293.848	-5.556

∇	**DP1**	**f(DP) =**	**-2066.116**
∇	**DP2**	**f(DP) =**	**-0.783**
∇	**DP3**	**f(DP) =**	**-160000.000**
∇	**DP4**	**f(DP) =**	**-400.000**
∇	**DP5**	**f(DP) =**	**-587.695**
∇	**DP6**	**f(DP) =**	**-11.111**

Lagrange Multiplier Method: ***∇f(DP) = λ * ∇g(DP)***

i =	∇_{DPi} f(DP) = DPi *	= λ *	∇_{DPi} g(DP)		
1	-2066.116	= λ *	1.09	λ =	-1899.877 **DP1**
2	-0.783	= λ *	1.28	λ =	-0.614 **DP2**
3	-160000.000	= λ *	-3.04	λ =	52672.378 **DP3**
4	-400.000	= λ *	6.26	λ =	-63.949 **DP4**
5	-587.695	= λ *	2.58	λ =	-227.590 **DP5**
6	-11.111	= λ *	3.99	λ =	-2.787 **DP6**

Equate λ's

DP1	DP2	DP3	DP4	DP5	DP6
-1899.877	-0.614	52672.378	-63.949	-227.590	-2.787

DP2	**=**	**3093.08920 DP1**			
DP3	**=**	**-0.00001 DP2**	**=**	**-0.036 DP1**	
DP4	**=**	**-823.66431 DP3**	**=**	**29.709 DP1**	
DP5	**=**	**0.28098 DP4**	**=**	**8.348 DP1**	
DP6	**=**	**81.66624 DP5**	**=**	**681.733 DP1**	

Substitute into Constraint Equation

Bottom term squared

-6526400.583 DP1 **= -0.5* β^2**

	For β= 1	
DP1	=	0.00028
DP2	=	0.85613
DP3	=	-0.00001
DP4	=	0.00822
DP5	=	0.00231
DP6	=	0.18870
Maximum Impact Force		
g(DP) =	**9.95 kN**	

	For β= 2	
DP1	=	0.00055
DP2	=	1.71226
DP3	=	-0.00002
DP4	=	0.01645
DP5	=	0.00462
DP6	=	0.37739
Maximum Impact Force		
g(DP) =	**11.85 kN**	

	For β= 3	
DP1	=	0.00083
DP2	=	2.56840
DP3	=	-0.00003
DP4	=	0.02467
DP5	=	0.00693
DP6	=	0.56609
Maximum Impact Force		
g(DP) =	**13.75 kN**	